Copyright
by
Emily June Boyd
2014

The Dissertation Committee for Emily June Boyd certifies that this is the approved version of the following dissertation:

Parameters that Affect Shaped Hole Film Cooling Performance and the Effect of Density Ratio on Heat Transfer Coefficient Augmentation

Committee:

David Bogard, Supervisor

Michael Crawford

Ofodike Ezekoye

Carlos Hidrovo

Thomas Kiehne

Parameters that Affect Shaped Hole Film Cooling Performance and the Effect of Density Ratio on Heat Transfer Coefficient Augmentation

by

Emily June Boyd, B.S.M.E.; M.S.

Dissertation

Presented to the Faculty of the Graduate School of
The University of Texas at Austin
in Partial Fulfillment
of the Requirements
for the Degree of

Doctor of Philosophy

The University of Texas at Austin

May, 2014

Dedication

To my incredibly supportive husband, Rodney, who commuted between St. Louis and Austin every weekend for the six years I worked on this degree.

Acknowledgements

I would like to thank Dr. David Bogard for his supervision of my research. I would also like to thank my labmates, many of whom helped me gather data for this dissertation: John McClintic, Kyle Chavez, Josh Anderson, Noah Mosberg, Robbie Stewart, Sean Klavetter, Gavin Packard, and Adam Vaclavik

Parameters that Affect Shaped Hole Film Cooling Performance and the Effect of Density Ratio on Heat Transfer Coefficient Augmentation

Emily June Boyd, Ph.D.
The University of Texas at Austin, 2014

Supervisor: David Bogard

Film cooling is used in gas turbine engines to cool turbine components. Cooler air is bled from the compressor, routed internally through turbine vanes and blades, and exits through discrete holes, creating a film of coolant on the parts' surfaces. Cooling the turbine components protects them from thermal damage and allows the engine to operate at higher combustion temperatures, which increases the engine efficiency. Shaped film cooling holes with diffuser exits have the advantage that they decelerate the coolant flow, enabling the coolant jets to remain attached to the surface at higher coolant flow rates. Furthermore, the expanded exits of the coolant holes provide a wider coolant distribution over the surface.

The first part of this dissertation provides data for a new laidback, fan-shaped hole geometry designed at Pennsylvania State University's Experimental and Computational Convection Laboratory. The shaped hole geometry was tested on flat plate facilities at the University of Texas at Austin and Pennsylvania State University. The objective of testing at two laboratories was to verify the adiabatic effectiveness performance of the shaped hole, with the intent of the data being a standard of comparison for future experimental and computational shaped hole studies. At first, measurements of adiabatic effectiveness did not match between the labs, and it was later found that shaped holes are extremely sensitive to machining, the material they are machined into, and coolant entrance effects.

In addition, the adiabatic effectiveness was found to scale with velocity ratio for multiple density ratios and mainstream turbulence intensities.

The second part of this dissertation measures heat transfer coefficient augmentation (h_f/h_0) at density ratios (DR) of 1.0, 1.2, and 1.5 using a uniform heat flux plate and the same shaped hole geometry. In the past, heat transfer coefficient augmentation was generally measured at DR = 1.0 under the assumption that h_f/h_0 was independent of density ratio. This dissertation is the first study to directly measure the wall and adiabatic wall temperature to calculate heat transfer coefficient augmentation at DR > 1.0. The results showed that the heat transfer coefficient augmentation was low while the jets were attached to the surface and increased when the jets started to separate. At DR = 1.0, h_f/h_0 was higher for a given blowing ratio than at DR = 1.2 and DR = 1.5. However, when velocity ratios are matched, better correspondence was found at the different density ratios. Surface contours of h_f/h_0 showed that the heat transfer was initially increased along the centerline of the jet, but was reduced along the centerline at distances farther downstream. The decrease along the centerline may be due to counter-rotating vortices sweeping warm air next to the heat flux plate toward the center of the jet, where they sweep upward and thicken the thermal boundary layer. This warming of the core of the coolant jet over the heated surface was confirmed with thermal field measurements.

Table of Contents

List of Tables

List of Figures

Nomenclature

AR	area ratio
Bi	Biot number, *ht*/*k*
d	film cooling hole diameter
DR	density ratio, ρ_c/ρ_∞
h	heat transfer coefficient
H	test section height
I	momentum flux ratio, $\rho_c U_c^2/\rho_\infty U_\infty^2$
k	thermal conductivity
L	film cooling hole length
M	blowing ratio, $\rho_c U_c/\rho_\infty U_\infty$
Ma	Mach number
p	film coolant hole pitch distance
q″	heat flux
Re	Reynolds number
T	temperature
Tu	turbulence intensity
U	mean velocity
VR	velocity ratio U_c/U_∞
x	downstream distance, parallel to the main flow
y	wall-normal coordinate
z	span-wise coordinate

GREEK

α	surface injection angle
β	shaped hole lateral expansion angle

γ	compound angle
δ	boundary layer thickness
ε	shaped hole laidback expansion angle
η	adiabatic effectiveness $(T_\infty - T_{aw})/(T_\infty - T_c)$
v	kinematic viscosity
θ	nondimensional temperature $(T_\infty - T)/(T_\infty - T_c)$

SUBSCRIPTS, ACCENTS

aw	adiabatic wall
c	coolant
f	with film cooling
iw	isoenergetic wall (with coolant at *DR* = 1.0)
w	wall
$\overline{x}$	lateral average
0	without film cooling
∞	mainstream

INTRODUCTION

1.1 Introduction to Film Cooling

Jet engines and thermal power plants operate using the Brayton cycle, which is shown in Figure 0-1. Air is compressed, mixed with fuel, and combusted which produces power and heat. The air and combustion products then travel through the turbine where work is extracted. In the case of jet engines, the work generated from the turbine is used to power the compressor. For power plants, the turbine powers an electrical generator.

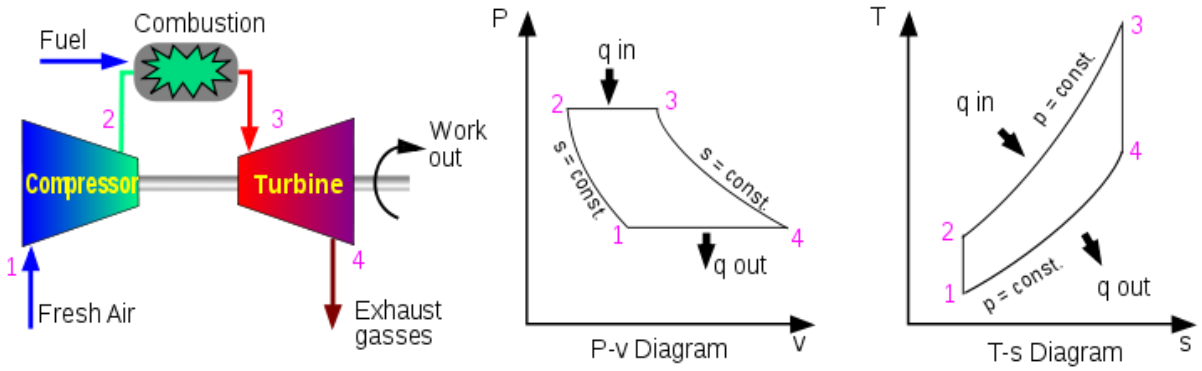

Figure 0-1 Diagram of Brayton cycle [1].

The cycle efficiency of an ideal air-standard Brayton cycle can be calculated by Equation 0-1. Increasing the combustion temperature, T_3, increases the thermal efficiency of the cycle.

$$\eta = 1 - \frac{T_4 - T_1}{T_3 - T_1}$$

Equation 0-1

Over the years, gas turbine designers have increased the combustion temperature up to the melting point of the turbine blade material. To further increase the combustion temperature, engineers are researching new materials and coatings that can withstand higher temperatures as well as the best methods for actively cooling the turbine vanes and blades with air from the compressor. This research focuses on the latter method.

To actively cool turbine vanes and blades, cool air is extracted from the compressor and fed through the center of the vanes and blades in the turbine, which internally cools the components. The coolant exits out of discrete holes in the turbine vanes and blades and creates a coolant film which protects the surface from heat damage. Figure 0-2 is a diagram of this film cooling process.

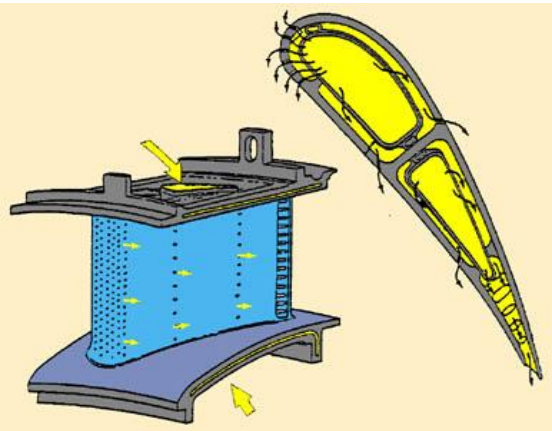

Figure 0-2 Illustration of film cooling [2].

Coolant holes can be cylindrical or they can be shaped. Shaped holes have a cylindrical base, but then expand into a diffuser up to the surface. Figure 0-3 shows the Solidworks drawing of the shaped hole design that was tested for this dissertation.

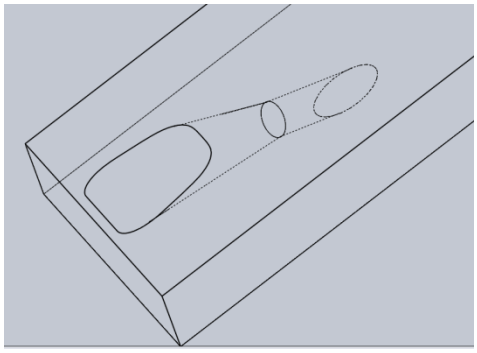

Figure 0-3 Model of the shaped hole designed by the Penn State University ExCCL Laboratory.

Shaped holes are very effective in film cooling because the diffuser reduces the momentum of the coolant exiting the hole which helps the jet stay attached to the surface. The diffuser also spreads the coolant laterally, providing more coolant surface coverage.

Some important parameters that are used to characterize film cooling are the density ratio, blowing ratio, momentum flux ratio, and velocity ratio. The density ratio, *DR*, is the ratio of the coolant density to the mainstream density, which is defined in Equation 0-2,

$$DR = \frac{\rho_c}{\rho_\infty} \approx \frac{T_\infty}{T_c},$$

Equation 0-2

where ρ_c is the density of the coolant and ρ_∞ is the density of the mainstream. Since the density of an ideal gas is inversely proportional to its temperature, the density ratio can also be viewed as the ratio of the mainstream temperature to the coolant temperature at similar pressures. Density ratios are about 2.0 in actual gas turbines [3]. The next three parameters characterize how much coolant is exiting the film cooling holes. The blowing ratio, M, is defined by Equation 0-3,

$$M = \frac{\rho_c U_c}{\rho_\infty U_\infty},$$

Equation 0-3

where U_c is the average velocity of the coolant in the cylindrical section of the holes and U_∞ is the velocity of the mainstream. The blowing ratio is the ratio of the mass flux of coolant to the mass flux of mainstream air. Another parameter, the momentum flux ratio, I, is the ratio of the coolant momentum flux to the mainstream momentum flux, which is given in Equation 0-4.

$$I = \frac{\rho_c U_c^2}{\rho_\infty U_\infty^2}$$

Equation 0-4

Equation 0-5 is the velocity ratio, VR, which is the ratio of the coolant velocity in the cylindrical section of the holes to the mainstream velocity.

$$VR = \frac{U_c}{U_\infty}$$

Equation 0-5

Gas turbine designers are interested in predicting and minimizing the surface temperature and heat flux entering vanes and blades. The adiabatic wall temperature, T_{aw}, is used to predict both of these. The adiabatic wall temperature is the surface temperature on an adiabatic surface, and it is presumed to be equal to the over-riding gas temperature that drives heat transfer into a conducting surface. The adiabatic wall temperature is nondimensionalized with the coolant temperature, T_c, and the mainstream temperature, T_∞, by Equation 0-6, which is termed adiabatic effectiveness.

$$\eta = \frac{T_\infty - T_{aw}}{T_\infty - T_c}$$

Equation 0-6

Equation 0-6 shows that if T_{aw} is equal to the coolant temperature, which would be optimum performance, $\eta = 1$. If $\eta = 0$, T_{aw} is equal to T_∞ which would mean the coolant jet is having no cooling effect.

Figure 0-4 depicts how the adiabatic wall temperature is presumed to be related to the actual wall temperature. Figure 0-4 a) shows film cooling of an attached jet over an adiabatic surface. A typical thermal profile above the wall is shown in red.

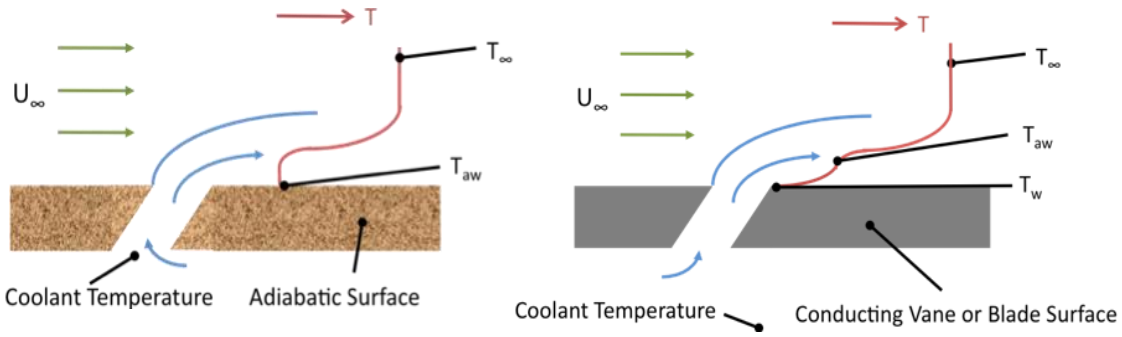

a) Film cooling on an Adiabatic Surface

b) Film Cooling on a Conducting Surface

Figure 0-4 a) Film cooling and thermal profile on an adiabatic surface b) Film cooling and thermal profile on a conducting surface

Since the surface is adiabatic, the temperature gradient is zero at the wall. Farther away from the wall, the jet continues to mix with the mainstream gas, and the temperature gradually increases until the edge of the jet is reached at T_∞. Figure 0-4 b) shows film cooling of an attached jet over a conducting surface. A thin thermal boundary layer exists between T_w and T_{aw}. T_w is usually lower than T_{aw} due to the internal cooling that conducts through the surface. In a conventional analysis, the driving temperature for heat transfer with film cooling is taken to be T_{aw}, which is equivalent to assuming that the edge of the thermal boundary layer is located at approximately T_{aw}. However, this assumption has been questioned by Harrison and Bogard [4]. Above the thermal boundary layer, the thermal profile gradually increases until the edge of the jet is reached at T_∞. The conventional equation for calculating heat flux entering the surface is given by Equation 0-7.

$$q'' = h_f (T_{aw} - T_w)$$

Equation 0-7

In Equation 0-7, h_f is the heat transfer coefficient with film cooling, which is different than the h that is typically used in heat transfer, where the driving temperature is T_∞. Because T_{aw} is used as the driving temperature, h_f is presumed to be independent of the coolant temperature. The reasons for this are discussed in Section 1.1.1. h_f can be determined experimentally by measuring q'', T_{aw}, and T_w. In addition to finding a heat transfer coefficient with film cooling, a heat transfer coefficient without film cooling, h_0, can be found using Equation 0-8.

$$h_0 = \frac{q''}{(T_\infty - T_w)}$$

Equation 0-8

In this case, with no film cooling, $T_{aw} = T_\infty$ or the recovery temperature in the case of high speed flows. Heat transfer coefficient results are often presented as h_f/h_0, which is called the heat transfer coefficient augmentation. It represents a percentage difference of the effect of adding film cooling versus no film cooling on the heat transfer coefficient.

To design gas turbines, designers multiply h_f/h_0 found in experiments by the h_0 in the actual turbine they are designing. They use experimental adiabatic effectiveness values to back calculate the actual adiabatic wall temperature using actual turbine coolant and mainstream temperatures. With these values, they can calculate the heat flux into the turbine vane or blade using Equation 0-7. This calculation is shown in Equation 0-9 to Equation 0-11, where the subscript *a* stands for actual turbine values, and the subscript *exp* stands for experimental values. In these calculations, T_{wa} is determined by a finite element analysis that uses the h_{fa} and T_{awa} as boundary conditions. q''_a can be found using a similar finite analysis using the internal heat transfer coefficient and conduction through the part surface.

$$T_{awa} = \eta_{\exp}(T_{\infty a} - T_{ca}) + T_{\infty a} \qquad h_{f\,a} = \left(\frac{h_f}{h_0}\right) h_{0a}$$

Equation 0-9 Equation 0-10

$$\longrightarrow \quad q''_a = \left(\frac{h_f}{h_0}\right)_{\exp} h_{0_a}[\eta_{\exp}(T_\infty - T_c)_a + T_{\infty a} - T_{wa}]$$

Equation 0-11

1.1.1 THE SUPERPOSITION APPROACH TO FILM COOLING

This section is intended to give a more detailed explanation for why the adiabatic wall temperature is used as a measure of film cooling performance. Characterization of film cooling performance relies on assuming the superposition of discrete solutions to the energy equation. This method has become so customary, despite its imperfections, that it is the dominate method that is used to analyze and measure film cooling performance. In fact, gas turbine designers have tailored their design process to design turbine components using the standard outputs from this superposition analysis, such as the adiabatic wall temperature and heat transfer coefficient augmentation. The only alternative to this method is the matched Biot number (*Bi*) model tests that were developed by the Turbulence and Turbine Cooling Research Laboratory at the University of Texas at Austin.

Film cooling research began in the late 1940s, and to make film cooling analysis easier, it was assumed that property differences between the coolant and mainstream were negligible. Given that actual gas turbine engines today operate at $DR = 2.0$, where the coolant density is twice that of the mainstream, this is a questionable assumption. Many of the first film cooling experiments did not use cooler secondary flow at all and ran tests to measure adiabatic effectiveness at $DR \leq 1.0$. Eckert describes superposition in [5, 6], which starts off with the assumption that property differences between the coolant and mainstream are negligible. In this case, the energy equation is linear and two temperature profiles can be superimposed. Film cooling, which in reality has a conducting wall with coolant cooler than the mainstream, is broken down into two problems. Problem A separates the effect of the conducting wall heat transfer from the film cooling, and includes the conducting wall boundary condition with uncooled jets operating at $DR = 1.0$. This provides the heat transfer coefficient h_f and the isoenergetic surface temperature T_{iw}, assuming q'' is known, which is shown in Equation 0-12.

$$q'' = h_f (T_{iw} - T_\infty)$$

Equation 0-12

Problem B isolates the effect of film cooling by operating the jets at $DR > 1.0$ while using an adiabatic wall boundary condition (this provides T_{aw}). If, in the actual film cooling case which combines the conducting wall with film cooling, we define the surface temperature to be T_w, the superposition of T_{aw}-T_∞ and T_{iw}-T_∞ should equal T_w-T_∞, which is shown in Equation 0-13.

$$(T_w - T_\infty) = (T_{aw} - T_\infty) + (T_{iw} - T_\infty)$$

Equation 0-13

Figure 0-5 depicts the superposition of temperatures profiles in the scenario where the wall is heated, which is what was used for the heat transfer coefficient measurements in this dissertation. The purple temperature profile, shown as case C, is the full film cooling scenario which includes the effect of the conducting wall and the coolant that is colder than the mainstream. Case A, shown in red, isolates the effect of a conducting wall while operating with jets at $DR = 1.0$. The blue temperature profile, case C, isolates the effect of the coolant by using an adiabatic testing surface and coolant at $DR > 1.0$. Using superposition, adding the temperature profiles in case A and case B should equal case C: A + B = C.

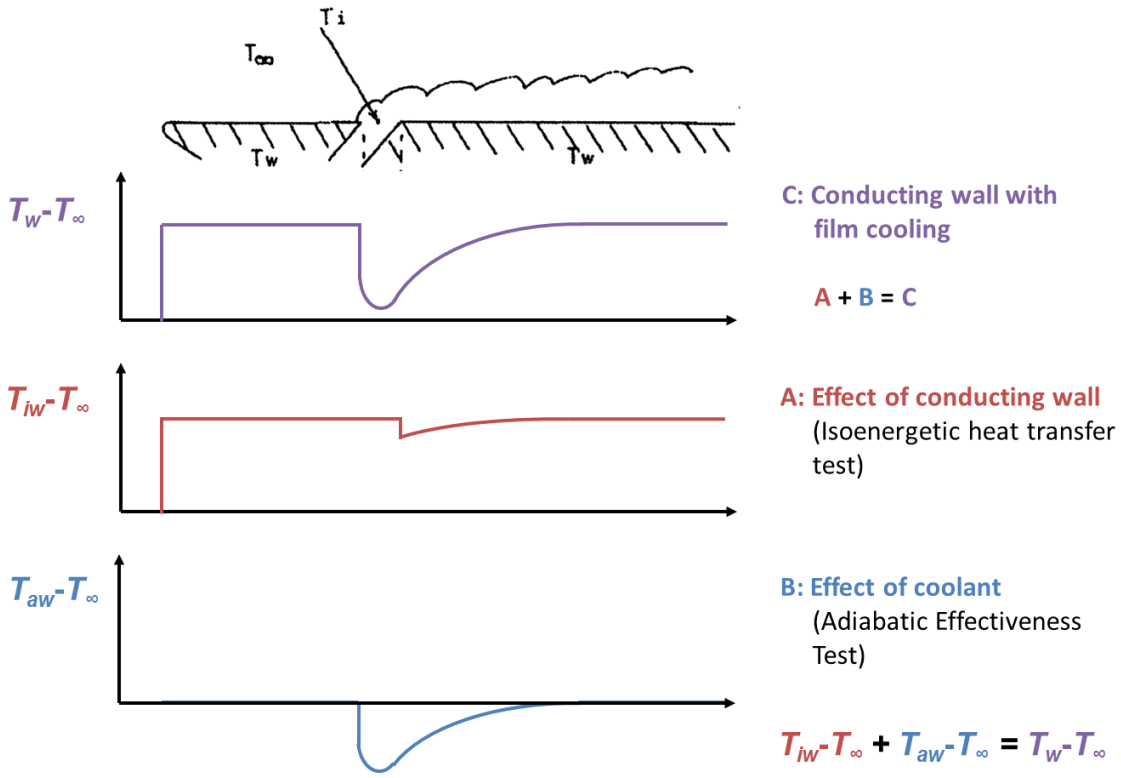

Figure 0-5 Illustration of superposition approach to film cooling. Modified from [7].

If superposition is valid, the heat transfer coefficient augmentation is the same in the actual film cooling scenario in case C as it is in case A. Equation 0-13 can be arranged to show $T_w - T_{aw} = T_{iw} - T_\infty$. For heat transfer coefficient augmentation measurements at DR = 1.0 (case A), h_f is measured from the difference between T_{iw} and T_∞. At DR > 1.0 (case C), h_f is measured from the difference between T_w and T_{aw}. Using superposition, the heat transfer coefficient measured at DR = 1.0 is equal to the heat transfer coefficient in the actual film cooling case, where DR > 1.0. If this is assumed to be true, then the heat transfer into the blade can be calculated using Equation 0-14.

$$q'' = h_f (T_w - T_{aw})$$

Equation 0-14

This analysis assumes that h_f is the same whether the density ratio of the coolant is 1.0 or much greater than 1.0. Perhaps this is part of the reason why researchers focused on measuring heat transfer coefficient augmentation at unit density ratio for so long. When they did this, most researchers found that the heat transfer coefficient augmentation on a flat plate was small and farther downstream was negligible. As a result, the majority of film cooling studies have focused on measuring adiabatic effectiveness, case B, rather than the heat transfer coefficient, case A.

1.1.2 METHODS FOR MEASURING HEAT TRANSFER COEFFICIENT AUGMENTATION

To accurately measure the heat transfer coefficients that would apply to an actual turbine part, the thermal boundary layer needs to be matched, which is not achieved by any of the current methods for measuring heat transfer coefficient augmentation. Many researchers assume that the thermal boundary layer on an actual turbine component can be approximated by an isothermal boundary condition. Yet, other researchers use a constant heat flux surface to measure heat transfer coefficients. In reality, neither boundary condition will truly give the correct thermal boundary layer condition, but it can be assumed that the thermal boundary layer thickness is thin relative to the size of the cooling jets due the high Reynolds number of the mainstream flow. Also, the thermal boundary layer in the vast majority of heat transfer coefficient studies starts downstream of the cooling jets. On an actual turbine component, the thermal boundary layer would start upstream of the holes, be slightly thicker, and would interact with the jets as soon as they exited from the coolant holes. The most common methods for measuring heat transfer coefficient augmentation are discussed below.

Direct Measurements of the Wall Temperature and Adiabatic Wall Temperature

This is the method that was used for the measurements in this dissertation. Many researchers have used this method to measure heat transfer coefficient augmentation at unit density ratio, but no one has used this technique to measure heat transfer coefficient augmentation at density ratios above one. This method directly measures heat transfer coefficients by measuring the heat flux, adiabatic wall temperature, and wall temperature that define the heat transfer coefficient with film cooling, which is shown in Equation 0-7. A heat flux plate, usually made from a thin, resistance foil heater, supplies a constant heat flux. The foil is usually placed downstream of the holes, so the thermal boundary layer is very thin. The heat flux can be calculated by multiplying the voltage drop across the plate by the current.

When measuring the heat transfer coefficient augmentation at unit density ratio, where the coolant jets are the same temperature of the mainstream, the wall temperature is measured by turning the heat flux plate on and measuring the surface temperature, at a given blowing ratio, at steady state. An infrared camera or surface thermocouples can be used to measure the surface temperature. At this density ratio, the driving temperature for heat transfer is the mainstream temperature, which is shown in Equation 0-12.

When measuring the heat transfer coefficient augmentation at density ratios other than one, there are two experiments required. The first is to measure the adiabatic wall temperature at the targeted blowing ratios and density ratios with the heat flux plate turned off. The second experiment is a repeat of the first experiment, except the heat flux plate is turned on, which provides T_w. The heat transfer coefficient with film cooling can be calculated using the heat flux, adiabatic wall temperature, and the wall temperature. A more detailed description of the experimental setup and procedure is provided in Section 1.6.2.

The advantage to using this method are that the heat transfer coefficients are measured using direct temperature measurements, and this technique does not rely on extrapolations or other assumptions to calculate the heat transfer coefficients. With

measurements at high density ratio, another advantage of using this technique is that it uses a realistic thermal field. The methods that use CO_2 to create a density ratio do not simulate the thermal fields of jets, which is discussed in more detail in the description of the heat/mass transfer analogy technique. The disadvantage of the direct temperature measurement technique is that the measurements at high density ratio can be difficult to make accurately due to higher uncertainty.

Linear Superposition

An overview of the linear superposition technique was written by Gritsch, et al. [8]. With this method, the heat flux is defined as Equation 0-15.

$$q'' = h_f (T_{aw} - T_w) = h(T_\infty - T_w)$$

Equation 0-15

which reduces to $h(\theta) = h_f (1 - \eta\theta)$

Equation 0-16

where $$\theta = \frac{T_\infty - T_c}{T_\infty - T_w}$$

Equation 0-17

In these equations, θ is the inverse of the nondimensional wall temperature and h is the classic heat transfer coefficient where T_∞ is used as the driving temperature for heat transfer. Equation 0-16 shows that h varies linearly with θ (this is valid if the energy equation is linear, with constant properties). With this method, an isothermal, conducting plate is placed downstream of the holes. The wall temperature can be controlled, such as by a water channel underneath the flat plate, which is what was used at Karlsruhe

Institute of Technology. The heat transfer coefficient, h, is found using measurements of T_∞, T_w, and q'', which is calculated using a finite element analysis of the isothermal, conducting plate. h is measured with the plate at multiple wall temperature values and a linear line of h versus θ is created. When this line is extrapolated to $\theta = 0$, h should equal h_f by Equation 0-16. This technique seems valid in theory, but some of the results have been questionable, showing extremely large increases in laterally averaged h_f/h_0. As an example, Saumweber and Schulz [9] presented laterally averaged h_f/h_0 results in excess of 2.5 for shaped holes spaced 6 hole diameters apart, which is shown in Figure 0-6.

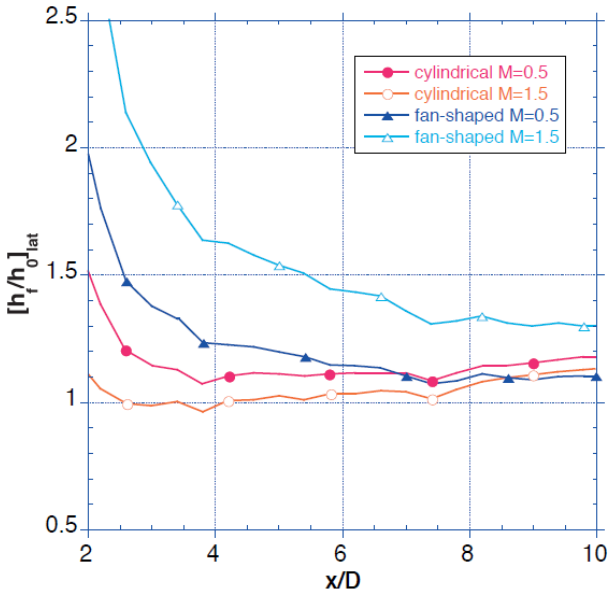

Figure 0-6 Plot of laterally averaged h_f/h_0 for shaped holes [9].

The test conditions in this paper were very similar to those in our facility, and we have never observed heat transfer coefficient augmentation values on this order by directly measuring T_{aw} and T_w.

Heat/Mass Transfer Analogy

The heat/mass transfer analogy is also used for measuring h_f, and it uses similar theory as the superposition technique just described. This method is typically performed at unit density ratio, but Ammari et al. [10] used it at a density ratio of 1.52 where the density ratio was created by using air in the mainstream and CO_2 as the coolant. With this technique, a swollen polymer surface is filled with a uniform concentration (often naphthalene), which simulates a constant temperature boundary condition, T_w = C. The polymer is coated on a non-subliminating surface, which is equivalent to an adiabatic surface [11]. The coolant and the mainstream lack naphthalene, which is analogous to operating at $T_c = T_\infty = 0$. From Equation 0-16, $\theta = 0$ and the mass transfer analogy that provides h will be equal to h_f, provided that the turbulent Prandtl number is equal to the turbulent Schmidt number for the analogy to hold. In a test, the gas jets subliminate the naphthalene and the rate of change of the naphthalene coating thickness is measured, which is proportional to the local mass/heat transfer coefficient. Laser interferometry can be used to produce a hologram of the surface that shows contours of the depth change [10], which is on the order of μm [11]. A depth gauge is typically used to measure the naphthalene thickness [11].

The advantages of this method is that there are no radiation or conduction losses, but sublimation occurs when not testing (like natural convection), so coating, testing, and measuring depths must be done quickly to minimize sublimation error. Other errors result from not knowing the properties of naphthalene accurately, which vary strongly with temperature [11]. In addition, even though CO_2 can be used to simulate higher density ratios, it does not match the analogous thermal field above the wall at that density ratio. Figure 0-7 shows an example, where the thermal field profile is shown in blue and the analogous concentration profile is shown in green. Since there is no naphthalene in the mainstream, the concentration is zero until the concentration boundary layer is reached. This causes the concentration boundary layer to differ from the thermal boundary layer, which is shown in the figure. The concentration boundary layer would be

more similar to the thermal boundary layer during an isoenergetic heat transfer coefficient experiment where the temperature of the mainstream and coolant jets are the same.

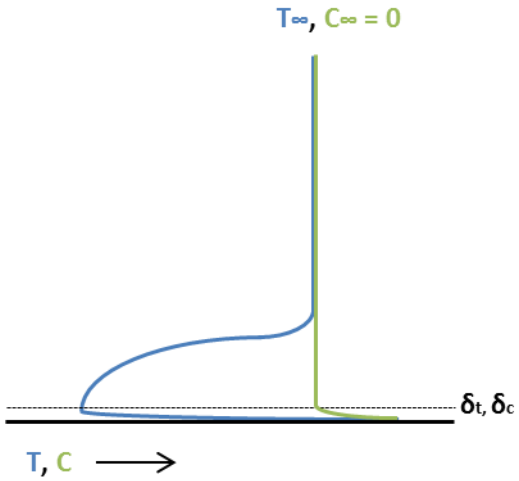

Figure 0-7 Comparison between a thermal boundary layer, and a concentration boundary layer using the mass transfer analogy.

Transient Liquid Crystal Technique

Another technique for measuring h_f is the transient liquid crystal thermography technique, although this technique can be done with any form of surface temperature measurement, not solely liquid crystals. A detailed description of the use of liquid crystals is included in a paper by Ekkad and Han [12]. With this technique, the test surface is coated with thermochromic liquid crystals. The liquid crystals turn red, green, and blue at certain temperature thresholds. At the beginning of the test, the surface is at uniform room temperature T_i and the liquid crystals are clear. When the test starts, hot mainstream air blows over the test surface and the coolant is ejected at temperature T_i. As the surface reaches certain temperature thresholds, the liquid crystals change color, and

the color changes are captured by a high resolution RGB camera. By tracking the temperature change with time and location on the test surface, a local heat transfer coefficient can be calculated by assuming a 1-D transient conduction into a semi-infinite solid. The equations for this are Equation 0-18 and Equation 0-19.

$$k\frac{\partial^2 T}{\partial x^2} = \rho C_p \frac{\partial T}{\partial t}$$

Equation 0-18

Boundary Conditions: at $t = 0$, $T = T_i$

at $x = 0$, $-k\frac{\partial T}{\partial x} = h_f (T_w - T_{aw})$

at $x \to \infty$ $T = T_i$

Equation 0-19 is the solution to Equation 0-18.

$$\frac{T_w - T_i}{T_{aw} - T_i} = 1 - \exp\left(\frac{h_f{}^2 \alpha t}{k^2}\right) erfc\left(\frac{h_f \sqrt{\alpha t}}{k}\right)$$

Equation 0-19

To make the semi-infinite solid assumption, the test plate must be made of a thick, low thermal diffusivity material. In the above equations, T_w is the temperature at which the liquid crystals change color, and t is the time at which the color change occurs. In Equation 0-19, there are two unknowns: T_{aw} and h_f. The solution to these variables can happen two ways. With the first method, the transient liquid crystals would need to change colors twice (e.g. from clear to red to green) in an experiment so that there would be at least two sets of values for Equation 0-18 at two different instances in time. With at

least 2 equations, T_{aw} and h_f can be solved for. With the second method, only one color change is measured per experiment, which creates the need for a second experiment so that there will be 2 equations for 2 unknowns. For the second experiment, a variable needs to be changed so that the first equation will not be reproduced. The variable that is often changed is heating the coolant instead of the coolant remaining at T_i as with the first experiment [12]. Doing this adds a complexity. The coolant pipes start at room temperature, T_i, and since this is a transient test, the coolant gradually warms up with time and cannot perform a step change. To be able to solve Equation 0-18 with this additional variable, the Duhamel Theorem is used to turn Equation 0-18 into a power series. The equations are solved numerically for each pixel on the testing surface. The advantage of this method is that the tests are quick (10-80 s), and the disadvantages are the low resolution of temperature measurements and the assumption that this is 1-D heat transfer. Since the coolant jets that lay on the surface create a non-uniform temperature boundary condition, the conduction into the wall will not be 1-D, as shown in the second boundary condition, it will be 3-D. Additional error comes from timing the changes in a transient test accurately.

1.1.3 Coordinate System and Presentation of Experimental Results

The coordinate system used in this dissertation defines the x direction in the streamwise direction, y in the vertical direction normal to the flat plate, and z in the lateral direction, which is depicted in Figure 0-8. The blue shaded region is the infrared imaging area used to process the data. It extends farther downstream than what is shown in the figure. Notice that $x = 0$ is defined at the downstream edge of the hole breakout.

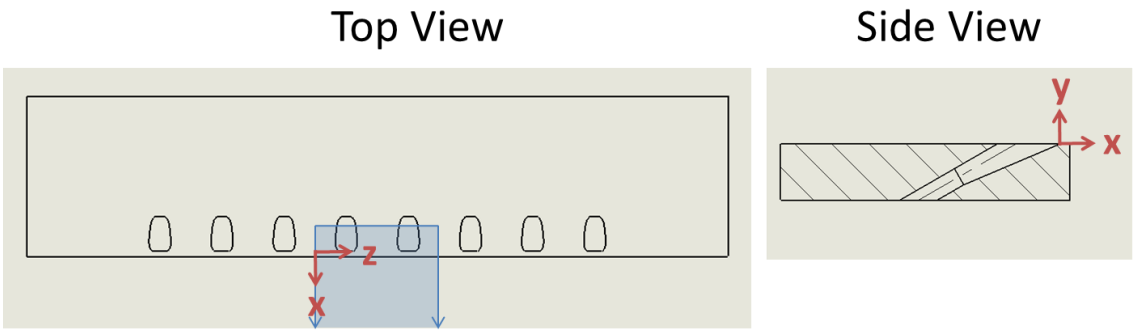

Figure 0-8 Coordinate system definition.

Results from experiments in this dissertation are presented three ways: contours, laterally averaged plots, and lateral plots. Contours are 2-D maps of the surface value being measured, such as adiabatic effectiveness or heat transfer coefficient augmentation. Figure 1-9 shows contours of adiabatic effectiveness downstream of cylindrical holes on a flat plate at a) M = 0.7 and DR = 1.5 and b) M = 1.2 and DR = 1.5. The areas where there is no data, from about x/d = 10 to 14, is where the data was obstructed from the joint of two salt crystal IR windows.

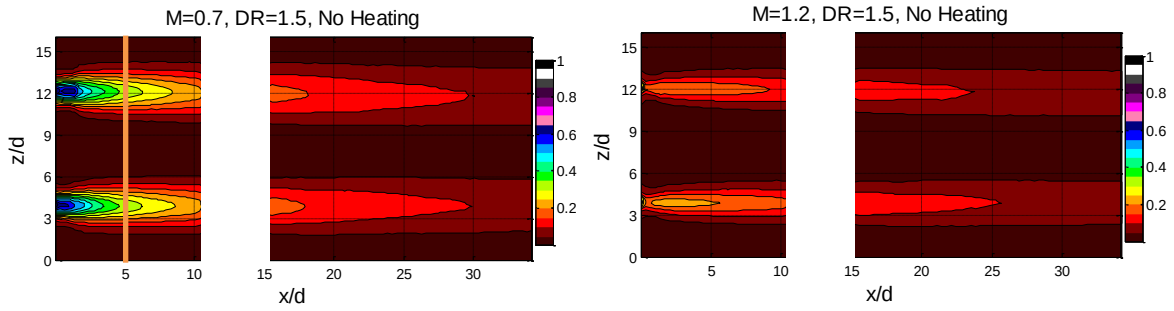

Figure 0-9 Contour plots of adiabatic effectiveness downstream of cylindrical holes at a) M = 0.7 and DR = 1.5 and b) M = 1.2 and DR = 1.5.

It is clear from comparing Figure 1-9 a) and Figure 1-9 b) that the adiabatic effectiveness of the jets decreases from $M = 0.7$ to $M = 1.2$, even though there is more coolant mass exiting the coolant holes for $M = 1.2$. This is because the film cooling jets are attached to the surface at $M = 0.7$, but are detached at $M = 1.2$. The normal momentum of the jets causes them to separate at high blowing ratios, and often the momentum flux ratio is better than blowing ratio for predicting jet separation [13].

Laterally averaged data are found by averaging local values at each x/d position, and an overbar is added to the variable to indicate that it is laterally averaged. For example, $\bar{\eta}$ at $x/d = 5$, which is shown by the orange line in Figure 1-9 a), would be equal to the average of the η values from $z/d = 0$ to 16 at $x/d = 5$. Laterally averaged values need to be averaged over a whole number of pitches, which is the spacing between holes. In Figure 1-9 a) the pitch is $8d$, so the averaging would need to be carried out for z/d values in multiples of 8 (in the case of Figure 1-9 a), there are two hole pitches that were used for averaging). Laterally averaged values are then plotted versus x/d, which is shown in Figure 0-10. Because the jets are separated at $M = 1.2$, $\bar{\eta}$ is lower than $\bar{\eta}$ at $M = 0.7$ where the jets are attached.

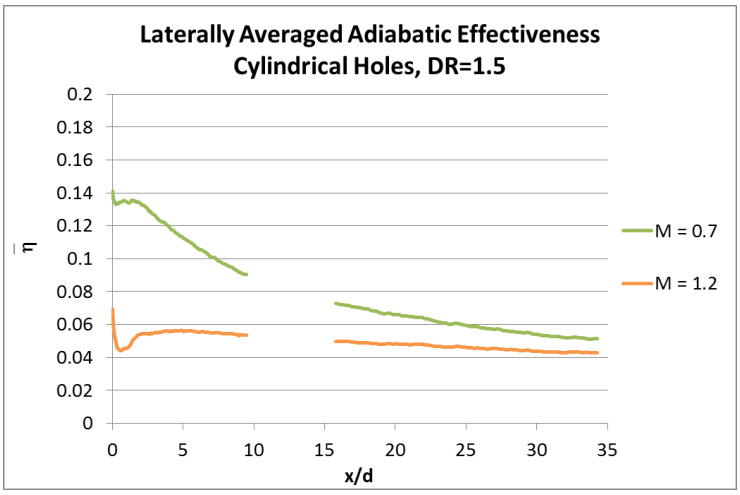

Figure 0-10 Plot of laterally averaged adiabatic effectiveness.

The hole pitch can have a large effect on laterally averaged results because if the holes are at a larger pitch, much of the effectiveness being averaged over is 0 between the jets. If the holes were spaced closer together, 3*d* for example, the laterally averaged effectiveness would be higher because there would be less space between the holes that would be averaged over.

Finally, the last form of presenting data is with lateral distributions. With these plots, a particular *x*/*d* position is chosen, and the adiabatic effectiveness, temperature, or heat transfer coefficient augmentation is plotted at this position versus *z*/*d*. An example is given below.

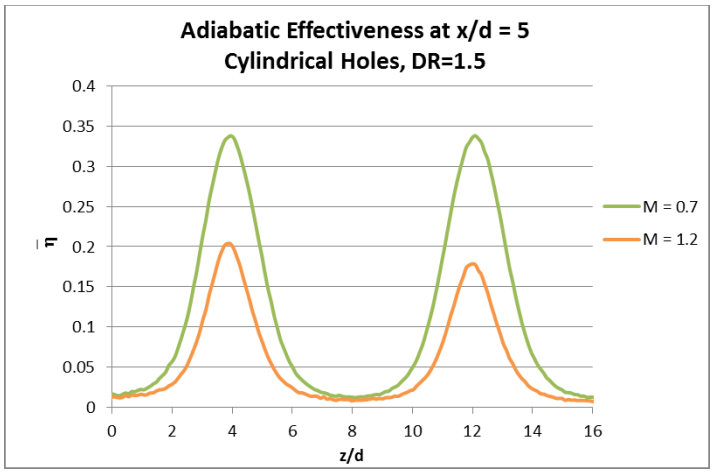

Figure 0-11 Plot of lateral effectiveness distribution at *x*/*d* = 5.

1.1.4 Definition of Hole Geometries

Coolant holes are positioned using two angles called the surface angle and the compound angle. Figure 1-12 is a schematic that shows these angles. The figure depicting the surface angle is shown with no compound angle.

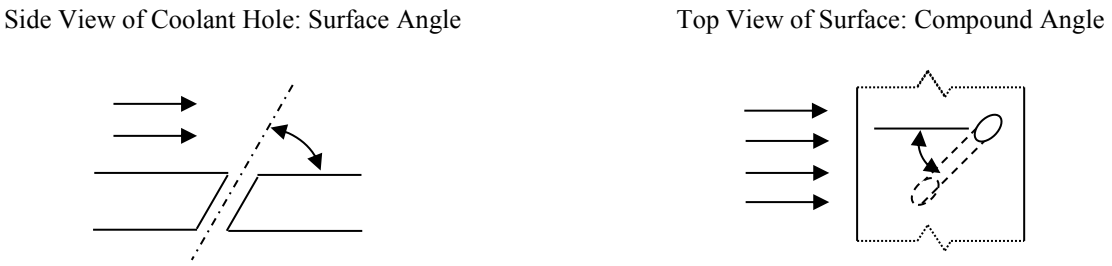

Figure 0-12 Schematic showing the definition of the surface angle, α, and the compound angle, γ.

The surface angle, α, is the angle that the hole makes with the mainstream from a side view of the hole. The compound angle, γ, is the angle the hole makes with the mainstream from the top view of the hole. For all of the geometries in this study, the compound angle was zero.

Shaped hole geometries are typically characterized by three angles, which are shown in Figure 0-13.

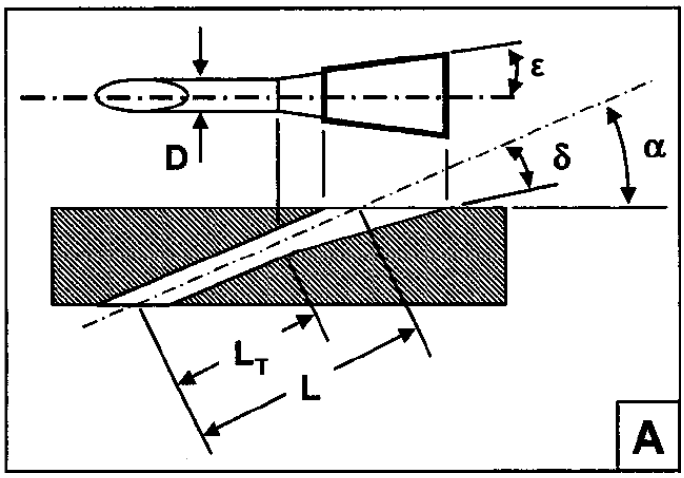

Figure 0-13 Diagram of shaped hole angles. Adapted from [14].

α is called the surface angle, which is the angle the hole makes with the surface in line with the mainstream flow. β is the lateral diffusion angle, which determines how wide the coolant spreads as it exits the holes. ε is the laidback expansion angle, which guides the coolant farther downstream and closer to the surface. Also shown in Figure 0-13 is the definition of the hole length. In a shaped hole, the metering hole is the cylindrical base indicated by L_T in the figure. L_T is the length of the metering hole, while L is the length of the entire hole. The length of the hole is often normalized by the metering hole diameter.

Figure 0-14 depicts the definition of the area ratio, AR, for a shaped hole, which is the ratio of the area at the exit of a film cooling hole (A_{exit}) if viewed from the surface angle divided by the metering area of the metering hole ($A_{entrance}$).

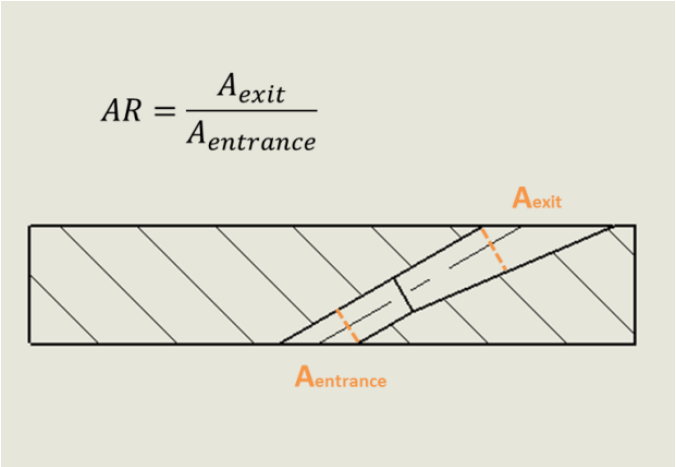

Figure 0-14 Definition of the area ratio (AR) for a shaped hole.

The goal in designing a high-performing shaped hole is to increase the expansion angles as much as possible without incurring separation inside the diffuser. When the expansion angles are too large, the flow separation causes a decrease in film cooling performance. This separation can be seen in results from Saumweber, Schulz, & Wittig [15], which are shown in Figure 1-15. The results show adiabatic effectiveness values for

shaped holes installed on a flat plate with a 14° lateral expansion and a 15° laidback expansion.

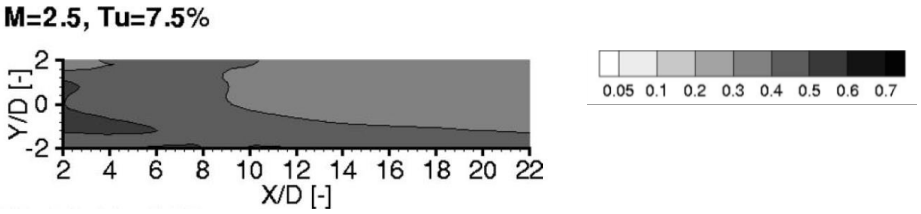

Figure 0-15 Adiabatic effectiveness downstream of shaped film cooling hole [14].

In this figure, the shaped hole is centered at y/d=0. One can see that the coolant has split into two jets and is biased to one side of the shaped hole. The performance can increase when the coolant splits like this, since the coolant spreads farther laterally, but the separation causes the shaped hole performance to become more unstable.

1.1.5 Flow Structure Inside a Shaped Hole

To understand film cooling performance of shaped holes, it's important to understand how they operate. As coolant travels through the hole, a boundary layer forms along the walls of the hole. Once the coolant exits the hole, the boundary layer curls and sheds vortical structures, which are then turned by the mainstream and form kidney vortices, or counter-rotating vortices, that are seen downstream [16]. These kidney vortices are shown in Figure 0-16. The kidney vortices are detrimental to film cooling performance because they entrain mainstream air into the jet and cause the jet to lift off the surface.

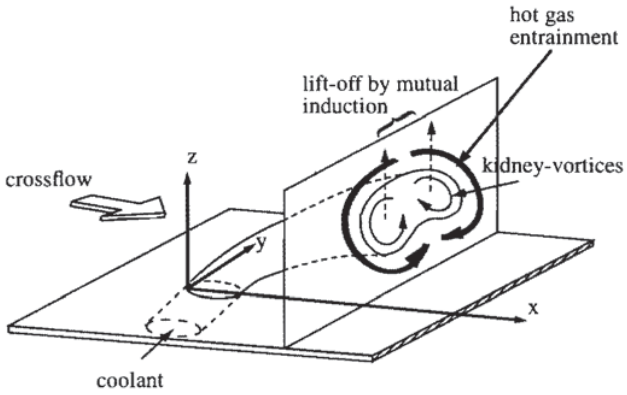

Figure 0-16 Kidney vortices (or counter-rotating vortices) generated by coolant exiting a film cooling hole [16].

Haven et al. [16] used Particle Image Velocimetry to show that there are two ways shaped holes can control the kidney vortices. Firstly, using a laterally expanded shaped hole increases the distance between the kidney vortices, which weakens them. Secondly, a second pair of vortices form, which the authors term "upper deck" vortices. Depending on the hole shape, the upper deck vortices can be kidney or anti-kidney vortices. If the anti-kidney upper deck vortices form, they can cancel out the lower deck vortices, which improves the film cooling performance. This study looked at a cylindrical hole, conical hole, fan-shaped hole, and laidback fan-shaped hole, all with the same *AR*. They found that the fan-shaped hole was best at canceling out the kidney vortices and also had better adiabatic effectiveness performance.

Within the hole, there are other important flow mechanisms taking place. Figure 0-17 shows velocity fields from within a fan-shaped hole that were generated using CFD. As coolant enters the metering hole from the bottom, a separation region forms on the downstream side of the hole, which is depicted on the bottom left figure as a bubble. This causes the coolant velocity to increase in the upstream part of the hole, which is known as the "jetting effect". In addition, if the shaped hole is over-expanded in the lateral

direction, a separation bubble will form in the diffuser, which is depicted in the bottom right of the figure. This is what causes the coolant jet to split in the diffuser.

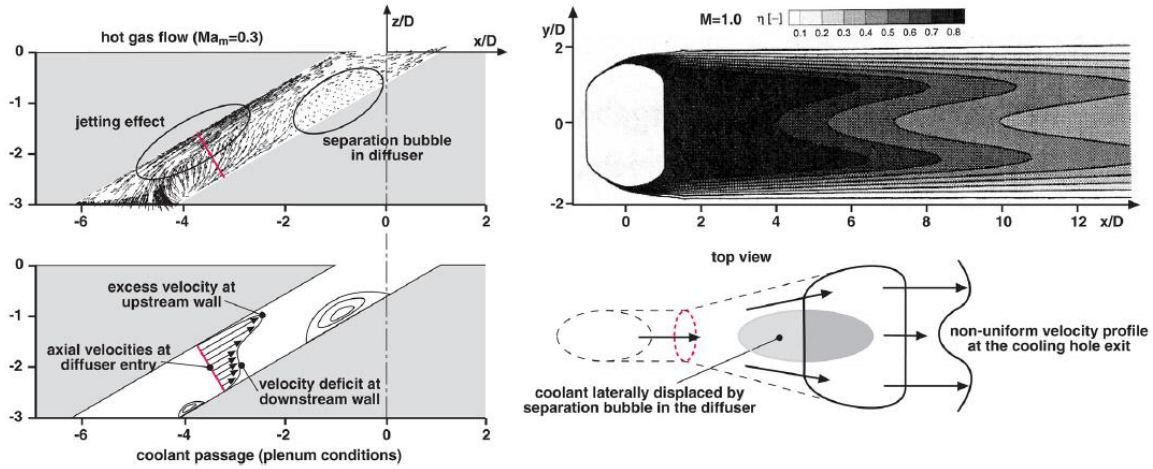

Figure 0-17 Computed velocity field inside a 14° laterally diffused shaped hole at M = 1.0, DR = 1.75, Ma_∞ = 0.3, Ma_c = 0, Tu = 2% [9].

1.2 Dissertation Objectives

This dissertation has two main objectives:

1. Quantify the Performance of a Newly-Defined Standard Shaped Hole

Shaped holes provide significant improvement in film cooling performance over cylindrical holes. Numerous researchers have studied shaped holes, but there is a catch. Research is often funded by industry, and the industry partner stipulates what data may be published in open literature. Industry prefers to keep publishable shaped hole geometries quite different from proprietary geometries, so much of the studies in literature use unrealistic, poor-performing shaped hole geometries. Researchers at NASA

have expressed a need for open literature data from a realistic shaped hole geometry to validate CFD predictions. Our lab collaborated with Dr. Karen Thole's lab at Pennsylvania State University (PSU) to test a more realistic hole geometry, which was defined by Robert Schroeder at PSU. The shaped hole has a 7° lateral expansion, 7° laidback expansion, and 30° surface angle (see Section 1.4.4 for more details). The goal of the project was to have both labs test the same hole geometry on similar flat plate facilities to validate the data being produced. This data was intended to serve as a standard for comparison for future CFD and experimental film cooling performance studies. However, this seemingly simple project evolved into a year-long investigation of the performance of shaped holes before the validation of the results could be made. This dissertation uses experimental data to analyze how adiabatic effectiveness performance from the aforementioned shaped hole is affected by machining, substrate material, and coolant entrance effects.

2. Measure the Heat Transfer Coefficient Augmentation at Density Ratios Above 1.0

To calculate the heat transfer entering a turbine vane or blade, the heat transfer coefficient augmentation, h_f/h_0 is needed. Most researchers measure h_f at unit density ratio (the coolant temperature is equal to the mainstream temperature) because it's easier to measure than at high density ratio and because it is generally presumed that the density ratio has little effect on h_f, even though gas turbines operate at density ratios close to 2. Presuming that h_f is independent of density ratio is an important step, and needs to be well understood.

Even though other researchers have studied heat transfer coefficient augmentation at $DR > 1.0$, the results are inconsistent. In addition, those researchers did not use direct measurements of T_w and T_{aw} to measure the heat transfer coefficient augmentation, and instead relied on other methods, which were described in Section 1.1.2, that required extrapolations and analogies that don't fully simulate the correct flow physics. This

dissertation presents heat transfer coefficient augmentation results downstream of shaped holes at DR = 1.0, 1.2, and 1.5 using direct temperature measurements. To the author's knowledge, this is the only study to do so. In addition, the thermal field was measured to give additional insight into film cooling performance.

1.3 Literature Review

1.3.1 Shaped Hole Geometry and Performance

Shaped holes produce higher adiabatic effectiveness than cylindrical holes [17, 18, 9, 19] by reducing the velocity and momentum of the coolant as it exits the hole, which allows the jets to stay attached to the surface at higher blowing ratios. Depending on the shaped hole geometry, other mechanisms also contribute to increased adiabatic effectiveness, which will be discussed subsequently. Even though shaped holes significantly increase adiabatic effectiveness, they also have detrimental effects such as increasing aerodynamic mixing losses [20, 21], increasing the heat transfer coefficient [9, 18, 22, 23, 24, 25, 26], and increased sensitivity to coolant entrance/cross-flow effects [18, 27] as compared to cylindrical holes. However, the increase in adiabatic effectiveness tends to out-weigh these deterrents, and several researchers have used the net heat flux reduction parameter to determine that this is the case [20, 17, 28].

Shaped hole adiabatic effectiveness performance depends largely on the shaped hole geometry, but it is common to see researchers report that adiabatic effectiveness on a flat plate continuously increases above M = 2.5 [18, 29, 30, 15, 9]. In comparison, jets downstream of cylindrical holes start to separate at $M \geq$ 0.5-0.7 [18, 9]. Shaped hole geometries can be complex, and their design parameters will be discussed in the following sections.

1.3.1.1 Lateral Expansion Angle

The lateral expansion angle increases adiabatic effectiveness by spreading the jet laterally and reducing its momentum normal to the surface. This improves coolant surface coverage, increases the distance between the counter rotating vortices, and weakens the counter-rotating vortex pair (CRVP), which reduces the jets' ability to lift off the surface [31]. These positive effects increase as the lateral expansion angle is increased. However, once the expansion angle becomes large, somewhere around 10-14° and above, a separation bubble forms in the center of shaped hole expansion and the coolant splits into two jets [18, 9], one on each side of the lateral expansion. On a simple flat plate, this can increase adiabatic effectiveness [18, 9] because the coolant is spread farther laterally on the surface. But, employing an over-expanded shaped hole in practice could be detrimental because the separation within the diffuser makes the shaped hole more unstable and sensitive to flow conditions [9]. Therefore, a shaped hole geometry that maximizes the lateral expansion angle without separation within the hole would be the most optimal, robust design.

Saumweber and Schulz [18] studied the effect of the expansion angle of a diffuser by comparing laterally averaged adiabatic effectiveness from three fan-shaped holes with lateral expansion angles of 6°, 10°, and 14° on a flat plate. All of the holes had $L/d = 6$ and $\alpha = 30°$. Their results showed that the effectiveness increased with increasing lateral expansion angle, up to $M = 2.5$ at $DR = 1.75$, which was the highest blowing ratio they tested. At $M = 0.5$, the laterally averaged adiabatic effectiveness between the three holes was very similar. However, at $M = 2.5$, there was a wide spread in performance between the hole geometries, with the hole with 14° lateral expansion performing best, and the 6° hole performing the worst. Jet splitting was present for blowing ratios of $M = 0.5$ and 2.5 for the 14° hole, at $M = 2.5$ for the 10° hole, and was not seen at $M = 0.5$ or 2.5 for the 6° hole.

1.3.1.2 Forward Expansion Angle

Like the lateral expansion angle, the forward expansion angle increases the exit area of the hole, which decreases the velocity and momentum of the coolant, and helps the jets stay attached to the surface at higher flow rates. The forward expansion angle also changes the angle of the jet relative to the surface at its exit, laying the jet more parallel to wall and reducing its velocity component normal to the wall, which also helps prevent jet separation. However, Thole et al. [32] showed that if the forward expansion angle is too large, the jet will bias toward the forward expansion and allow mainstream ingestion into the upstream side of the hole.

The closest study to systematically varying the forward expansion angle was completed by Gritsch et al. [29]. They looked at the effect varying the area ratio of a laidback fan-shaped hole while keeping the hole breakout width constant, which in effect, is the same as varying the forward expansion angle. The researchers varied the area ratio between 3.5 and 4.2 with corresponding forward expansion angles of 4° and 8°, respectively, while the lateral expansion angle remained constant at 4°. At M = 0.5, 1.0, 1.5, 2.0, and 2.5, DR = 1.7, there was no effect of varying the forward expansion angle on laterally averaged adiabatic effectiveness. This could be because the jets had not started to detach by M = 2.5, and if higher blowing ratios, where jet detachment started to occur were tested, there would be an effect of increasing the forward expansion angle.

Thole et al. [32] measured the flow field downstream of a cylindrical hole, a 14° laterally diffused fan-shaped hole, and a 14° laterally diffused and 15° forward diffused shaped hole at DR = 1.0 and M = 1.0. They found that the shaped hole with the forward diffusion was most effective at reducing the velocity gradients and the jet penetration normal to the wall. However, the shaped holes had higher turbulence levels exiting the holes because the expansion angles of the hole were so large and there was separation within the diffuser. Another disadvantage of the forward and laterally diffused hole was that the coolant biased toward the downstream portion of the hole, which allowed

ingestion of the mainstream into the upstream portion of the hole. The authors suggested that the holes could be improved by reducing the expansion angles at the expense of lateral coolant coverage.

1.3.1.3 Laterally Diffused Shaped Holes versus Forward Diffused Holes

A few studies have compared purely laterally diffused shaped holes (fan-shaped holes) with purely forward diffused shaped holes [17, 18] and all found that the laterally diffused holes produced higher adiabatic effectiveness and stayed attached to the surface at higher blowing ratios than the forward diffused holes. According to Saumweber and Schulz [18], the forward diffused holes maintain more of a velocity component normal to the wall, which leads the jets to separate from the surface at lower blowing ratios. In contrast, the laterally diffused shaped holes spread the coolant more in the lateral direction, reducing the penetration of the jet normal to the wall. Another explanation is that diffusing the jet in the lateral direction widens the distance between the counter-rotating vortex pair, which makes them weaker, and helps the jet stay attached to the surface at higher blowing ratios. This is an advantage that purely forward diffused shaped holes do not have.

1.3.1.4 Combined Lateral and Forward Diffused Holes

An ideal shaped hole geometry will include both lateral diffusion and forward diffusion, because both expansion angles add to film cooling performance in different ways, which were discussed in Sections 1.3.1.1 and 1.3.1.2. But, over-expanding can lead to different types of jet separation within the hole expansion, which can make the film cooling performance unstable. The most effective combination of forward and lateral expansion angles is not clear because film cooling performance depends on other geometric parameters, such as the length of the metering hole and the length of the

diffuser, and there are simply too many shaped hole geometry combinations to test all of them. There have been some CFD studies that have attempted to optimize a shaped hole geometry, such as the one by Lee and Kim [33], but the optimized shaped hole geometry is often unrealistic since CFD is not yet at the point where it can accurately predict film cooling performance with shaped holes.

1.3.1.5 Surface Angle

For both cylindrical and shaped holes, a shallower surface angle reduces the velocity component normal to the wall, which helps the jets stay attached to the surface. Heneka [34] showed that as the surface angle decreases, and the hole become more parallel with the mainstream, the film cooling performance increases. However, shallower surface angles are more difficult to machine and require longer hole lengths, which increases the pressure losses across the coolant holes [30]. Aside from the leading edge, typical surface angles range from 30°-35° in turbine components.

Saumweber and Schulz [18] varied the surface angle of cylindrical holes and 14° laterally expanded fan-shaped holes. Three surface angles of 30°, 45°, and 60° were tested at DR = 1.75 on a flat plate. At the low blowing ratio of 0.5, both hole geometries showed that there was no effect of the surface angle. At higher blowing ratios, where there was some degree of jet separation occurring for the cylindrical holes, but not the shaped holes, the two hole geometries showed opposite trends. For the cylindrical holes at M = 2.5, the α = 30° and 45° holes performed similarly, but $\bar{\eta}$ for the α = 60° holes performed about 50% better. This is because the jets were separated from the surface, and as the surface angle was increased to 60°, the jets interacted more with the mainstream, which spread the colder coolant closer to the wall and increased the effectiveness. For the shaped holes at M = 2.5, $\bar{\eta}$ increased with decreasing surface angle, with the difference in $\bar{\eta}$ being 20%, between the α = 30° and 60° cases.

1.3.1.6 Hole Length

The length of shaped holes is characterized by the ratio of the hole length to the metering (cylindrical) hole diameter. The total L/d includes the length of the metering section as well as the expansion, and the metering L_T/d includes only the length of the metering section. For cylindrical holes, Lutum and Johnson [35] found that adiabatic effectiveness remained constant for $L/d > 5$. As the metering L_T/d increases, the flow will become more fully-developed inside the hole before it exits, and the velocity profile will have a longer distance to recover from the "jetting effect" that is caused by the coolant separating at the hole entrance. This effect was described further in section 1.1.5.

Saumweber and Schulz [18] looked at the effect of L/d for a cylindrical hole and a fan-shaped hole with a 14° lateral expansion. For cylindrical holes, at $M = 0.5$, 1.0, and 1.5 and $DR = 1.75$, varying L/d from 6 to 10 produced almost no effect. For the shaped holes, the total L/d was also varied from 6 to 10, but only the metering L_T/d was changed (from $L_T/d = 2$ to 6) and the length of the shaped hole diffuser was held constant. There was also no effect of varying the metering L_T/d except at $M = 2.5$, where holes with total $L/d = 10$ performed 15% lower. Contours of adiabatic effectiveness showed that the shaped holes with the shorter metering length produced jets that split. When the metering L_T/d was increased, the splitting ceased and the jet was more uniform. The authors mentioned that as L_T/d is increased, the velocity distribution in the metering section of the hole becomes more uniform and the jetting effect is reduced. This prevents separation in the expansion of the hole, which prevents the jet from splitting, which also decreases the adiabatic effectiveness at $M = 2.5$ since the jet is not spreading as much laterally.

Gritsch et al. [29] looked at the effect of hole length (L/d) by keeping the cylindrical portion of a shaped hole constant at $L_T/d = 2$, but varying the diffuser length. The forward and lateral expansion angles of the hole diffusers were varied in order to maintain the same area ratio. The researchers found that there was no effect as the total L/d was varied between 7.5, 9.5, and 11.5. The lateral expansion angles were kept

roughly the same, 6-7°, for holes with three different diffuser lengths, but the forward expansion angle was changed from 11° for L/d = 7.5 to 4° for L/d = 9.5 to 2° for L/d = 11.5.

1.3.1.7 Relevant Studies to the 7°-7°-7° Shaped Hole Performance

Aside from the data produced at UT and PSU, to the author's knowledge, there are no other studies in literature that have tested shaped holes with a 7° forward expansion and a 7° lateral expansion. The studies that compare best were tested at the Karlsruhe Institute of Technology.

Saumweber and Schulz [18] measured the heat transfer coefficient augmentation downstream of fan-shaped holes that were laterally expanded by 6°, 10° and 14° with no forward expansion. The holes were spaced 6d. The hole shape was different from the 7°-7°-7°, but the testing conditions were very similar to what were used for this dissertation. The measurements were taken on a flat plate with plenum conditions at the coolant hole entrance. The mainstream Mach number was 0.3, and the turbulence intensity was 5.2%. The paper presents adiabatic effectiveness results at M = 0.5 and 2.5 at DR = 1.75. At M = 0.5, the performance for all three hole geometries was similar, being about $\bar{\eta}$ = 0.3 at x/d = 2 and dropping off to $\bar{\eta}$ = 0.13 at x/d = 12. At M = 2.5, there was a large difference in performance. At x/d = 2, the 14° fan-shaped hole reached $\bar{\eta}$ = 0.48, the 10° hole was at $\bar{\eta}$ = 0.36, and the 6° hole was $\bar{\eta}$ = 0.22. Clearly, the 6° hole had separated by M = 2.5, since its performance at this blowing ratio was lower than at M = 0.5, but it's difficult to ascertain the blowing ratio that produced the peak performance from any of the holes, since data from only two blowing ratios were presented.

Saumweber and Schulz published another paper that had the same testing conditions, but had a slightly higher turbulence intensity of 7.5%. This study used a 14° laterally expanded fan-shaped hole, which is the same geometry that was used in the

study discussed in the previous paragraph. Laterally averaged adiabatic effectiveness for $M = 0.5$ and 2.5 was also presented in this paper. Comparison between the results of this study and the aforementioned study show that at $Tu = 7.5\%$, the laterally averaged adiabatic effectiveness is about $\bar{\eta} = 0.04$ lower than at 5.2%.

Gritsch et. al. [29] presented laterally averaged adiabatic effectiveness results from a shaped hole with a 7° lateral expansion and an 11° forward expansion, which had an area ratio of 3.5 and 6d hole spacing. The external Mach number was 0.3, and the density ratio was 1.7. Results at $M = 0.5$, 1.5, and 2.5 were presented. At $M = 2.5$, the jets were still attached and performing well, with the laterally averaged adiabatic effectiveness being 0.55 at the hole exit and dropping down to $\bar{\eta} = 0.22$ by 30d downstream.

1.3.1.8 Scaling Adiabatic Effectiveness

It is highly desirable to know what flow parameter scales adiabatic effectiveness at multiple density ratios. Currently, most researchers use the blowing ratio to characterize the coolant flow rate, but this parameter usually does not scale adiabatic effectiveness results at multiple density ratios, and its use is an artifact from some of the first film cooling studies that found M scales results for 2-D slot geometries. The main flow rate parameters that are used to scale adiabatic effectiveness with density ratio are the blowing ratio, momentum flux ratio, and velocity ratio. Most of the scaling studies have found that the momentum flux ratio and velocity ratio are more likely to work as scaling parameters, although none of the studies have been able to firmly and consistently establish a scaling factor that works for multiple hole geometries. There are few studies that have looked at scaling adiabatic effectiveness at multiple density ratios with shaped holes. Most of the studies that have looked at scaling adiabatic effectiveness were completed with cylindrical holes, so those results will also be included here.

Goldstein et al. [36] looked at scaling of 10° fan-shaped holes oriented 35° from the mainstream. Two types of coolant were used to create the density ratios: slightly heated air ($DR \approx 1.0$), and Freon ($DR = 3.5$). The authors concluded that the centerline adiabatic effectiveness scaled with the momentum flux ratio at the hole exit, which was defined assuming a perfect expansion in the 10° fan-shaped hole.

Foster and Lampard [37] looked at scaling of centerline adiabatic effectiveness of a row of holes oriented normal to the mainstream on a flat plate. The density ratio was varied between 1.5 – 4.26, using the mass/heat transfer analogy and mixing varying amount of Freon with air to achieve the correct density ratio. Their results did not scale with M, I, or VR.

Pederson et al. [38] used the heat/mass transfer analogy to measure adiabatic effectiveness downstream of a row of cylindrical holes spaced 3d and at a surface angle of 35°. The density ratio ranged between 0.75 and 4.17 by mixing different concentrations of air, CO_2, and F-12 refrigerant. While the jets were attached, the momentum flux ratio scaled the results at some x/d positions, but the authors mentioned that the collapse of the data was not as pronounced farther downstream. When the jets were detached, the centerline adiabatic effectiveness scaled with velocity ratio at several positions downstream of the holes.

Forth et al. [1985] measured heat transfer coefficients and adiabatic effectiveness downstream of a single row of cylindrical holes with a surface angle of 30° using superposition. They tested at $DR = 0.81$, 1.22, 1.67, and 2.0 and $Ma_\infty = 0.55$. They found that when the jets were attached to the surface (weak injection regime) the laterally averaged adiabatic effectiveness at $x/d = 2$ scaled best with momentum flux ratio. When the jets started to detach from the surface (strong injection regime) the laterally averaged adiabatic effectiveness at $x/d = 2$ scaled with velocity ratio. Even though the momentum flux ratio and velocity ratio scaled the adiabatic effectiveness results well, the authors proposed a "weak injection" scaling parameter and a "strong injection" scaling

parameter, both of which were functions of the plenum pressure, plenum total pressure, and the mainstream pressure and total pressure. The authors did not mention whether I, VR, the weak injection parameter, or the strong injection parameter scaling held at distances farther downstream. However, the authors did show that the strong injection parameter scales effectiveness results at $x/d = 8$ for results from Foster and Lampard [37] and Pedersen et al. [38]. In a follow-up study, Forth et al. [39] confirmed their prior results, showing that at four density ratios, data at all downstream distances collapsed with momentum flux ratio while the jets were attached and the data collapsed when scaled with velocity ratio at all distances downstream when the jets were detached. Their paper also showed that this was true for a double row of cylindrical holes.

Sinha et al. [13] looked at scaling film cooling performance with blowing ratio, momentum flux ratio, and velocity ratio for a row of cylindrical holes at a surface angle of 35° and $p/d = 3$. The density ratio was varied between 1.2, 1.6, and 2.0. The results showed that the laterally averaged adiabatic effectiveness did not scale with any of the parameters, but the momentum flux ratio was able to predict the degree of jet separation immediately downstream of the hole as the density ratio was varied.

1.3.1.9 Mainstream Effects

Mainstream Mach Number

In the past, it was assumed that mainstream Mach number effects were negligible, as long as the flow was subsonic and the boundary layer was matched. But, the studies that showed that this was the case were completed using cylindrical holes [40, 27]. This assumption has only recently been studied with shaped holes. Saumweber and Schulz [9] looked at the effect of the mainstream Mach number on performance of cylindrical and 14° fan-shaped holes on a flat plate. As the mainstream Mach number was increased from 0.15 to 0.45, results from the cylindrical holes showed that the laterally averaged

adiabatic effectiveness decreased slightly, by $\bar{\eta}$ = 0.03. However, as the Ma_∞ was increased, the boundary layer thickness decreased by 7.8%, and the authors attributed the difference in performance to a change in boundary layer thickness. In contrast, the shaped holes performed differently because the increased Mach number changed the way the coolant filled out the shaped holes. At Ma_∞ = 0.15, the coolant from the fan-shaped holes split, but when the Mach number was increased to 0.45, the jets started to bias to one side of the shaped hole at high blowing ratios, which decreased the adiabatic effectiveness. It's possible that if this study were repeated using a shaped hole with smaller expansion angles that the performance would be less sensitive to changing the mainstream Mach number.

Mainstream Turbulence Intensity

The mainstream turbulence intensity has been shown to affect cylindrical and shaped holes in a similar manner. If the coolant jet is attached to the surface, increasing the mainstream turbulence intensity decreases the adiabatic performance due to the enhanced mixing of the coolant with the mainstream. If the jets have detached from the surface, increasing the mainstream turbulence increases that adiabatic effectiveness because the enhanced mixing pushes the detached cooler air toward the wall.

Saumweber and Schulz [9] looked at the effect of mainstream turbulence intensity for cylindrical and 14° fan-shaped holes. For cylindrical holes, while the jets were attached at low blowing ratios (M = 0.5, DR = 1.75), increasing the turbulence intensity from 2%, 5.2%, and 7.5% gradually decreased the adiabatic effectiveness performance. At M = 1.5, when the cylindrical holes were detached, the opposite trend was true. As the turbulence intensity increased, the jets widened and were pushed closer to the surface. The authors explained that when jets are attached, the increased turbulence intensity eats away at the shear layer between the jet and mainstream, decreasing its effectiveness. When the jets are detached, the turbulence intensity causes more mixing, which pushes colder coolant toward the surface and widens the jets. When Saumweber and Schulz did a

similar analysis with fan-shaped holes, they found that increasing the turbulence intensity gradually decreased adiabatic effectiveness at M = 0.5 and M = 2.5 at DR = 1.75. Decreasing performance with increasing turbulence intensity was not observed at M = 2.5 like with the cylindrical holes most likely because the jets were still attached to the surface. Compared to cylindrical holes, the shaped holes were more sensitive to increasing the turbulence intensity, and showed larger degradations, percentage-wise, than shaped holes. Bons et al. [41] also studied the effect of mainstream turbulence on film cooling with cylindrical holes, and their results agreed with the trend seen in Saumweber and Schulz's [9] study.

Saumweber et al. [15] also studied the effect of free-stream turbulence on film cooling with shaped holes. The study was similar to Saumweber and Schulz [9], but in addition to testing cylindrical and 14° laterally diffused shaped holes, they also tested a shaped hole with a 14° lateral diffusion and a 15° forward diffusion. Their conclusions were the same as [9], where increasing the turbulence intensity, from 3.6%, 7.5%, and 11% in this case, decreased the adiabatic effectiveness of the cylindrical holes at low blowing ratios and increased the adiabatic effectiveness at higher blowing ratios where the jets were detached. For both shaped holes, increasing the turbulence intensity decreased adiabatic effectiveness at all blowing ratios, up to M = 2.5 at DR = 1.7, which was the highest blowing ratio tested. Again, the shaped hole performance never decreased with increasing blowing ratio, indicating that there was no gross separation at the blowing ratios tested.

Turbulent Length Scale

Saumweber and Schulz [9] varied the turbulent length scale from 1d to 1.8d, and saw no effect for cylindrical and shaped holes. Saumweber et al. [15] found that changing the turbulence length scale from 2.1d to 3.5d produced a very slight increase in laterally averaged adiabatic effectiveness downstream of cylindrical holes. Increasing the

turbulent length scale widened the jets and increased the centerline effectiveness close to the holes.

1.3.1.10 Entrance and Cross Flow Effects

Cross-flow Effects

Studies that have looked at the effect of coolant cross-flow on adiabatic effectiveness have shown that when coolant is fed by cross-flow, versus by a plenum, film cooling performance increases for cylindrical holes [27, 18, 22, 42, 19], but can decrease for shaped holes, especially if the cross-flow is perpendicular to the mainstream [27, 18, 22, 42, 19].

Saumweber et al. [27] compared the effects of cross-flow intensity and direction on cylindrical holes and 14° laterally expanded fan-shaped holes. Contours of adiabatic effectiveness at $M = 1.0$ and $DR = 1.8$ were used to compare the performance. The study included coolant cross-flow Mach numbers of 0 (plenum condition), 0.3, and 0.6. When the coolant cross-flow was oriented parallel to the mainstream, the cylindrical and shaped holes performed slightly better with increasing coolant Mach number. However, when the coolant cross-flow was oriented perpendicular to the mainstream, the performance of the cylindrical holes decreased at $Ma_c = 0.3$, but increased significantly at $Ma_c = 0.6$. The performance of the shaped holes continually decreased with increasing perpendicular coolant cross-flow Mach number. The perpendicular cross-flow changed the way the coolant filled out the diffuser of the shaped hole, causing the coolant to bias to one side of the hole, which decreased the performance.

Saumweber and Schulz [18] varied the internal cross-flow from a plenum condition to a perpendicular cross-flow with an internal Mach number of 0.29 and 0.59 using a fan-shaped hole with a 6° lateral expansion. As the cross-flow increased, the laterally averaged adiabatic effectiveness decreased and the jet biased to one side of the shaped hole. In contrast, the performance of cylindrical holes increased with increasing

internal cross-flow. At an internal Mach number of 0.6 and M = 1.0, the spatially averaged adiabatic effectiveness of the shaped holes reduced to the same level as the cylindrical holes.

Saumweber and Schulz [22] compared film cooling effectiveness downstream of cylindrical and 14° laterally expanded fan-shaped holes with and without cross-flow that was perpendicular to the main flow at Ma_c = 0.3. For cylindrical holes, adding cross-flow widened the film cooling jets and increased the adiabatic effectiveness over the plenum-fed coolant condition. For the fan-shaped holes, adding the cross-flow decreased the film cooling effectiveness for all blowing ratios tested: 0.5, 1.5, and 2.5.

Gritsch et al. [42] tested the effect of cross-flow oriented perpendicular to the mainstream flow with cylindrical, fan-shaped, and laidback fan-shaped holes. All of the shaped hole expansion angles were 14°, but the forward expansion of the laidback hole was 15° and only extended 1d from the hole breakout. Plenum conditions were compared at Ma_c = 0.3 and 0.6, DR = 1.75, and M = 0.5, 1.0, 1.5, and 2.0. Except at M = 0.5, the performance of the cylindrical holes improved with increasing internal Mach number. It delayed jet detachment and kept the jet closer to the wall. However, for both types of shaped holes, the perpendicular cross-flow was always detrimental to adiabatic effectiveness performance.

Gritsch et al. [19] looked at the effect of internal cross-flow on adiabatic effectiveness using cylindrical, fan-shaped, and laidback fan-shaped holes (the same shaped holes described in the previous paragraph). They varied the internal cross-flow Mach number between 0 and 0.6 and the cross-flow was oriented to be parallel to the mainstream and perpendicular to the mainstream. The testing conditions were DR = 1.85 and M = 0.5, 1.0, and 1.5. They found that for the cylindrical holes, adding cross-flow in either direction increased the adiabatic effectiveness. For the fan-shaped hole, the parallel cross-flow increased the performance and the perpendicular cross-flow decreased the performance.

Entrance Effects

Unfortunately, coolant entrance effects on film cooling performance using shaped holes haven't been studied much, even though the results of this dissertation indicate that they are very important. Lim et al. [20] looked at the effects of contouring the inlet to shaped hole and observed the effect on aerodynamic losses and net heat flux reduction. The contour to the hole inlet was the same as the external shaped hole geometry (17.5° lateral expansion, no forward expansion). Basically, they tested a hole that had a shaped hole expansion at the entrance and a shaped hole expansion at the exit that was mirrored along the z axis. Their study used a flat plate facility at $DR = 1.0$, and their results showed that contouring the inlet to the hole significantly reduced aerodynamic losses inside the hole, but did not affect aerodynamic mixing losses external to the hole. The net heat flux reduction for the holes with the inlet contouring was lower than for shaped holes without internal contouring, but was still significantly higher than the *NHFR* for cylindrical holes. Adiabatic effectiveness results were not presented.

Porter [43] proposed that hole inlet conditions should be specified by the inlet velocity ratio, which they define as the ratio of the mean cross-flow velocity normal to the hole to the mean velocity in the coolant hole. They claim that this is the best way describe inlet flow conditions, versus the cross-flow Mach number or Reynolds number, since this parameter affects the velocity distribution inside the coolant holes by taking the angle of the hole into account. The researchers used CFD and experimentation to show that as the inlet velocity ratio increased, the jetting effect in a shaped coolant hole decreased, but did not experimentally show how this affected film cooling performance downstream of the coolant holes.

Hyams and Leylek [44] performed a CFD study that looked at the effect of contouring the entrance to a cylindrical film cooling hole. The holes in the study were at a 35° surface angle, and the contoured hole had a filleted radius around the entire perimeter of the hole. The fillet at the hole entrance ranged from $0.35d$ at the upstream edge of the hole to $0.44d$ at the downstream edge of the coolant hole entrance. The flow

field between the hole with the contoured entrance and a cylindrical hole without a contoured entrance was compared. Contouring the hole entrance created a more uniform velocity profile exiting the hole and reduced the turbulence intensity by about a third. However, the vorticity of the jet and the adiabatic effectiveness downstream of the coolant hole exit remained largely unchanged. The authors attributed this to the jet shear layer between the jet and mainstream dominating film cooling performance. It would be interesting to see if this result would hold true in an experiment.

1.3.1.11 Effect of Hole Imperfections

The effect of hole imperfections on film cooling performance is a very important aspect. Often, research labs are able to precisely machine complicated, scaled-up shaped hole geometries, and it's not clear whether this precision matches the precision that is used to machine actual turbine components. Variability in shaped hole geometries due to machining or material differences could greatly affect film cooling performance, especially for shaped holes, but few studies have looked at this.

Heneka et al. [34] looked at the effect of machining a shaped hole with sharp edges in the diffuser. Normally, shaped holes have filleted radii in the expansion, and in this study, the holes were manufactured with sharp edges, and no fillets. The adiabatic effectiveness results were compared to those of Colban et. al. [30] who published effectiveness results from a shaped hole with the same expansion angles, but had fillets machined into the diffuser shape. The results showed that the sharp-edged holes performed better than the smooth shaped holes for the lower blowing ratio of $M = 0.5$. The results were roughly equal at $M = 1.5$. As the blowing ratio was increased, adiabatic effectiveness performance peaked for the sharp-edged shaped holes at $M = 2.0$. The rounded shaped holes increased in performance up to $M = 4.0$, which was the highest blowing ratio presented.

Jovanovic et al. [2006] did a study on the effect of imperfections in a cylindrical hole. They placed a half-torus-shaped circular ring inside a shaped hole at 0.2d, 1.2d, and 2.5d, from the hole exit, and the hole was 10d long. The half torus was 1/8d. The experiments were completed using a water channel at $DR \approx 1$. When the blockage was positioned closest to the hole exit, at 0.2d, the imperfection increased the adiabatic effectiveness performance at $VR = 0.25$ and had little effect at higher velocity ratios. When the imperfection was located 1.2d into the hole, the adiabatic effectiveness decreased for $VR = 0.5 - 1.5$. When the half torus was located 2.5d into the hole, there was no effect on adiabatic effectiveness.

1.3.2 Effect of Density Ratio on Heat Transfer Coefficient Measurements

The effect of density ratio on heat transfer coefficient measurements has been studied in the past, but no researchers have used direct measurements of the wall temperature and adiabatic wall temperature to measure h_f, which is what was done to obtain the data in this dissertation. Other researchers have used the mass/heat transfer analogy, transient, or superposition techniques to measure the heat transfer coefficients and these techniques, along with their advantages and disadvantages, are described in section 1.1.2. There is fairly good consensus in the literature about heat transfer coefficient augmentation at unit density ratio, but the results at $DR > 1.0$ vary quite widely for both cylindrical and shaped holes.

1.3.2.1 Results at Unit Density Ratio

In the past, it has been assumed that heat transfer coefficient augmentation is independent of density ratio (as suggested by the superposition analysis of Eckert [6]), and most experiments were run at $DR = 1.0$ since this is a simpler experiment and results

in more precise measurements. Many of these studies were completed with cylindrical holes spaced 3*d* [45, 26, 46, 47], which showed relatively low heat transfer coefficient augmentation values. For low blowing ratios, $M < 1.0$, the heat transfer coefficient augmentation downstream of the coolant holes was $\overline{h_f/h_0} = 0.75\text{-}1.1$. For higher blowing ratios with detached jets, such as at $M = 2.0$, [45, 26, 46] showed slightly larger values of $\overline{h_f/h_0} = 1.15\text{-}1.3$.

Heat transfer coefficient augmentation using shaped holes for film cooling has been measured by [47, 28, 9, 15]. Yu et al. [47] used unit density ratio coolant to measure heat transfer coefficient augmentation downstream of cylindrical holes and shaped holes with 10° forward and lateral expansion angles. They found that the heat transfer coefficient augmentation was similar for cylindrical and shaped holes, with $\overline{h_f/h_0} = 0.8$ immediately downstream of the holes and increasing to 1.0 by $x/d = 7$. The authors attributed the decrease in $\overline{h_f/h_0}$ downstream of the holes to the jets thickening the thermal boundary layer, although they did not verify that this was the case.

1.3.2.2 Effect of Density Ratio using Cylindrical Holes

To establish the effect of density ratio on heat transfer coefficients downstream of cylindrical holes, Baldauf et al. [23] used a row of holes with $p/d = 3$, $\alpha = 30°$, and $Tu = 1.5\%$. They varied the wall temperature and used superposition to deduce the heat transfer coefficients that would occur for $T_c = T_\infty$. For $DR = 1.2$, they found $\overline{h_f/h_0} < 1$ for $M < 1$, and $x/d = 0$ to 15 downstream, while $\overline{h_f/h_0}$ approached 1 farther downstream. At higher blowing ratios, when the jets were detached from the surface, $\overline{h_f/h_0}$ increased with increasing blowing ratio up to $\overline{h_f/h_0} = 1.3$ at $M = 2.5$. At $DR = 1.8$, $\overline{h_f/h_0} = 1.0$ at all distances downstream for the attached jets, and when the jets detached from the surface, $\overline{h_f/h_0}$ increased with increasing blowing ratio up to $M = 2.5$, where $\overline{h_f/h_0}$ was about 1.2.

The effect of density ratio on heat transfer coefficient augmentation with film cooling using cylindrical holes was also studied by Ammari et al. [25] and Ekkad et al. [24]. They used CO_2 for the higher density coolant, DR = 1.5, and air as the low density coolant, DR = 1.0. Ammari et al. [25] used the mass transfer analogy to measure heat transfer coefficients downstream of a row of cylindrical holes at α = 35° and p/d = 3. At a fixed density ratio, the laterally averaged heat transfer coefficient augmentation increased with increasing blowing ratio. At a fixed blowing ratio, $\overline{h_f/h_0}$ decreased with increasing density ratio. The authors attributed the trend with density ratio to the lower density jets having greater momentum than the higher density jets. For both density ratios, $\overline{h_f/h_0}$ ranged from about 1.2-1.4 3d downstream of the holes and dropped off to 1.0 farther downstream.

Ekkad et al. [24] used the transient liquid crystal method to measure heat transfer coefficients downstream of cylindrical holes with α = 35°, p/d = 4, and a mainstream turbulence level of Tu = 8.5%. The results showed that except at the highest blowing ratio of M = 2.0, increasing the density ratio at M = 0.5 and 1.0 increased $\overline{h_f/h_0}$. At a given density ratio, $\overline{h_f/h_0}$ increased with increasing blowing ratio. Just downstream of the holes $\overline{h_f/h_0}$ ranged from 1.0 to 1.2 depending on the density ratio and blowing ratio.

1.3.2.3 Effect of Density Ratio using Shaped Holes

Most of the studies that looked at the effect of density ratio on heat transfer coefficient augmentation using shaped holes were completed at the Karlsruhe Institute of Technology. The study that compares best to the current study at high density ratio was completed by Saumweber and Schulz [9]. In this study, heat transfer coefficients downstream of fan-shaped holes with a 14° lateral expansion, 30° surface angle, and p/d = 6. Heat transfer coefficients were determined using superposition and varying the wall temperature. The researchers found that at DR = 1.75 and x/d = 2, $\overline{h_f/h_0}$ = 1.55 for M = 0.5

and $\overline{h_f/h_0}$ > 2.5 for M = 2.5. This study showed that the heat transfer coefficient augmentation was significantly large.

Saumweber et al. [15] performed a similar study where they tested the effect of mainstream turbulence intensity on heat transfer coefficients downstream of cylindrical, fan-shaped, and laidback fan-shaped holes using coolant at DR = 1.7. The fan-shaped hole had 14° lateral expansions and the laidback fan-shaped hole had 14° lateral expansions with a 15° forward expansion. All holes were spaced at p/d = 4. At Tu = 3.6%, all of the holes showed h_f/h_0 < 1 which increased to above 1.0 farther downstream. When the turbulence intensity was increased to 11%, h_f/h_0 for both shaped holes was 1.0-1.1 for M = 0.5. As the blowing ratio was increased to 1.5 and 2.5, h_f/h_0 = 1.5-1.75 downstream of holes and then decreased to 1.3-1.6 by 20d downstream.

Gritsch, Schulz, and Wittig [28] used the superposition technique to measure heat transfer coefficients from 2-8d downstream of cylindrical holes, fan-shaped holes, and laidback fan-shaped holes at α = 30° and p/d = 3. The mainstream was at a Mach number of 0.6 and Tu < 2%. At DR = 1.85, M = 0.5-1.5, and x/d = 2, $\overline{h_f/h_0}$ = 0.7 for the fan-shaped hole and $\overline{h_f/h_0}$ = 0.6 for the laidback fan-shaped hole. By 8d downstream, the heat transfer coefficient augmentation had increased for both types of holes, but still remained below 1.0.

Saumweber and Schulz [18] measured the heat transfer coefficient augmentation downstream of fan-shaped holes that were laterally expanded by 6° and 14° and were spaced 6d. The hole shape is different from the 7°-7°-7°, but the testing conditions are very similar to what were used for this dissertation. The measurements were taken on a flat plate with plenum conditions at the coolant hole entrance. The mainstream was Mach number was 0.3, the turbulence intensity was 5.2%, and the heat transfer coefficients were measured using superposition. Results at M = 0.5, 2.5 and DR=1.75 were presented for both hole geometries, and are shown in Figure 0-18. At M = 0.5, $\overline{h_f/h_0} \approx 2$ at 2d

downstream of the metering hole centerline, and by 6d, $\overline{h_f/h_0}$ = 1.1-1.2. At M = 2.5, $\overline{h_f/h_0}$ = 3 at x/d = 2.5 and dropped to $\overline{h_f/h_0}$ = 1.7 by 6d downstream.

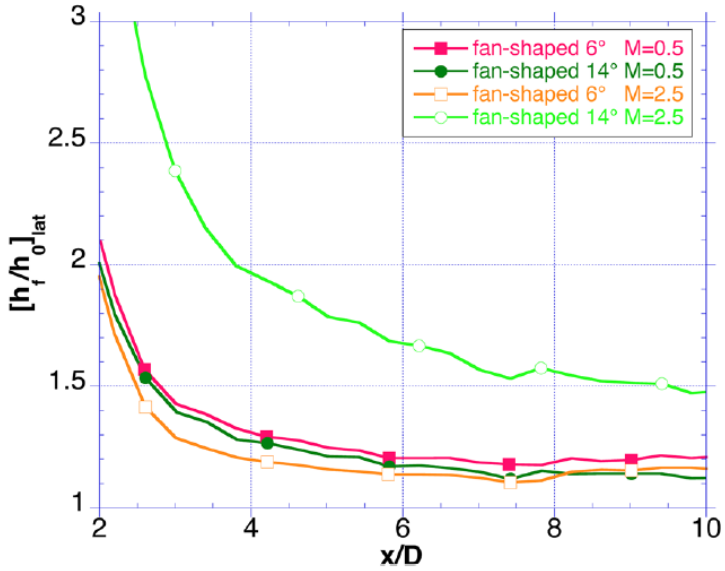

Figure 0-18 Laterally averaged heat transfer coefficient augmentation using 14 laterally expanded fan-shaped holes at DR = 1.75 [18].

Saumweber and Schulz [9] published another paper using the same test setup and parameters as described in the previous paragraph, except the mainstream turbulence intensity was slightly higher at 7.5% versus 5.2%. The results are shown in Figure 0-19. For 14° laterally expanded fan-shaped holes, at M = 0.5, $\overline{h_f/h_0}$ = 1.55 at x/d = 2 and dropped off to $\overline{h_f/h_0}$ = 1.0 by x/d = 10. At M = 2.5, $\overline{h_f/h_0}$ = 2.5 at x/d = 3 and dropped off to $\overline{h_f/h_0}$ = 1.4 by x/d = 10.

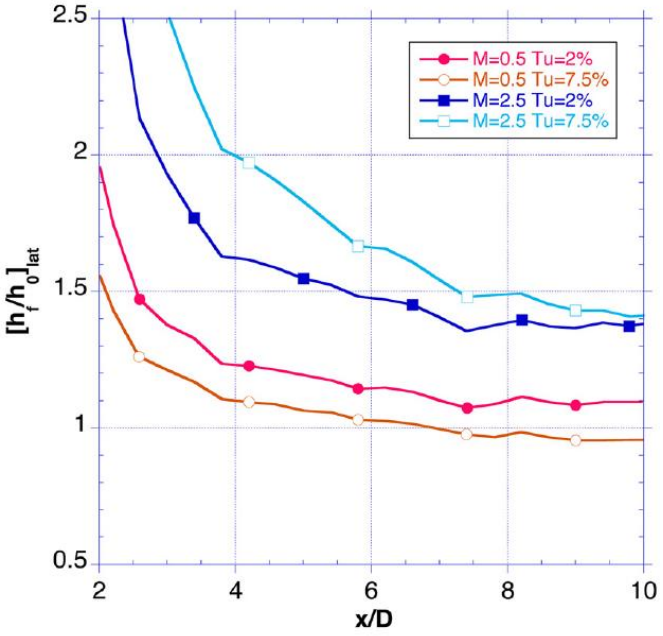

Figure 0-19 Laterally averaged heat transfer coefficient augmentation using 14 laterally expanded fan-shaped holes at *DR* = 1.75 [9].

For using the same testing conditions at the same lab, with the same shaped hole geometry, the variation between the results from [18, 9] are quite inconsistent. A small difference in turbulence intensity should not cause the results to vary this much.

1.3.3 THERMAL FIELD MEASUREMENTS

There are very few studies in literature that include thermal field measurements on a flat plate. The only reliable studies used cylindrical holes at low blowing ratios (*M* = 0.4-0.5) where the film cooling jets were attached to the surface. Kohli and Bogard [48] measured thermal fields downstream of cylindrical holes with a surface angles of 35° and 55° at *DR* = 1.6. The α = 35° holes were at *M* = 0.5 and the α = 55° holes were tested at *M* = 0.4. The results showed that the jets at both surface angles were attached and

extended to about y/d = 10. However, the nondimensional coolant temperature from the jet with the 55° surface angle decayed much faster as it traveled downstream than the α = 35° jet. In another study, Kohli and Bogard [49] used a cold-wire to measure the thermal field downstream of cylindrical holes at M = 0.4 and DR = 1.05. The jet was also attached at this condition. The study compared the centerline thermal field profile to a profile with matched momentum flux ratio at DR = 1.6. The profiles were very similar, with nondimensional temperatures extending the same distance downstream and vertically above the walls at both density ratios. This suggests that the flow field scaled with momentum flux ratio, but no other testing conditions were compared. Other results from the study showed that the random mean squared temperature was highest in the core of the jet and dissipated at the edges of the jet.

EXPERIMENTAL METHODS AND UNCERTAINTY

1.4 Experimental Facility

1.4.1 FLAT PLATE FACILITY AND TEST SECTION

Flat Plate Facility

Adiabatic effectiveness, heat transfer coefficient augmentation, and thermal fields were measured in a closed-loop wind tunnel facility at the Turbulence and Turbine Cooling Research Laboratory at the University of Texas at Austin (UT). A diagram of the facility is shown in Figure 0-1.

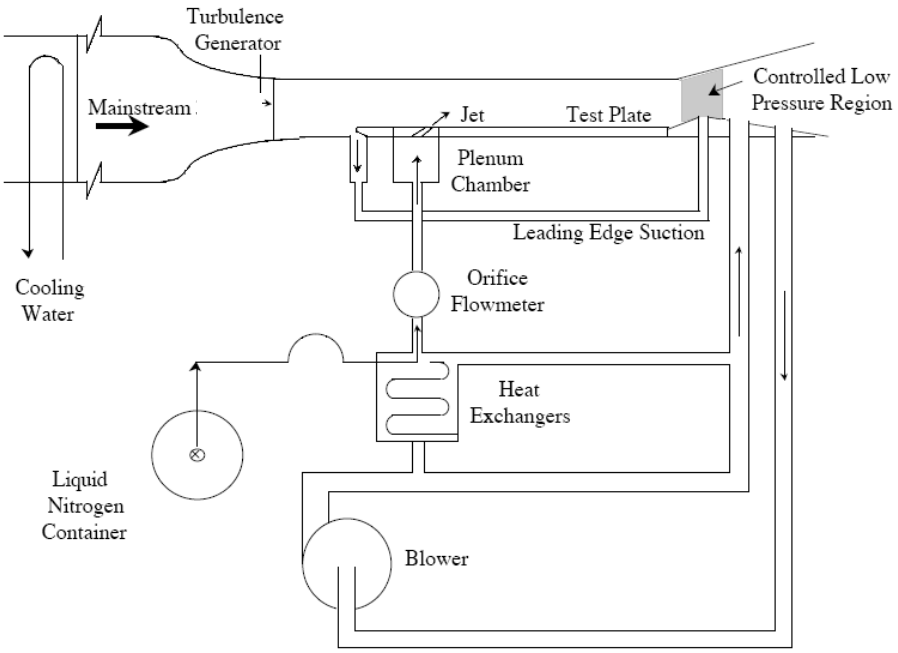

Figure 0-1 Diagram of flat plate testing facility

Experiments were run with the mainstream at 303 K and cold nitrogen gas was used as coolant to produce density ratios of 1.2 and 1.5. Liquid nitrogen tanks were used to supply coolant. The liquid nitrogen was warmed to nitrogen gas as it traveled through copper pipe heated by the ambient room and also through a heat exchanger with air supplied by a blower. The coolant flow rate was measured with an orifice meter and then traveled up to a coolant plenum that dispersed the coolant before it exited from film cooling holes. The following discussion will describe the details of the test section.

Test Section

Figure 0-2 shows a schematic of the wind tunnel test section. The test section was 5.4 inches (13.7 cm) high and 24 inches (61 cm) wide in the span-wise direction. Each component of the test section is described below.

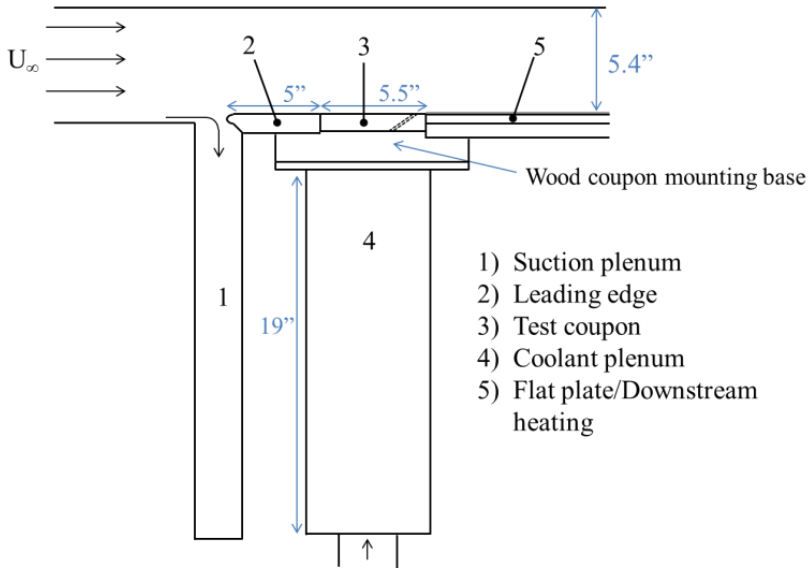

Figure 0-2 Diagram of wind tunnel test section.

1) Suction Plenum

The approach boundary layer on the bottom of the wind tunnel was bled off into a suction plenum so that a fresh boundary layer could form along the flat plate. A 10 in. PVC pipe connected the suction plenum to a constricted region downstream of the test section (shown in Figure 0-1). The constriction was adjustable, which was used to adjust the level of suction. The suction was set by measuring the mainstream velocity upstream of the test section and the mainstream velocity at the coolant hole location with Pitot-static probes. The two velocities were compared to make sure the suction plenum was siphoning off the correct amount of the approach flow to stagnate on the leading edge. Using this method of adjusting the suction level was validated using Particle Image Velocimetry flow visualization, which showed that the approach flow stagnated on the leading edge when the mainstream velocity readings were used in the manner described. The mainstream velocity in the y direction is shown in the PIV flow visualization image in Figure 0-3.

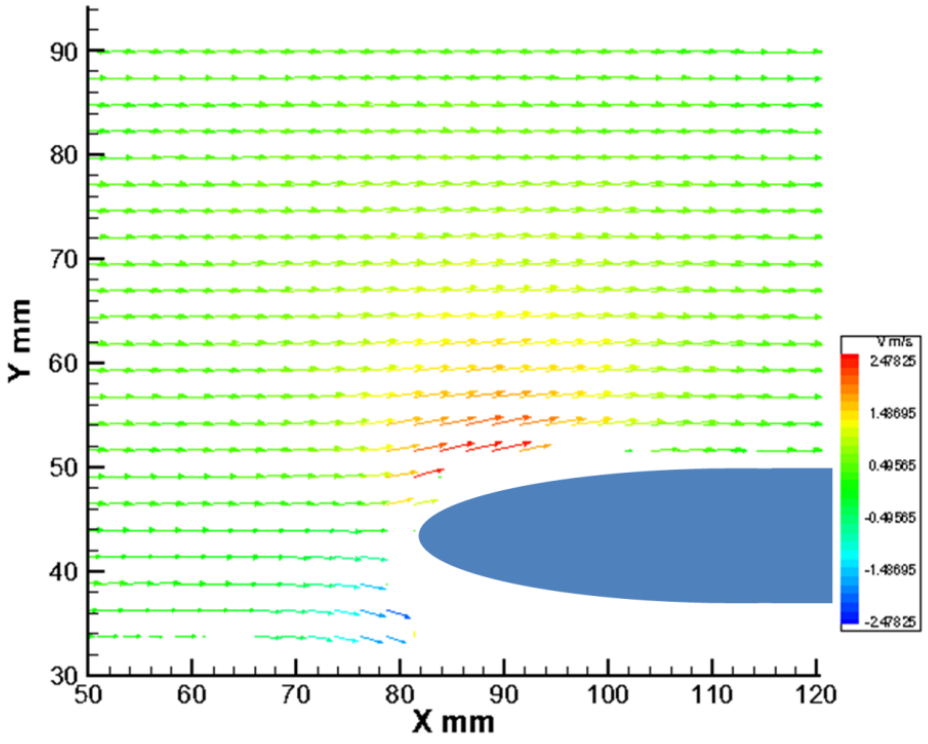

Figure 0-3 Velocity in the *y* direction using PIV flow visualization for determining correct suction level.

2) Leading Edge

The leading edge was a half ellipse so that the approach mainstream air would stagnate, preventing a separation bubble on the flat plate. A 1/16 in. (1.6 mm) diameter boundary layer trip was installed 1.5 in. (3.8 cm) downstream of the leading edge, which promoted a fully turbulent boundary layer (boundary layer measurements will be discussed in Section 1.5.1).

3) Test Coupon

The test coupon was made out of closed-cell polyurethane foam manufactured by General Plastics Manufacturing Company. The thermal

conductivity was 0.44 W/m·K. Shaped holes were machined into the coupon at UT's Mechanical Engineering Machine Shop using a CNC. More information on the shaped hole geometry is provided in Section 1.4.4.

4) Coolant Plenum

The coolant plenum had an open internal cross-section of 17.5 in. in the span-wise direction and 4.5 in. in the downstream direction. The internal height of the plenum was 18 in. The coolant entered through a 3 in. PVC pipe at the bottom of the plenum and was dispersed by three fine screens spaced evenly in the plenum. The even dispersion of coolant in the plenum was verified by taking infrared images of the jets operating across the span of the plenum and finding that they had consistent performance.

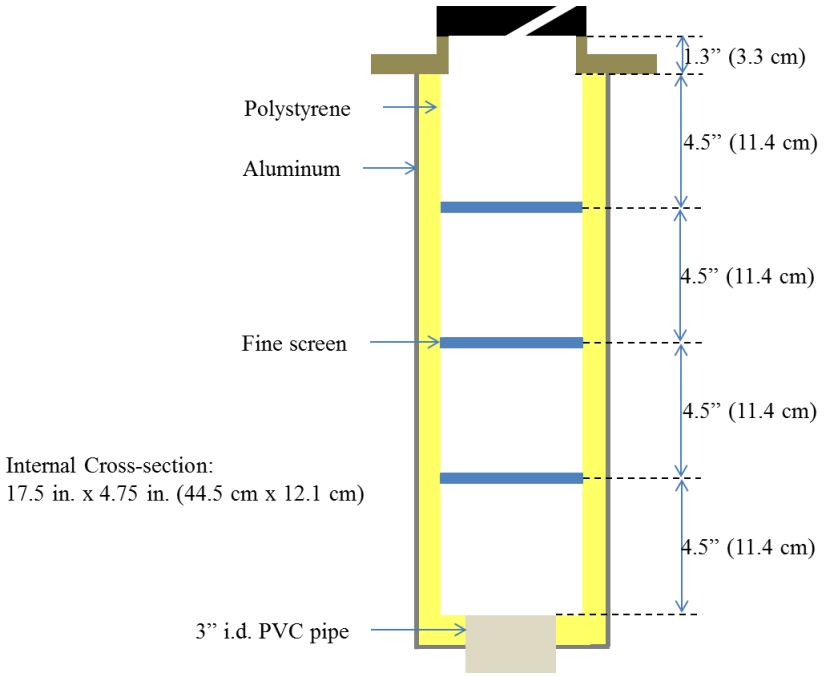

Figure 0-4 Diagram of the internal plenum geometry at UT.

5) Flat Plate/Downstream Heating

A flat plate was installed downstream of the test coupon, which consisted of 0.5 in. thick polystyrene foam mounted on top of 0.75 in. thick Birch plywood. Four inches of fiberglass insulation, which is not depicted in Figure 0-2, was attached to the bottom of the plate to reduce conduction losses. For the heat transfer coefficient experiments, a 0.5 mil thick stainless steel foil was attached on top of the polystyrene foam. The foil is discussed further in Section 1.4.5.

1.4.2 INFRARED CAMERA MEASUREMENTS

A FLIR P20 infrared (IR) camera was mounted on top of the wind tunnel test section to measure the surface temperature on the flat plate. The camera viewed the flat plate through a salt crystal window, which is invisible to infrared radiation. All testing surfaces were painted with a flat black latex paint to provide a uniform emissivity.

The IR camera temperature readings were calibrated with surface thermocouples. Separate calibration tests that used thermocouples installed on thin copper plates were used to create the calibration. The copper plates provided a more uniform temperature, which helps to create a more accurate IR camera calibration. Photographs of the copper plates are shown in Figure 0-5. The picture on the left shows the side view of the plates, which are less than 0.5 mm thick. The thermocouples were electrically insulated from the copper plates and then painted with the same paint used on the flat plate. The picture on the right shows the calibration plate after it has been painted. There are also silver tick marks which help the test operator locate the thermocouple junction in infrared camera images.

Figure 0-5 Photographs of copper IR camera calibration plates.

Five calibration tests were completed by Sean Klavetter and Noah Mosberg to create a standard IR calibration curve for this project. For each test, 3-4 calibration plates were installed at different distances downstream of the coolant holes, and the calibrations between the plates were very consistent. The data from the calibration tests were compiled to produce the IR calibration curve shown in Figure 0-6. The scatter of the calibration points increases at lower temperatures as the lower temperature limit that the IR camera can read is approached.

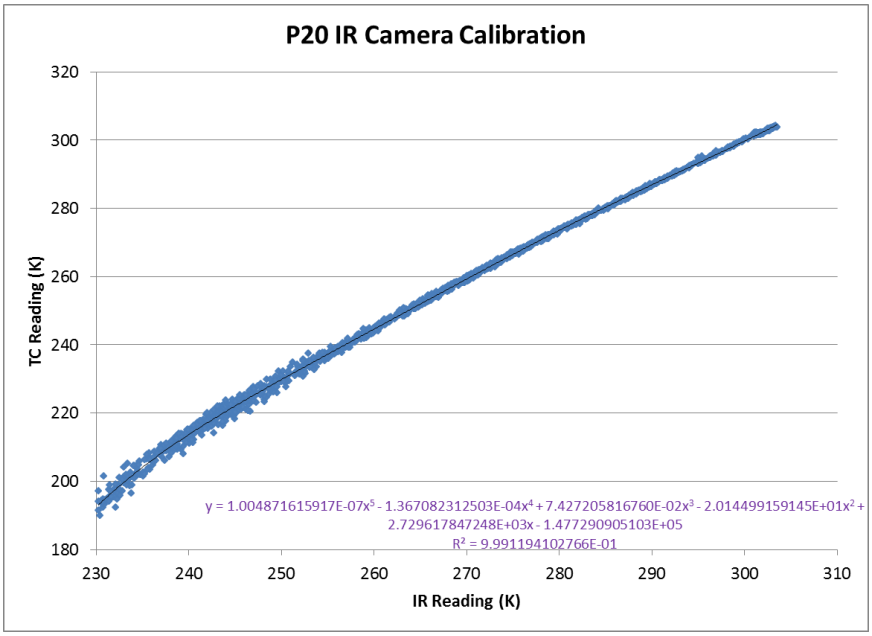

Figure 0-6 IR camera calibration

1.4.3 Measurement of Coolant Temperature and Mainstream Temperature

To calculate the adiabatic effectiveness, the adiabatic wall temperature is nondimensionalized with the coolant temperature and the mainstream temperature. The coolant temperature was measured with a bead-type thermocouple in the center of the plenum, 1.5 in. (3.8 cm) beneath the coolant hole entrances. As a reference for how much the coolant warmed from the coolant temperature measurement location to the coolant hole entrances, thermocouples were installed at the entrances of two coolant holes on each coupon tested. A photograph of this is shown in Figure 0-7. The hole entrance thermocouples were installed on holes just outside the viewing area of the IR camera in case their installation had an effect on the coolant entering and exiting the holes. The photograph isn't quite taken at the appropriate angle to show that the thermocouple

installed in the center of the hole is indeed in the center when viewing directly into the coolant hole. For this particular coupon, an additional thermocouple was installed at the edge of the coolant hole to observe the temperature profile of the coolant at the edge and center of the coolant hole.

Figure 0-7 Photograph of a thermocouple installed at the coolant hole entrance.

There were three bead-type thermocouples installed upstream of the suction plenum to measure the mainstream temperature. The three thermocouples were spaced even distances in the lateral direction of the wind tunnel and were located in the center of the test section vertically. The thermocouple that was located laterally in the center of the test section was used for the mainstream temperature reading, since the IR measurements were also taken in the center of the test section. The other two thermocouples mainly served as references to double check the center thermocouple reading and to serve as backups, in case the center thermocouple broke.

1.4.4 SHAPED HOLE GEOMETRY

The shaped hole geometry used for all of the experiments in this project was designed by Pennsylvania State University's (PSU's) EXCCL laboratory. The geometry features a 7° forward and lateral expansion and a surface angle of 30°, which is shown in Figure 0-8. The hole diameter was 9.0 mm and eight holes were spaced at p/d = 6, in a single row. PSU tested the same hole geometry, but their hole diameter was reduced to 8.47 mm, and their test section was narrower in the span-wise direction, so they tested five holes.

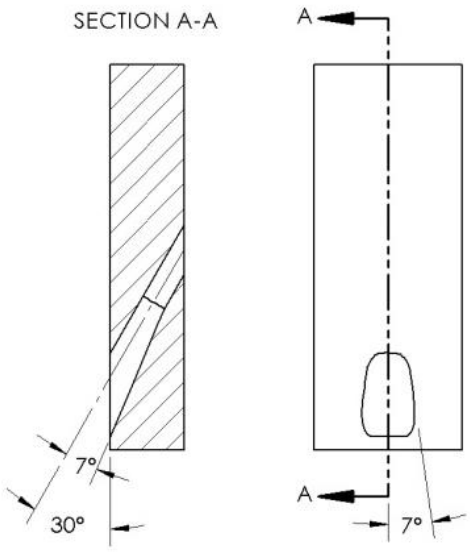

Figure 0-8 7°-7°-7° shaped hole geometry designed at PSU

Table 0-1 lists more details on the shaped hole geometry.

Table 0-1 Summary of coolant hole geometry parameters

Metering Hole Diameter, d	9 mm
Surface Angle, α	30°
Lateral Expansion, β	7°
Forward Expansion, ε	7°
Compound Angle, γ	0°
Area Ratio, AR	2.5
Breakout Width/d	2.1
Metering Length, L_T/d	2.5
Total Length, L/d	6
Diffuser fillet radius	0.5d
Hole Pitch, p/d	6
Number of holes	8

1.4.5 HEAT FLUX PLATE

The heat transfer coefficients were measured using a uniform heat flux plate, which was located just downstream of the coolant holes and spanned from x/d = 1.1 to 33. Measuring heat transfer coefficients at high density ratio produces a non-isothermal boundary condition on the top of the heat flux plate. A very thin heat flux foil was used to minimize heat conduction to the core of the jets. The effect of the foil thickness was tested by comparing lateral plots of adiabatic effectiveness (with the heat flux plate turned off) downstream of cylindrical holes using a) bare polystyrene foam b) polystyrene foam with 1 mil foil on top and c) polystyrene foam with 2 mil foil on top. The comparison is shown in Figure 0-9 at x/d = 7, DR = 1.5, and M = 0.5, 0.7, 1.0 and 1.5. The figures show that as the stainless steel foil thickness was increased, the jet peaks

decreased. Even with a very thin 1 mil foil, the effectiveness values did not quite achieve the same peak as the foam without foil. To minimize the effect of lateral conduction, the heat flux plate used for this dissertation was constructed using 0.5 mil or 0.0127 mm thick 304 stainless steel shim foil. The foil was manufactured by Trinity Brand Industries, which had a thickness tolerance of ± 5%.

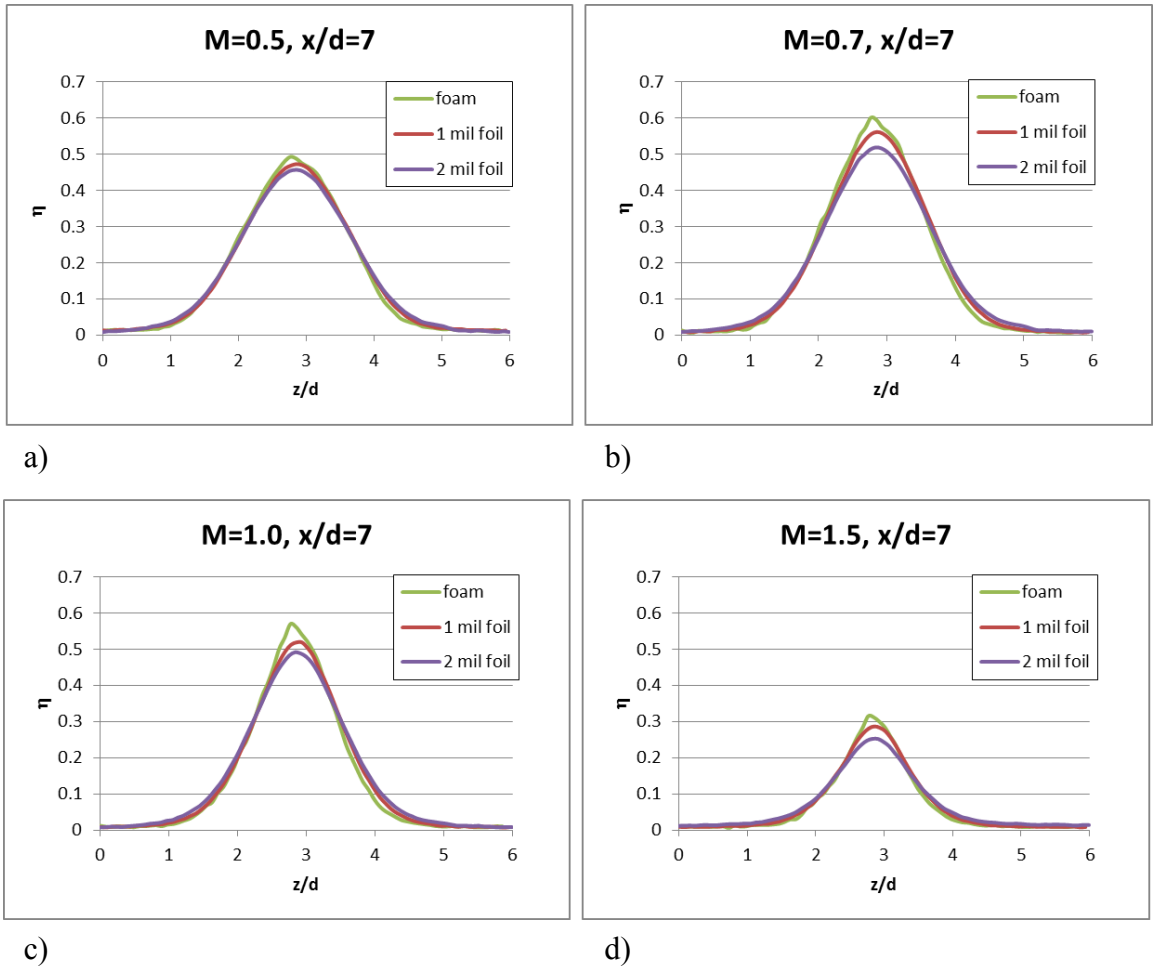

Figure 0-9 Comparison of lateral plots of adiabatic effectiveness at x/d = 7 with the plate surface being bare polystyrene foam, polystyrene foam covered with 1 mil stainless steel foil, and polystyrene foam covered with 2 mil stainless steel foil. Blowing ratios of a) M = 0.5, b) M = 0.7, c) M = 1.0, and d) M = 1.5 at DR = 1.5 are compared.

Stainless steel was used because it has a relatively low thermal conductivity compared to other metals. One half inch thick copper busbars were attached to the ends of the foil and the busbars were connected to a constant voltage power supply, which ran at about 48 A and 5.7 V across the busbars. The thickness of the busbars was found to be important, not for even current distribution within the busbars, but for making uniform contact with the foil after the busbars were clamped together. Thin busbars can deform, changing the contact resistance between the busbars and the foil which leads to non-uniform current distribution. Also, a high purity silver grease was used between the busbars and the foil to promote even current distribution in the foil.

Attaching the foil without creating ripples and air pockets underneath is critical to obtaining a uniform heat flux. Several different attachment methods were tried. The most successful procedure consisted of priming and painting the heat flux foil to give it some structural integrity to resist crinkling. Then, the foil was attached to a polystyrene substrate using 3M 5952 VHB tape, which proved to be much better at preventing air bubbles than epoxies or spray glues. Once the heat flux foil was attached, the uniformity of the heat flux was tested by orienting the plate vertically, which created a thermal boundary layer caused by natural convection. The temperature distribution on the plate was measured with an IR camera and was uniform laterally. Then, the plate was rotated 90° and the temperature distribution was uniform laterally in that direction as well, demonstrating that the heat flux being generated was uniform. Laying the heat flux plate flat does not work for testing heat flux uniformity because natural convection forms plumes of warm air along the plate which will create non-uniform temperatures, even though the heat flux is uniform. The temperature was uniform laterally within ± 0.75 K when the heat flux plate was heated 35 K above the ambient temperature.

The heat flux generated using the aforementioned test setup was uniform, but the heat flux generated during an experiment was not, since the electrical resistivity of stainless steel varies with temperature. During an experiment, the temperature of the foil can vary as much as 100 K between locations where cold jets are located and regions

where jets are absent. To see what effect this would have on the current distribution, Kyle Chavez created a 3-D model of the heat flux plate using Comsol Multiphysics®, which showed that the change in resistivity with temperature produced a uniform current distribution that was within ± 1.5%. Figure 0-10 shows the current distribution at $M = 2$ and $DR = 1.5$ using electrical resistivity as a function of temperature. $M = 2$ was chosen because it was the most effective blowing ratio and should therefore serve as a worst case scenario.

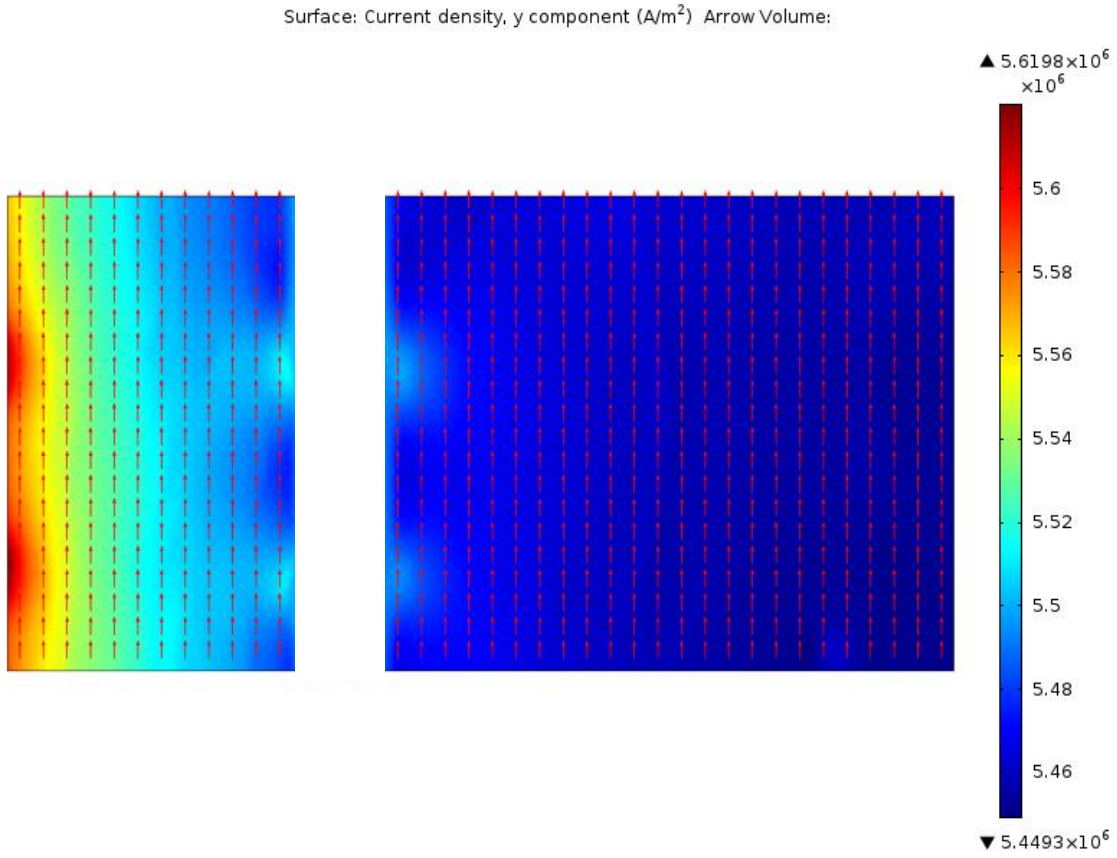

Figure 0-10 Comsol Multiphysics® model of current distribution in the heat flux foil at $M = 2$ and $DR = 1.5$.

Using this information, the heat flux generated by the heat flux foil was calculated using a constant current and the local resistivity, which was a function of the surface temperature. This function is plotted in Figure 0-11 which shows that the electrical resistivity can change up to 13% for foil temperature ranges at DR = 1.5. The local resistivity was converted to a local resistance using the foil dimensions, and the heat flux was calculated using Equation 0-1.

$$q'' = I^2 R$$

Equation 0-1

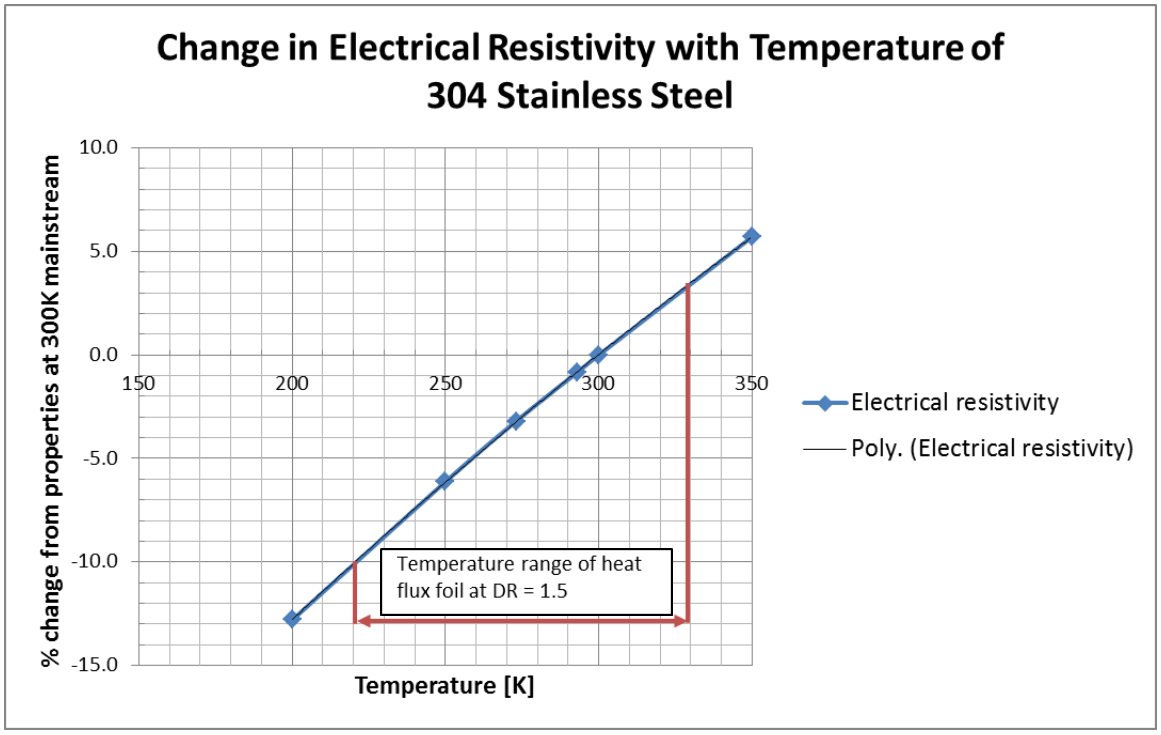

Figure 0-11 Variation of electrical resistivity of 304 stainless steel with temperature [50].

1.4.6 Radiation and Conduction Corrections

The heat flux measurements were corrected to account for radiation, which comprised 14-16% of the calculated heat flux. The foil was mounted on several layers of insulation, which are shown in Figure 0-12. Underneath the foil were uniform layers of 0.5 in. (1.3 cm) of polystyrene, 0.75 in. (1.9 cm) of plywood, and 4 in. (10 cm) of fiberglass insulation. Because the plate was well insulated with no coolant underneath, no backside conduction corrections were made to the heat flux measurements. The temperature of the heat flux plate was kept below 340 K so as not to exceed the temperature limits of the polystyrene it was mounted to. A 30 K temperature difference was maintained between the heat flux plate and the mainstream for the heat transfer coefficient experiments.

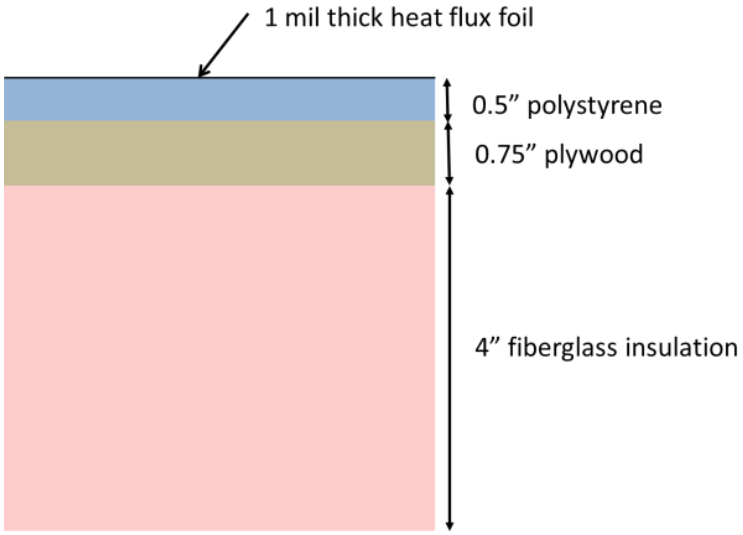

Figure 0-12 Diagram of insulation beneath the heat flux foil.

1.4.7 THERMAL FIELD PROBE

The thermal field was measured by traversing a thermocouple made from 1 mil (0.0254 mm) diameter wire, which was manufactured by Omega Engineering. However, the thermocouple from Omega had to be altered and installed on a probe before it could be used. The thermocouple had to be soldered to larger thermocouple wires, which is shown in Figure 0-13 a). This connects the 1 mil thermocouple to insulated wires and prevents them from breaking. The thermocouple was epoxied to a fish hook that was insulated with shrink tubing, which is shown in Figure 0-13 b). The fish hook was used for its shape because it could be angled in such a way as to allow the thermocouple to reach farther downstream than a straight rod. The fish hook was then epoxied to a 12 in. tungesten rod. Tungten was chosen to reduce vibration from the mainstream velocity while taking measurements.

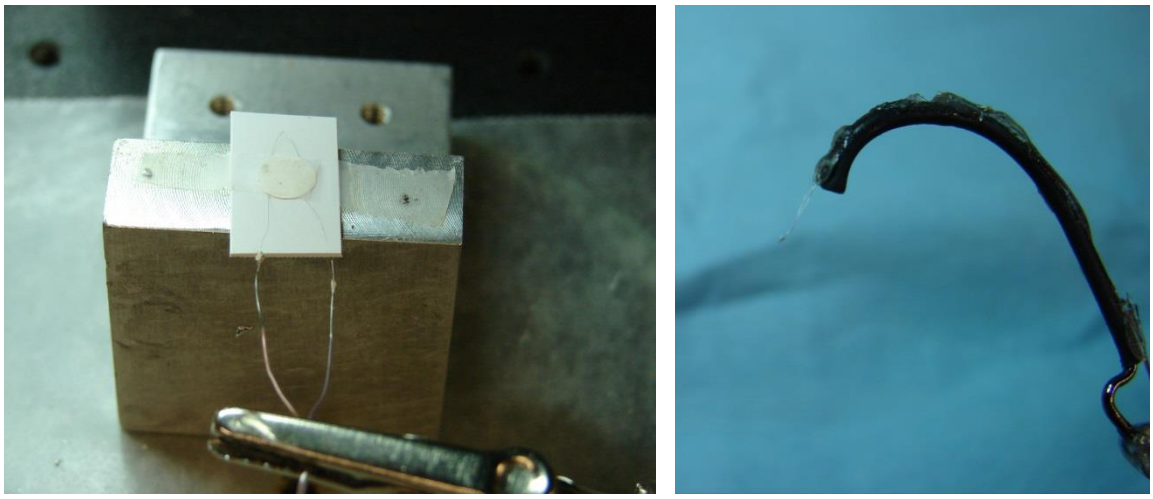

a) b)

Figure 0-13 Photographs of the thermocouple used for the thermal field measurements a) attachment of larger thermocouple wires to the 1 mil wires b) thermocouple mounted on the probe

1.5 Testing Parameters

Table 0-2 lists the testing parameters used by UT and PSU for this study. In the table, Re_∞ is based on the mainstream velocity, mainstream kinematic viscosity, and the metering hole diameter.

Table 0-2 Summary of test parameters

	UT	PSU
DR	1.0, 1.2, 1.5	1.2, 1.5
M	0.5, 1.0, 1.5, 2.0, 2.5, 3.0	0.5, 1.0, 1.5, 2.0, 2.5, 3.0
T_∞	303 K	295 K
U_∞	9.9 m/s	10 m/s
Re_∞	5600	5400
Tu	0.5%, 5.0%	0.5%, 5.4%

1.5.1 Boundary Layer Measurements at $Tu = 0.5\%$

Before the adiabatic effectiveness downstream of the 7°-7°-7° was measured, the approach boundary layer between UT and PSU was matched at $Tu = 0.5\%$. UT measured the boundary layer using a hot-wire, and PSU used Laser Doppler Velocimetry. When the project began, PSU had already measured their approach boundary layer, and UT had to match it. Figure 0-14 is a diagram of where the trip and hot-wire measurements were located. The hot-wire measurements were $4.5d$ upstream of the coolant holes to match where PSU completed their boundary layer measurements, which is shown with a black "X". A trip was installed, shown as a red dot, to ensure that the boundary layer was fully turbulent and to control the boundary layer thickness. The boundary layers downstream

of several combinations of trip sizes and locations were measured to match PSU's boundary layer, and in the end, a 1/16 in. (1.6 mm) diameter trip located 1.5 in. downstream of the leading edge matched PSU's boundary layer.

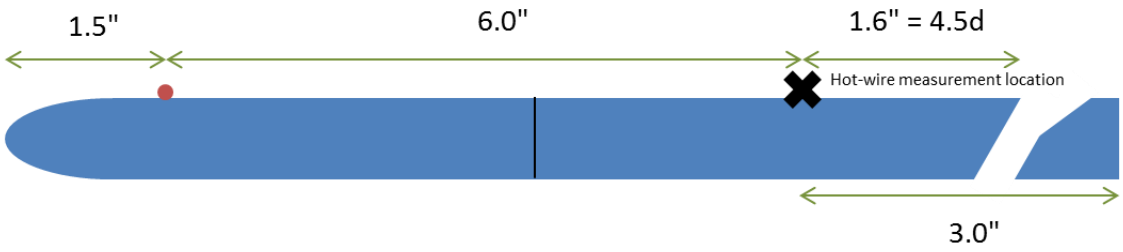

Figure 0-14 Diagram of hot-wire measurement location (black X) and trip location (red dot).

To test the repeatability of the boundary layer measurements, the boundary layer was measured with the trip in place. Then, on a different day, the trip was removed, replaced, and the boundary layer was measured again. The results of the measurements are shown in Table 0-3. The boundary layer was measured on 8/25/12 and 8/20/12, and the column "UT Average" is the average of the two measurements, which are the final parameters used to quantify the boundary layer at UT. In the table, note that δ* is the displacement thickness, θ is the momentum thickness, u_τ is the shear velocity, and H is the shape factor.

Table 0-3 Comparison of boundary layer measurements at UT and PSU.

	UT 8/25/12	UT 8/20/12	UT Average	PSU
d [mm]	9.0	9.0	9.0	8.47
δ [mm]	11.4	10.4	10.9	10.1
δ^* [mm]	1.34	1.40	1.37	1.52
θ [mm]	1.05	1.04	1.04	1.02
u_τ [m/s]	0.50	0.51	0.50	0.51
δ/d	1.3	1.2	1.2	1.2
δ^*/d	0.12	0.13	0.13	0.18
θ/d	0.12	0.12	0.12	0.12
Re_θ	622	613	617	677
Re_∞	5342	5298	5320	5461
H	1.28	1.34	1.31	1.45

Figure 0-15 shows the nondimensional boundary layer measurements taken at UT and PSU compared to the 1/7th power law, which is $U/U_\infty = (y/\delta)^{1/7}$. The measurements agree well.

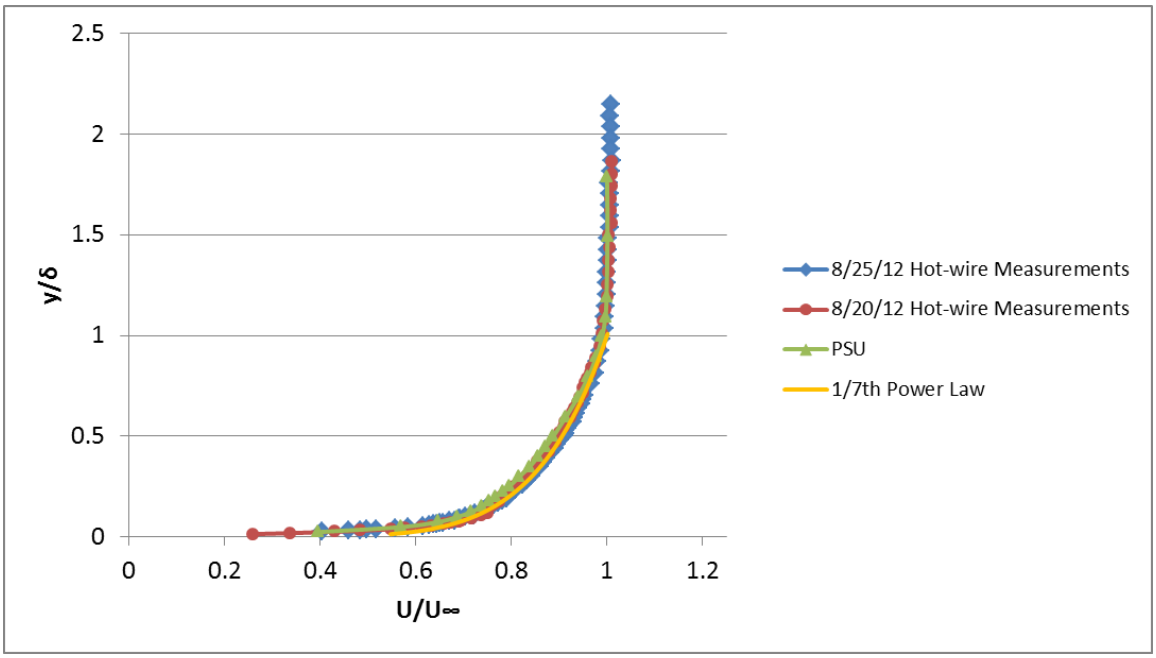

Figure 0-15 Boundary layer measurements taken at UT and PSU compared to the 1/7th power law at $Tu = 0.5\%$.

1.6 Experimental Methods

The following sections describe how adiabatic effectiveness, heat transfer coefficient augmentation, and thermal field experiments were operated.

1.6.1 Adiabatic Effectiveness Measurements

Adiabatic effectiveness experiments were run at DR = 1.2 and 1.5. An infrared camera was used to measure the adiabatic wall temperature. At each test condition, the density ratio and blowing ratio were held constant until steady state was reached. Infrared images and corresponding temperature and flow measurements values were recorded in

one minute intervals for 8-10 minutes. This proved to be plenty of time, as the surface temperature data reached constant values, or steady state, after 4-5 minutes. From the images taken at each test condition, an IR image was selected as being representative of the data set. The IR temperature readings were put through the IR camera calibration to produce adiabatic wall temperature values. The adiabatic wall temperatures were then converted to adiabatic effectiveness by nondimensionalizing T_{aw} with T_c and T_∞ that were recorded with Labview at the time each IR camera image was taken.

1.6.2 HEAT TRANSFER COEFFICIENT MEASUREMENTS

The heat transfer coefficient with film cooling is defined in Equation 0-7, which is repeated here for convenience: $q'' = h_f (T_{aw} - T_w)$.

Unit Density Ratio

Heat transfer coefficients with film cooling at unit density ratio were found by measuring T_{iw}, which is the surface temperature of the heat flux plate while turned on, with an IR camera. At unit density ratio, the driving temperature for heat transfer is T_∞, so h_f is simply found with Newton's Law of Cooling.

Density Ratio > 1.0

Calculating the heat transfer coefficients at DR = 1.2 and 1.5 required two experiments: an adiabatic effectiveness experiment with the heat flux plate turned off, and a heat transfer coefficient experiment with the heat flux plate turned on. The following steps were used to calculate the heat transfer coefficient with film cooling at high density ratio:

1. T_{aw} was measured with the heat flux plate turned off (experiment 1)
2. T_{aw} was nondimensionalized into η

3. The wall temperature was measured with the heat flux plate on (experiment 2)
4. The T_{aw} that was used to calculate h_f was back calculated from η measured in the first experiment, using T_∞ and T_c from the second experiment to account for any small differences in T_∞ and T_c between the two experiments.

These steps are depicted in Figure 0-16. The subscript "1" in the figure refers to experiment 1 and the subscript "2" refers to experiment 2. For the data in this paper, experiments 1 and 2 were run back-to-back, which eliminated test-to-test uncertainty.

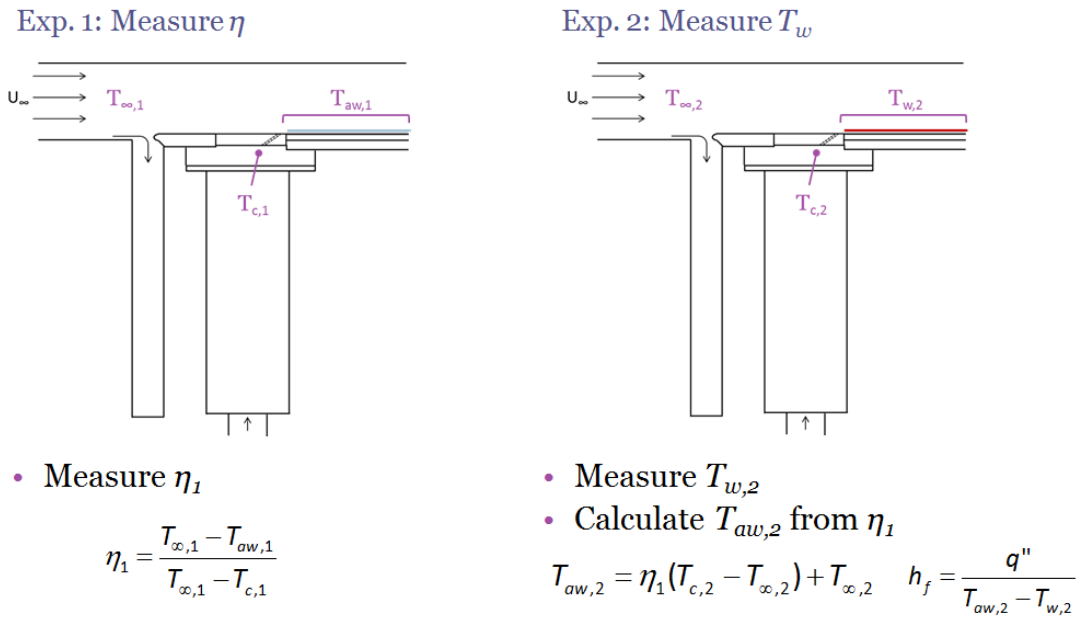

Figure 0-16 Diagram of experiments and variables used to calculate heat transfer coefficients at $DR > 1.0$

Measurement of h_0

The heat transfer coefficient without film cooling, h_0, was measured with the coolant holes taped over so that they would not disturb the hydrodynamic boundary layer. As with measuring h_f at unit density ratio, the heat flux plate was turned on and T_w was measured with the IR camera. h_o was calculated using Newton's Law of Cooling by using T_w, T_∞, and q''.

1.6.3 THERMAL FIELD MEASUREMENTS

The thermal field was measured by traversing a thermocouple made from 1 mil (0.0254 mm) diameter wire installed on a probe. A Zaber T-LSR traverse with 2 μm accuracy in the wall-normal direction and 15 μm accuracy in the streamwise direction was used to control the probe's location. For these tests, most of the results were taken at $DR = 1.2$ because the flow conditions had to be held for several hours to get enough data points for the thermal field measurements. Frost tends to become a problem when holding higher density ratios for long periods of time, and the slightest bit of it can become a problem, since it cannot be brushed away without risking damaging the thermocouple probe. These were two-person experiments, where one person controlled the traverse and the other person maintained the flow conditions and watched the thermocouple's location with respect to the wall. John McClintic controlled the traverse for all of these experiments. John also designed a special window for the wind tunnel that had grooves cut into it that allowed the traverse to move downstream and laterally at certain fixed positions. Measurements were taken at $x/d = 0.0$, 5.0, 10.0, and 14.66. $x/d = 15$ was not achievable to due portions of the wind tunnel obstructing the traverse's movement. While taking a profile, the traverse was lowered at even increments until the thermocouple was close the wall. At this point, the probe was moved in much finer increments until the thermocouple temperature stopped changing, which indicated that the thermocouple was touching the wall. The wall location was then defined at that distance.

1.7 Uncertainty

A thorough uncertainty analysis was completed for the film cooling experiments. There were two issues that affected the data: an increased adiabatic effectiveness between the jets where there was no coolant, and the coolant temperature measurement location. The largest sources of error were from the bias and precision uncertainty of the IR camera measurements, and in the case of measuring heat transfer coefficients at DR=1.2 and 1.5, the uncertainty of η provided an additional dominate source of uncertainty. All uncertainties were calculated to within 95% confidence using the methods described in Kline & McClintock [51] and Moffat [52].

1.7.1 Uncertainty of Density

The uncertainty in density ratio should be very low since the calculation of density using the ideal gas law depends on two fairly easy measurements: temperature and static pressure. While completing this uncertainty analysis it was discovered that there were some correctable bias errors in the calculation of density in the mainstream, orifice, and plenum. First, the ideal gas constant for air was used instead of nitrogen, even though the coolant loop and mainstream are pure nitrogen. While air is composed of mostly nitrogen, the ideal gas constants vary slightly, with the constant for air being 286.9 J/kg·K and the gas constant for nitrogen being 296.8 J/kg·K, 3.5% higher. Secondly, the static pressures at the orifice, plenum, and mainstream were not measured and standard atmospheric pressure was used to calculate density instead. The correctable pressure biases produced, at most, one third of the bias error, with the rest of the error resulting from using the R value for air instead of nitrogen. Fortunately, since the Labview program used the wrong R value for all of the density calculations, it produced a negligible effect on density ratio and blowing ratio calculations for the experiments. The error changed the mainstream velocity from the targeted 9.7 m/s to 9.9 m/s, but the error

was too small to have much effect on the blowing ratio calculation. The error in density calculation increases density ratios by 0.005 and decreases blowing ratios by 0.006. These values are so small that no adjustments were made to the reported density ratios and blowing ratios.

1.7.2 UNCERTAINTY OF BLOWING RATIO

The blowing ratio calculation depends on the coolant density, mainstream density, mainstream velocity, coolant hole diameter, pressure drop across the coolant orifice, and constant C. Constant C is a lumped coefficient that is a function of the pipe diameter, orifice diameter, and orifice discharge coefficient, which is itself a function of Reynolds number at the orifice, pipe diameter, orifice diameter, and the location of the pressure taps with respect to the orifice. The correlation for the discharge coefficient came from Fluid Mechanics Measurements by Goldstein [53], which states that the accuracy of the correlation is within 0.2%. Equation 0-2 was used to calculate the blowing ratio.

$$M = \frac{\rho_c}{U_\infty \rho_\infty} \frac{C\sqrt{\frac{\Delta P_B}{\rho_o}}}{8\frac{\Pi}{4}d^2}$$

Equation 0-2

The uncertainty in blowing ratio is largest at M = 0.5 at DR = 1.2 and 1.5 because the uncertainty at low flow rates is dominated by the bias uncertainty of the pressure transducer, which is has a zero that can drift as much as 0.02 in. H_20 at 23°C or 5 Pa throughout an experiment. As the flow rate increases, the effect of the pressure transducer drift on the uncertainty of the blowing ratio decreases and the uncertainty becomes

dominated by the bias error of the mainstream velocity, which is itself dominated by its pressure transducer's bias uncertainty.

1.7.3 UNCERTAINTY OF IR CAMERA MEASUREMENT

To determine the precision uncertainty of the IR camera, IR temperature measurements at z/d = 6, mid-pitch between the coolant jets, were compared. The temperatures between the jets where there was no coolant should have only been affected by changes in mainstream temperature. At each density ratio and blowing ratio condition, IR camera readings at z/d = 6 were averaged and all of the mainstream temperatures were averaged. Each IR camera reading at z/d = 6 was subtracted from the average, which was then subtracted from the difference between the mainstream temperature reading and the mainstream temperature average. The calculations used are written in Equation 0-3 to Equation 0-5. In total, eighty images at steady-state were used for the calculation of precision uncertainty, which produced $U_p = \pm$ 0.67 degrees.

$$D_{x/d,i,M,DR} = (T_{IR,x/d,i,M,DR} - \overline{T}_{IR,M,DR}) - (T_{\infty,x/d,i,M,DR} - \overline{T}_{\infty,M,DR})$$

Equation 0-3

$$S_x = \sqrt{\frac{\sum D^2_{x/d,i,M,DR}}{N-1}}$$

Equation 0-4

$$U_p = \pm 2S_x$$

Equation 0-5

The IR camera bias uncertainty was found by comparing five IR camera calibrations. Figure 0-17 shows the IR camera calibrations that were completed by Sean Klavetter and Noah Mosberg. The calibration shown in black is the average calibration

produced from compiling all of the data from the five experiments, and this was the IR camera calibration that was used to process the IR camera data for this project.

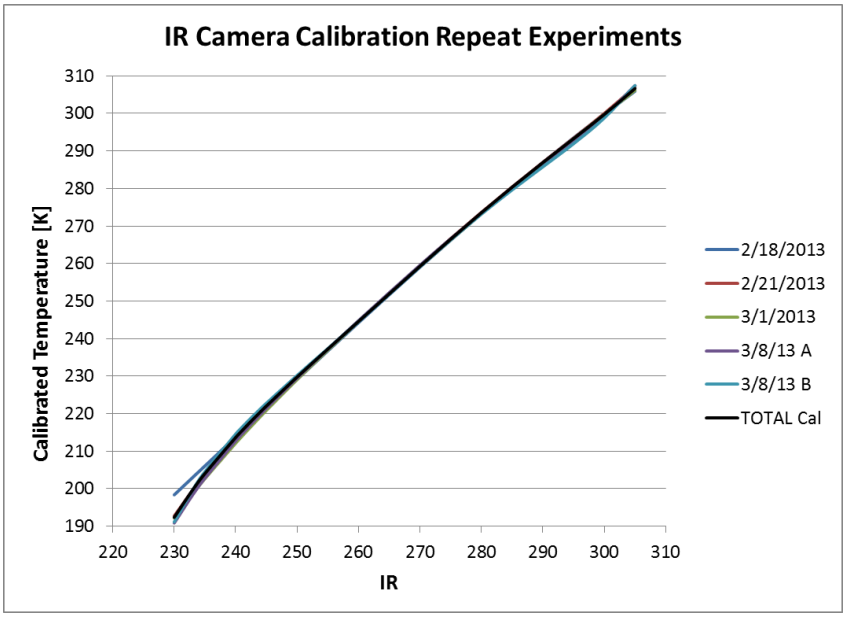

Figure 0-17 Plot of five IR camera calibrations. The IR camera calibration that was created using data from all five experiments and used to process the IR temperature data is shown in black.

The bias uncertainty is a function of IR temperature, which can be seen by observing the deviations between the calibration curves at the highest and lowest temperatures in Figure 0-17. The bias uncertainty was calculated in increments of 5 degrees from IR = 230 to 305 degrees. For each temperature, the standard deviation was calculated based upon the five IR calibrations and using the total calibration value as the mean. The equations for the uncertainty calculation are shown in Equation 0-6 and Equation 0-7. The t statistic corresponding to 5 samples, or 4 degrees of freedom, to 95% confidence is 2.776.

$$S_x = \sqrt{\frac{\sum_{i=1}^{N=5}(T_i - T_{TOTALCAl})^2}{N-1}}$$

Equation 0-6

$$U_b = \pm \frac{2.776 S_x}{\sqrt{5}}$$

Equation 0-7

Figure 0-18 shows the IR camera's bias uncertainty as a function of IR temperature.

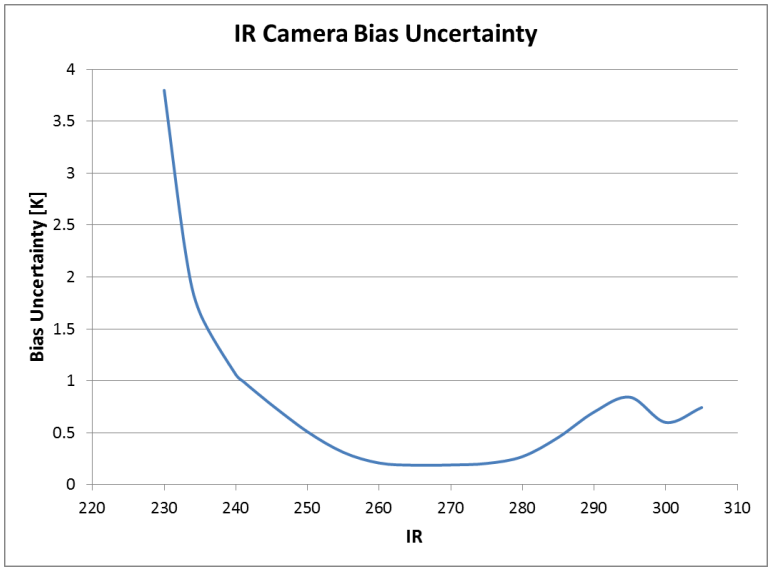

Figure 0-18 IR camera bias uncertainty as a function of IR camera temperature.

For IR temperatures greater than 245 degrees, the uncertainty is within ± 0.85 degrees, which corresponds to effectiveness values below 0.85 at *DR* = 1.5. At *DR* = 1.2, all of the IR camera measurements fall within ± 0.85 degrees. As the effectiveness

increases, or the IR camera reads colder temperatures, the uncertainty shoots up to ± 2.2 degrees at a corresponding η = 1.0 at DR = 1.5.

$U_b = \pm 0.85$ degrees for $\eta \leq 0.85$ at DR = 1.5

for all η at DR=1.2

$U_b = \pm 2.2$ degrees for η = 1.0 at DR = 1.5

The uncertainty of the IR camera increases with decreasing temperature because the IR camera is designed to read certain wavelengths of radiation. As the IR camera reaches its upper wavelength limit and lower temperature limit of 230 degrees, the uncertainty of the readings increases.

1.7.4 UNCERTAINTY OF ADIABATIC EFFECTIVENESS

Adiabatic effectiveness is dependent on temperature measurements of the coolant, mainstream, and adiabatic wall. It is also a function of the amount of coolant exiting the holes since any small change or uncertainty in coolant flow will affect the adiabatic wall temperature that is measured. Equation 0-8 shows how the uncertainty was calculated.

$$U = \sqrt{\left(\frac{\partial \eta}{\partial T_{aw}}\delta T_{aw}\right)^2 + \left(\frac{\partial \eta}{\partial T_{\infty}}\delta T_{\infty}\right)^2 + \left(\frac{\partial \eta}{\partial T_c}\delta T_c\right)^2 + \left(\frac{\partial \eta}{\partial VR}\delta VR\right)^2}$$

Equation 0-8

The coolant temperature and mainstream temperature come from individual thermocouple measurements, and the adiabatic wall temperature is measured by the IR camera. Equation 0-8 shows that adiabatic effectiveness is a function of velocity ratio,

but adiabatic effectiveness could just as easily be a function blowing ratio or momentum flux ratio. For this particular hole geometry, it was found that adiabatic effectiveness scales best with velocity ratio, which is shown in Figure 0-19 a), which is a plot of area averaged adiabatic effectiveness versus velocity ratio at three different density ratios. Figure 0-19 b) shows a curve fit that was generated to calculate the uncertainty of the adiabatic effectiveness as a function of velocity ratio.

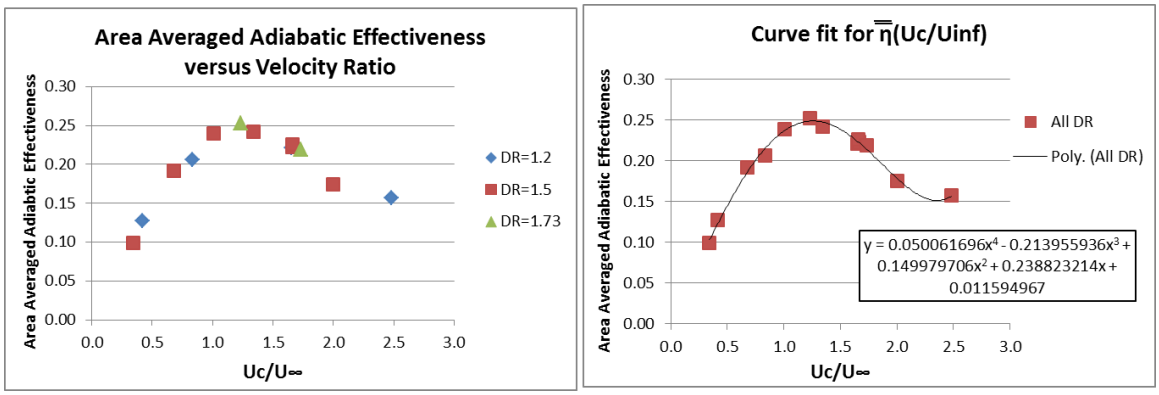

a) b)

Figure 0-19 a) Plot of area averaged adiabatic effectiveness scaling with velocity ratio b) Plot of a curve fit for area averaged adiabatic effectiveness as a function of velocity ratio.

The advantage of using the curve fit for area averaged adiabatic effectiveness over adiabatic effectiveness is that it produces one curve fit that is not a function of downstream distance. To verify that using a function for area averaged adiabatic effectiveness would produce the same derivative as a function of adiabatic effectiveness, a plot of adiabatic effectiveness versus velocity ratio at x/d = 5, 10, 15, 20 is presented in Figure 0-20.

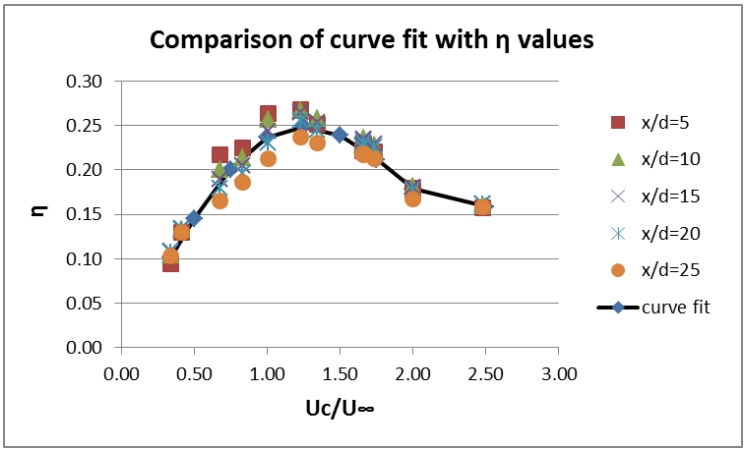

Figure 0-20 Plot of curve fit of area averaged adiabatic effectiveness versus velocity ratio compared to adjusted data of adiabatic effectiveness versus velocity ratio at *x*/*d* positions of 5, 10, 15, 20, and 25.

Depending on the *x/d* position, the adiabatic effectiveness values are different, with the locations closest to the film cooling holes having higher effectiveness. All of the *x/d* profiles shown in Figure 0-20 have been offset from their original values to line up with the curve fit because the point of Figure 0-20 is the ensure that the curve fit provides the same derivative as the adiabatic effectiveness versus velocity ratio curves at the different *x/d* positions. Only the derivative is important because it's what is used in the uncertainty calculation. As Figure 0-20 shows, the curve fit of area averaged adiabatic effectiveness aligns well with the adiabatic effectiveness data at several *x/d* positions. The uncertainty of adiabatic effectiveness versus velocity ratio was calculated using Equation 0-9. To use this equation, the precision and bias uncertainty of the velocity ratio had to be calculated, $\delta U_{p,VR}$ and $\delta U_{b,VR}$, respectively, which depended on the blowing ratio, coolant density, and mainstream density.

$$\delta U = \sqrt{\left(\frac{\partial \eta}{\partial VR}\delta U_{p,VR}\right)^2 + \left(\frac{\partial \eta}{\partial VR}\delta U_{b,VR}\right)^2}$$

Equation 0-9

The uncertainty of adiabatic effectiveness can depend on the particular adiabatic effectiveness value, since Figure 0-18 shows that the bias uncertainty of the IR calibration curve depends on the temperature being measured. Figure 0-21 is a plot of the uncertainty of adiabatic effectiveness for different adiabatic effectiveness values at the density ratios and blowing ratios tested.

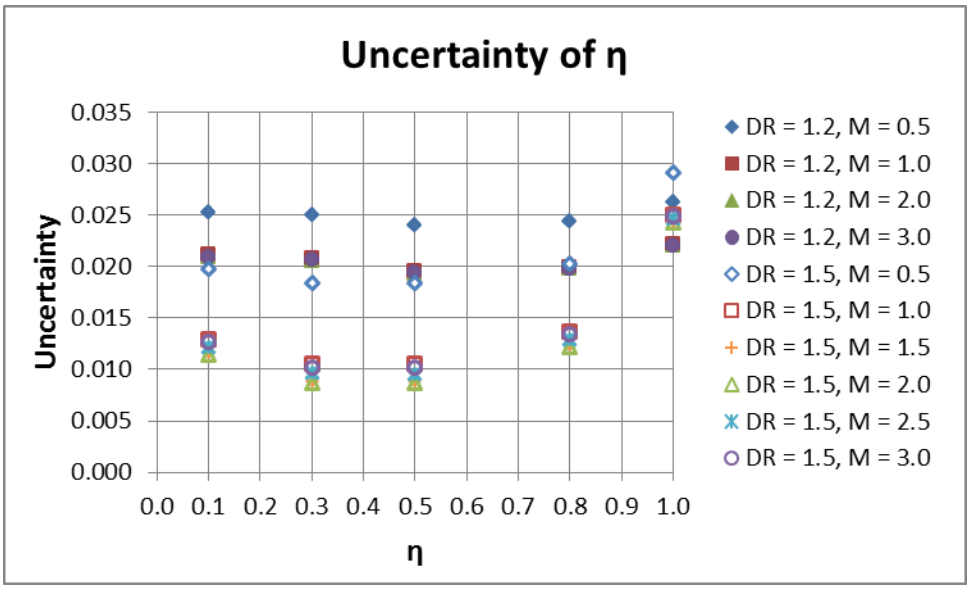

Figure 0-21 Uncertainty of adiabatic effectiveness as a function of adiabatic effectiveness, blowing ratio, and density ratio.

At M = 0.5, the uncertainty is higher than the uncertainty at all other blowing ratios because the uncertainty of the velocity ratio is highest at low flow rates. At low flow rates, the pressure transducer's zero drift dominates the uncertainty of the velocity ratio

measurement. Aside from the data at M = 0.5, the data in Figure 0-21 shows that the uncertainty at DR = 1.5 hovers around 0.01-0.13, and the uncertainty at DR = 1.2 is around 0.02. At DR = 1.5, the uncertainty is lower because the temperature differences are larger—T_{aw} and T_c are colder with respect to T_∞—and the larger temperature difference helps reduce the effect of uncertainties on the calculation of η.

1.7.5 Uncertainty of the Heat Transfer Coefficient

There are two different methods for calculating the heat transfer coefficient, depending on the density ratio of the coolant. At DR = 1.2 and 1.5, the calculation of the heat transfer coefficient depends on q'', ε, T_∞, T_c, the IR camera measurement of $T_{w,}$ and η, which is measured during a different test. Measuring the heat transfer coefficient at unit density ratio only relies on q'', T_{iw}, ε, and T_∞, which requires a different uncertainty analysis than the heat transfer coefficient measurements at high density ratio. Equation 0-10 was used to calculate the uncertainty of h_f at DR = 1.2 and 1.5. The heat flux generated from the heat flux plate based upon the voltage and current, q'', is adjusted with a radiation correction. The heat flux plate was painted with a matte black acrylic paint, and the emissivity was assumed to be 0.98 ± 0.02.

$$h_f = \frac{q'' - \sigma\varepsilon(T_w^4 - T_\infty^4)}{T_w - (\eta(T_c - T_\infty) + T_\infty)} \quad \text{at } DR = 1.2 \text{ \& } 1.5$$

Equation 0-10

The uncertainty in h_f was calculated at η = 0.3 and 0.5. To complete the uncertainty analysis properly, the locations in the centerline of the jets where η = 0.3 and 0.5 during the adiabatic effectiveness experiment were found, and the corresponding T_w temperatures from the heat transfer experiment were found at the same locations. Higher η values were not considered because the heat flux plate was not present between x/d = 0

and 2, where the higher values are located, so T_w could not be found in those locations. Figure 0-22 a) shows the results of the uncertainty analysis of h_f versus M as a function of η and DR and Figure 0-22 b) shows the uncertainty analysis of h_f as a function of h_f as a function of η and DR. As can be seen in Figure 0-22 a), the heat transfer coefficient is a strong function of M, especially at M = 0.5. The uncertainty in h_f is dominated by the uncertainty in η and T_w and can be assumed to be within ± 6 W/m^2·K. The areas with the lowest uncertainty are the areas where the adiabatic effectiveness is highest: downstream of the jets, closest to the film cooling holes. In these regions there is a larger temperature difference between the surface and the mainstream when measuring η, which reduces the uncertainty of h_f.

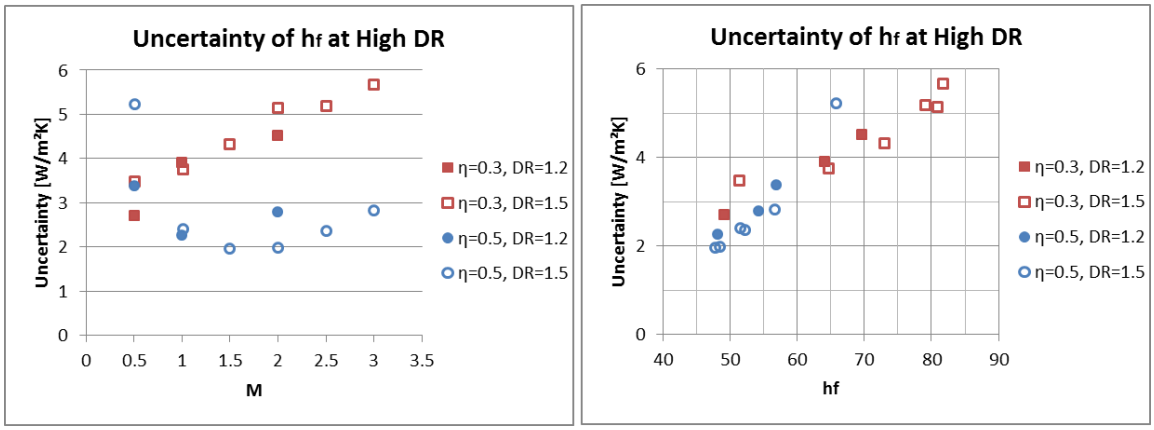

a) b)

Figure 0-22 a) Uncertainty of h_f as a function of M for η = 0.3, 0.5 and DR = 1.2, 1.5. b) Uncertainty of h_f as a function of h_f for η = 0.3, 0.5 and DR = 1.2, 1.5.

At M = 0.5 and DR = 1.2, the uncertainty is less than at M = 0.5 and DR = 1.5, which is counterintuitive. The uncertainty is dominated by adiabatic effectiveness and Equation 0-10 shows that η is multiplied by the temperature difference between the

coolant and mainstream. The temperature difference is lower at DR = 1.2 than at 1.5, which decreases the effect of the uncertainty of η.

Equation 0-11 shows the equation that was used to calculate h_f at unit density ratio.

$$h_f = \frac{q'' - \sigma\varepsilon(T_{iw}^4 - T_\infty^4)}{T_{iw} - T_\infty} \qquad \text{at } DR = 1.0$$

Equation 0-11

The uncertainty of h_f at unit density ratio was dominated by bias and precision uncertainties of T_{iw} as well as the bias uncertainty of ε. As the temperature difference between the wall and mainstream increases, the uncertainty of h_f decreases. Figure 0-23 a) shows the uncertainty of h_f versus h_f and Figure 0-23 b) shows the percentage uncertainty of h_f versus h_f.

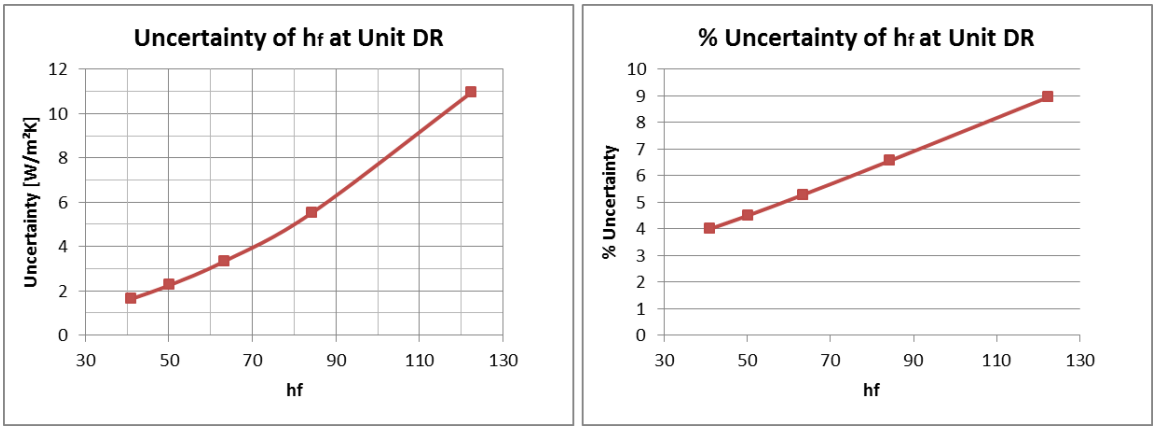

a) b)

Figure 0-23 a) Uncertainty of h_f versus h_f at unit density ratio
b) Percentage uncertainty of h_f versus h_f at unit density ratio

There will be increased heat transfer coefficients downstream of the jets as well as at the start of the heat flux plate where a new, very thin thermal boundary layer begins, producing an almost infinite heat transfer coefficient that decreases with increasing downstream distance. The lowest T_w temperature that the IR camera can resolve at the upstream edge of the heat flux plate corresponds to an h_f of 122 W/m^2·K, which would produce an uncertainty of ± 11 W/m^2·K, or ± 9% uncertainty. The uncertainty over most of the rest of plate will be within 6% uncertainty. What is interesting to note is that at *DR* = 1.0, the uncertainty will increase downstream of the jets due to the smaller temperature difference between the surface and mainstream, but at high density ratio, the uncertainty will decrease since the uncertainty of η decreases with higher effectiveness values in the jet. The uncertainty values shown in Figure 0-23 a) and b) are also applicable to the uncertainty of h_0 since it's the same measurement only without the mainstream temperature jets operating.

Figure 0-24 shows the uncertainty of h_f/h_0 at high density ratio. Like the uncertainty of h_f, the uncertainty of h_f/h_0 is dominated by the uncertainty of η, and is lower at regions where adiabatic effectiveness is larger. The uncertainty downstream of the jets can be assumed to be ± 0.10 and farther downstream ± 0.16, which is quite high, making it difficult to meaningfully compare results in terms of h_f/h_0.

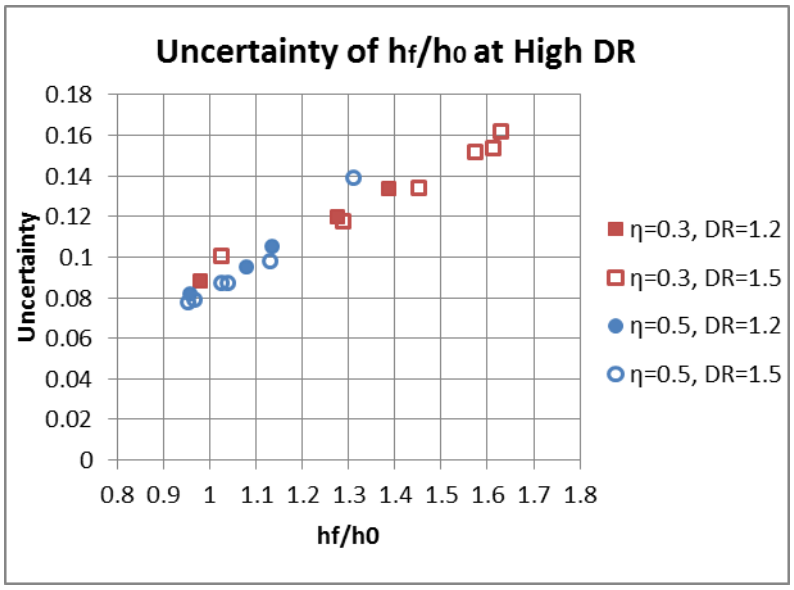

Figure 0-24 Uncertainty of h_f/h_0 at high DR versus M for DR = 1.2 and 1.5.

The uncertainty of h_f/h_0 at DR = 1.0 is lower, with the uncertainty of the heat transfer coefficient augmentation being within ± 0.06 to 0.10 for the measurements taken, which is shown in Figure 0-25.

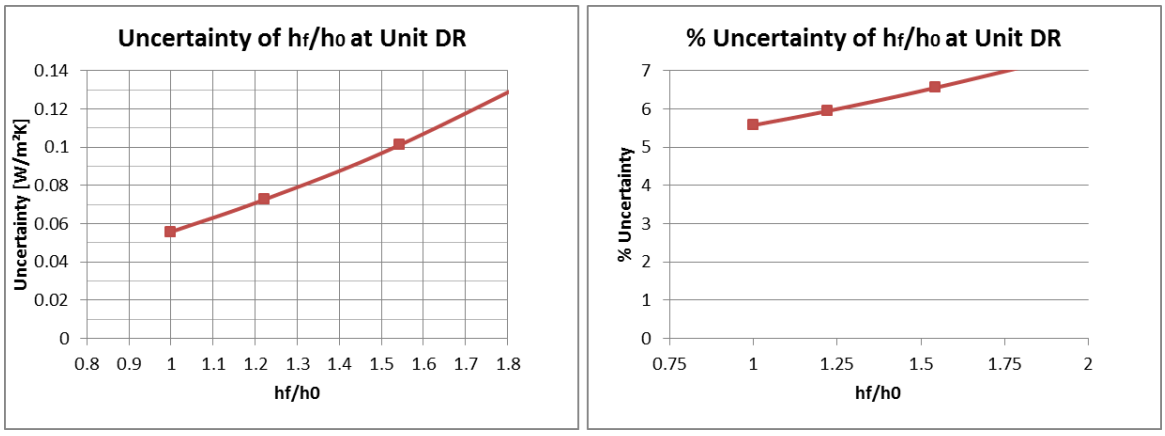

a) b)

Figure 0-25 Uncertainty of h_f/h_0 at unit density ratio.

1.7.6 UNCERTAINTY OF THERMAL FIELD MEASUREMENTS

The microthermocouple that was used for the thermal field measurements was calibrated using a thermocouple bath. The thermocouple was calibrated from 250-340 K and the calibration curve is shown in Figure 0-26. A thermistor was used as the standard temperature and was accurate within ± 0.01 K. The thermistor would not measure temperatures below 273 K, so for the temperatures from 250-273 K, the thermocouple calibration bath readout was used, which was accurate to ± 0.05 K. Figure 0-26 is a plot of the thermistor or thermocouple bath readout versus the thermocouple reading Labview. There was a standard NIST type E thermocouple calibration imbedded Labview, so the thermocouple calibration is really calibrating the thermistor reading to the NIST calibration, which is why the calibration is linear, not a polynomial.

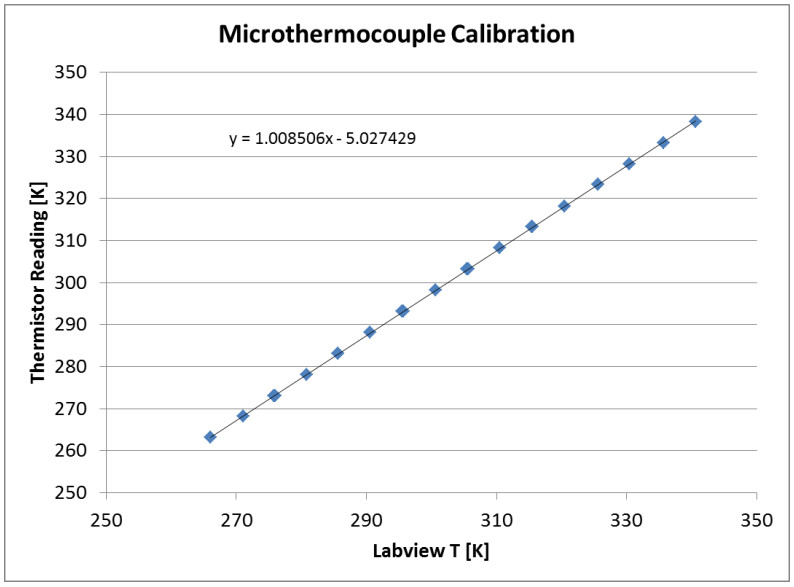

Figure 0-26 Microthermocouple calibration

The bias uncertainty of the thermocouple was found using a standard error of fit analysis. Equation 0-12 was used to calculate the standard deviation, where m and b are

the slope and intercept of the calibration, x is the thermocouple reading, and y is the thermistor reading. Equation 0-13 and Equation 0-14 were used to calculate the uncertainty of the slope and the uncertainty of the intercept, respectively.

$$S = \sqrt{\frac{\sum_{i=1}^{N}(y_i - mx_i - b)^2}{N-2}}$$

Equation 0-12

$$\delta m = S\sqrt{\frac{N}{(N\sum_{i=1}^{N}x_i^2) - (\sum_{i=1}^{N}x_i)^2}}$$

Equation 0-13

$$\delta b = S\sqrt{\frac{\sum_{i=1}^{N}x_i^2}{(N\sum_{i=1}^{N}x_i^2) - (\sum_{i=1}^{N}x_i)^2}}$$

Equation 0-14

This analysis produced a bias uncertainty of ± 0.5-0.6 K, depending on the temperature. The precision uncertainty was found from repeat thermocouple measurements of the same temperature, which was calculated to be ± 0.04 K. The total uncertainty is ± 0.05-0.06 K.

1.7.7 ADIABATIC EFFECTIVENESS BIAS BETWEEN COOLANT JETS

An ongoing issue with the adiabatic effectiveness data was an increased adiabatic effectiveness between the coolant jets. The coolant holes were spaced fairly far apart—6*d*—and the jets should not spread enough laterally to touch one another until far downstream. The contour plots of adiabatic effectiveness show that there was a region

between the jets with increased adiabatic effectiveness where there was no coolant. At DR = 1.2, η = 0.04 and at DR = 1.5 η = 0.035 between the jets where there was no coolant. This would correspond to a surface temperature that was 2-4 K lower than expected, depending on the density ratio. Without knowing the cause of the temperature offset, it's hard to adjust the data to account for it. Interestingly, this error was present in Penn State University's data as well, although to a lesser degree. The issue of increased adiabatic effectiveness between coolant jets was revisited several times over the course of a year to try and pin down the cause. The following potential causes were studied:

1. Bias of the IR camera calibration at mainstream temperature
2. Conduction error through the bottom of the flat plate
3. A cool boundary layer

1. Bias of the IR Camera Calibration

When a calibrated temperature doesn't look correct, the first thing to check is the accuracy of the calibration. Figure 0-27 shows five IR calibrations as well as the final combined IR calibration used to process the data, which shown in black. The orange dot corresponds to the average IR temperature between the coolant jets for an experiment on the x axis and the average mainstream temperature taken during the same experiment on the y axis. If η = 0 between the jets for that experiment, the calibration curve would need to go through the orange data point. Comparing the scatter of the IR calibration curves to where the orange point is, clearly the orange point is outside the range of scatter, which would indicate that the IR temperature being measured between the jets is real, and not a calibration error.

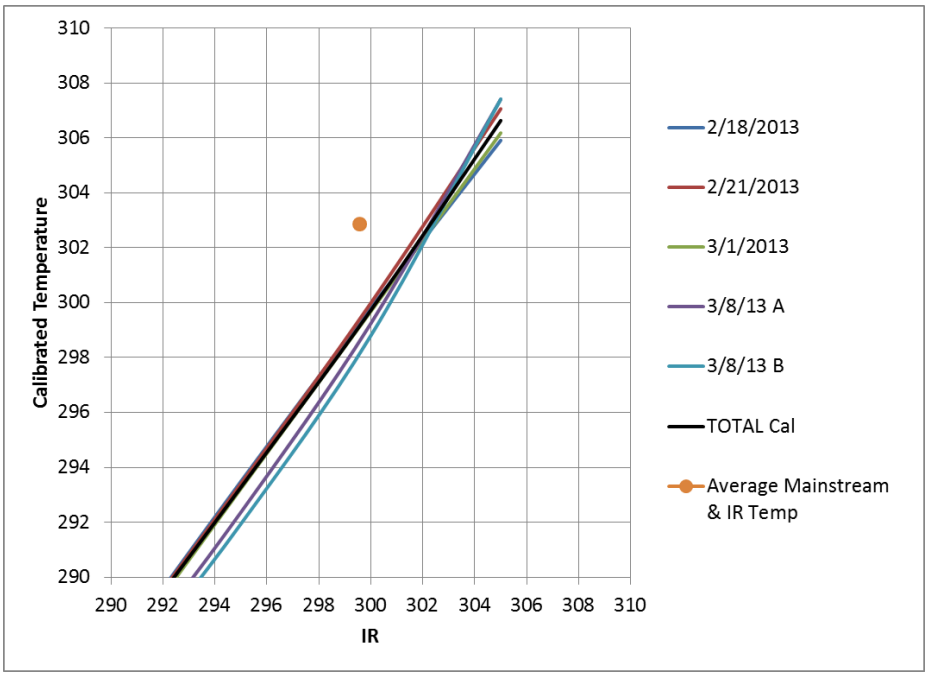

Figure 0-27 Repeated IR camera calibrations compared to where the IR camera curve would need to lie for $\eta = 0$ between coolant jets.

One could speculate that there is an error in the calibration process that would produce an error at room temperature, but any of those potential sources, such as thermocouple conduction error or difference in emissivity between the test surface and the thermocouples used to calibrate the IR camera have already been identified and do not exist in the IR camera calibration method used. Another possibility that was explored was a thermocouple calibration error in which the copper calibration plates would read a different mainstream temperature than the thermocouple used to measure the mainstream. This theory was also eliminated by suspending the copper calibration plates in the mainstream, which showed that they read the same temperature as the mainstream thermocouple.

2. Conduction Error Through the Bottom of the Flat Plate

Another obvious source that could cause the increased effectiveness between the jets is conduction error through the bottom of the flat plate. As mentioned above, the temperature of the mainstream was warmer than the temperature of the lab. This could cause heat to be transferred from the warmer wind tunnel to the cooler lab, cooling the surface. Upon closer examination, this can't be the cause of the increased effectiveness between the jets because there is only a 7 K difference between the mainstream temperature and lab temperature, and the decreased temperature between the jets is on the order of 3-4 K. The plate consisted of 0.5 inches of polystyrene foam, and underneath were 0.75 inches of plywood and 4 inches of fiberglass insulation. This amount of insulation coupled with the fact that the heat transfer coefficient in the wind tunnel is much higher than the stagnate air in the lab rules out the possibility of conduction error causing the increased adiabatic effectiveness between the jets.

3. A Cool Boundary Layer

There could have been a cool boundary layer that was cooling the surface between the jets, causing increased adiabatic effectiveness. A boundary layer could develop along the sides of the wind tunnel because the mainstream is heated and, with the exception of the bottom of the test section, the sides of the wind tunnel are uninsulated. Another source of a cool boundary layer could be from the mainstream flowing over the coupon, which is cooler due to the coolant plenum being underneath it. Both sources could supply the thermal boundary layer together, compounding the effect.

To observe whether there was a boundary layer along the sides of the wind tunnel due to heating the mainstream, a gas type thermocouple was traversed along the bottom of the test section 4 inches upstream of the suction slot. The measured profile is shown in Figure 0-28.

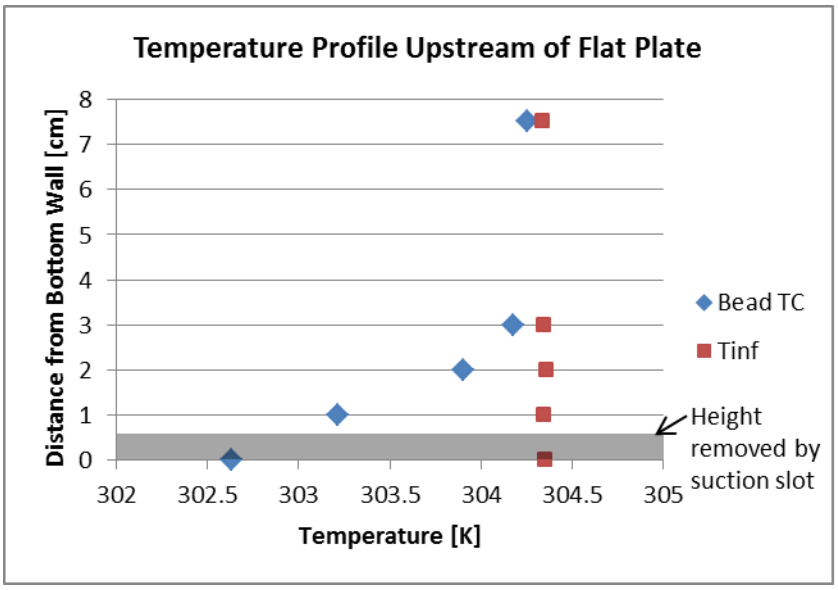

Figure 0-28 Cool thermal boundary layer measured 4 inches upstream of the suction slot along the bottom of the test section.

The measured mainstream is shown in red and the thermocouple readings are in blue. The grayed out area indicates the approximate height of air that would be removed from the tunnel by the suction slot. Comparing the blue profile at the edge of gray box to the mainstream temperature, the profile is about 1.4 K cooler than the mainstream. The boundary layer is thick, so it's possible for it to survive some distance as it travels over the flat plate. Figure 0-29 shows thermal boundary layer measurements 1.5 inches upstream of the coolant holes on the flat plate. The lab temperature is usually 295-296 K, and the figure shows a blue profile that was taken with the mainstream set at 298 K and a red profile with the mainstream set at 303 K, which is normal mainstream operating temperature. In addition to measuring the thermal boundary layer with a bead thermocouple, a surface thermocouple was attached to the surface to provide a more accurate surface temperature measurement. Those points are shown with open symbols.

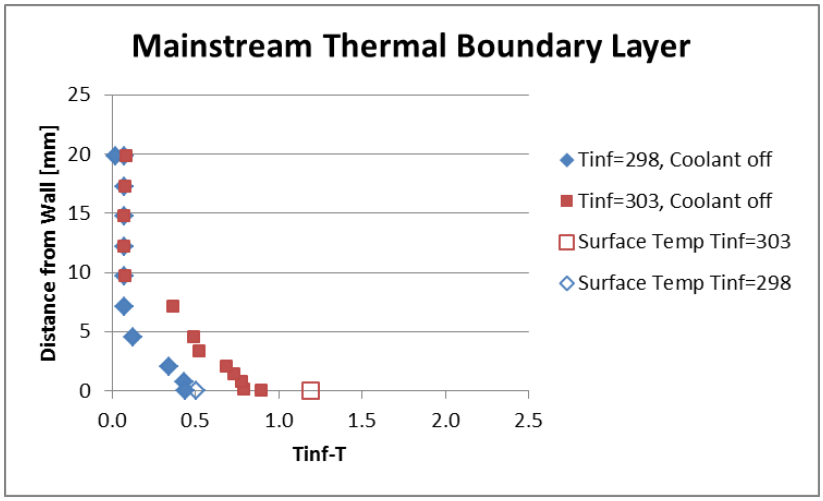

Figure 0-29 Thermal boundary layer measurements 1.5 inches upstream of coolant holes with slightly heated mainstream and fully heated mainstream.

The figure verifies that there is indeed a cool boundary layer that grows in strength with increased mainstream temperature.

Another experiment involved attaching thermocouples installed on thin copper plates (the same plates used to calibrate the IR camera) to the bottom surface of the wind tunnel. When the plates were attached to flat plate, they consistently read 1.2 degrees cooler than the mainstream. When the same copper plates were suspended in the center of the test section, all of the plates agreed with the mainstream temperature reading with 0.2 K.

The experiments just described helped confirm that there was a cool boundary layer that developed along the length of the wind tunnel that propagated over the flat plate. However, the experiments only explained a 1-1.2 K difference between the plate surface and the mainstream. The effectiveness between the jets showed a 3.5-4 K difference, so the source of the other 2-2.5 K cooling effect has yet to be explained. In another test, one film cooling hole was blocked with tape while the surrounding jets remained active at M = 2.0, DR = 1.5. Figure 0-30 shows the adiabatic effectiveness

downstream of the blocked jet at $z/d = 6$. Even when there was no jet interaction present, there was increased effectiveness starting at 0.04 at $x/d = 2$ that decayed very slowly down to 0.03 at $x/d = 23$. The slow decay would indicate that the boundary layer was thick, otherwise it would dissipate quickly on the insulated surface.

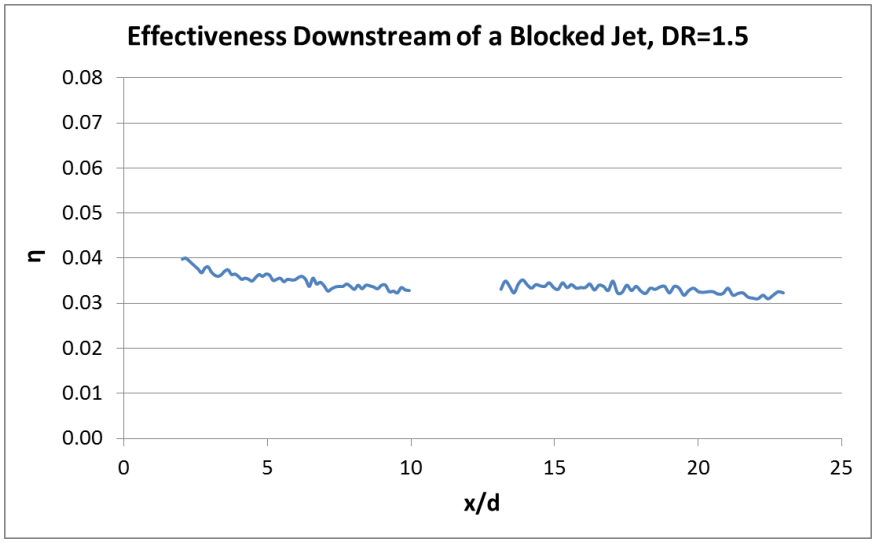

Figure 0-30 Adiabatic effectiveness downstream of a blocked jet while other jets are blowing at $M = 2.0$, $DR = 1.5$, $z/d = 6$.

Figure 0-31 shows lateral plots of adiabatic effectiveness at $x/d = 3$, 8, and 20 from the same experiment where one coolant hole was blocked. The top three plots show the lateral profiles at full scale, and the figures underneath are zoomed-in views of the same plots, which clearly show the lower effectiveness values.

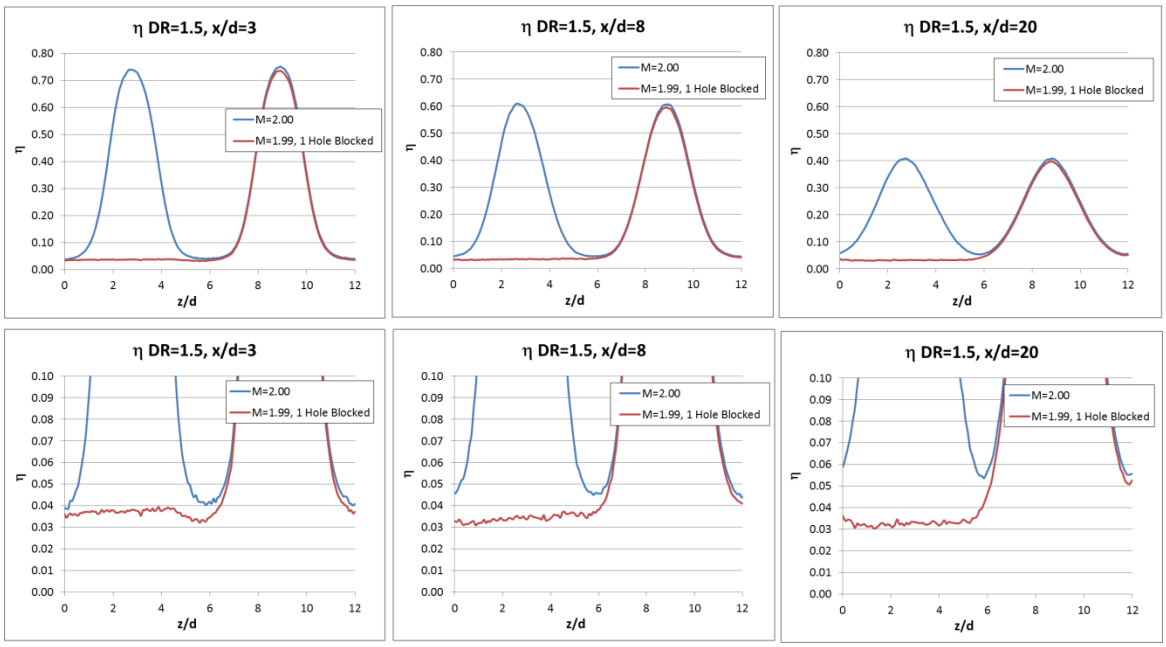

Figure 0-31 Lateral plots of adiabatic effectiveness with both coolant holes active (blue) and with one coolant hole blocked (red).

The figure shows that at $x/d = 3$, the coolant jets had not joined, but by $x/d = 8$, the jets started interacting. It can also be seen that the increased effectiveness is not caused by any lateral spreading of the jet or lateral conduction through the foam.

To test whether a cooled plenum exacerbates the cool boundary layer, two coolant holes were taped over and coolant was fed through the plenum at $DR = 1.46$. The coolant was able to escape from 6 holes that were not taped over. A surface thermocouple and a thin copper plate with a surface thermocouple on top were installed on the surface $8.5d$ downstream. Figure 0-32 shows the results.

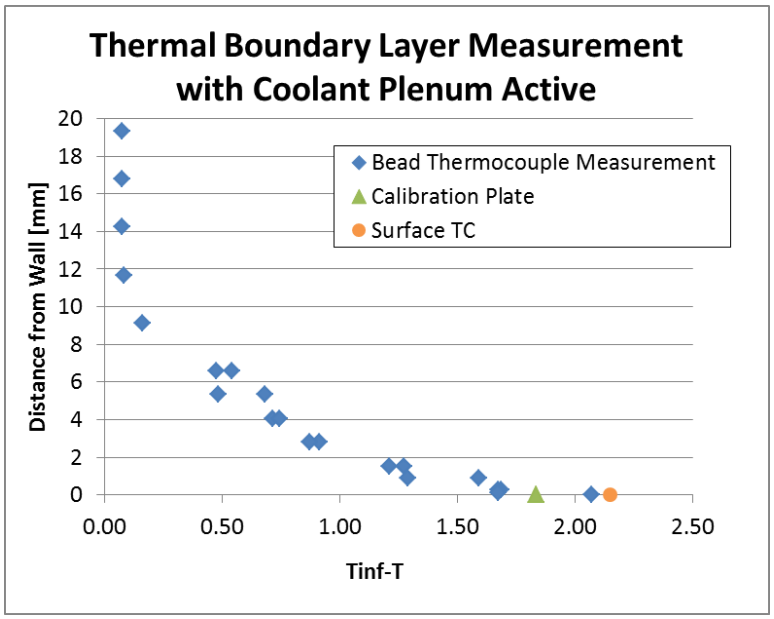

Figure 0-32 Thermal boundary layer measured 4*d* downstream of coolant holes with coolant flowing through plenum.

The yellow dot indicates the temperature of the surface thermocouple and the green triangle indicates the temperature of the copper plate. The relationship between the two thermocouples and the thermal boundary layer profile was as expected. The surface thermocouple read slightly cooler than the bead thermal profile measurement since it was directly attached to the surface. The thermocouple on the copper plate read slightly warmer since it was slightly raised off the surface and may also have created a flow disturbance that would warm the thermocouple. Figure 0-32 shows that the temperature of the surface was about 2.2 K cooler than the mainstream, which was twice what was measured without the plenum operating. This would indicate that the increased effectiveness between the jets was due in part to an approach boundary layer from the bottom of the wind tunnel and part due to the mainstream flowing over the coupon that was cooled by the coolant in the plenum. The 2.2 K temperature difference between the surface and mainstream shown in Figure 0-32 still doesn't show a 3.5-4 K decrease in

temperature at the wall as what would be indicated by the effectiveness measurements, and it's uncertain as to whether there is another source causing the additional increase or whether it can be attributed to uncertainty.

The data at PSU showed similar increased effectiveness between jets, which was of similar magnitude as UT's at $DR = 1.5$. At $DR = 1.2$, the effectiveness between the jets stayed the same or was slightly increased in UT's data, but decreased in PSU's data. For the following discussion, data at $M = 0.5$ will be used as an example, since the trends to be discussed are easiest to notice at this blowing ratio, but the same trends are present for other blowing ratios. Figure 0-33 is a plot of lateral η profiles at $M = 0.5$, $DR = 1.5$, and $x/d = 0$, 3, 8, and 20. The figure is zoomed-in to look at effectiveness values between the jets, and it compares UT's data to PSU's data using the exact same cooling holes that were machined in polystyrene at PSU and tested at both labs.

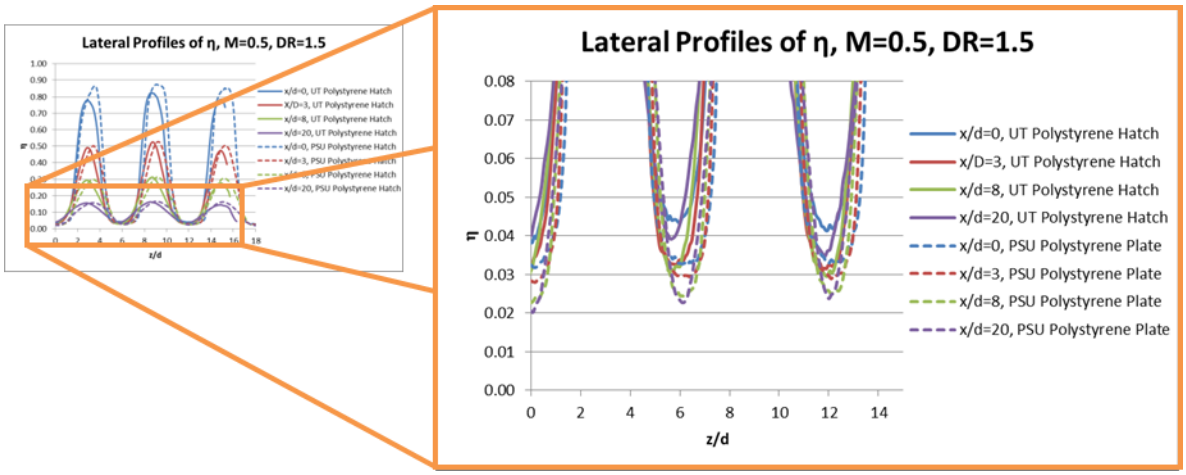

Figure 0-33 Zoomed-in view of lateral plot of η at $x/d = 0$, 3, 8, and 20 at $M = 0.5$ and $DR = 1.5$.

Focusing on the effectiveness values between the jets at z/d = 6 and 12, there is a clear trend. For PSU's data, in the dashed lines, η between the jets was highest at x/d = 0 and gradually dropped with increasing x/d. For UT's data, the effectiveness between the jets was also highest at x/d = 0, decreased for x/d = 3 and 8, and then increased again at x/d = 20. It appears that there was a cool boundary layer that slowly dissipated with downstream distance for both data sets, but at x/d = 20, the jets started to merge in UT's data which increased the effectiveness between the jets. For PSU's data, it appears that the jets didn't merge, at least up to x/d = 20, which is why the effectiveness between the jets continued to decrease with increasing downstream distance. Figure 0-34 shows a similar plot at DR = 1.2

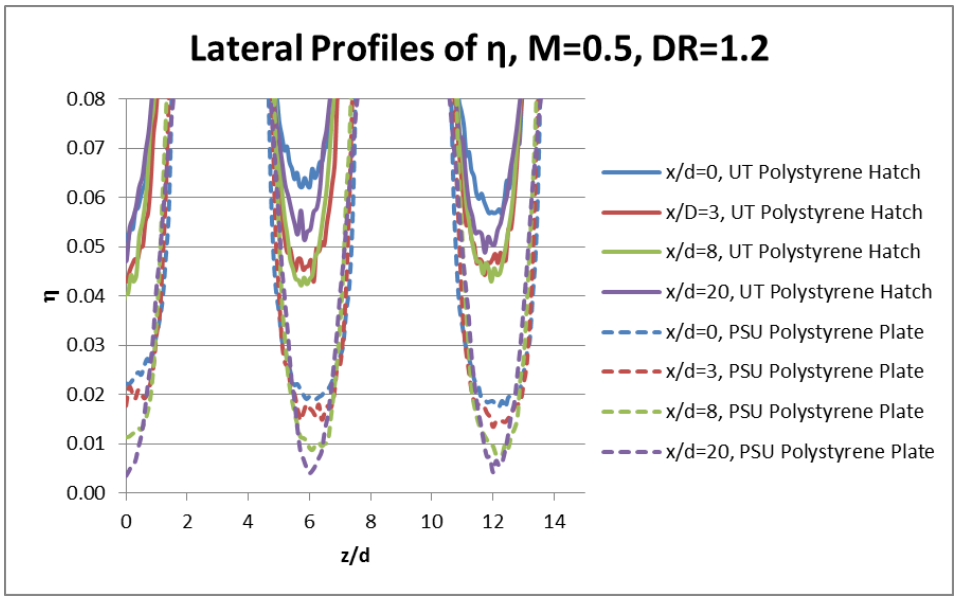

Figure 0-34 Zoomed-in view of lateral plot of η at x/d = 0, 3, 8, and 20 at M = 0.5 and DR = 1.2.

The same trend of mid-pitch effectiveness versus x/d is present. At DR = 1.5, the increased effectiveness between the jets was of similar magnitude between PSU's and

UT's data. However, at DR = 1.2, the effectiveness between the jets decreased in PSU's data, while it increased in UT's. Without knowing more about PSU's test setup, it's hard to speculate why the trend between the two labs does not hold at DR = 1.2. If the increased effectiveness between the jets were only due to conduction from the plenum through the polystyrene, it would make sense for the effectiveness to scale with density ratio i.e. as the coolant gets colder, the temperature between the jets would decrease, but effectiveness would stay the same. However, PSU's data shows that the effectiveness between the jets is lower at DR = 1.2 than at 1.5, but UT's data shows the opposite trend where the effectiveness between the jets is higher at DR = 1.2 than at DR = 1.5. One way to explain the effectiveness increasing between the jets at DR = 1.2 is that the magnitude of the thermal boundary layer developing along the sides of the wind tunnel remains constant at DR = 1.2 and DR = 1.5, so when η is calculated, the same 1 K cooler surface temperature appears as η = 0.01 at DR = 1.5 and η = 0.02 at DR = 1.2. It's possible that part of the cold boundary layer scales with density ratio, but part of it is constant despite density ratio, which would increase the effectiveness between the jets more at DR = 1.2 than at DR = 1.5

Figure 0-35 shows lateral profiles at additional x/d positions for M = 0.5 and DR = 1.2 and further demonstrates the trend of effectiveness between the jets with downstream distance previously mentioned.

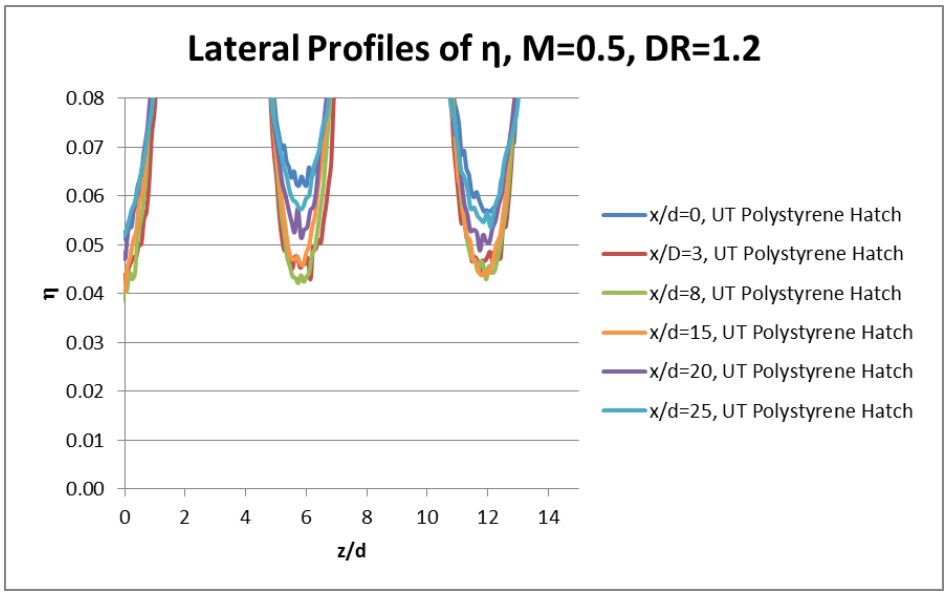

Figure 0-35 Lateral profiles of UT's data at $DR = 1.2$ and $x/d = 0$, 3, 8, 15, 20, and 25.

The effectiveness between the jets was highest at $x/d = 0$, which then started to decrease up to $x/d = 8$, and then increased up to $x/d = 25$. The reduced temperature between the jets could be due to a cold boundary layer that decayed up to $x/d \approx 8$ until the jets started to merge, at which point the effectiveness between the jets started to increase with increasing x/d. Figure 0-36 shows the contour plot of adiabatic effectiveness at $DR = 1.2$ and $M = 0.5$ and depicts approximately where the jets started to merge at this blowing ratio and density ratio.

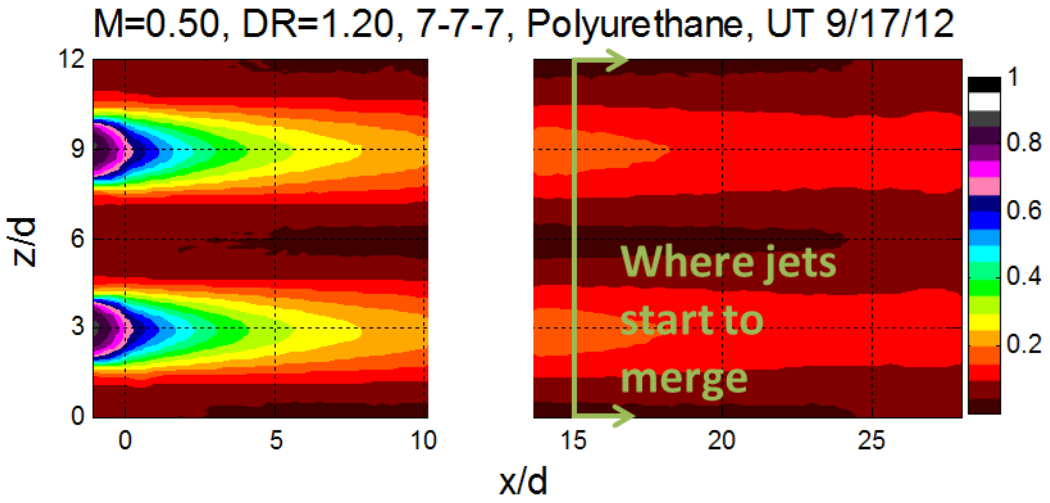

Figure 0-36 Contour of η at M = 0.5, DR = 1.2. Jets start to merge together at approximately x/d = 15.

Two tests were run, in which one used a coupon made out of polystyrene and another used a coupon made out of polyurethane. Polyurethane's thermal conductivity is 50% larger than the thermal conductivity of polystyrene. Figure 0-37 shows a lateral plot of adiabatic effectiveness at M = 0.5 and DR = 1.5 comparing results from coupons made of the two different materials, which contained the same shaped hole geometry. There was no clear trend that would indicate that increased conduction through the polyurethane coupon was causing greater increases in effectiveness between the jets.

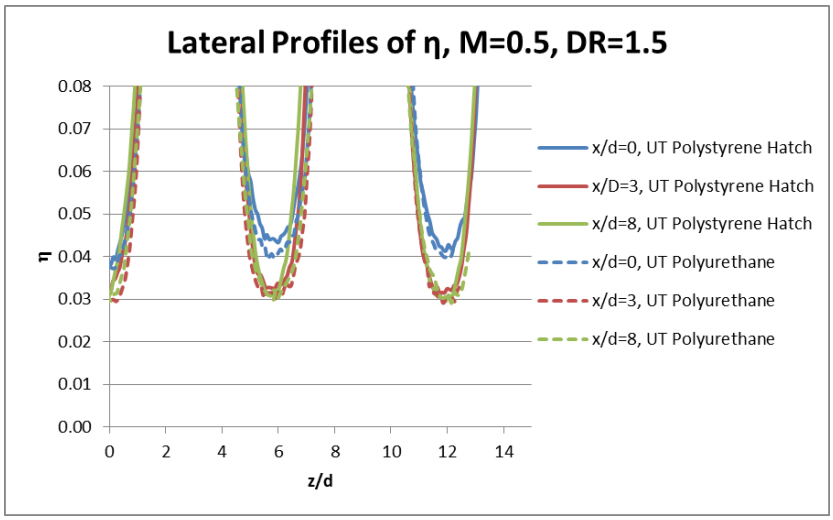

Figure 0-37 Lateral profiles at $M = 0.5$, $DR = 1.5$ comparing coupons made out of polystyrene ($k = 0.029$ W/m^2·K) and polyurethane ($k = 0.044$ W/m^2·K) with the same hole geometry.

Figure 0-38 shows another confounding data set. A test was operated with the mainstream temperature reduced to 296 K from the normal operating condition of 303 K, which should have decreased, if not eliminated any approaching boundary layer that formed along the sides of the wind tunnel. The effectiveness between the jets may have decreased at $x/d = 0$, but the other downstream positions agreed quite well between the two tests.

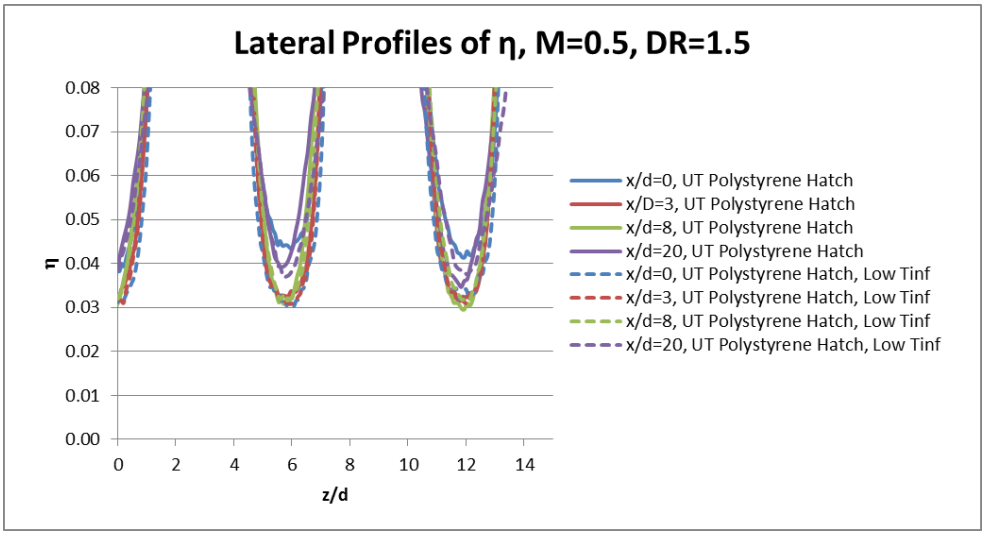

Figure 0-38 Lateral plots of η at x/d = 0, 3, 8, and 20 at M = 0.5 and DR = 1.5. Solid lines show data taken with the mainstream heated to 303 K and dashed lines show data taken with the mainstream at 296 K, approximately the temperature of the lab.

Now the question remains: how should this effect be included in the uncertainty analysis? The measurement of the increased adiabatic effectiveness between the jets was real, and with the data available, the best explanation is that it was due to a cool thermal boundary layer that developed along the sides of the wind tunnel, which was then exacerbated by flowing over a cold foam coupon that was cooled by the coolant plenum. With this scenario, a cool boundary layer would certainly cool the areas of the plate that aren't affected by the coolant jets, but it is unclear what effect the boundary layer would have in the regions where the jets are located. Therefore, it's not appropriate to uniformly subtract η = 0.035 at DR = 1.5 and η = 0.04 at DR = 1.2 because the area underneath the jet may not be affected by the thermal boundary layer. For this reason, no correction due to the boundary layer effect was made to the data.

1.7.8 BIAS ERROR FROM COOLANT TEMPERATURE MEASUREMENT LOCATION

In the past, UT measured the coolant temperature at the entrance of the coolant holes to account for any additional warming that was taking place in the plenum. When verification of the 7°-7°-7° shaped hole performance began and testing parameters between PSU and UT were matched, UT changed the coolant temperature location from the coolant hole entrance to 1.5 inches beneath the coupon inside the plenum to match what was used at PSU. When the plenum temperature is compared to two bead thermocouples installed at coolant hole entrances, it is significantly lower at low blowing ratios, providing a source of error, which would decrease the reported density ratios and blowing ratios and increase reported adiabatic effectiveness values. Since the goal of this project was to reproduce PSU's film cooling results, the coolant temperature location was not changed, but the results will be biased from those that would use the coolant temperature exiting the holes, which is how adiabatic effectiveness is defined. Figure 0-39 shows the bias error of measuring T_c in the plenum versus at the coolant hole entrance.

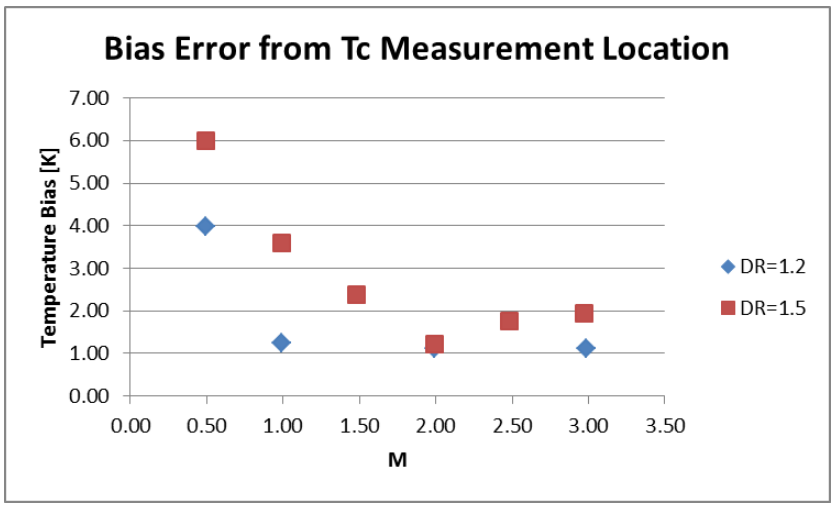

Figure 0-39 Bias error associated with measuring T_c in the plenum versus at the entrance of the coolant holes.

The figure shows that as the blowing ratio decreases, the bias error increases. This is because at low *M*, the coolant will stay in the plenum longer, giving it more time to warm. The plenum is heavily insulated, with 0.75 inch polystyrene lining the inside and a 4 inch layer of fiberglass insulation wrapped around the outside. The warming seen between where the plenum thermocouple is located and the coolant hole entrance most likely comes from conduction through the coupon. The data at *DR* = 1.2 and 1.5 does not collapse because for a given blowing ratio, the temperature difference between the coolant and mainstream at *DR* = 1.5 is twice the amount as at *DR* = 1.2, which will lead to a greater temperature difference between the plenum and hole entrances. In addition, the coolant velocity at *DR* = 1.2 is higher than at *DR* = 1.5 for a given blowing ratio, which would also reduce the degree of warming.

One caveat of using the hole entrance temperatures from two thermocouples is that the temperatures varied between them, especially at low *M*, which increases the bias uncertainty of the measurement. The thermocouples were attached to the coupon very carefully so that the thermocouple beads were positioned in the center of the coolant holes to provide a consistent location for the measurement of the entering the holes. The variation between the temperature readings is most likely due to the unsteadiness of the coolant flow. For instance, at a given blowing ratio and density ratio, there may be several degrees of variation between the two coolant hole entrance thermocouples readings, but if several points at the same density ratio and blowing ratio are averaged, the averaged values agree much better.

Table 0-4 shows an analysis of the coolant temperature for an experiment. The third column is the plenum thermocouple reading, the fourth column is the bias associated with measuring the coolant temperature in the plenum, the fifth column is the a nominal hole entrance temperature found by adding the bias to the plenum temperature, and the sixth column is the bias error of measuring the coolant temperature at the hole entrance. The last column is the percentage bias uncertainty of the coolant hole entrance

thermocouple reading. Upon examining this column, the bias uncertainty is significant at the low blowing ratios of $M = 0.5$ at $DR = 1.2$ and $M = 0.5$ and 1.0 at $DR = 1.5$

Table 0-4 Uncertainty of coolant temperature due to the measurement location. Temperatures are in Kelvin.

		Nominal Values				
DR	M	Plenum	Bias	Hole Entrance	Ub Hole Ent.	%
1.19	0.50	252.3	3.99	256.3	3.50	1.37
1.20	0.99	252.6	1.25	253.9	1.00	0.39
1.21	2.00	250.0	1.12	251.1	0.50	0.20
1.22	3.01	248.7	1.12	249.8	0.10	0.04
1.45	0.50	204.2	6.00	210.2	6.00	2.85
1.47	1.01	204.0	3.60	207.6	3.00	1.45
1.47	1.49	203.9	2.39	206.3	2.00	0.97
1.48	1.99	203.5	1.21	204.7	0.90	0.44
1.50	2.50	201.5	1.75	203.2	0.70	0.34
1.50	3.00	198.9	1.95	200.9	0.80	0.40

If the bias in the temperature reading is taken into account, it can affect the nominal readings of density ratio, blowing ratio, adiabatic effectiveness, and heat transfer coefficient at $DR = 1.2$ and 1.5. Table 0-5 shows the nominal density ratio reading and the density ratio after it has been adjusted for the coolant temperature bias. The last column shows the uncertainty in density ratio, which is greatest at low blowing ratios. It should be noted that these values also include adjustments made to the calculation of coolant density, which was discussed in Section 1.7.1. The largest adjustments in density ratio are at the lower blowing ratios. At $M = 3.0$, the density ratio increases because the adjustment from accounting for static pressure in the plenum overpowered the correction from the coolant temperature bias, which was only 1-2 K.

Table 0-5 Change in density ratio from adjusting the bias due to the coolant measurement location.

DR		
Nominal Value	**Adjusted Bias**	**Uncertainty**
1.20	1.19	0.02
1.20	1.20	0.01
1.21	1.21	0.01
1.21	1.22	0.01
1.49	1.45	0.04
1.49	1.47	0.02
1.49	1.47	0.02
1.49	1.48	0.01
1.50	1.50	0.01
1.51	1.50	0.01

Table 0-6 shows that adjusting the coolant temperature has almost no effect on blowing ratio, so there is no need to correct the nominal readings.

Table 0-6 Change in blowing ratio from adjusting the bias due to the coolant measurement location.

		M		
DR	**Nominal Value**	**Adjusted Bias**	**Uncertainty**	**% U of Adjusted M**
1.18	0.50	0.50	0.07	13.51
1.19	1.00	0.99	0.04	3.72
1.21	2.00	2.00	0.04	1.98
1.22	3.00	3.01	0.06	1.84
1.44	0.51	0.50	0.09	17.77
1.46	1.01	1.01	0.04	4.45
1.47	1.50	1.49	0.04	2.74
1.48	2.00	1.99	0.04	2.16
1.50	2.51	2.50	0.05	2.03
1.52	3.00	3.00	0.06	2.00

Figure 0-40 shows the uncertainty of η versus η at DR = 1.2 and 1.5. The values are similar as in the original analysis, except at M = 0.5 where the uncertainty increases dramatically. This is due to the high bias uncertainty of the coolant temperature at the lowest blowing ratios.

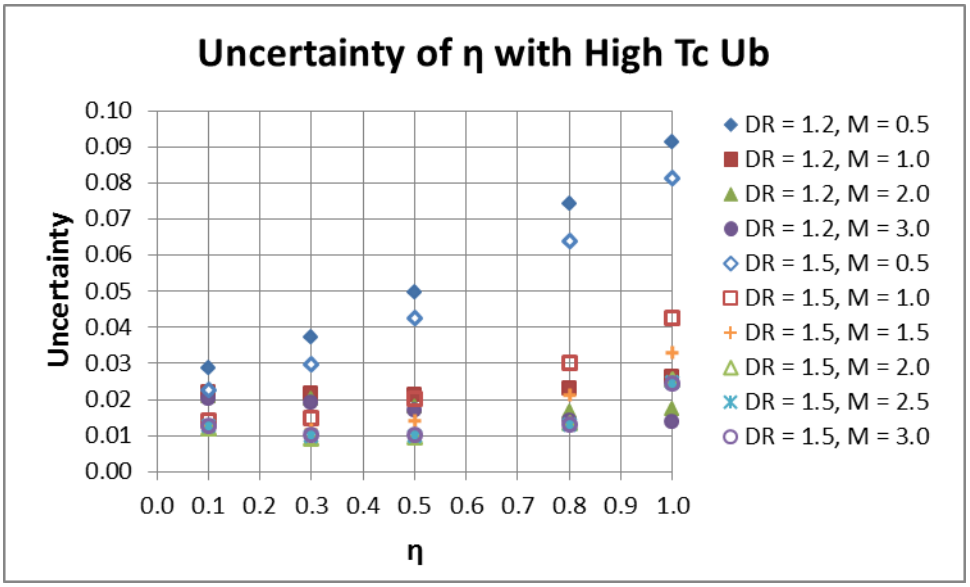

Figure 0-40 Uncertainty of adiabatic effectiveness with high T_c bias error.

The bias in coolant temperature affects the heat transfer coefficients at DR = 1.2 and 1.5, but not 1.0. Figure 0-41 a) and b) show the uncertainty of h_f using the adjusted coolant temperature and its associated uncertainty. The uncertainty is a few percent higher than the initial analysis for all blowing ratios, but the uncertainty shoots up higher at M = 0.5 at DR = 1.2 and 1.5. Once again, this is due to high bias uncertainty of measuring the coolant temperature at low blowing ratios.

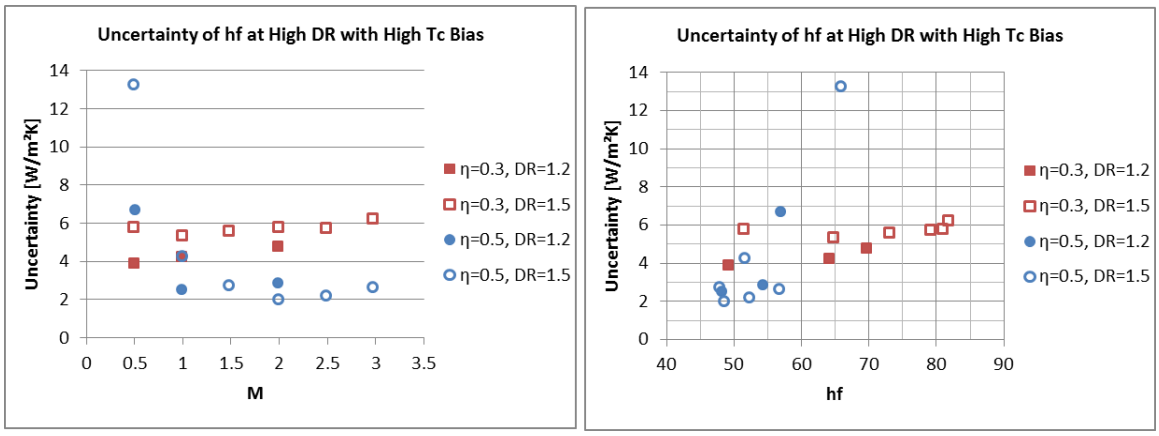

a) b)

Figure 0-41 a) Uncertainty of h_f versus M with high T_c bias
b) Uncertainty of h_f versus h_f with high T_c bias

Figure 0-42 a) and b) show a similar trend. The uncertainty of h_f/h_0 did not change much at higher blowing ratios compared to the original analysis, but becomes very large at $M = 0.5$.

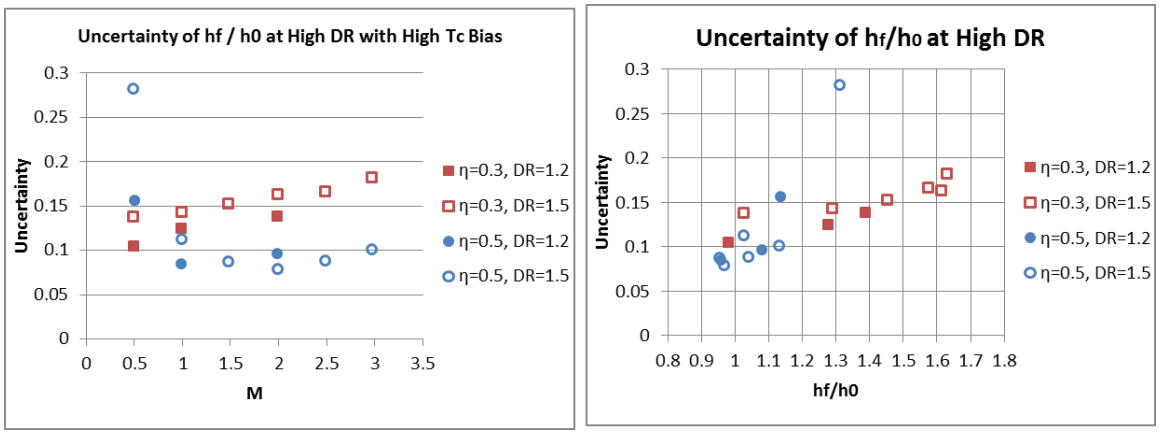

a) b)

Figure 0-42 a) Uncertainty of h_f/h_0 versus M with high T_c bias.
b) Uncertainty of h_f/h_0 versus h_f/h_0 with high T_c bias.

From the above analysis it can be concluded that making an accurate coolant temperature measurement at low blowing ratios is difficult. Measuring the coolant temperature in the plenum provides a steady temperature, but does not account for any additional warming of the coolant that takes place between the plenum and the coolant holes. Measuring the coolant temperature at the coolant hole entrances accounts for warming of the coolant, but provides an unsteady measurement that has large bias errors at low blowing ratios.

1.7.9 REPEATABILITY

One of the best ways to get a better understanding of the uncertainty associated with measurements is to compare repeat measurements in-test as well as test-to-test. Three in-test repeatability measurements were taken, and one test was repeated. Figure 0-43 and Figure 0-44 show in-test repeatability measurements

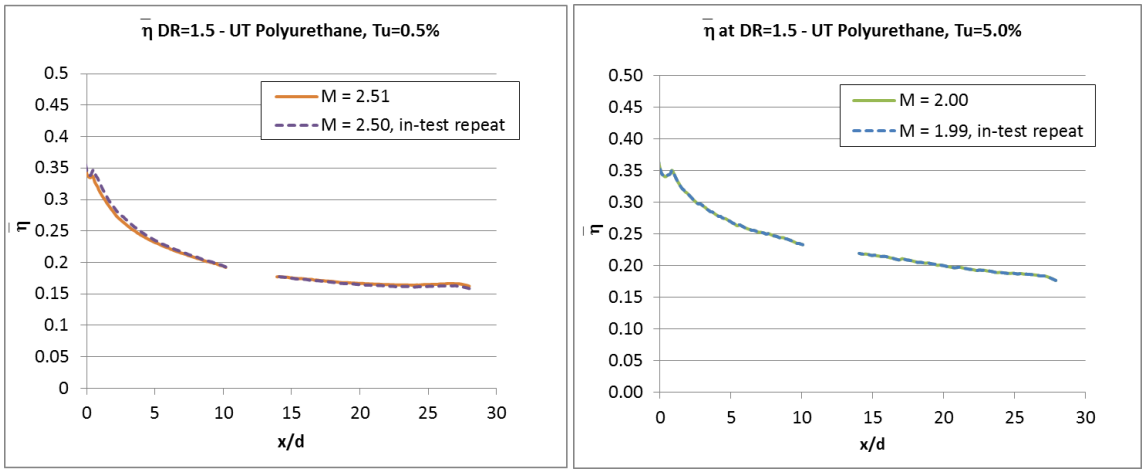

a) b)

Figure 0-43 In-test repeatability using the UT Polyurethane coupon at a) *Tu* = 0.5% and b) *Tu* = 5.0%

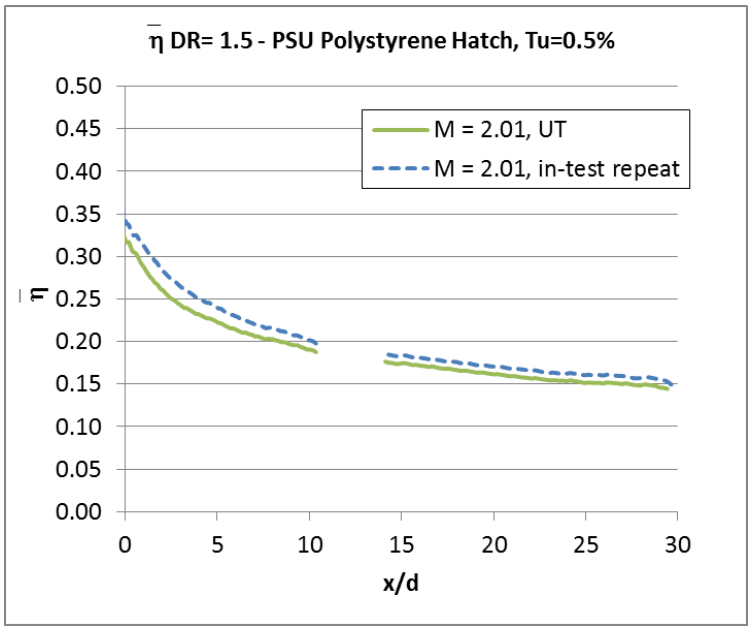

Figure 0-44 In-test repeatability for the PSU Polystyrene Hatch Coupon

1.7.10 Uncertainty Analysis Summary

The uncertainty has been calculated for two different scenarios:

1. Nominal measurements with the coolant temperature measurement 1.5 inches beneath the coupon
2. A bias correction of the coolant temperature to account for warming that takes place between the plenum and hole entrances

Deciding which uncertainty analysis to use depends on how the data is being compared. In the case where UT's adiabatic effectiveness data is being compared to PSU's data, the uncertainty analysis from scenario 1 should be used for the data since PSU measured the coolant temperature in the plenum. If UT's data is being compared to

data where the coolant temperature is defined at the exit of the coolant holes, the uncertainty analysis under scenario 2 should apply since it accounts for the bias errors and uncertainties in the measurement of the coolant temperature.

The issue of measuring increased adiabatic effectiveness between the jets, despite the lack of cooling in those locations, was discussed. The best explanation for this, given the present data, is that there is a cool boundary layer that forms along the sides of the wind tunnel when the mainstream is heated. The cool boundary layer may be exacerbated by flowing over the coupon which is cooled by the plenum underneath. Because it is uncertain what effect this would have on the adiabatic effectiveness underneath the jets, no correction was made to the data.

Table 0-7 summarizes the uncertainty of adiabatic effectiveness. At each density ratio, most of the uncertainties for the different blowing ratios fell onto one another except at $M = 0.5$, which has been set aside as a special case.

Table 0-7 Uncertainty of η for uncertainty scenarios 1 and 2.

Uncertainty of η			
Uncertainty Scenario	**DR=1.2**	**DR=1.5**	**M=0.5 (DR=1.2 & 1.5)**
1. Nominal Analysis	± 0.020	± 0.010	± 0.025
2. Including Tc bias	± 0.020	± 0.015	± 0.070

The uncertainties of heat transfer coefficients are a function of the test conditions, and it is recommended that the reader reference the charts provided earlier in this chapter to get an accurate estimate of uncertainty at a particular condition. But for certain reference conditions, Table 0-8 is provided as an example.

Table 0-8 Uncertainty of heat transfer coefficients at certain reference conditions.

Uncertainty of Heat Transfer Coefficients			
Variable	**DR**	**1. Nominal Analysis**	**2. Including Tc Bias**
hf, at 70 W/m²·K	1.2, 1.5	± 4.5 W/m²·K	± 6 W/m²·K
hf, at 70 W/m²·K	1.0	± 4 W/m²·K	± 4 W/m²·K
hf/h0 at 1.3	1.2, 1.5	± 0.12	± 0.14
hf/h0 at 1.3	1.0	± 0.08	± 0.08

RESULTS

1.8 Verification of 7°-7°-7° Shaped Hole Adiabatic Effectiveness Performance

1.8.1 The First Experiment

Before running the first experiment to test the 7°-7°-7° shaped hole design, several testing parameters between the University of Texas (UT) and Pennsylvania State University (PSU) were established and most of them were matched. Testing parameters such as the boundary layer thickness, mainstream Reynolds number, density ratios, turbulence intensity, and blowing ratios were matched between the two labs (more information is given in Chapter 2). However, the plenum geometry and test coupon material differed. The plenums in both facilities had been constructed prior to this project and should have easily simulated a plenum condition (very low, uniform velocity at the entrance of the coolant holes) despite the geometrical and internal configuration differences. PSU chose to machine its coupon out of polystyrene (more commonly known as Styrofoam™) because it was a material they were familiar with and it provided a low thermal conductivity (k = 0.029 W/m·K [54]). UT chose to machine its test coupon out of polyurethane foam due to its durability and machinability. The disadvantage of using polyurethane over polystyrene is its higher thermal conductivity (k = 0.044 W/m·K [55]), which is 52% higher than polystyrene. After weighing the property differences between the two materials, UT decided that machining accuracy and coupon durability were more important than the increased thermal conductivity and chose to machine the coupon out of polyurethane.

For the first test, PSU machined their shaped holes out of one long piece of polystyrene that started several hole diameters upstream of the coolant holes and extended several feet downstream of them. At UT, the holes were machined into a

coupon, or hatch, that covered the plenum, and the coupon connected to upstream and downstream sections to make a flat plate.

The targeted testing conditions for UT's first experiment are listed in Table 0-1. There was no generated mainstream turbulence for the first experiment, and the turbulence intensity at both labs was 0.5%.

Table 0-1 Targeted parameters for UT's first 7°-7°-7° shaped hole test.

	***DR* = 1.2**	***DR* = 1.5**	***DR* = 1.73**
M	0.5, 1.0, 2.0, 3.0	0.5, 1.0, 1.5, 2.0, 2.5, 3.0	2.13, 3.0

Figure 0-1 shows UT's results from the first 7-7-7 shaped hole test at a) DR = 1.2 and b) DR = 1.5. At DR = 1.2, the effectiveness continuously increases with increasing blowing ratio up to M = 2.0, and at M = 3.0 the effectiveness drops. At DR = 1.5, the performance peaks at M = 1.5. At M = 2.0, $\bar{\eta}$ decreases slightly downstream of the holes, most likely due to the jet lifting off the surface. At M = 3.0, the jets separate from the surface at all positions downstream.

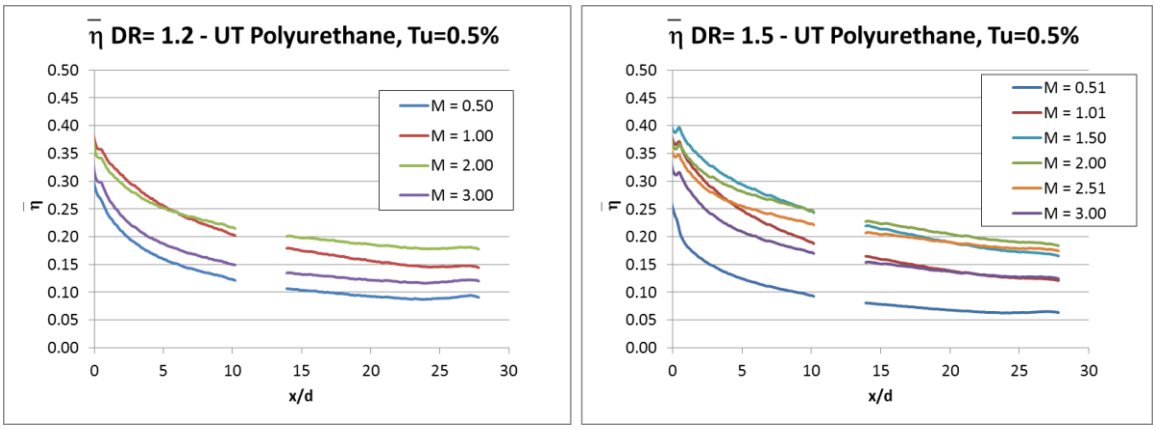

a) b)

Figure 0-1 Results from first 7°-7°-7° test at UT a) *DR* = 1.2 b) *DR* = 1.5 using the UT Polyurethane coupon.

Figure 0-2 shows surface contours of adiabatic effectiveness for *DR* = 1.5 and *M* = 0.5, 1.0, 1.5, 2.0, 2.5, and 3.0. Showing the full range of contours demonstrates how the adiabatic effectiveness performance changed as the blowing ratio was increased. The lowest effectiveness was at *M* = 0.5, which is the contour on the top left. At *x*/*d* = 0, the film cooling performance was already low, with η = 0.60 exiting the holes, while the contours at higher blowing ratios show η > 0.90. This suggests that the coolant was not filling out the entire shaped hole expansion and there could have been some mainstream ingestion in the hole. The performance increases with increasing blowing ratio, as the coolant fills out the shaped hole more and more, and peaks at *M* = 1.5 and 2.0. It is interesting to compare these two blowing ratios because the laterally averaged adiabatic effectiveness was similar between them, which is shown in Figure 0-1 b), but the contours are fairly different. At *M* = 1.5, the jets spread more laterally, but at *M* = 2.0 the adiabatic effectiveness in the center of the jets was higher and the jets narrowed slightly. The effectiveness in the center of the jets doesn't decrease until *M* = 3, so at *M* = 2 and 2.5, the reduced performance is localized to the edges of the jets, and not the center. This

behavior is unique to shaped holes. With cylindrical holes, the reduced adiabatic effectiveness due to separation is seen at all areas, not just the jet edges, as the jet lifts off the surface.

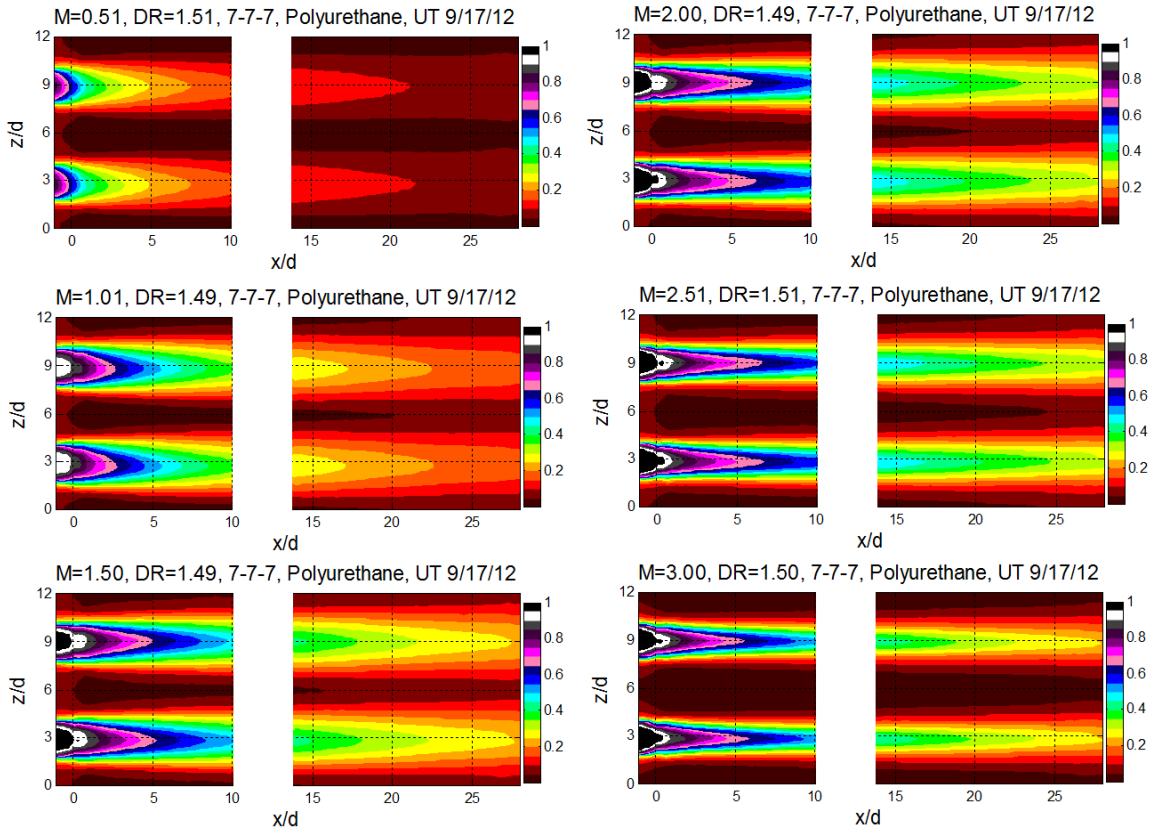

Figure 0-2 Surface contours of adiabatic effectiveness at Tu = 0.5%, DR = 1.5 and M = 0.5, 1.0, 1.5, 2.0, 2.5, and 3.0 using the UT Polyurethane coupon.

Figure 0-3 shows results that were taken at different blowing ratios and density ratios, but had the same momentum flux ratio. The two curves agree well, indicating that the effectiveness may scale reasonably well with momentum flux ratio, although the blowing ratios to match the momentum flux ratio are not far apart. The data in blue at M

= 2.13 and *DR* = 1.73 is absent upstream of *x/d* = 2.5 because the surface temperatures were too cold for the IR camera to read accurately.

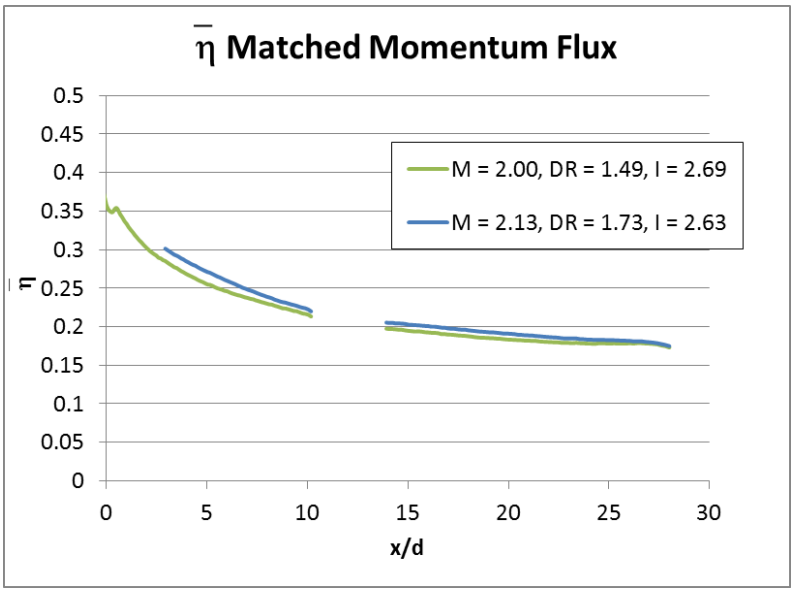

Figure 0-3 Results with matched momentum flux from first experiment using the UT Polyurethane coupon.

Figure 0-4 shows laterally averaged adiabatic effectiveness values versus blowing ratio at a) *x/d* = 8 and b) *x/d* = 17. The results did not scale with blowing ratio, even at low blowing ratios where the jets were attached to the surface. Figure 0-5 shows that the data scales well with momentum flux ratio, but it scales even better with velocity ratio, which is shown in Figure 0-6. The data scales fairly well with both momentum flux ratio and velocity ratio, but the data is more tightly grouped together when plotted versus velocity ratio. For example, the data points at *DR* = 1.2, 1.5, and 1.73, which span from *I* = 3.3 to 5.2 in Figure 0-5 a) and b) have approximately the same laterally averaged value and prevent the data from collapsing nicely. Those same data points are plotted in Figure 0-6 a) and b). They have almost the same velocity ratio of 1.65-1.74 and also the same $\bar{\eta}$,

indicating that the data scales with *VR*. All of the coupons tested for this project scaled best with velocity ratio.

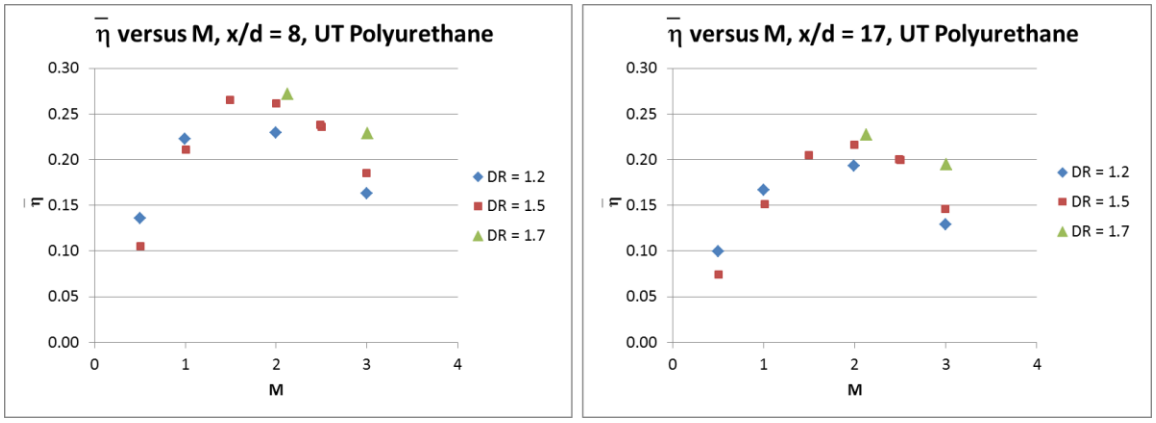

a) b)

Figure 0-4 Laterally averaged adiabatic effectiveness versus blowing ratio at a) $x/d = 8$ and b) $x/d = 17$ at $Tu = 0.5\%$.

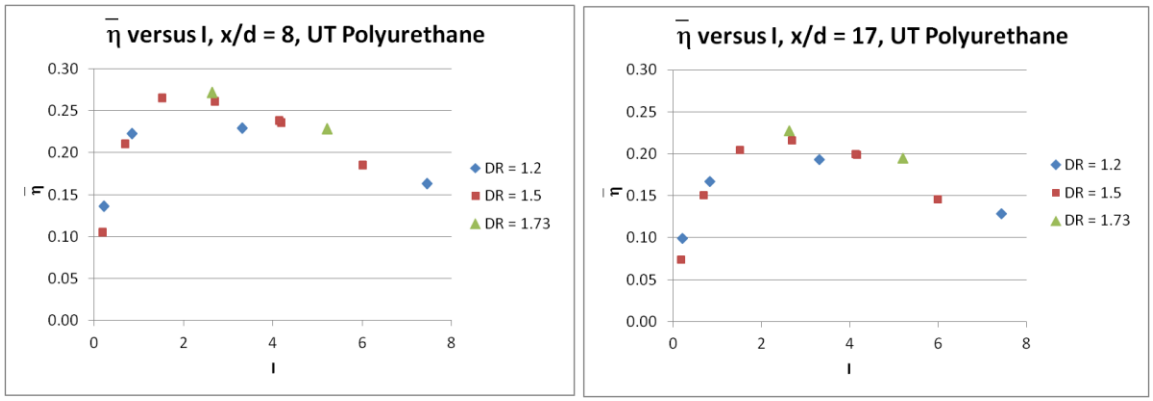

a) b)

Figure 0-5 Laterally averaged adiabatic effectiveness versus momentum flux ratio at a) $x/d = 8$ and b) $x/d = 17$ at $Tu = 0.5\%$.

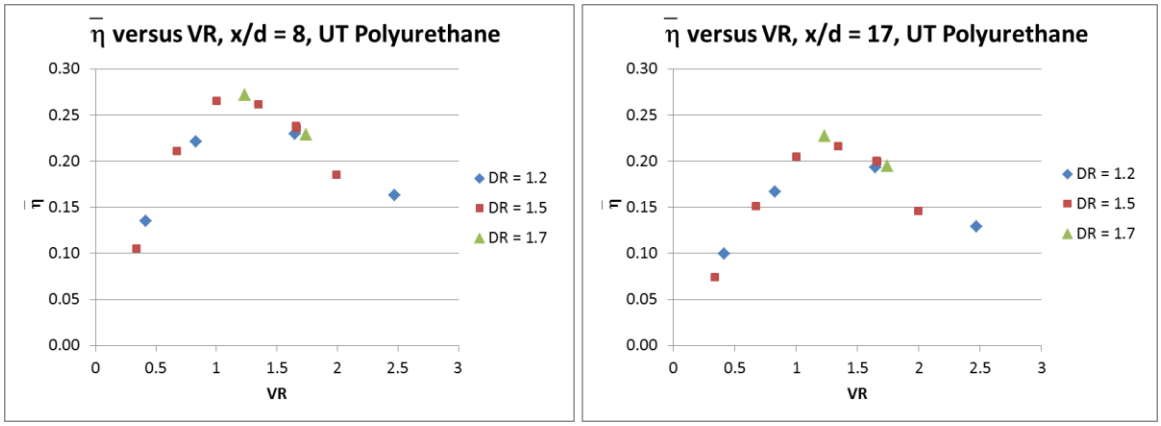

a) b)

Figure 0-6 Laterally averaged adiabatic effectiveness versus velocity ratio at a) $x/d = 8$ and b) $x/d = 17$ at $Tu = 0.5\%$.

Figure 0-7 shows a comparison between the results from UT and PSU at $DR = 1.2$. At $M = 0.5$ and 1.0, blue and red, respectively, the results match well, but at $M = 2.0$, the $\bar{\eta}$ dropped, which suggests that the jets separated from the surface, while the jets at UT did not. At $M = 3.0$, the coolant jets at UT and PSU were both detached, with PSU's laterally averaged adiabatic effectiveness being lower than UT's.

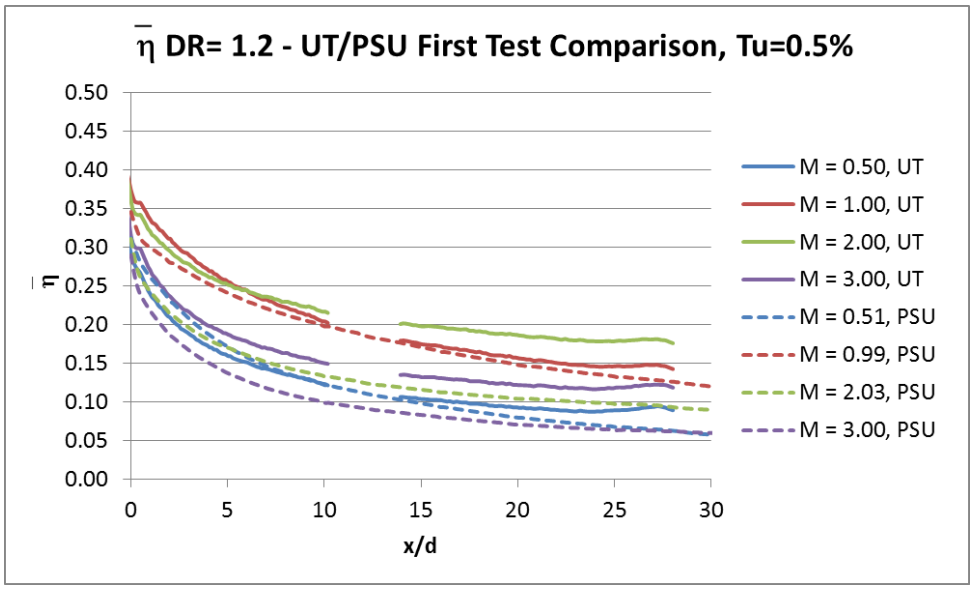

Figure 0-7 Laterally averaged adiabatic effectiveness comparison between the UT Polyurethane and PSU Polystyrene Plate at *DR* = 1.2.

Figure 0-8 is a comparison between the results from UT and PSU at *DR* = 1.5. At this density ratio, none of the blowing ratios between the labs match. At *M* = 0.5 and 1.0, UT's results are lower than PSU's, but at *M* = 2.0 and 3.0, UT's results are higher than PSU's. This outcome prompted speculation as to what could cause the results between the two labs to differ. Firstly, the fact that UT's coolant jets stay attached at higher blowing ratios could have been caused by PSU's coolant flow rate being too low or UT's coolant flow rate being too high. Secondly, since UT's wind tunnel test section is shorter than PSU's, the ejection of the jets could have caused acceleration of the mainstream due the jets occupying more volume in the test section than at PSU. The mainstream acceleration could have push the jets closer to the surface, keeping them attached at higher blowing ratios.

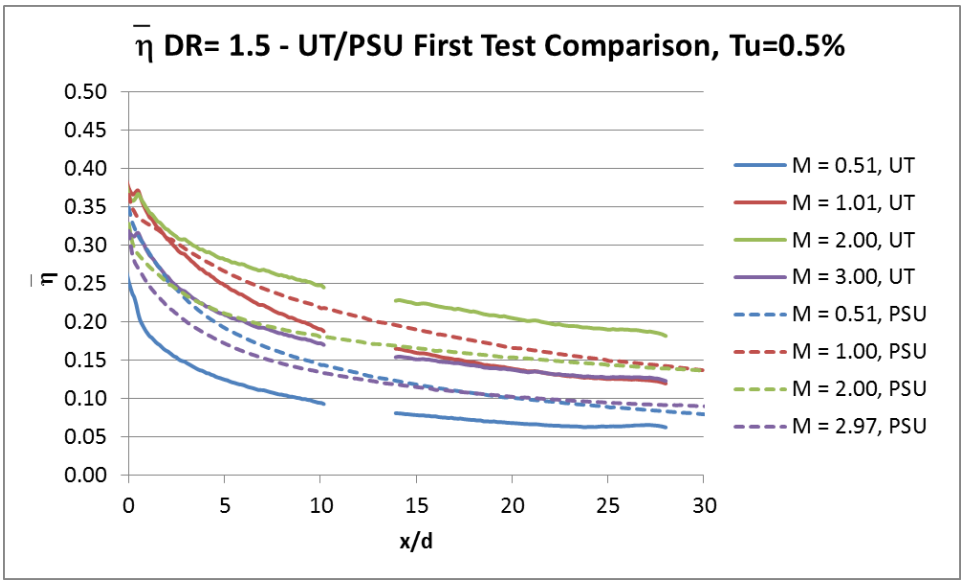

Figure 0-8 Laterally averaged adiabatic effectiveness comparison between UT Polyurethane and PSU Polystyrene Plate at *DR* = 1.5.

The results shown in Figure 0-7 and Figure 0-8 prompted the investigation of the possible issues mentioned, as well as several others that were tested over the course of a year. Table 0-2 outlines the possible causes of the differing results that were tested for this project, and each is discussed in the following sections, 1.8.2-1.8.7. They are presented chronologically in the order that they were investigated.

Table 0-2 Testing parameters investigated as causes for differing results between UT and PSU.

	Testing Parameter	Testing Method
1.8.2	Material/machining difference	• Have PSU machine a coupon out of polystyrene for UT to test • Have UT machine a coupon out of polyurethane for PSU to test
1.8.3	Mainstream velocity acceleration due to jet injection.	• Test a reduced-size coupon to decrease the percentage volume occupied by the jets in the test section to reduce mainstream acceleration
1.8.4	Difference between plenums and entrance effects	• Have UT construct a new plenum that matches PSU's internal plenum geometry
1.8.5	Incorrect flow rate measurement	• Check flow rate measurement with a laminar flow element • Compare measurements of the pressure drop across the holes to PSU's pressure drop measurements
1.8.6	Extreme sensitivity of shaped hole geometries to machining and material differences	• Test the same coupon at PSU and UT
1.8.7	Difference in plenum inlet flow conditions	• Change the coolant piping leading into the plenum at UT

In addition, there were several 7°-7°-7° hole coupons machined and tested throughout the course of this project, and Table 0-3 provides the nomenclature used for each coupon or test plate in subsequent figures. The reader can refer back to this table to remind him or her which coupon corresponds to which label.

Table 0-3 Nomenclature used to describe coupons and test plates used for this project.

Coupon Name	Material	Machining Location	User
UT Polyurethane	Polyurethane	UT	UT
UT Polystyrene	Polystyrene	PSU	UT
UT Polyurethane, d=4 mm	Polyurethane	UT	UT
PSU Polystyrene Plate	Polystyrene	PSU	PSU
PSU Polystyrene Hatch	Same as polystyrene plate, but cut to a smaller size		PSU & UT
PSU Polyurethane	Polyurethane	UT	PSU
PSU Smooth Polystyrene	Polystyrene	PSU	PSU

The results presented in the previous figures are from a test PSU conducted with their polystyrene plate. Later, they cut the polystyrene plate to make it into a coupon that fits over their plenum, like what was done at UT, to see if it would have an effect on the results. When they ran this test, they tested additional blowing ratios to match the blowing ratios UT used (M = 0.5, 1.0, 1.5, 2.0, 2.5, and 3.0) at DR = 1.5. The results from testing the same holes in plate form and in hatch form agreed very well, showing PSU's excellent repeatability and that there was no effect from testing the polystyrene holes in the form of a plate or hatch. The following figures throughout the rest of this chapter use the results from the PSU polystyrene plate when data at DR = 1.2 is being compared, since PSU did not test the PSU Polystyrene Hatch at DR = 1.2. However, when results at DR = 1.5 are being compared, the PSU hatch results will be used since they include additional blowing ratios (M = 1.5 and 2.5) that were not tested in the PSU Polystyrene Plate experiment. The two PSU tests agree well and can be used interchangeably, which is shown in Figure 0-9.

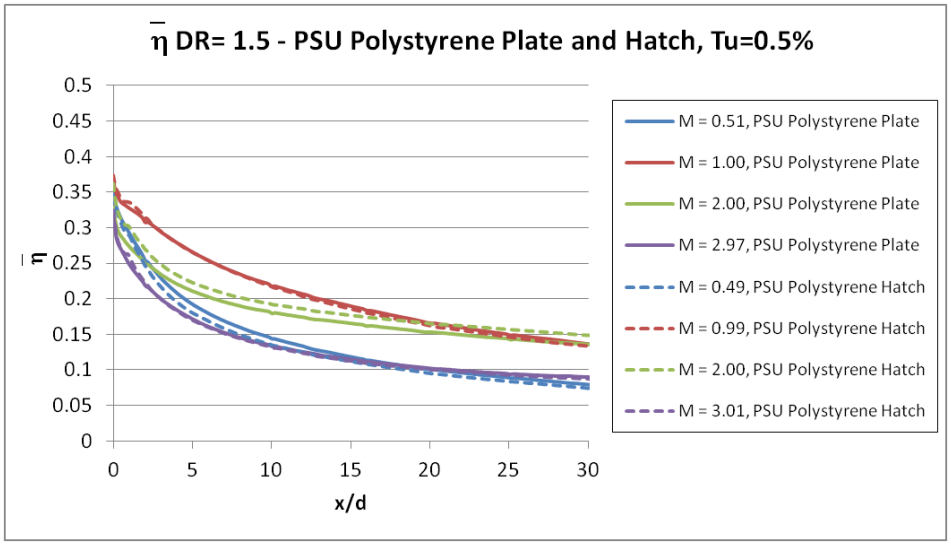

Figure 0-9 Comparison of PSU's test with PSU Polystyrene Plate and the PSU Polystyrene Hatch at DR = 1.5 and Tu = 0.5%.

Several adiabatic effectiveness experiments were run for this project, and their testing conditions are summarized in Table 0-4. The reader can refer back to this table to be clear on the testing parameters that were used for experiments at UT. The section column refers to the section of the dissertation where the experiment is discussed. The Re_∞ column refers to the mainstream Reynolds number that was used for the experiment, where its definition is based upon the mainstream velocity and kinematic viscosity and the coolant hole metering diameter. The plenum design refers to the internal plenum configuration used for the experiment, which is discussed in Section 1.8.4. The coolant piping configuration column refers to the coolant piping design used, which is discussed in Section 1.8.7. The repeat column indicates whether a test was repeated.

Table 0-4 Test parameters for all adiabatic effectiveness experiments.

Section	Test Geometry	DR	Re_∞	*Tu*	Plenum Design	Coolant Piping	Repeat
3.1.1, 7, 9 10, 11, 12	UT Polyurethane	1.2, 1.5, 1.73	5600	0.5%	UT	Original	X
3.1.3	UT Polyurethane, *d*=4 mm	1.2, 1.5	5600	0.5%	UT	Original	
3.1.4	UT Polystyrene	1.2, 1.5	5600	0.5%	PSU	Original	
3.1.6	PSU Polystyrene Hatch	1.2, 1.5	5600	0.5%	UT	Original	
3.1.7, 9	UT Polyurethane	1.2, 1.5	5600	0.5%	UT	New	
3.1.8, 9	UT Polyurethane	1.2, 1.5	5600	5.0%	UT	Original	
3.1.9	UT Polyurethane	1.2, 1.4, 1.6	5600	5.0%	UT	New	
3.1.10	UT Polyurethane, *d*=4 mm	1.2, 1.5	2500	0.5%	UT	Original	

1.8.2 Material/Machining Difference

The first possible cause of the disagreement of results between UT and PSU that was investigated was a difference in material and machining. As mentioned in Section 1.8.1, PSU's test plate was machined out of polystyrene at PSU, and UT's coupon was machined out of polyurethane at UT. To see if there was a difference in machining and material, both universities built a coupon for the other university to test: PSU had their machinist build a coupon out of polystyrene for UT to test (labeled UT Polystyrene), and UT's machinist made a coupon out of polyurethane at UT for PSU to test (labeled PSU Polyurethane).

Unfortunately, it was later discovered that the test that UT had conducted with the UT Polystyrene coupon had an unquantifiable coolant leak, so the results from that test will not be presented in this section. However, a test with the UT Polystyrene coupon was completed with a different internal plenum configuration and those results are presented in Section 1.8.4.

When PSU received the polyurethane test piece that was machined at UT, PSU noticed that there was a faint rifling pattern on the inside of the metering section of the shaped holes, which is shown in Figure 0-10. The dark interior is from spray painting the opposite side of the coupon black, and some of the spray paint coated the inside of the holes. PSU was not able to quantify the roughness of the interior of the coolant holes, and from the photograph, the rifling appears to be very small, albeit the effect looks exacerbated due to the black spray paint. PSU noted that the rifling was only observable in the metering section of the coolant holes and not in the diffuser section of the holes.

Figure 0-10 Photo of "rifling" at the coolant hole entrance in the PSU polyurethane test piece. Photo taken by Robert Schroeder at PSU.

The test coupon built at UT for PSU was 22.75 in. (57.8 cm) long in the streamwise direction, which is considerably longer than the size UT's test coupons, which are 5.5 in. (14.0 cm) in the streamwise direction. Such a long piece could barely fit into the CNC machine at UT, and the machinist had to attach a long tool extension to machine the coolant holes. It is possible that some chatter from the long tool extension

could have caused this pattern. Figure 0-11 shows the Solidworks drawing of the polyurethane test piece that was machined at UT.

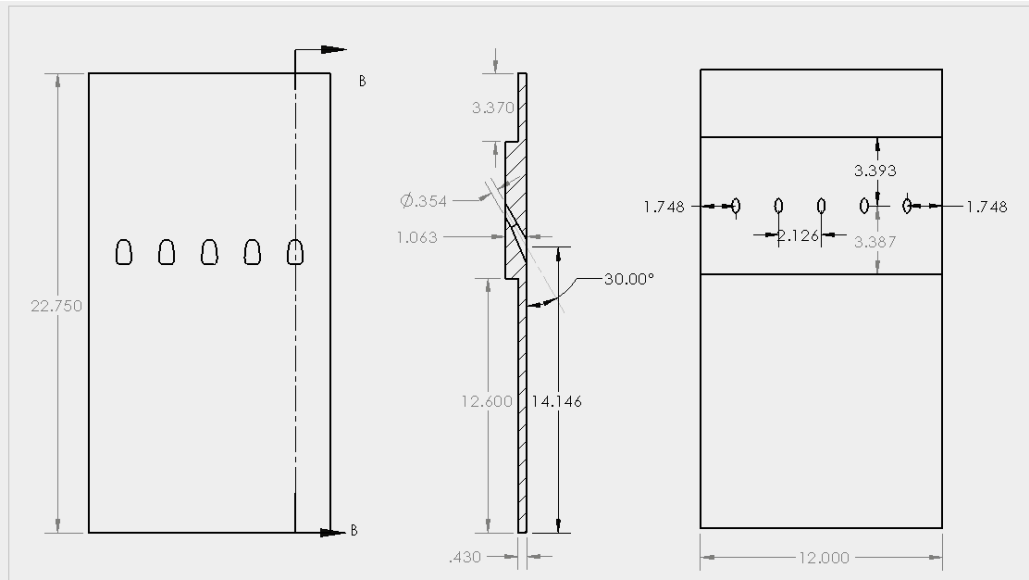

Figure 0-11 Solidworks drawing used to machine polyurethane test coupon for testing at PSU. Drawing is in inches.

To try to understand what was causing the rifling pattern, UT had its machinist machine some test holes to see if he could reproduce the rifling. Figure 0-12 shows a photo of the holes that the machinist at UT made. There were two drill bits in the shop, one was in mint condition and the other had a chipped edge. The machinist made two holes, one with each drill bit, to make sure the chipped bit did not cause the rifling pattern. The hole pictured on the left of the picture was machined with the drill bit in mint condition and the hole on right was machined with a chipped drill bit. Both holes were very smooth, despite the long tool extension and the quality of drill bits.

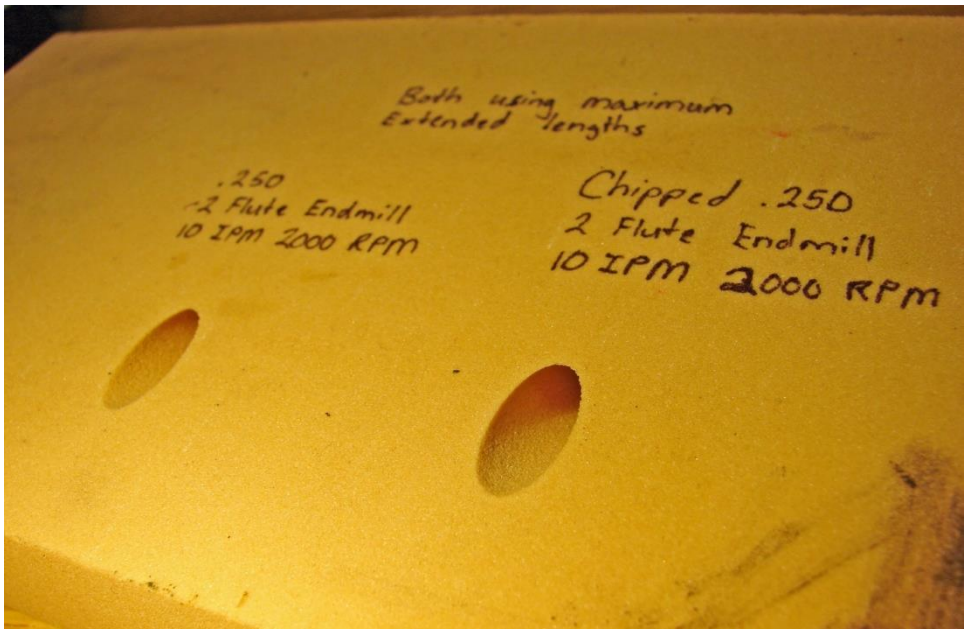

Figure 0-12 Photograph of metering section of coolant holes machined using a long tool extension, the same method used to machine the PSU polyurethane coupon.

All of the coupons made at UT were closely inspected to see if this pattern was present in other coupons, but it was not, and the rifling appears to have been an anomaly that occurred only with the PSU Polyurethane coupon.

PSU tested the PSU Polyurethane test piece at $DR = 1.5$ and $M = 0.5$, 1.0, 1.5, 2.0, 2.5, and 3.0. They did not test at $DR = 1.2$, which is why there is no data at that density ratio presented in this dissertation. Figure 0-13 compares the results at $DR = 1.5$ from the PSU Polyurethane Piece, PSU Polystyrene Hatch and UT Polyurethane coupon at $Tu = 0.5\%$.

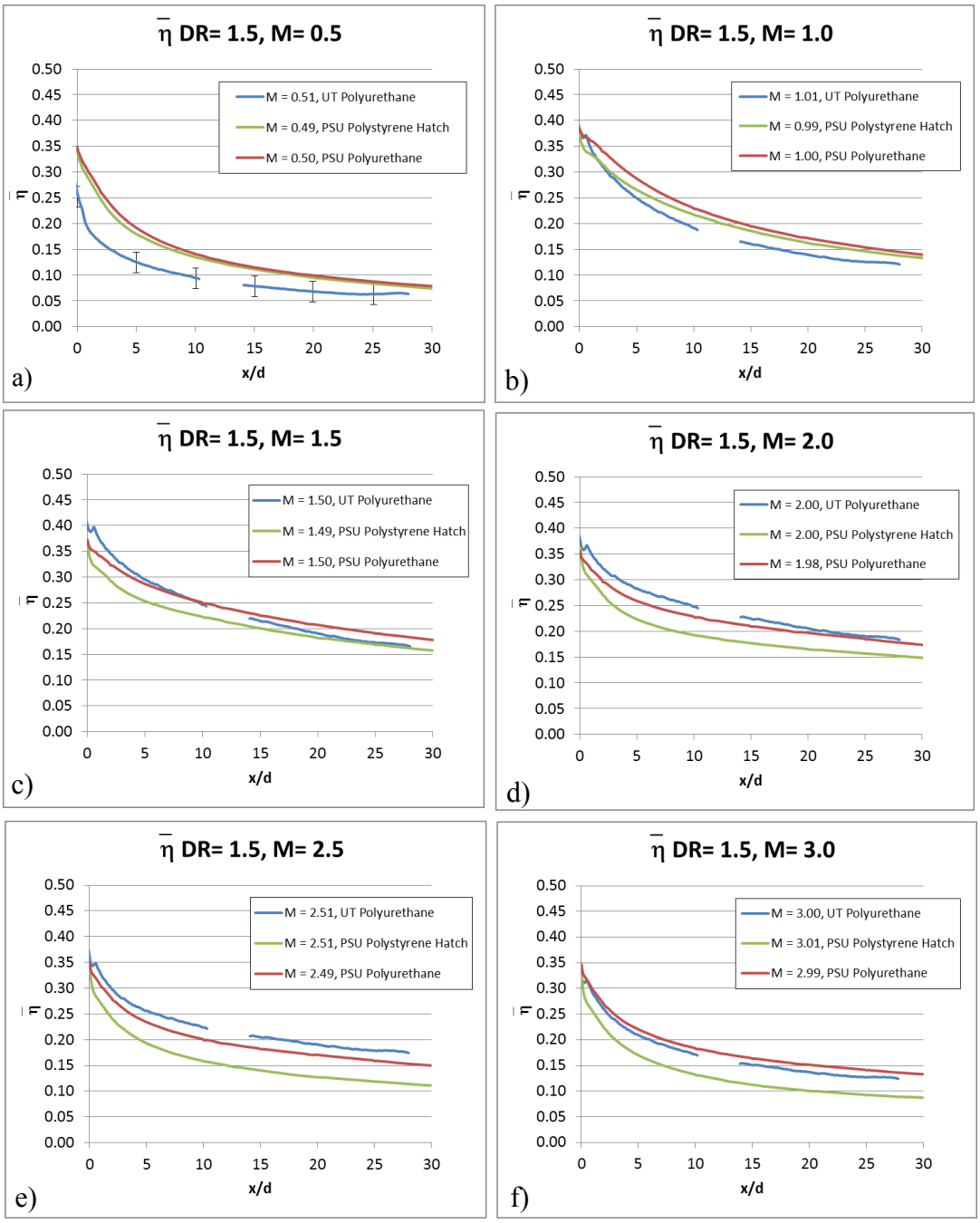

Figure 0-13 Comparison of UT Polyurethane, PSU Polystyrene Hatch, and PSU Polyurethane results at $DR = 1.5$ and $Tu = 0.5\%$ a) $M = 0.5$ b) $M = 1.0$, c) $M = 1.5$ d) $M = 2.0$ e) $M = 2.5$ f) $M = 3.0$.

At M = 0.5 and 1.0 the results from the PSU Polystyrene Hatch and the PSU Polyurethane agree quite well, with the results from the UT Polyurethane coupon being lower. From M = 1.5 to 3.0, the performance of the polyurethane coupons merge together and agree well, with the effectiveness from the PSU Polystyrene Hatch being lower. At the time this comparison was originally carried out, PSU had an IR camera calibration error that was present at low temperatures causing high effectiveness values to be biased lower (all of the data in this dissertation is corrected). At the time, none of the data sets matched at all, and UT and PSU were still left with no explanation as to why the results were different. In hindsight, the results matched well except at M = 0.5 and 1.0. The uncertainty of UT's data at M = 0.5, DR = 1.5 is $\eta \pm 0.02$, which not enough to make up for the 0.1 gap between the UT Polyurethane and PSU Polyurethane results. There is larger uncertainty of the coolant temperature and coolant flow rate at M = 0.5, and to get UT's M = 0.5 data to increase from η = 0.10 to 0.15, the coolant temperature would have to be 33 K warmer, which is far out of range of the 6.0 ± 6.0 K uncertainty in coolant measurement that was discussed in Section 1.7. Figure 0-14 shows a comparison of contours at M = 0.5 and DR = 1.5 for the three test coupons. Clearly, the PSU Polystyrene Hatch (center) and the PSU Polyurethane (bottom) contours agree well, but the effectiveness values for the UT Polyurethane coupon (top) are lower. The jets from the UT Polyurethane coupon spread the same distance laterally as the jets from the PSU coupons, but the effectiveness drops off at smaller x/d values. Focusing on the region inside the holes at $x/d < 0.0$ for the UT Polyurethane coupon, the effectiveness levels in the shaped hole and expansion exit are much lower than in the PSU contours. This suggests that the coolant is not filling out the expansion and there is mainstream ingestion in the hole. There are two possible reasons that this could have happened for the UT Polyurethane coupon and not the PSU Polyurethane coupon. Firstly, there could have been different coolant entrance effects at UT and PSU from using different plenum and coolant piping designs, which could have caused the data at low blowing ratios to differ. Secondly, PSU's coupon had a faint rifling pattern in the metering section of the coolant

holes, which could have improved film cooling performance at the low blowing ratios, and could have caused the polyurethane coupons at UT and PSU to perform differently. What is interesting, is reflecting back on the original comparison between the UT Polyurethane and PSU Polystyrene Hatch results in Figure 0-7 and Figure 0-8, the UT *M* = 0.5 data was lower than PSU's at *DR* = 1.5, but not at *DR* = 1.2. This could be because the coolant velocity is higher at *DR* = 1.2 than at 1.5, and the coolant fills out the hole expansion better.

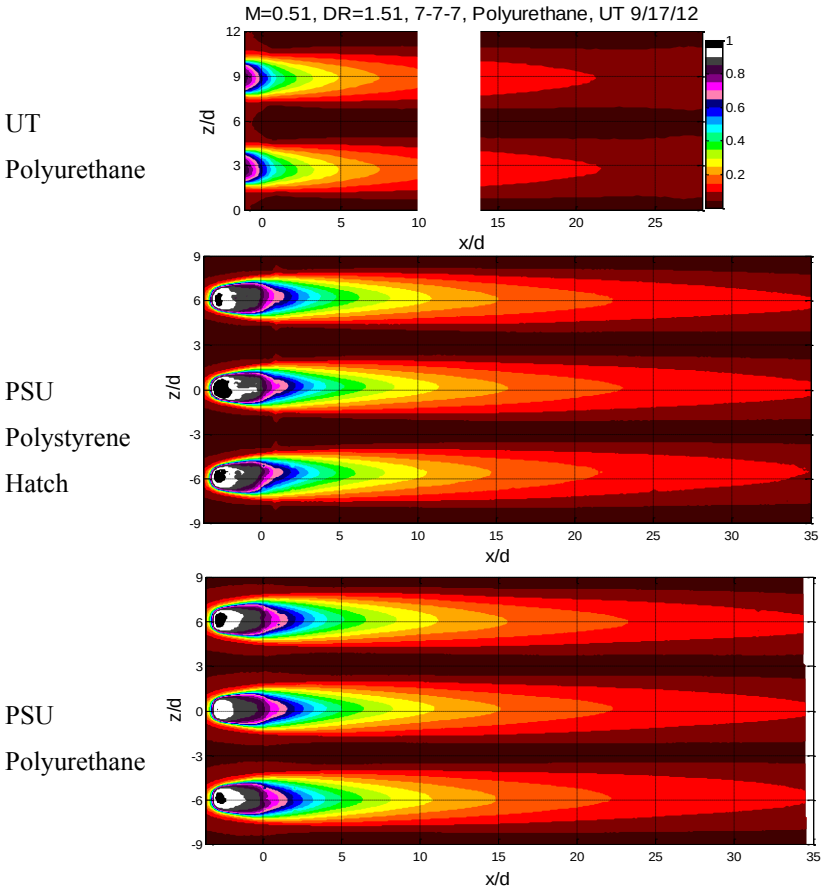

Figure 0-14 Contours of adiabatic effectiveness at *M* = 0.5, *DR* = 1.5, *Tu* = 0.5% using the UT Polyurethane (top), PSU Polystyrene Hatch (center), and PSU Polyurethane (bottom).

1.8.3 MAINSTREAM VELOCITY ACCELERATION DUE TO JET INJECTION

One theory as to why the results between the two labs did not agree was that UT's test section height was shorter (13.65 cm or 15.2 hole diameters) than PSU's test section height (29.2 cm or 34.5 hole diameters). In UT's test section, the ratio of the volume occupied by the jets to the volume of the tunnel would be larger, and if too large, could cause the mainstream velocity to accelerate downstream of the coolant injection, creating a pressure gradient that could change the way the jets perform.

As a first step, a Pitot-static probe was positioned 5 cm downstream of the coolant holes and the mainstream velocity was measured with room temperature air exiting the holes. When the jets were operating, the mainstream velocity was 1.7% higher than when the jets were not operating. A quick calculation that presumed the jets produced a blockage of the mainstream 2d in diameter (thermal field measurements presented in section 1.9.6 show the jet protrudes 2d into the mainstream) yielded a 1.5% acceleration of the mainstream, which is reasonably consistent with this measurement. The mainstream was set to operate at 9.9 m/s, so accounting for the 1.7% acceleration would mean the mainstream was actually at 10.07 m/s. This showed that the jets did cause some acceleration of the mainstream, but not very much. As a second step, a new test coupon was machined with reduced-scale holes that had diameters chosen to match the test section height to hole diameter ratio at Penn State University. The coupon contained 4.00 mm diameter holes, producing a test section height to hole diameter ratio of $H/d = 34.5$.

Testing parameters, such as the mainstream velocity and the boundary layer thickness needed to be changed to scale with the original testing conditions. The mainstream velocity was changed from 9.9 m/s to 22.25 m/s to match the Reynolds number based on the mainstream velocity, mainstream kinematic viscosity, and the metering hole diameter. It was not possible to scale the boundary layer thickness with the hole diameter for this test. The original tests with $d = 9$ mm holes had $\delta/d = 1.2$ with a trip installed. For the reduced hole diameter test, the boundary layer trip was removed,

which produced the thinnest boundary layer possible. Using Prandtl's relation for turbulent boundary layer thickness, which is given in Equation 0-1, the boundary layer thickness was approximated to be 1.5d, which is just slightly greater than the 1.2d used for the d = 9 mm experiments.

$$\frac{\delta}{x} \approx \frac{0.37}{Re_x^{1/5}}$$

Equation 0-1

In this equation, the Reynolds number is based on the mainstream velocity, mainstream kinematic viscosity, and the distance downstream of the leading edge on the flat plate, x. This relation was found to be fairly accurate when compared to boundary layer measurements that were taken without a trip at U_∞ = 9.9 m/s. The correlation produced a boundary layer thickness of 6.8 mm while the measurements were 7.6 mm (5% less). Based upon what is in literature, a larger δ/d should reduce adiabatic effectiveness [56], although it's possible that this small of a difference in boundary layer thickness would not have much of an effect.

Figure 0-15 a) and b) show laterally averaged adiabatic effectiveness results at DR = 1.2 and Figure 0-16 a) and b) show laterally averaged adiabatic effectiveness results at DR = 1.5. All of these figures compare results using the UT Polyurethane coupon (d = 9 mm) to the UT Polyurethane, d = 4 mm coupon.

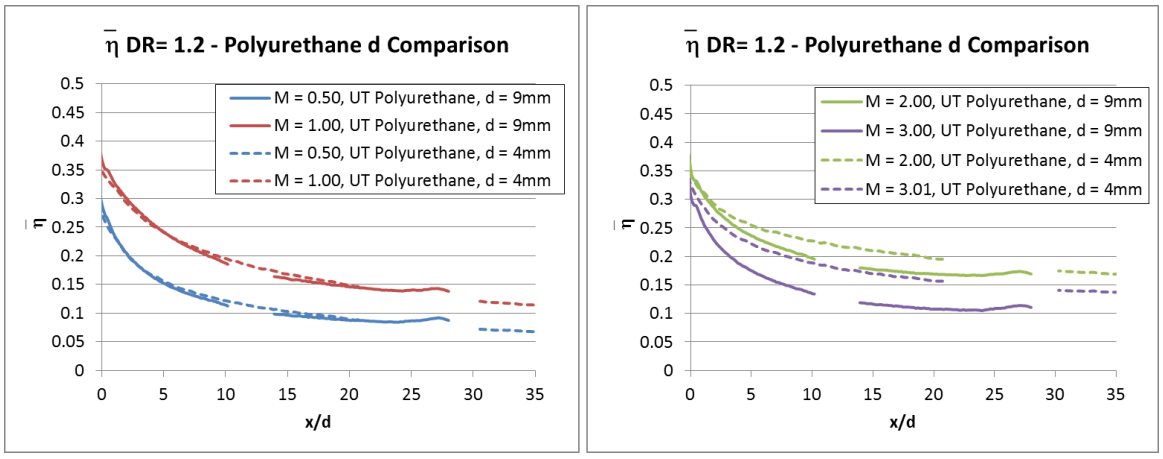

a) b)

Figure 0-15 Comparison between polyurethane coupons with different hole diameters at $DR = 1.2$, $Tu = 0.5\%$ a) $M = 0.5$ and 1.0 b) $M = 2.0$ and 3.0

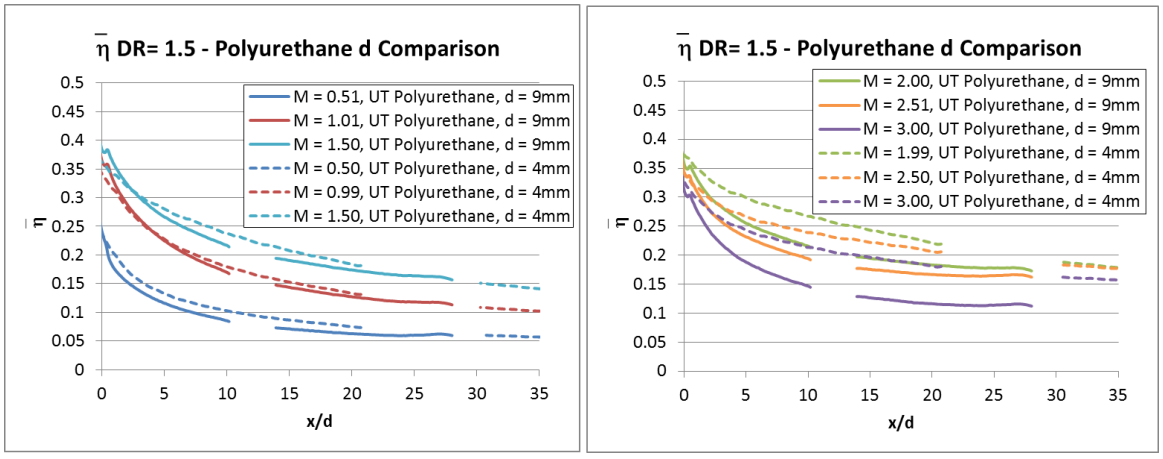

a) b)

Figure 0-16 Comparison between polyurethane coupons with different hole diameters at $DR = 1.5$, $Tu = 0.5\%$ a) $M = 0.5$, 1.0, and 1.5 b) $M = 2.0$, 2.5 and 3.0

The results from Figure 0-15 a) and Figure 0-16 a) show the comparison of results from 9 mm diameter holes and 4 mm diameter holes at low blowing ratios. The data using the two different hole diameters agreed very well while the jets were attached at these blowing ratios. However, at $M = 2.0$ and above, shown in Figure 0-15 b) and Figure 0-16 b), when the jets started to detach from the surface, the results between the two tests diverge. The test with $d = 4$ mm stay attached at $M = 2.0$, while the jets with $d = 9$ mm holes start to detach. If mainstream acceleration were an issue, it would create a favorable pressure gradient and the jets from the 9 mm holes would stay better attached than the jets from the 4 mm holes. The results above show the opposite effect, and it is likely that the difference in the results at the higher blowing ratios is due to the differences in separation within the shaped hole. Separation is very sensitive, and the difference in the degree of separation could be due to differences in machining, especially since the shaped holes with 4 mm diameter are so much smaller than the 9 mm diameter shaped holes. There could also be an effect of surface roughness since the ratio of the surface roughness height to diameter ratio will be different between the two coupons. Despite the different degrees of separation produced from the two coupons, the mainstream acceleration is negligible, since the jets from the 4 mm diameter holes performed better than the jets from the 9 mm diameter holes and is therefore not the cause of UT's Polyurethane coupon results staying attached at higher blowing ratios than PSU's coupons' results.

1.8.4 Differences Between Plenums and Entrance Effects

Another theory that could explain the differing results between UT and PSU was that there could be different entrance effects when the coolant enters the shaped holes. This made particular sense when comparing results at $M = 0.5$ and $DR = 1.5$ between the two labs, which is shown in the laterally averaged adiabatic effectiveness plot in Figure 0-7 and the surface contours of adiabatic effectiveness in Figure 0-14. The largest difference in adiabatic effectiveness was at this blowing ratio and it seemed as though the

coolant was not filling out the shaped holes at the UT like it was at PSU. One theory speculated that there could be different coolant entrance effects between the two labs, such as different turbulence intensity and coolant uniformity. To make sure that the internal plenum geometry was not causing this, the University of Texas fabricated the inside of a second plenum to match the internal geometry of Penn State University's plenum as much as possible. The internal plenum designs are shown in Figure 0-17 and Figure 0-18.

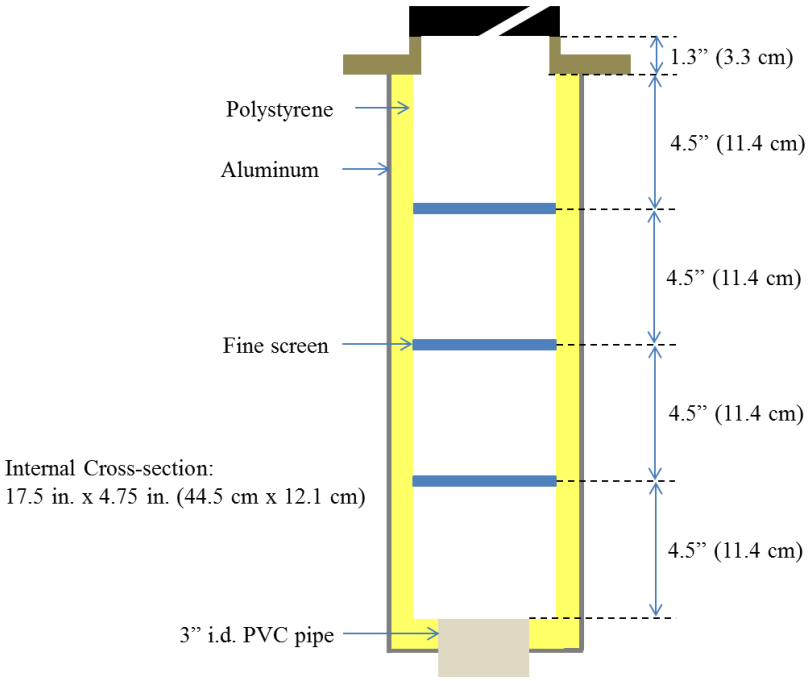

Figure 0-17 Internal plenum geometries: University of Texas design

The original internal plenum design had a 3 in. i.d. PVC coolant pipe entrance. The coolant was then evenly distributed inside the plenum by 3 fine screens evenly spaced inside the plenum. The screens are depicted in blue in Figure 0-17. The plenum

was made out of aluminum and was lined with 0.75 in. (1.9 cm) thick polystyrene to insulate it, which is shown in yellow. For experiments, the plenum is also insulated on the outside with 4 inch thick sheets of fiberglass insulation.

A second spare plenum was used to mimic PSU's internal plenum geometry. To match PSU's design, the plenum needed to be shortened, and this was done by extending the PVC pipe entrance into the plenum. The coolant entered the plenum through a 3" i.d. PVC pipe which then connected to a 2" i.d. PVC pipe, which was the entrance pipe diameter PSU used. The coolant exited the PVC pipe, hit a splash plate, and then went through a porous plate that was specifically machined to match the porous plate at Penn State University. From there it went through a fine mesh screen. The dimensions shown are as-built dimensions and PSU's corresponding dimensions are shown in red.

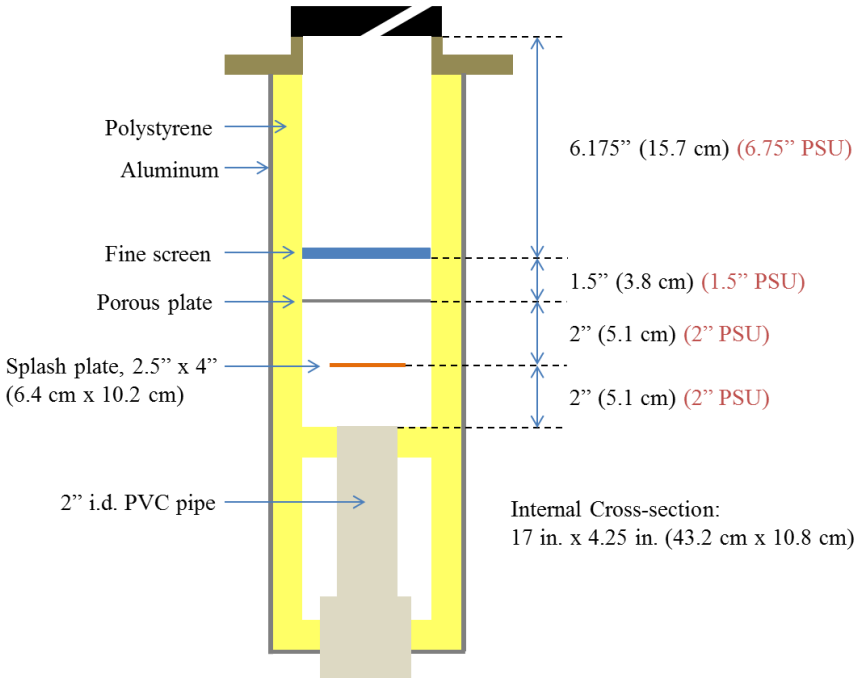

Figure 0-18 Internal plenum geometry used by UT to match the internal plenum geometry used by PSU. Dimensions are as-built.

Figure 0-19 shows the Solidworks drawing of the porous plate that was machined to match PSU's porous plate.

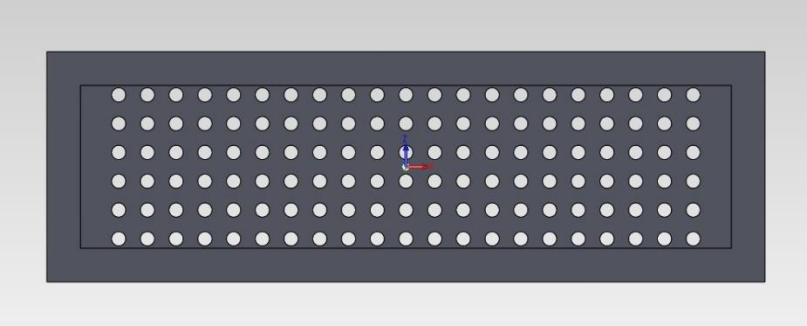

Figure 0-19 Solidworks drawing of the porous plate machined to replicate the porous plate at PSU. View shows the perimeter of the plate that is covered by polystyrene insulation.

All of the holes were drilled inline. The hole diameter in the porous plate was matched to PSU's porous plate (d = 3/8 in. or 0.95 cm), since the coolant hole diameters were roughly the same, being 9 mm at UT and 8.47 mm at PSU. UT scaled the number of holes with the plenum internal cross-sectional area of UT's and PSU's plenums. UT's plenum cross-sectional area was 75 in.^{2} and PSU's was 72.25 in.^{2} with 130 holes. This calculation is shown in Equation 0-2.

$$72.25\ in.^2\ \frac{130\ holes}{75\ in.^2} = 125.23\ \rightarrow 126\ holes$$

Equation 0-2

Scaling the number and size of holes in the porous plate helps to insure that the turbulent length scale inside the plenum would be matched. The fine mesh screen that was used in both of UT's plenums and PSU's plenum was the same: 0.24 mm diameter wire spaced 2mm.

UT attempted to match the internal geometry of PSU's plenum to the extent that was possible, but one difference that could not be accounted for was the plenums had different aspect ratios. The plenum cross-section, which is defined as the open internal area of the plenum, was 7.5 in. x 10 in. for PSU's plenum and was 4.25 in. x 17 in. for UT's plenum. Figure 0-20 is a scaled depiction of the plenum cross sections, showing the different aspect ratios of the plenums used by PSU (blue) and UT (orange). PSU's splash plate was 4 in. x 4 in., and because of the different plenum aspect ratios, UT had to reduce its splash to 2.5 in. x 4 in. to accommodate its smaller depth.

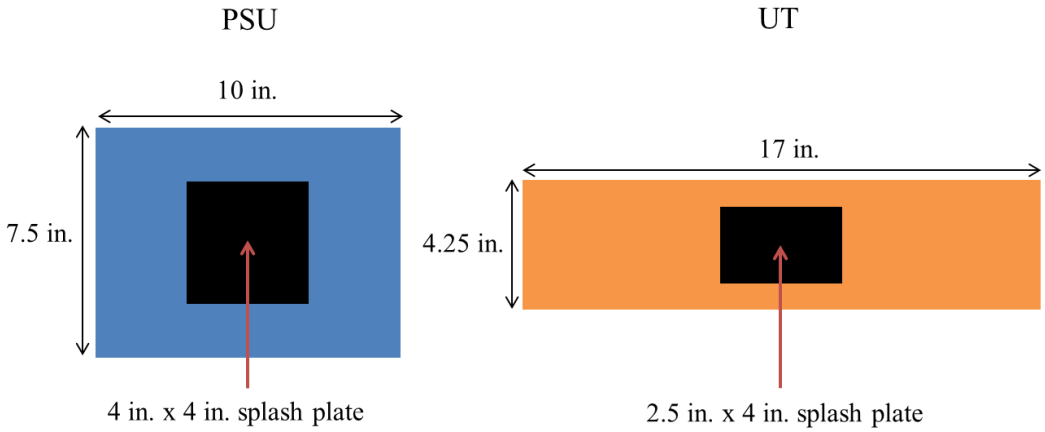

Figure 0-20 Scaled representation of the cross sectional area of PSU's plenum (blue) and UT's plenum (orange).

Figure 0-21 shows photographs from the construction of the UT plenum with similar PSU internal geometry. In the photographs, the yellow blocks are polystyrene insulation, and the red lining the seams is silicone. The picture on the top left shows the plenum after the 2 in. PVC pipe has been extended into the plenum to shorten its length. The picture on the top right shows the splash plate after it was installed, which is orange.

The picture on the bottom left shows the porous plate after it was installed, and finally, the picture on the bottom right show the fine mesh screen after it was installed.

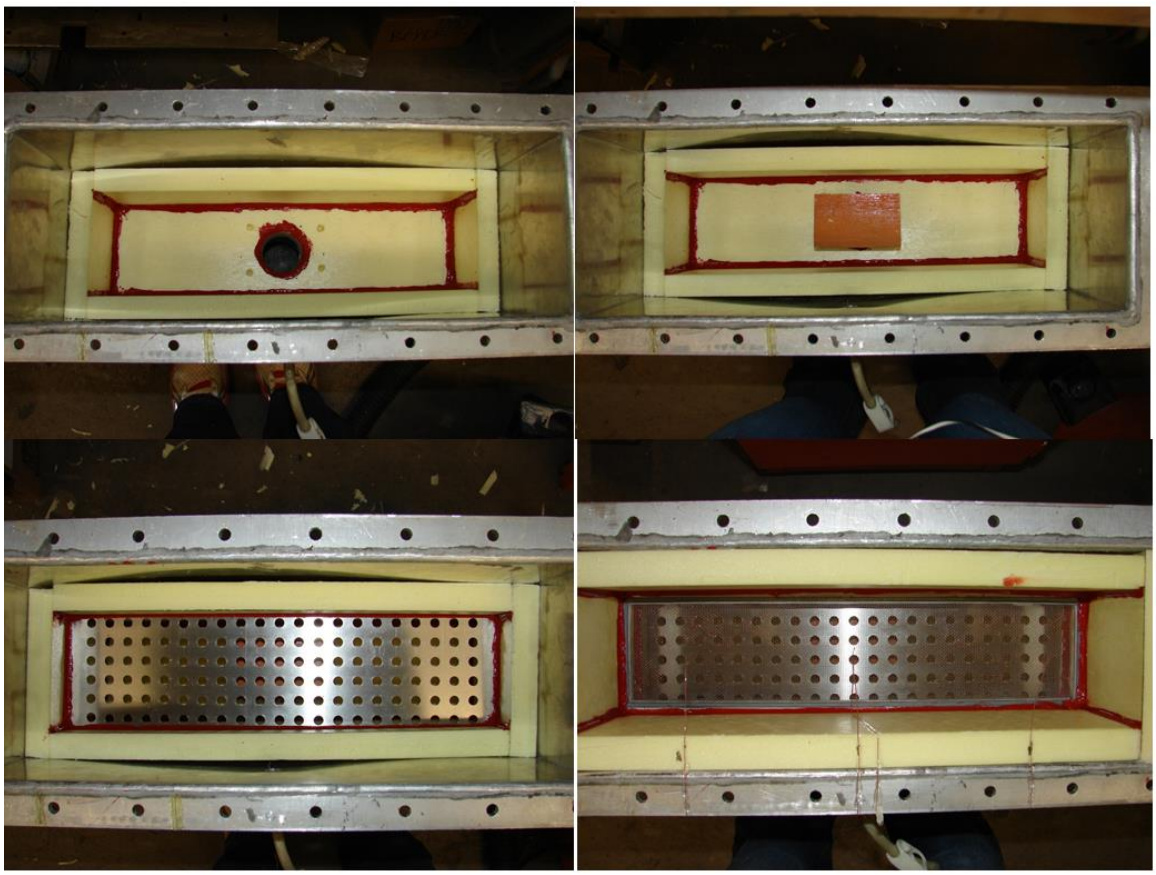

Figure 0-21 Construction of UT's plenum with the PSU internal plenum design.

UT tested the UT polystyrene coupon on the plenum with the PSU internal configuration. UT's traditional method of attaching polyurethane coupons to the plenum with silicone did not work with polystyrene. After the silicone delaminated from the polystyrene and created a leak during two experiments, the attachment method had to be changed. To get around silicone not adhering well to polystyrene, a Plexiglass liner was

machined to be sandwiched between the polystyrene coupon and the mounting base. Liquid Nails Foamboard Adhesive was used to attach the Plexiglass liner to the polystyrene and then silicone attached the Plexiglass liner to the wooden mounting base. This method worked well, and there were no leaks.

Figure 0-22 a) and b) show results from testing the UT polystyrene coupon. For this test, UT used a polystyrene coupon that PSU machined and a plenum that had a similar internal geometry to PSU's. At this point, everything that could possibly be matched, with exception of testing the exact same coupon, had been matched. Yet, the correspondence of results between the labs was worse than ever. Figure 0-22 a) shows the results at DR = 1.2. Interestingly, there was not a large drop in effectiveness at the higher blowing ratios. There appears to be some separation downstream of the coolant holes at M = 2.0 and 3.0, but there is some reattachment farther downstream. This is a unique result that was not seen in any of the previous tests. Again, at DR = 1.5, shown in Figure 0-22 b), there isn't a significant drop-off at high blowing ratios, although there appears to be some separation downstream of the holes for M = 2.0 to 3.0, with some reattachment farther downstream.

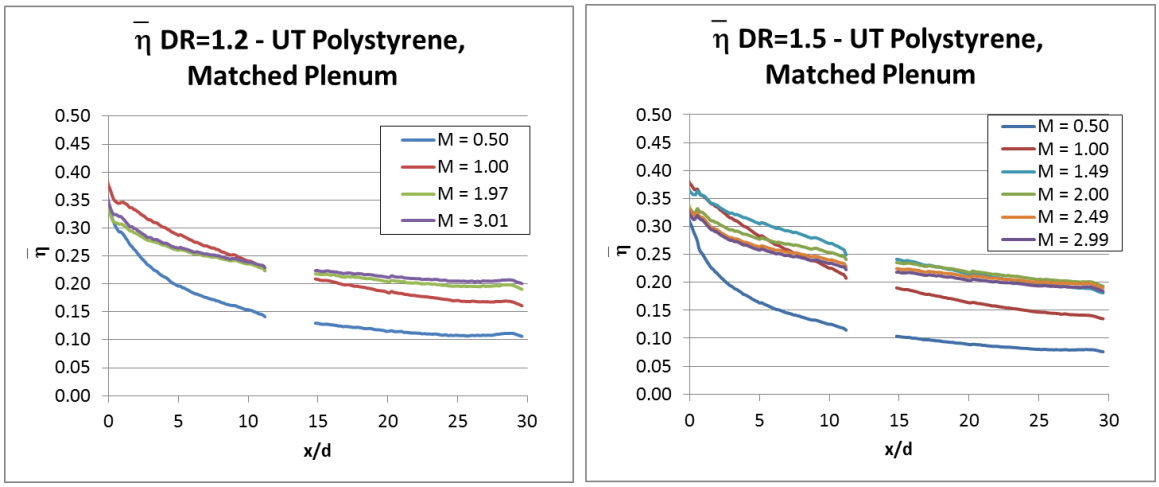

a) b)

Figure 0-22 Results from UT Polystyrene coupon with a plenum matching PSU's internal plenum geometry a) DR = 1.2 b) DR = 1.5.

Figure 0-23 a) and b) compare results from the UT polystyrene coupon with the matched PSU internal plenum geometry to results from the PSU polystyrene plate at *DR* = 1.2. The results don't match at any of the blowing ratios tested, with the largest differences being at the higher blowing ratios of *M* = 2.0 and 3.0. The $\bar{\eta}$ from the UT polystyrene coupon stayed relatively high at these blowing ratios, while the $\bar{\eta}$ from the PSU polystyrene plate did not, indicating the jets separated.

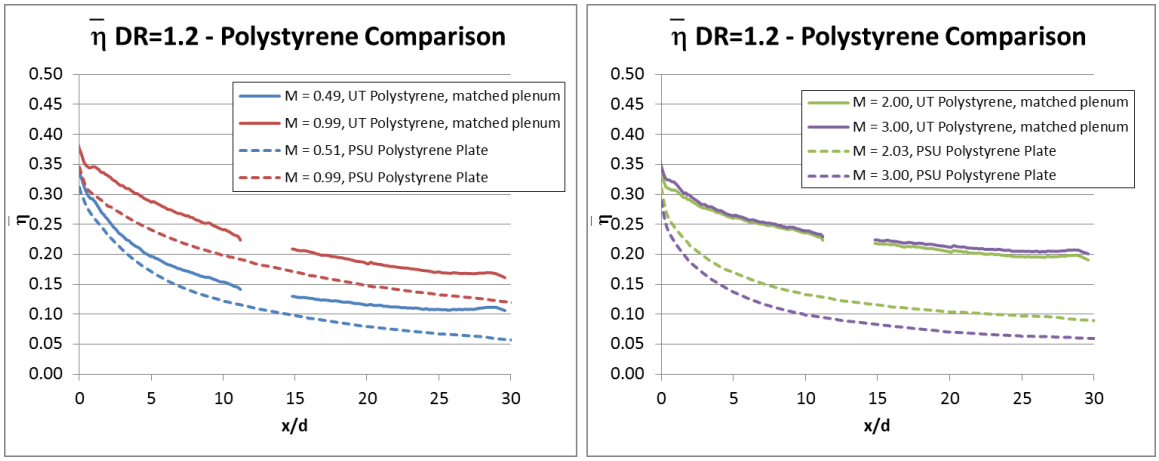

a) b)

Figure 0-23 Comparison of UT Polystyrene with matched PSU internal plenum geometry and PSU Polystyrene Hatch at *DR* = 1.2 and a) *M* = 0.5 and 1.0 b) *M* = 2.0, and 3.0

Figure 0-24 shows the results at *DR* = 1.5 comparing UT's data with the UT Polystyrene coupon to data from the PSU Polystyrene Hatch. At this density ratio, the data at *M* = 0.5 and 1.0 matches very well, but starts to diverge more and more as the blowing ratio is increased. The biggest difference between the two data sets is that the jets from the UT Polystyrene coupon with the similar internal plenum geometry remain effective at higher blowing ratios, while the jets from the PSU Polystyrene Hatch do not.

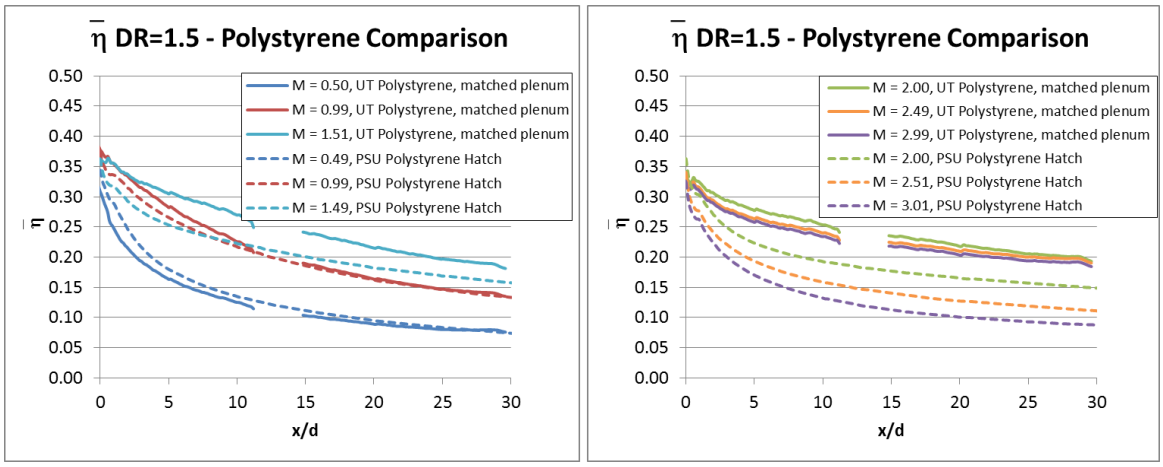

a) b)

Figure 0-24 Comparison of UT Polystyrene coupon with matched PSU internal plenum geometry and PSU Polystyrene Hatch at DR = 1.5 a) M = 0.5, 1.0, and 1.5 b) M = 2.0, 2.5, and 3.0

One interesting thing to note is that at M = 0.5 and DR = 1.5, UT's results match PSU's as to where other coupons had produced adiabatic effectiveness results that were much lower than PSU's at M = 0.5. It seems as though the performance at this blowing ratio is either especially sensitive to the coupon material/machining or coolant entrance effects that could have been altered due to the different internal plenum geometry.

It turns out that altering a UT plenum to be similar to the internal plenum geometry at PSU causes non-uniform coolant distribution, which is shown in Figure 0-25. This is a contour plot of adiabatic effectiveness at M = 1.5 and DR = 1.5, and clearly the jet at z/d = 9 performs worse than the jet at z/d = 3. This trend was seen at all blowing ratios except M = 0.5. Figure 0-26 is a surface plot of adiabatic effectiveness at $M \approx$ 1.0-1.5 and DR = 1.5 with the UT Polystyrene coupon and UT internal plenum design. The contours use the same coupon, but different internal plenum designs. The blowing ratio for this surface plot is uncertain since this test had a coolant leak. However, the figure can still give qualitative insight as to how well the jets perform compared to one another. Both jets perform similarly, suggesting that the coolant non-uniformity seen in Figure

0-25 was due to the internal plenum design and not the manufacturing of the UT polystyrene test coupon.

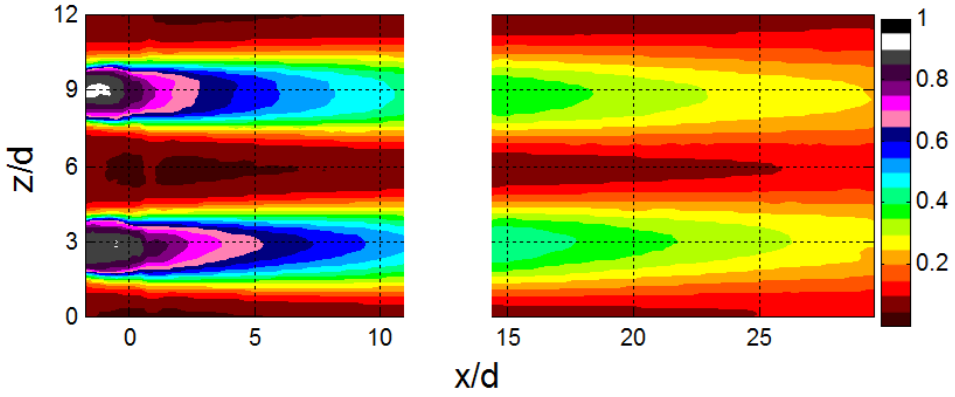

Figure 0-25 Contour plot of adiabatic effectiveness at M = 1.5, DR = 1.5, with the UT Polystyrene coupon and the PSU internal plenum design.

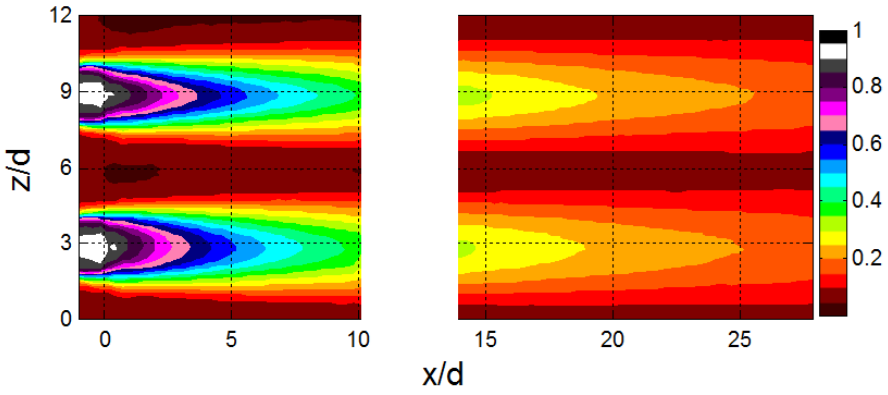

Figure 0-26 Contour plot of adiabatic effectiveness at $M \approx$ 1.0-1.5, DR = 1.5, with the UT Polystyrene coupon and the UT internal plenum design.

At the time this data was analyzed, PSU and UT decided that the best next step was to check that the flow rates were being measured properly at both facilities.

1.8.5 INCORRECT FLOW RATE MEASUREMENT

At this point in the project, UT and PSU still did not know what was causing the discrepancy in their test results and why every coupon tested performed differently. Obtaining the correct flow rate measurement is critical for these experiments, so both labs verified their flow rate measurements with laminar flow elements. PSU found that the venturi meter that they used to measure the flow rate of their coolant was accurate up to ± 0.25% of its 50 ACFM full scale, which would translate to ± 6.25% at $M = 0.5$ and $DR = 1.5$, the lowest flow rate that is measured for this project.

UT attached the laminar flow element to the coolant line and measured the flow rate reading from Labview versus the flow rate measured with the laminar flow element. The flow rate reading from Labview agreed with the flow rate measurement of the laminar flow element within ± 7% at the equivalent flow rate at $M = 0.5$, $DR = 1.5$. As the flow rate increased, the measurements between the two devices became closer. At an equivalent flow rate that would be present at $M = 1.0$ at $DR = 1.5$, the Labview readout was within 0.6% of the laminar flow element reading. However, the uncertainty analysis shows that the uncertainty of the pressure drop measurement for $M = 0.5$, $DR = 1.5$ was ± 0.07 in. H_2O at 23°C, which corresponds to ± 13% for a total uncertainty of M = 0.5 ± 0.09. The higher uncertainty results from zero drift of the pressure transducer that can occur throughout an experiment, but may not exist in the flow rate check comparison with the laminar flow element. In the end, UT verified that the Labview readout from the test setup corresponded to the laminar flow element reading, and an incorrect flow rate measurement was not causing the difference in results between UT and PSU.

Additionally, both labs measured the pressure drop across the coolant holes, which is another way of verifying that the flow rate and blowing ratio calculations were correct. To make this measurement, a pressure tap was installed inside the plenum at roughly the same distance from the coolant holes as what was used at PSU. A Pitot-static probe was installed just upstream of the coolant holes and the change in static pressure

between the plenum and coolant hole exit was measured. Figure 0-27 shows the pressure drop across the coolant holes versus blowing ratio at *DR*=1.5.

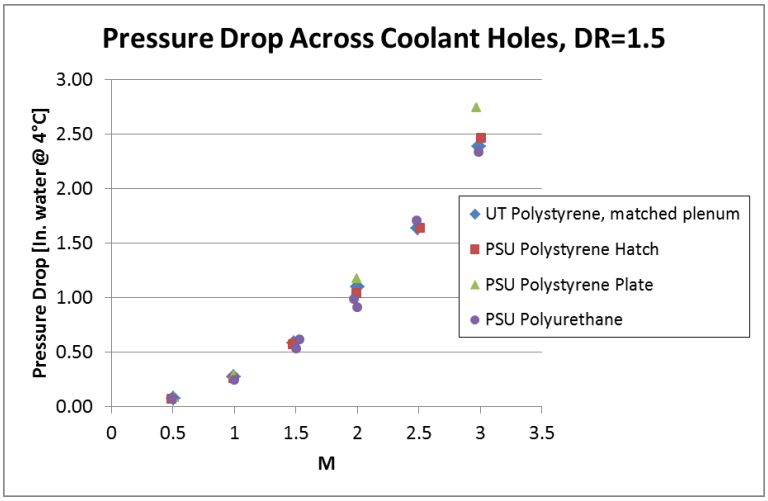

Figure 0-27 Comparison of pressure drop across film cooling holes at different blowing ratios for three PSU tests (PSU Polystyrene Plate, PSU Polystyrene Hatch, and PSU Polyurethane) and one UT test (UT Polystyrene).

This figure shows the pressure drop across the coolant holes versus blowing ratio for three PSU tests (PSU Polystyrene Hatch, PSU Polystyrene Plate, and PSU Polyurethane) compared to one UT test (UT Polystyrene with the PSU internal plenum geometry design). UT's pressure drops match very well with PSU's, indicating that the two labs were measuring the same blowing ratios that they were reporting. At M = 0.5, the scale on Figure 0-27 is too large to see the variation pressure drop measurements, but the value for UT's data point is 0.07 in. H_2O at 4°C and PSU's range from 0.07 to 0.08 in. H_2O at 4°C. Therefore, the difference in adiabatic effectiveness results between the two labs cannot be attributed to different coolant flow rate measurements.

1.8.6 Extreme Sensitivity of Shape Hole Geometries to Machining and Material Differences

Up to this point in the project, none of the experiments that had been completed provided an explanation as to why the results did not match between the labs. As a last effort, UT and PSU decided to test the exact same coupon. PSU mailed UT the PSU Polystyrene Hatch. The results from testing the PSU Polystyrene Hatch at UT and PSU at *DR* = 1.5 are shown in Figure 0-28. For this experiment, UT used the original UT plenum design, since the PSU plenum design caused the jets to be non-uniform. UT's laterally averaged adiabatic effectiveness values were produced by averaging over two hole pitches from *z/d* = 0 to 12, which was the same range used to process the other experiments mentioned in this chapter.

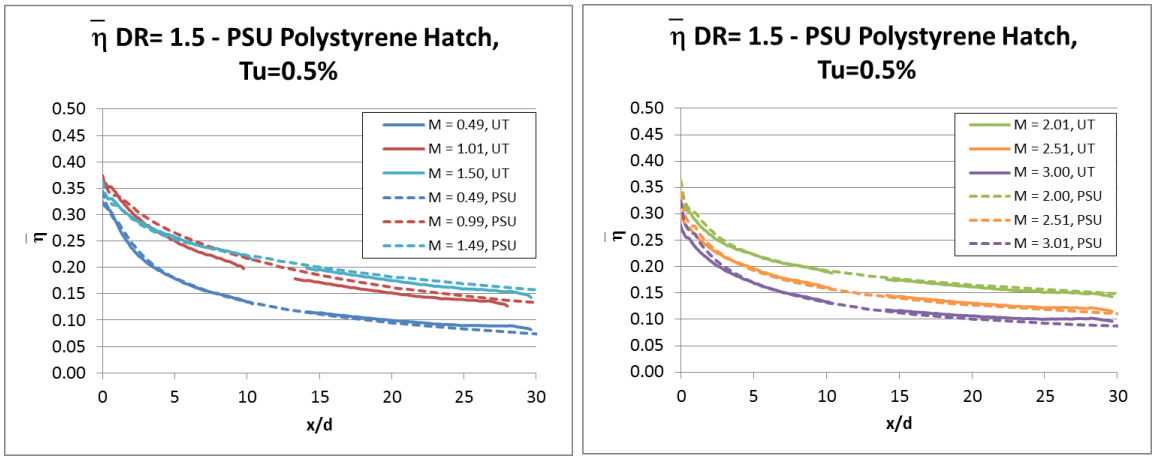

a) b)

Figure 0-28 Laterally averaged adiabatic effectiveness results from the PSU Polystyrene Hatch tested by UT and PSU at *DR* = 1.5 a) M = 0.5, 1.0, and 1.5 b) *M* = 2.0, 2.5, and 3.0.

Finally, UT and PSU produced results that finally matched, even at *M* = 0.5. However, looking solely at laterally averaged adiabatic effectiveness results is a little

misleading in this case. Even though UT tested the coupon with the original UT internal plenum design, the coolant flow between the holes was not very uniform at high blowing ratios. Figure 0-29 shows how the flow is uniform between holes at low blowing ratios. The top surface contour shows adiabatic effectiveness measured at UT at $M = 0.5$ and $DR = 1.5$, and the bottom contour shows the corresponding data measured at PSU.

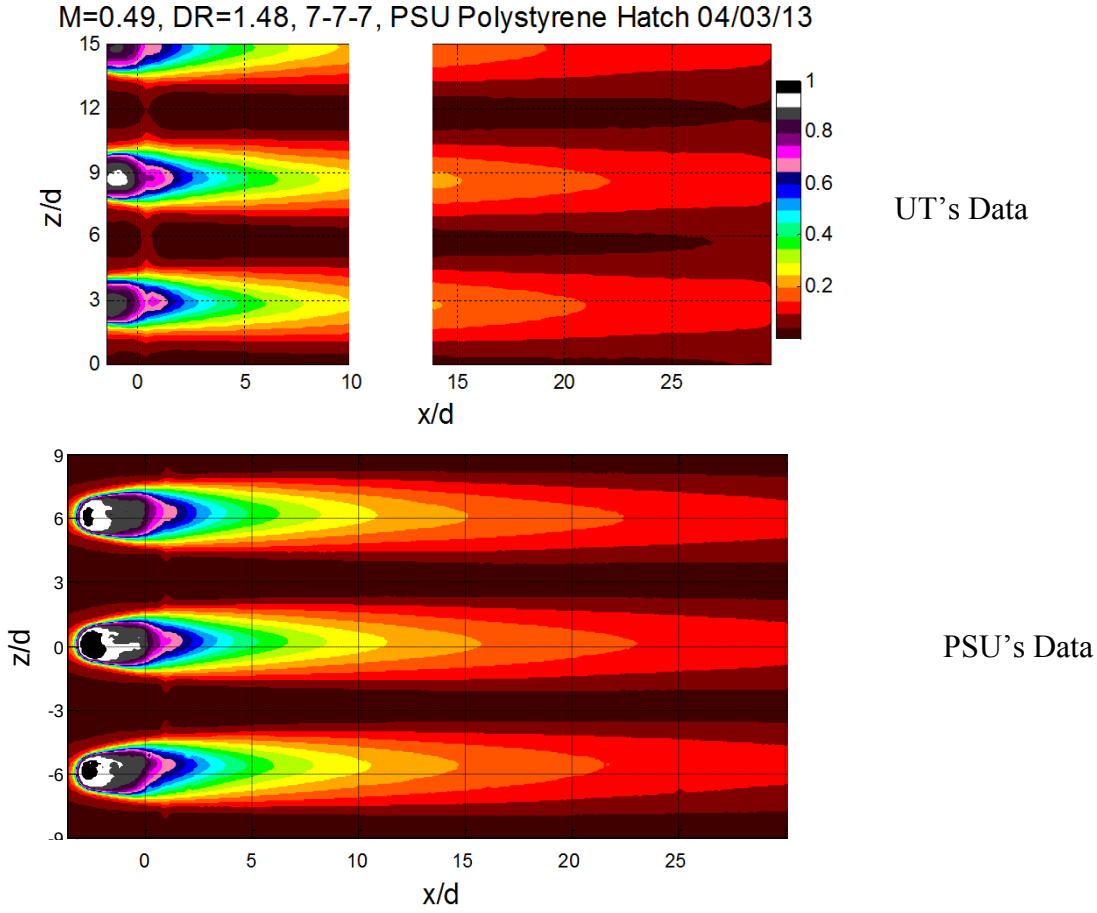

Figure 0-29 Contour of adiabatic effectiveness for the PSU polystyrene hatch tested at $M = 0.5$ and $DR = 1.5$ at UT (top) and PSU (bottom).

From the contours it can be seen that the effectiveness values are very similar. A comparison of UT's data to PSU's data in terms of lateral distributions of η at x/d = 0, 3, 8, and 20 is shown in Figure 0-30. The peak effectiveness between the three jets is very similar.

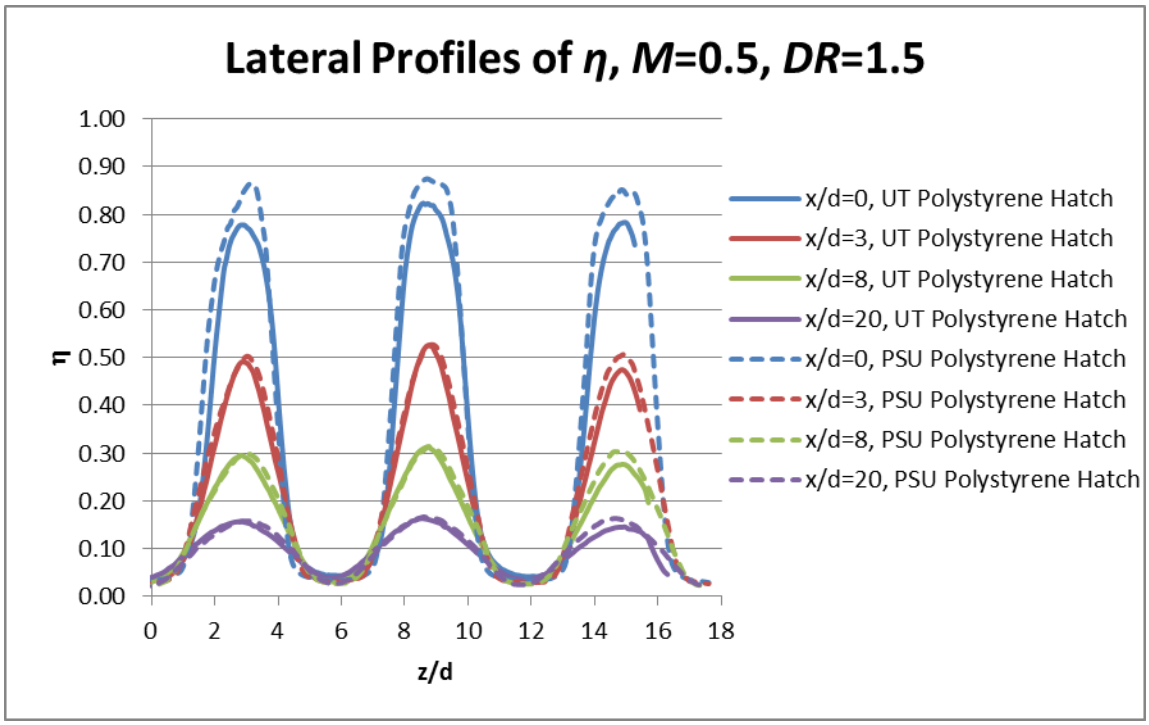

Figure 0-30 Lateral profiles of η comparing results from UT and PSU using the PSU Polystyrene coupon at x/d = 0, 3, 8, and 20.

At DR = 1.5, from M = 1.5 up to 3.0, UT's jets start to become non-uniform. This is shown in Figure 0-31, which compares UT's contour plots of η to PSU's at M = 2.0, DR = 1.5.

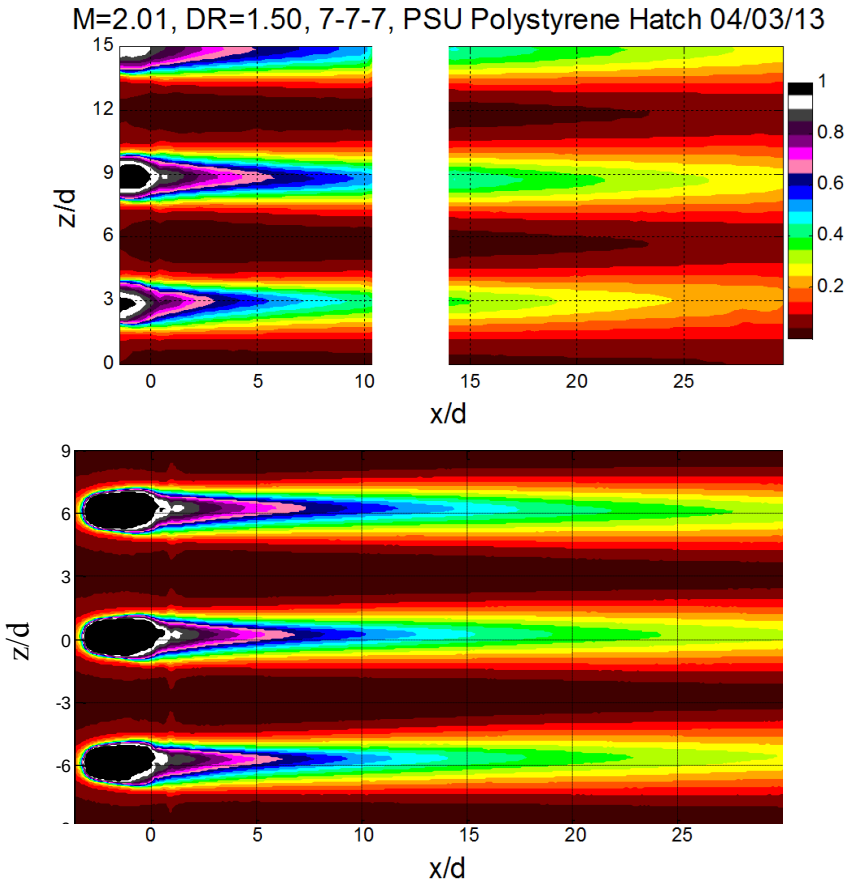

Figure 0-31 Contour of adiabatic effectiveness for the PSU Polystyrene Hatch tested at $M = 2.0$ and $DR = 1.5$ at UT (top) and PSU (bottom).

UT's contour plot, at the top, shows that the jet at $z/d = 15$ performs the best, and the jet at $z/d = 3$ performs the worst. PSU's contour shows that the jet at $z/d = 6$ (the same jet as at $z/d = 15$ in UT's contour plot) performs the best and the performance decreases for the jets as z/d decreases. However, the variation in jet performance at PSU was much less that what was seen at UT.

The lateral η distributions for $M = 2.0$, $DR = 1.5$ are shown in Figure 0-32. The jet peaks for UT's data, in the solids lines, are less than the jet peaks for PSU's data, which are in the dashed lines. Yet, the adiabatic effectiveness between the labs is the same

because UT's jets spread laterally slightly more than they do at PSU. Also, by averaging over the lower performing hole at z/d = 3 and a higher performing hole at z/d = 9, the variation of performance between the jets at UT is averaged out, and the averages align with PSU's data. It would be useful to know how the two remaining film cooling holes perform, but unfortunately, the IR window is not wide enough to allow the IR camera to image them.

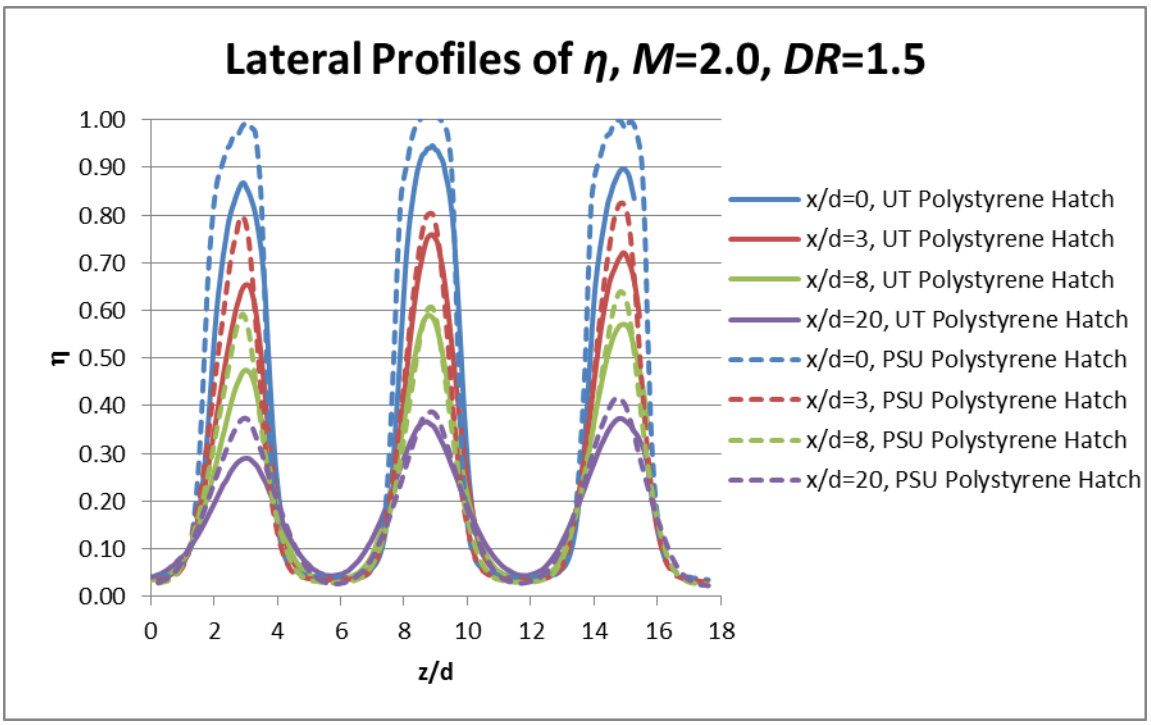

Figure 0-32 Lateral profiles of η comparing results from UT and PSU using the PSU polystyrene coupon at x/d = 0, 3, 8, and 20.

At DR = 1.2, the jets were also uniform at low blowing ratios and non-uniform at high blowing ratios of M = 2.0 and above. The non-uniformity could have been caused by hole-to-hole machining variation in addition to the fact that the PSU Polystyrene Hatch only had five coolant holes. UT's plenum is wider than PSU's (refer to Figure 0-20) and

UT normally tests eight holes that span across the entire width of the plenum. Having only 5 holes leaves extra volume on the sides of the plenum where the coolant can recirculate, which could cause some variation in temperature and turbulence at the hole entrances. This was investigated by looking at temperature measurements in the plenum compared to the thermocouples installed at the coolant hole entrances. Figure 0-33 a) shows the coolant temperature measurements that were taken while testing the UT Polyurethane coupon, which had eight coolant holes. This figure is representative of the temperature variations between the plenum temperature (1.5 in. beneath the coupon) and hole entrance thermocouples for all of the coupons that had eight holes that spanned across the entire width the plenum. The coolant entrance thermocouples were installed at the center of holes 2 and 7, if the holes are numbered from one side to the other, and surface temperatures were measured over holes 4 and 5. The coolant temperatures around 200-210 K were points taken at DR = 1.5 and temperatures around 250 K were points taken at DR = 1.2. For low blowing ratios, the temperature difference between the thermocouples was large, but decreased as the blowing ratio increased. This is the trend that was seen in all of the other film cooling tests that were run with eight holes spanning across the entire plenum.

Figure 0-33 b) shows the coolant temperatures that were measured while testing the PSU Polystyrene Hatch at UT. The coolant hole entrance thermocouples were installed on holes 1 and 5, while the three center holes were imaged with the IR camera for the data presented.

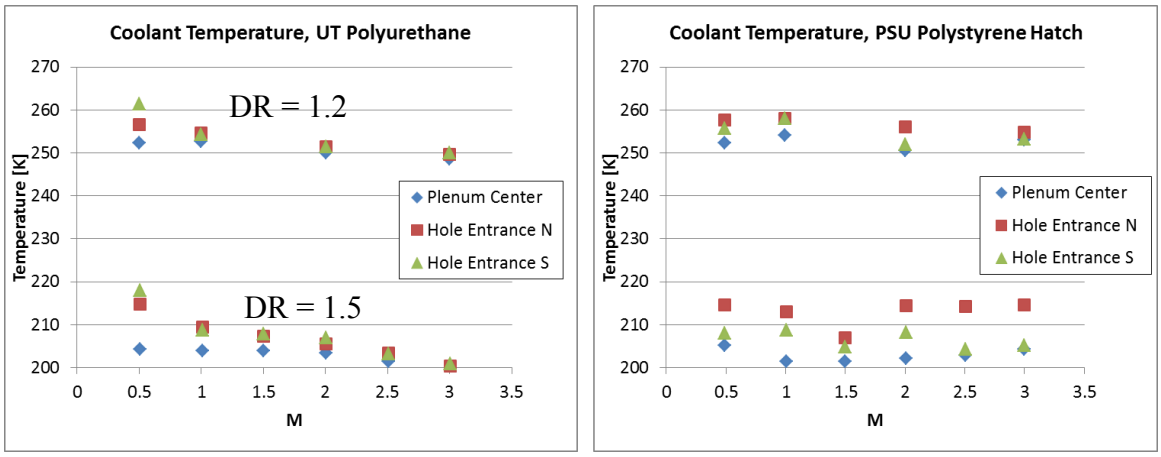

a) b)

Figure 0-33 a) Coolant temperature measurements from the UT polyurethane coupon test, which contains eight coolant holes.
b) Coolant temperature measurements from the PSU polyurethane coupon that contains five film cooling holes and was tested at UT.

The coolant temperature measurements shown in Figure 0-33 b) do not collapse with increasing blowing ratio, and vary as much as 10 K at $DR = 1.5$ and $M = 2.5$ and 3. Testing five holes instead of eight will also reduce the flow rate in the plenum, being about 38% less than the flow rate with eight holes. But, if the temperature variation of the coolant thermocouples were due to a lower coolant flow rate, the temperature variation should still be reduced at higher blowing ratios, and it's not. This indicates that the coolant temperature variation is due to the number of holes, not the flow rate through the plenum. The fact that there is this much variation in coolant temperature at high blowing ratios would also indicate that the velocity and turbulence profiles at the coolant hole entrances vary as well. All of these effects would produce non-uniform temperature and blowing ratios exiting the holes. There isn't a direct correspondence between the variation of the coolant thermocouple measurements and the non-uniformity between the jets, since the non-uniformity is not present at $M = 0.5$, where the variation between the thermocouples is still significant, but Figure 0-33 b) does show that there is some

unsteady effect that is taking place in the plenum when only five coolant holes are tested. Indeed, larger fluctuations in coolant temperature readings were observed during this test.

The results between UT and PSU didn't agree as well at DR = 1.2, but this is partly due to increased adiabatic effectiveness between the jets in UT's data, and very little increased adiabatic effectiveness between the jets in PSU's data, which is discussed later. Figure 0-34 shows laterally averaged adiabatic effectiveness at DR = 1.2 and compares UT's results, which are the solid lines, to PSU's results in the dashed lines.

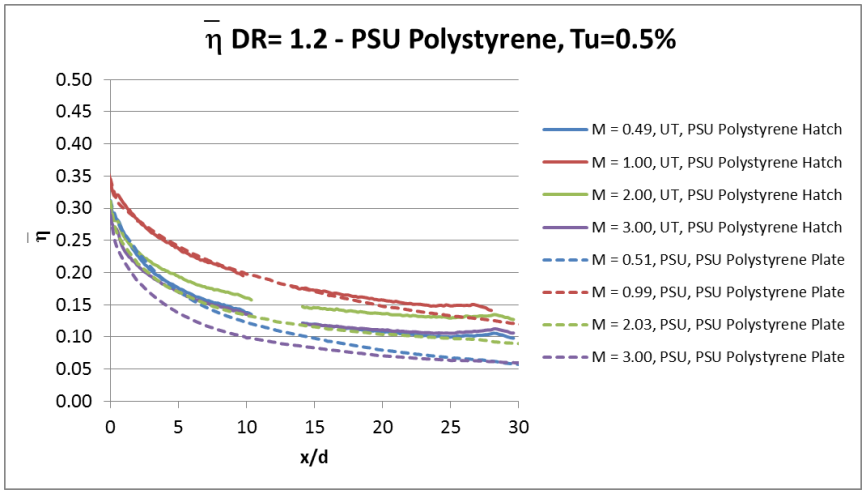

Figure 0-34 Laterally averaged adiabatic effectiveness at DR = 1.2 for data taken with the PSU Polystyrene Hatch.

As mentioned, with the exception of M = 1.0, the laterally averaged results between UT and PSU do not agree well. If the results from the two labs are separated, a clear trend forms. Figure 0-35 a) shows UT's laterally averaged adiabatic effectiveness results and Figure 0-35 b) shows PSU's.

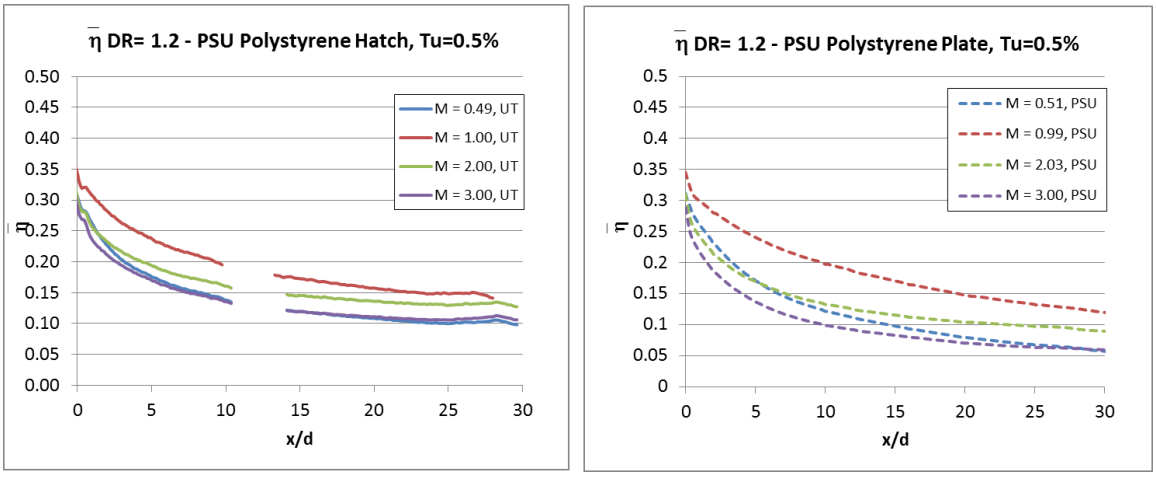

Figure 0-35 a) Laterally averaged adiabatic effectiveness from the PSU Polystyrene Hatch measured at UT at $DR = 1.2$.
b) Laterally averaged adiabatic effectiveness from the PSU Polystyrene Hatch measured at PSU at $DR = 1.2$.

The figures show the same trend with blowing ratio. The laterally averaged adiabatic effectiveness starts out low at $M = 0.5$ and increases up to its peak at $M = 1.0$ and then decreases with increasing blowing ratio. Figure 0-36 shows lateral distributions of η at $M = 2.0$, $DR = 1.2$ and $x/d = 0$, 3, 8, and 20.

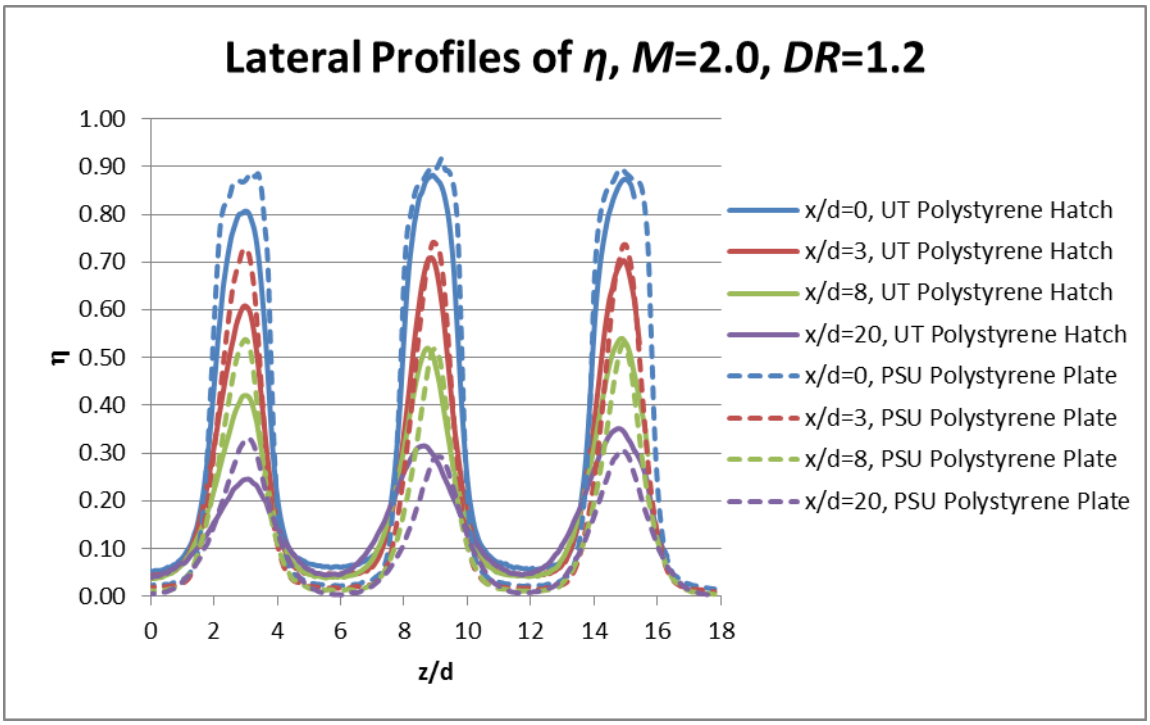

Figure 0-36 Lateral distributions of η using the PSU Polystyrene Hatch at M = 2.0, DR = 1.2 and x/d = 0, 3, 8, and 20.

Interestingly, the peaks of the jets line up quite well, with the exception of the underperforming jet at z/d = 3. What is different is the adiabatic effectiveness between the jets, which is about 0.05 in UT's data and 0.02 in PSU's data. If UT's adiabatic effectiveness is shifted down uniformly to match PSU's effectiveness between the jets, the data matches much better, which is shown in Figure 0-37.

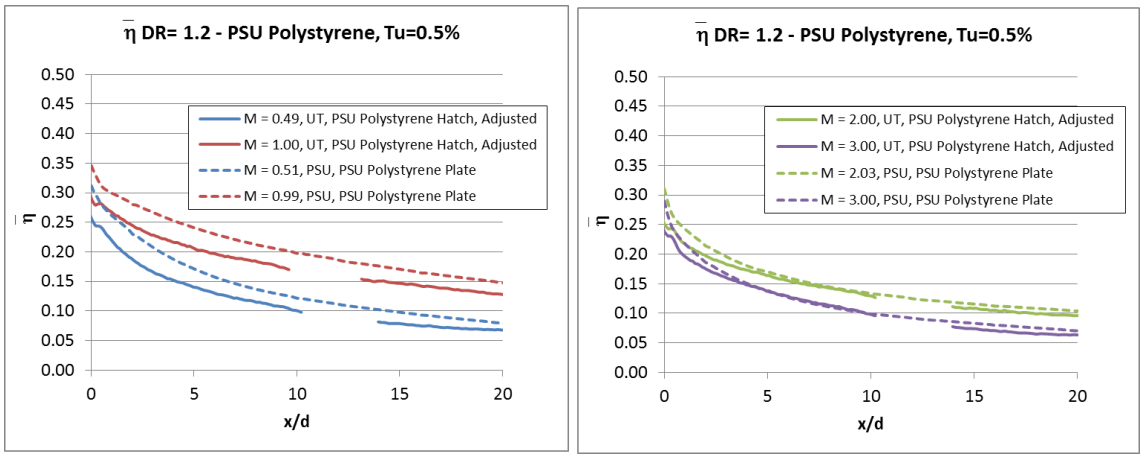

Figure 0-37 Comparison of UT and PSU laterally averaged effectiveness at DR = 1.2 after UT's data has been shifted down to match PSU's effectiveness between jets.

The adjustment has decreased the laterally averaged adiabatic effectiveness for all blowing ratios. Now, the agreement between UT's and PSU's data is better than the original comparison in Figure 0-35 except at M = 1. In the original comparison, UT's and PSU's data at M = 1.0 agreed very well, so decreasing the effectiveness caused the data at this blowing ratio to not match as well. At M = 2.0 and 3.0 UT's shifted data and PSU's data agree very well. Shifting UT's entire lateral average values down by the difference of effectiveness between UT's and PSU's data between the jets is probably an overcorrection, since the source of error is most likely confined to area between the jets, and not inside them. But, this kind of analysis is helpful in demonstrating that the difference in the results between the two labs isn't as large as it initially appears. The difference seems to be due to an error in the effectiveness measurements between the jets, possibly due to a cold approaching boundary layer in UT's case. It should be pointed out that this error is enhanced at DR = 1.2, and not at DR = 1.5, because it appears to be a bias error, and a bias in temperature reading at DR = 1.2 will have a larger effect because there is a smaller temperature difference between the coolant and mainstream.

PSU machined another coupon out of polystyrene, this time instructing the machinist to be very careful with the quality of the holes. This coupon is labeled PSU Smooth Polystyrene in the results. Figure 0-38 shows laterally averaged adiabatic effectiveness results for all of the polystyrene coupons tested, which includes the UT Polystyrene, PSU Polystyrene Hatch, and the PSU Smooth Polystyrene. These plots include the PSU Polystyrene Hatch data measured at PSU.

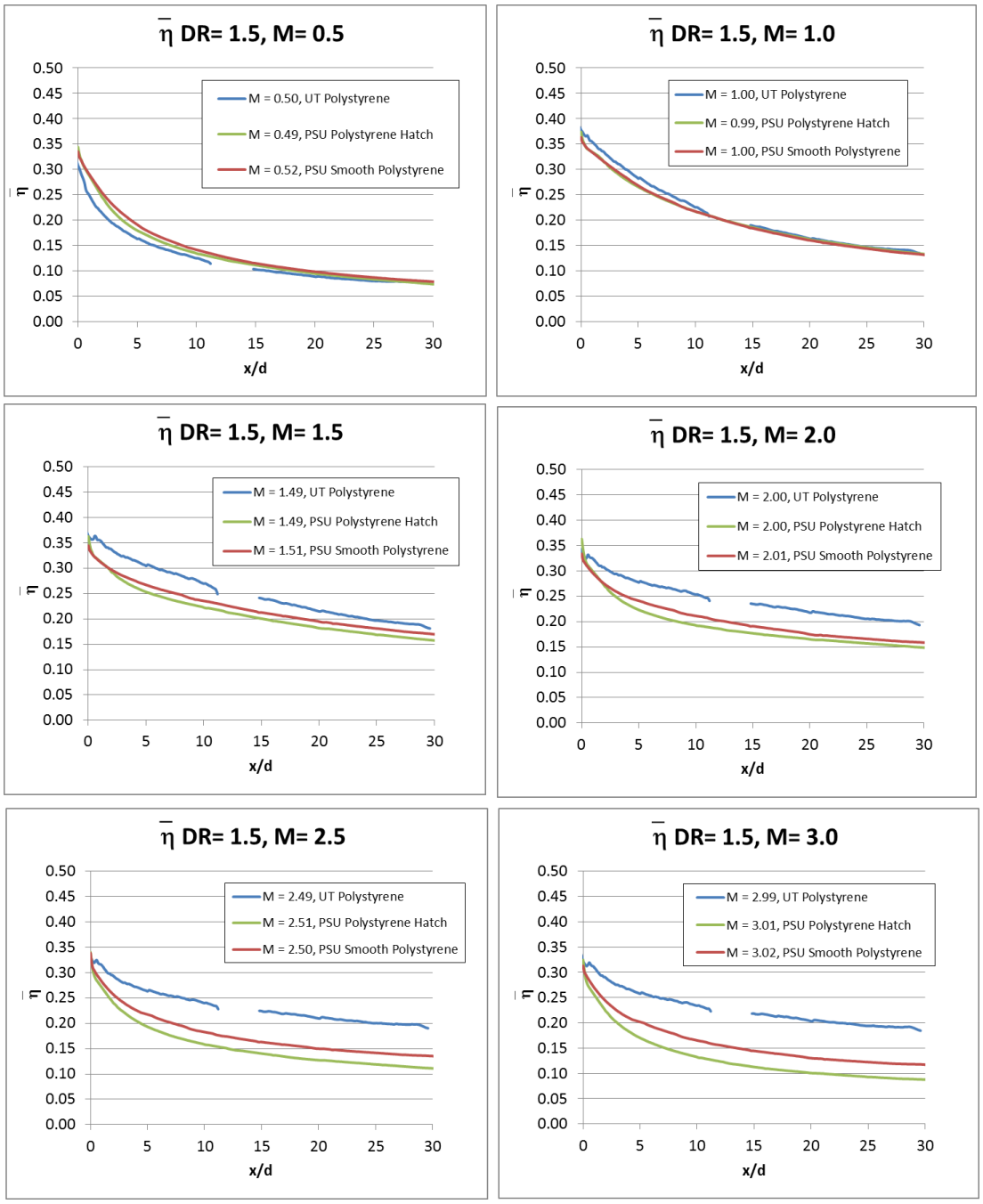

Figure 0-38 Comparison of all polystyrene coupons at DR = 1.5 and a) M = 0.5 b) M = 1.0 c) M = 1.5 d) M = 2.0 e) M = 2.5 f) M = 3.0

At M = 0.5 and 1.0, the results taken with the three coupons agree extremely well. Jet detachment starts to begin at M = 1.5 for the results taken with the PSU Polystyrene Hatch and the PSU Smooth Polystyrene, while separation does not occur with the data taken with the UT Polystyrene coupon. As the blowing ratio increases, the results taken with the different coupons start to diverge. The laterally averaged adiabatic effectiveness taken with the UT Polyurethane coupon doesn't drop like the results from the other two coupons, which can be attributed to differences in the machining of the coupon and/or to different coolant entrance effects than at PSU, even though the plenum design that was similar to PSU's was used for this test. The laterally averaged adiabatic effectiveness of the PSU Polystyrene Hatch and the PSU Smooth Polystyrene agree quite well, but start to diverge from one another by up to $\bar{\eta}$ = 0.03 at M = 3, which is outside of PSU's uncertainty. It appears that the results from all three coupons agree when the jets are fully attached, but once detachment starts to take place, slight variations in material, roughness, and machining start having a large effect. This figure shows that machining the same holes in the same material using the same machinist does not necessarily mean the results will be the same.

To summarize, the data between UT and PSU agree much better when the labs test the same coupon, suggesting that there is sensitivity of shaped holes to both machining and the coupon material. UT's results from testing the PSU Polystyrene Hatch had their issues. When the hatch was tested at DR = 1.5, the jets were non-uniform, but the lateral averages lined up very well with PSU's. The non-uniformity was mostly likely due to a combination of hole-to-hole machining variation and testing a coupon with five holes, instead of eight. Five holes did not span the width of plenum, causing different coolant entrance effects.

At DR = 1.2, UT's laterally averaged adiabatic effectiveness results were higher than PSU's. The peaks of the jets lined up well, but the effectiveness between UT's jets was higher than PSU's. If UT's data were uniformly shifted down so that the adiabatic

effectiveness between the jets equaled PSU's adiabatic effectiveness between the jets, the laterally averaged results between UT and PSU agreed much better.

Results from three polystyrene coupons made at PSU were compared. All three matched extremely well while all of the jets were attached at $M = 0.5$ and $M = 1.0$, but once separation began, the results started to diverge, especially for the UT Polystyrene coupon.

1.8.7 Difference in Plenum Inlet Flow Conditions

In the fall of 2013, a new test section and coolant piping system were built for a different research project. In the process, the coolant piping that led up to the plenum was changed to simpler configuration. The original coolant piping is shown in Figure 0-39 a) and the updated coolant piping is shown in Figure 0-39 b). The original coolant piping design was more complex because, at the time, leading edge experiments were being tested in the same test section, which required the coolant to be raised vertically above the plenum, to the height of the test section. Several times, over several years, the uniformity of the coolant exiting the row of jets was measured, and was found to be uniform hole-to-hole. As a result, it was concluded that the plenum and coolant piping design was working properly.

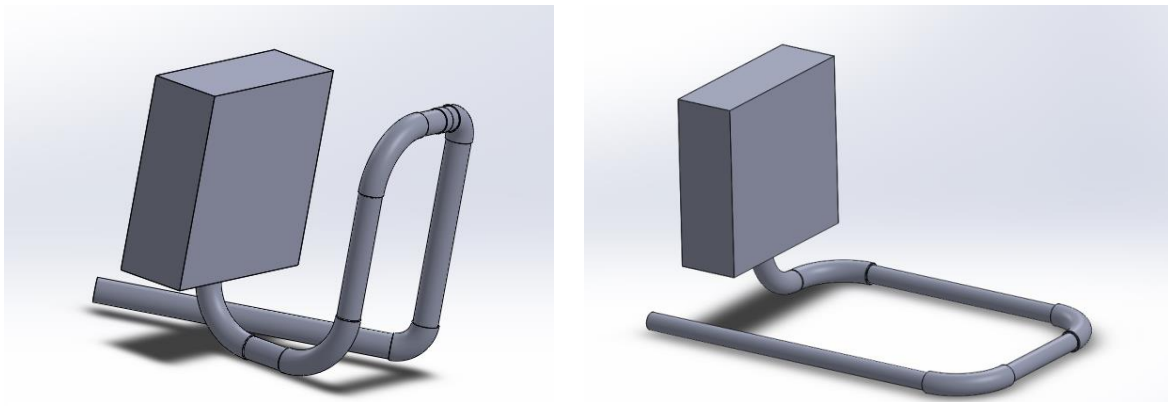

a) b)

Figure 0-39 a) Original coolant piping configuration b) Updated coolant piping configuration

After the new test section was built, a repeat experiment using the UT Polyurethane coupon with the UT Plenum was run. Initially, the test was repeated to check the M = 0.5 data point, which had been shown to be curiously low in previous experiments. When the experiment was run, the results at multiple blowing ratios were different than when the UT Polyurethane coupon was tested a year prior. Figure 0-40 compares the difference in results from testing the UT Polyurethane coupon with the UT plenum at DR = 1.2 with the original piping configuration and the new piping configuration. Except at M = 1.0 and 3.0, the results are very different. The comparison is similar at DR = 1.5, which is shown in Figure 0-41, and only the results at M = 1.0 agree well at this density ratio.

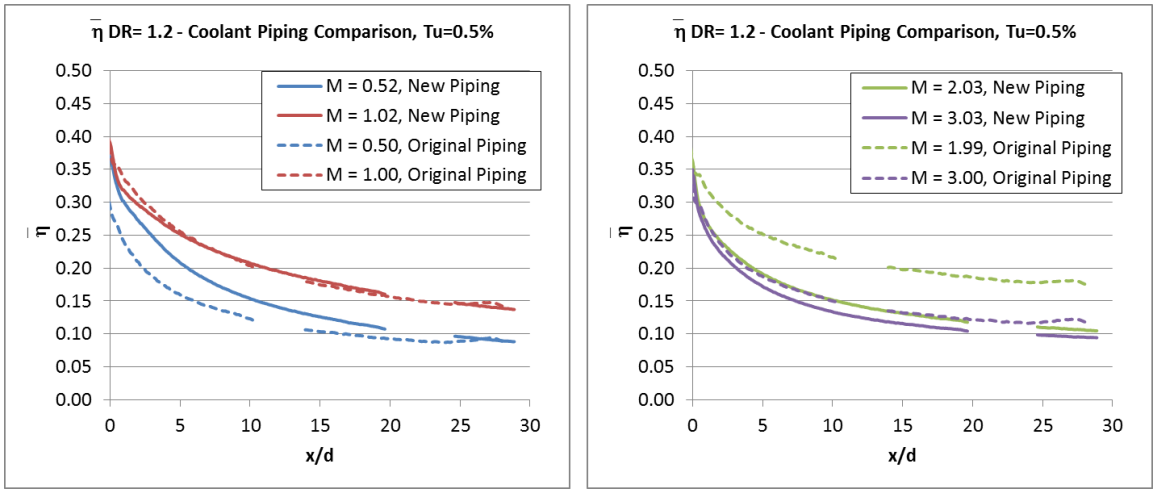

a) b)

Figure 0-40 Comparison between results taken with the new coolant piping and old coolant piping configurations at DR = 1.2 a) M = 0.5 and 1.0 b) M = 2.0 and 3.0 using the UT Polyurethane coupon and the UT plenum.

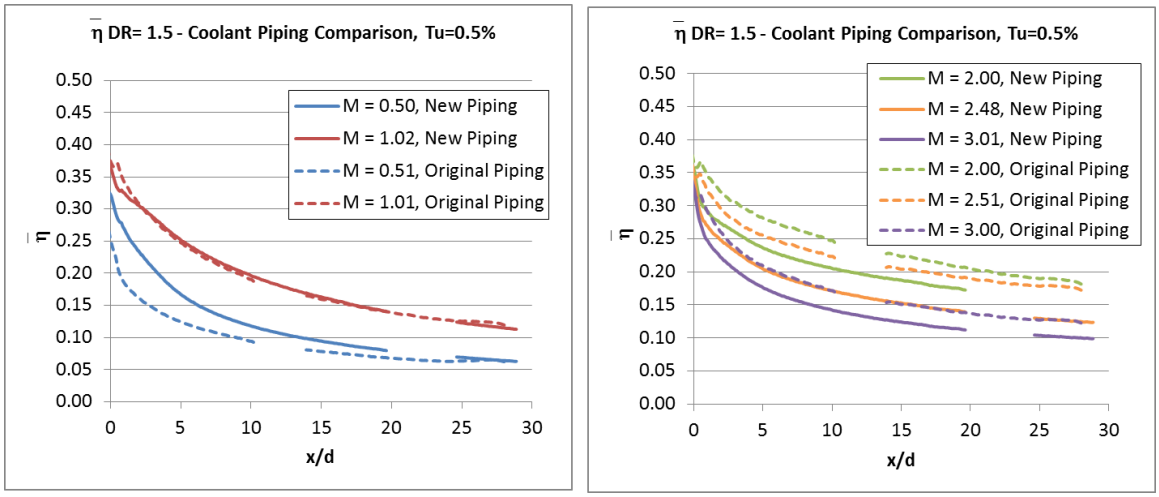

a) b)

Figure 0-41 Comparison between results taken with the new coolant piping and old coolant piping configurations at DR = 1.5 a) M = 0.5 and 1.0 b) M = 2.0, 2.5, and 3.0 using the UT Polyurethane coupon and the UT plenum design.

In addition to new coolant piping, the new test section used a venturi meter to measure the flow rate, while an orifice meter had been used in the past. Also, new pressure transducers were purchased, which were used for the coolant flow rate measurement and mainstream velocity measurement. Of course, these variables could also cause the change in results shown in Figure 0-40 and Figure 0-41. But, as discussed in Section 1.8.5, the coolant flow rate measurement used in the original piping configuration had been tested by using a laminar flow element as a standard (which was also used to calibrate the venturi meter in the new coolant piping system) and also by measuring the pressure drop across the coolant holes during a test, which aligned well with PSU's measured pressures. If the flow rate measurement was not at fault, the only possible explanation for the difference in results is that the coolant piping was affecting the shaped hole performance.

When the results using the new coolant piping configuration are compared to PSU's Smooth Polystyrene results, the data correspond well. Figure 0-42 compares results at $DR = 1.2$ and Figure 0-43 compares results at $DR = 1.5$.

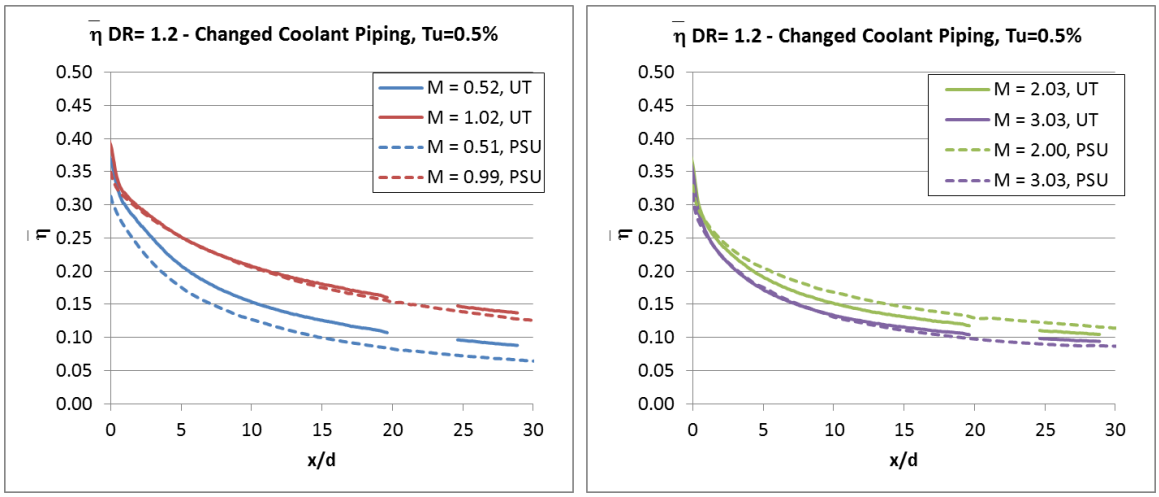

a) b)

Figure 0-42 Comparison of laterally averaged adiabatic effectiveness between UT (UT Polyurethane), with changed coolant piping into the plenum, and PSU (PSU Smooth Polystyrene) at *DR* = 1.2.

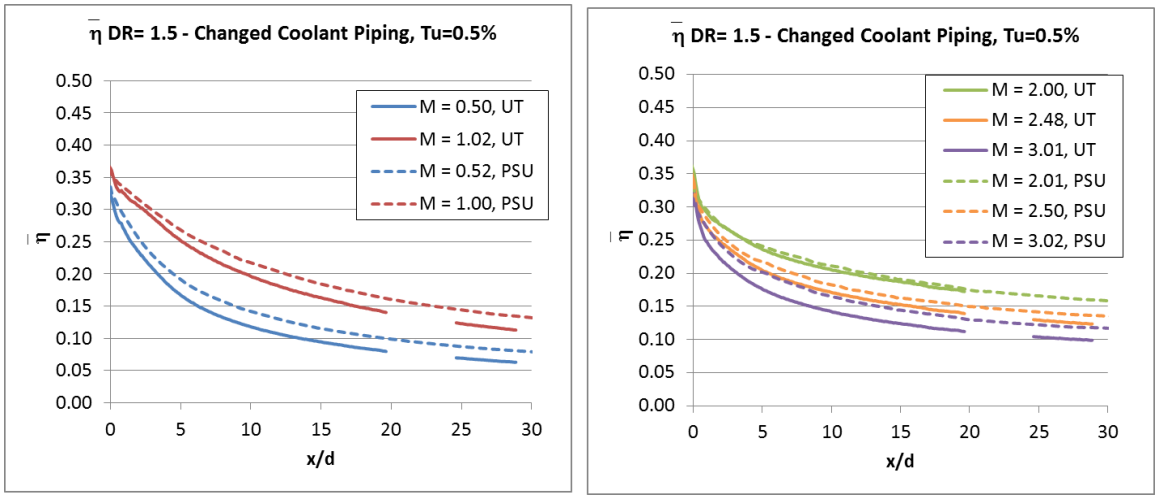

a) b)

Figure 0-43 Comparison of laterally averaged adiabatic effectiveness between UT (UT Polyurethane), with changed coolant piping into the plenum, and PSU (PSU Smooth Polystyrene) at *DR* = 1.5.

Figure 0-44 shows contours of adiabatic effectiveness at M = 2.0 and DR = 1.5. The top contour was measured at PSU using the PSU Smooth Polystyrene plate and the bottom contour was measured at UT using the UT Polyurethane coupon with the updated coolant piping system. By comparing the two surface contours, it can be seen that the adiabatic effectiveness between the two labs is very similar, and it's not coincidental that the laterally averaged results match in Figure 0-43 b).

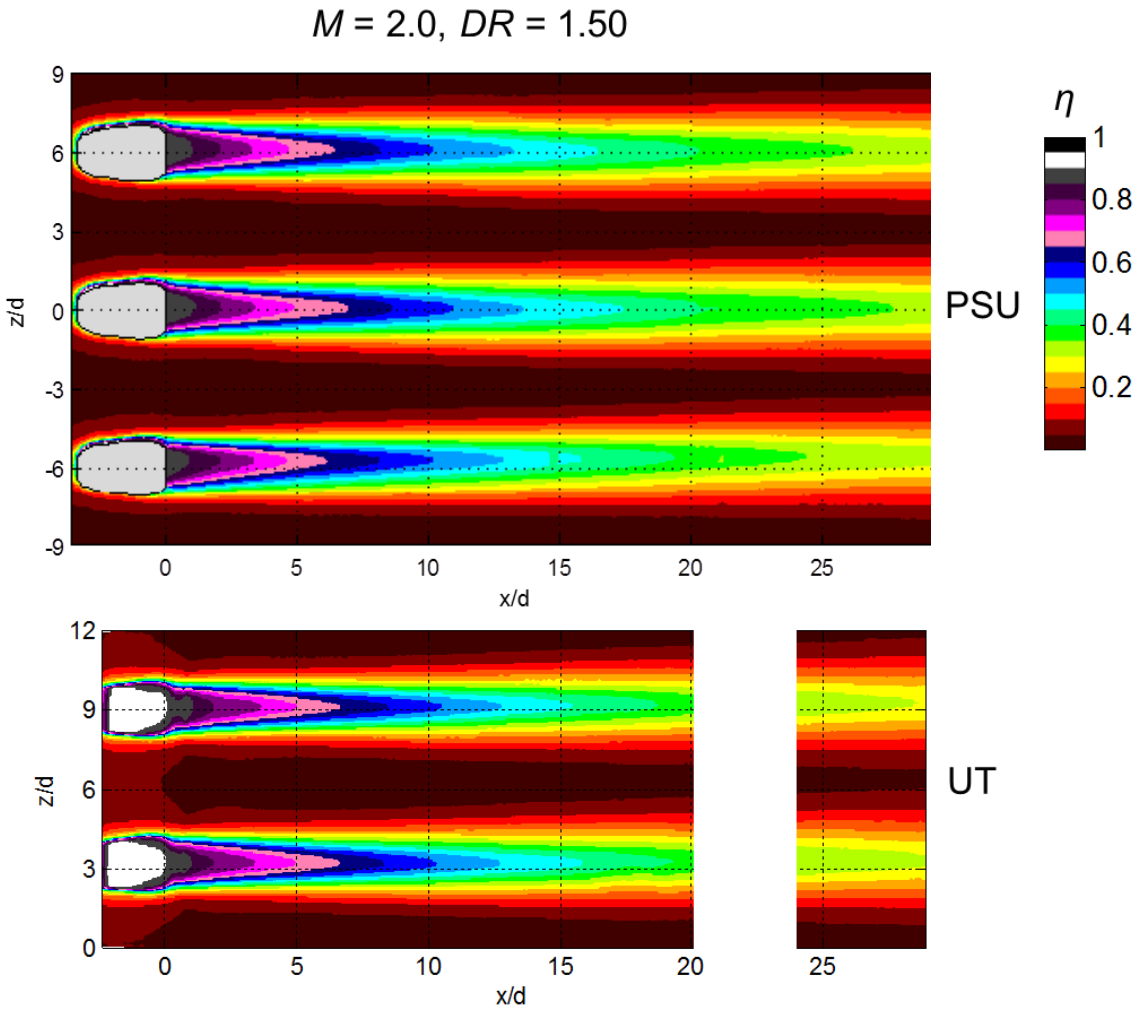

Figure 0-44 Comparison of adiabatic effectiveness contours at M = 2.0 and DR = 1.5 for PSU (top) and UT (bottom). PSU contour used the PSU Smooth Polystyrene and UT contour uses the UT Polyurethane.

If it is assumed that the changes in UT's data can be attributed to the coolant piping configuration leading up to the plenum, this is a very interesting result. There must have been a difference in the coolant flow conditions approaching the shaped holes between using the two coolant piping configurations. PSU's coolant piping is more similar to the new coolant piping configuration. In their configuration, the coolant flows in the upstream direction, centered along the width of the test section, and then turns vertically into the plenum. UT's new coolant configuration flows in the same direction as PSU's, but runs off-center of the test section width, then turns toward the center of the test section width before it turns vertically into the plenum, which is shown in Figure 0-39 b). The results in this section have shown that the shaped holes are extremely sensitive to inlet flow conditions.

It was surprising that changing the coolant piping leading to the plenum caused the adiabatic effectiveness results to change and match PSU's results because it was thought that altering the plenum's internal configuration to match PSU's, which was discussed in Section 1.8.4, would account for changes in coolant inlet conditions. Since the altered PSU internal plenum geometry did not cause the results to match, there are two possible explanations. First of all, only the UT Polystyrene coupon was tested using the internally redesigned plenum, and the machining quality of that coupon could have caused differences in the results. Secondly, the internal plenum geometry was rebuilt to match PSU's plenum geometry as closely as possible, but PSU's plenum and UT's plenum had different aspect ratios. This, accompanied with the different cooling piping configurations could mean that that flow conditions between UT and PSU, even when UT matched PSU's internal plenum geometry, had different coolant inlet flow conditions.

1.8.8 Results at Moderate Turbulence

PSU tested their PSU Smooth Polystyrene Plate at a moderate turbulence intensity of 5.4%. PSU modeled their turbulence grid after the grid used at UT so that the

turbulence intensity and length scale would be matched. Josh Anderson measured the turbulence intensity in UT's wind tunnel to be 5.0%. Figure 0-45 compares laterally averaged adiabatic effectiveness results at low (0.5%) and moderate (5.0%) mainstream turbulence intensity using the UT Polystyrene coupon. The results for the two turbulence levels are similar and just within the experimental uncertainty of $\bar{\eta} \pm 0.02$, so no definite conclusions on the effect of turbulence intensity can be drawn. Based upon what is in literature, increasing the turbulence intensity should degrade the performance of the shaped holes [9, 15], but the opposite trend is seen here. However, those studies were completed at a higher mainstream Mach number of 0.3 and with a very different shaped hole geometry.

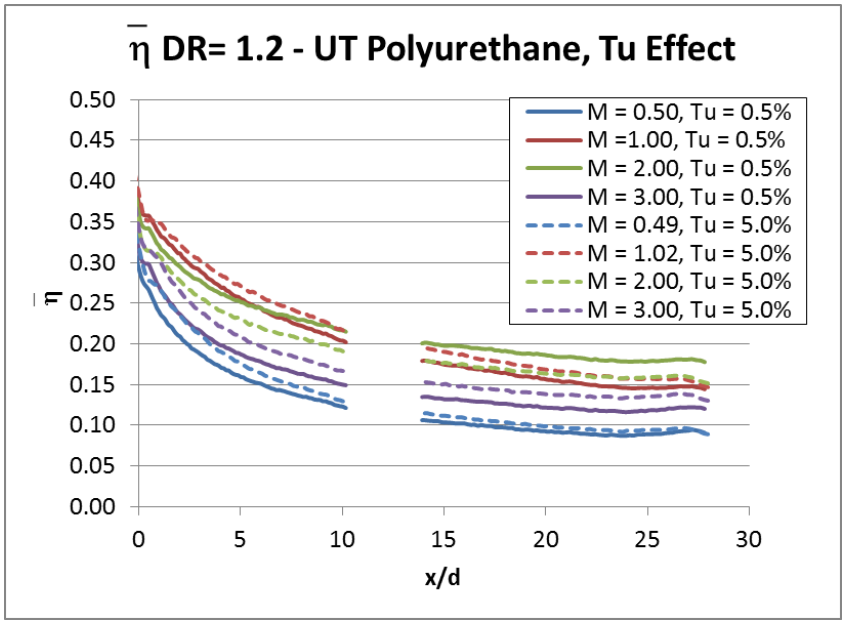

Figure 0-45 Comparison of laterally averaged adiabatic effectiveness at Tu = 0.5% and 5.0% at DR = 1.2 using the UT Polyurethane coupon.

Figure 0-46 shows the effect of turbulence intensity at DR = 1.5. Again, the difference in results at Tu = 0.5% and 5.0% is just within the experimental uncertainty of $\bar{\eta} \pm 0.01$, except the difference in performance at M = 0.5 is substantial. Increasing the turbulence intensity at M = 0.5 increases the laterally averaged adiabatic effectiveness performance significantly. This could be because the higher mainstream turbulence intensity spreads the coolant in the expansion, which increases the performance.

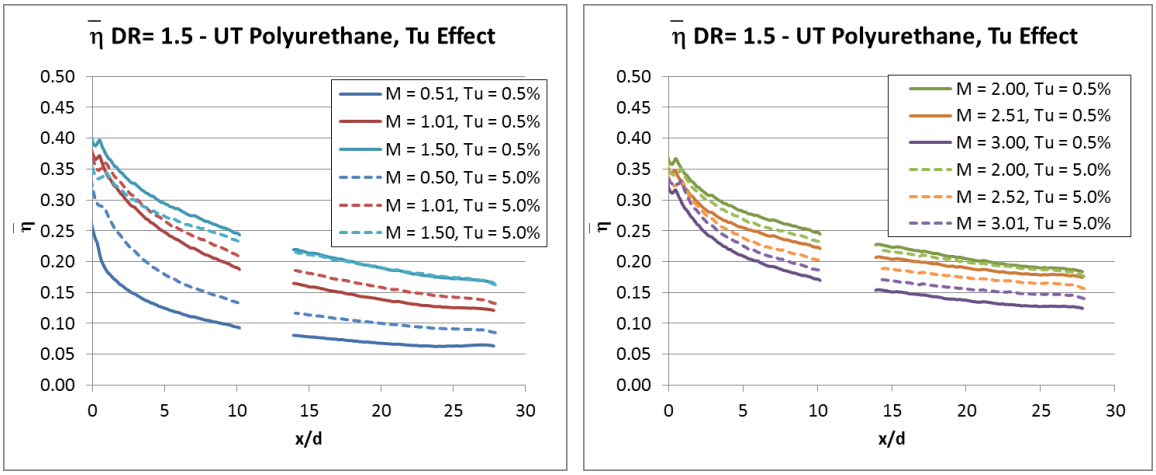

Figure 0-46 Comparison of laterally averaged adiabatic effectiveness at Tu = 0.5% and 5.0% at DR = 1.5 using the UT Polyurethane coupon.

Figure 0-47 compares moderate turbulence data taken at UT and PSU at DR = 1.5. UT used the UT Polyurethane coupon and PSU used the PSU Polystyrene Plate.

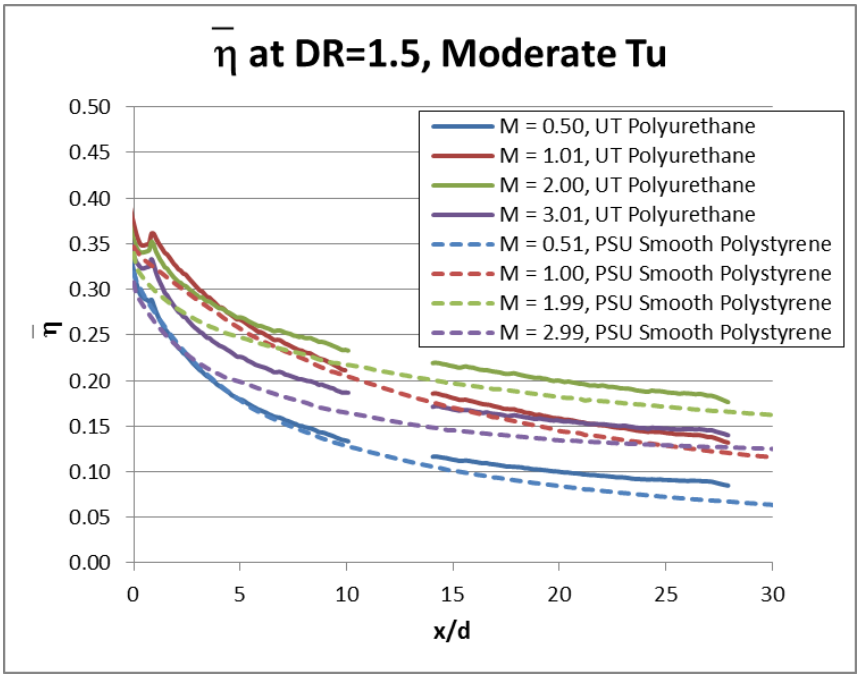

Figure 0-47 Comparison between results with the UT polyurethane coupon and the PSU smooth polystyrene plate at moderate turbulence intensity.

The results agree quite well, with UT's results being about $\bar{\eta}$ = 0.02 higher at some blowing ratios, which would be within uncertainty between the two labs. However, the results using the two coupons don't agree as well at low turbulence intensity, which is shown in Figure 0-48.

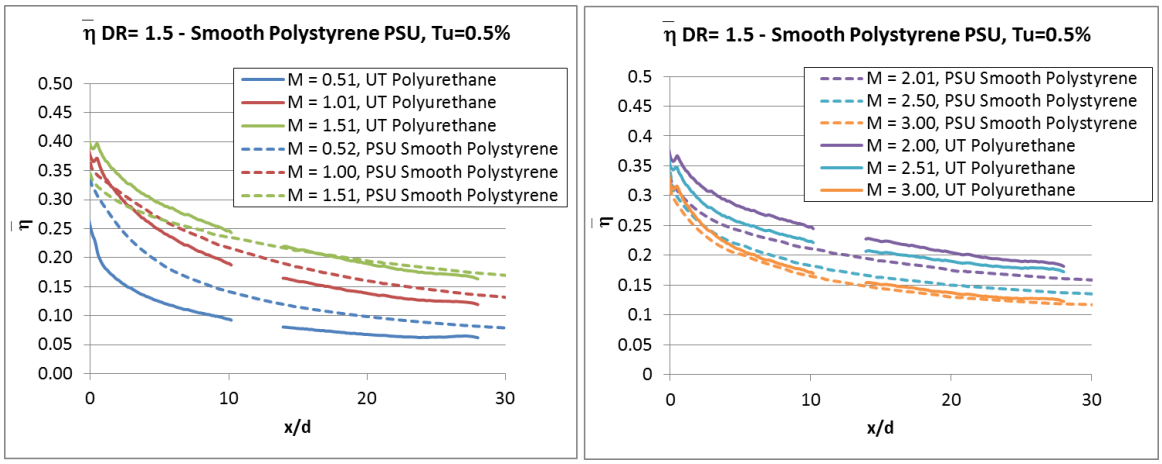

Figure 0-48 Comparison of laterally averaged adiabatic effectiveness at DR = 1.5 and Tu = 0.5% between the UT Polyurethane coupon and the PSU Smooth Polystyrene coupon results.

The results agree well at M = 1.5 and 3.0, but are up to 0.04 different at other blowing ratios. M = 0.5 is a special case, where UT's results are much lower, as has been discussed earlier in this chapter. The results from both labs peak between M = 1.5 and 2.0 and then show similar drop-off as the jets detach more and more.

Adding mainstream turbulence caused the data from two coupons to agree reasonably well that didn't agree at low mainstream turbulence. However, the change in UT's data from using low to moderate turbulence was within experimental uncertainty, except at M = 0.5 and DR = 1.5.

1.8.9 Scaling Adiabatic Effectiveness at Low and Moderate Turbulence Intensity

Understanding how adiabatic effectiveness scales with density ratio is important because it would allow researchers and turbine designers to use adiabatic effectiveness results at one density ratio to predict the performance at a different density ratio. This is

especially useful since many film cooling studies do not match the density ratio of 2.0 that is actually used in gas turbine engines. In addition, understanding how the performance of jets scales will provide insight into the flow physics of the jets. First scaling at low turbulence intensity will be discussed and then scaling at moderate turbulence. Scaling was analyzed using data taken with the original coolant piping system and the new coolant piping system, which was discussed in Section 1.8.7. Josh Anderson operated the tests with the new coolant piping system. All of the data used to discuss scaling in this section used the UT Polyurethane coupon.

1.8.9.1 Low Turbulence Intensity

Original Coolant Piping System

Scaling at Tu = 0.5% using the original coolant piping system was briefly discussed in Section 1.8.1. The laterally averaged adiabatic effectiveness was found to scale best with velocity ratio. Scaling with momentum flux ratio did fairly well, but not as well as velocity ratio. Scaling with blowing ratio was found to be poor. Figure 0-6, which shows how the results scale with velocity ratio at DR = 1.2, 1.5, and 1.73 is repeated here as Figure 0-49 for convenience.

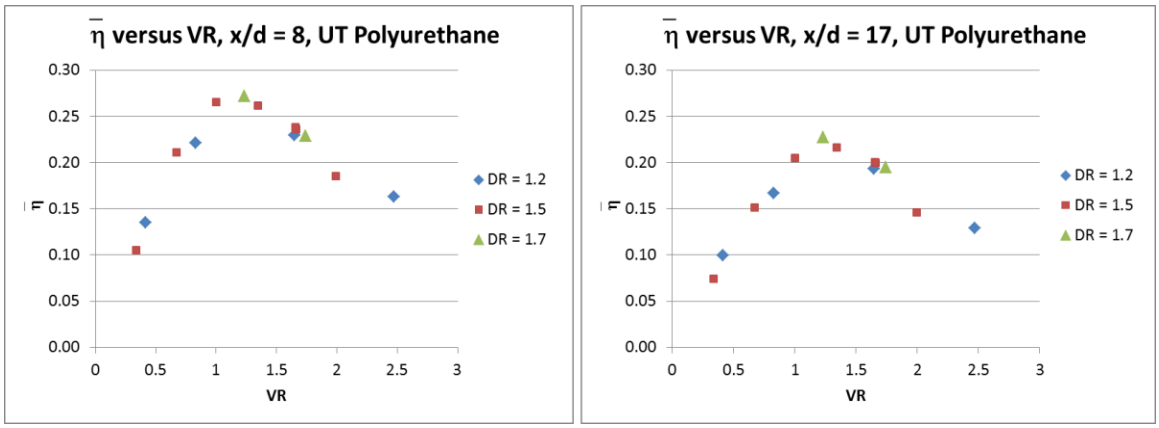

a) b)

Figure 0-49 Scaling with *VR* at *Tu* = 0.5% and a) *x*/*d* = 8 and b) *x*/*d* = 17 using the original coolant piping system and the UT Polyurethane coupon. Repeated from Figure 0-6.

New Coolant Piping System

Since the laterally averaged adiabatic effectiveness performance was different when using the new coolant piping system versus the original coolant piping, one would expect the scaling to change as well. However, it did not, and the laterally averaged adiabatic effectiveness still scales best with velocity ratio. Figure 0-50 shows how $\bar{\eta}$ scales with *M*, Figure 0-51 shows how $\bar{\eta}$ scales with *I*, and Figure 0-52 shows how $\bar{\eta}$ scales with *VR*. Each figure has a plot a) at *x*/*d* = 8 and b) at *x*/*d* = 17. These *x*/*d* positions are representative of scaling at all *x*/*d* positions. Clearly, *VR* is the best scaling parameter and the quality of scaling is comparable to what was seen with the original coolant piping system shown in Figure 0-49.

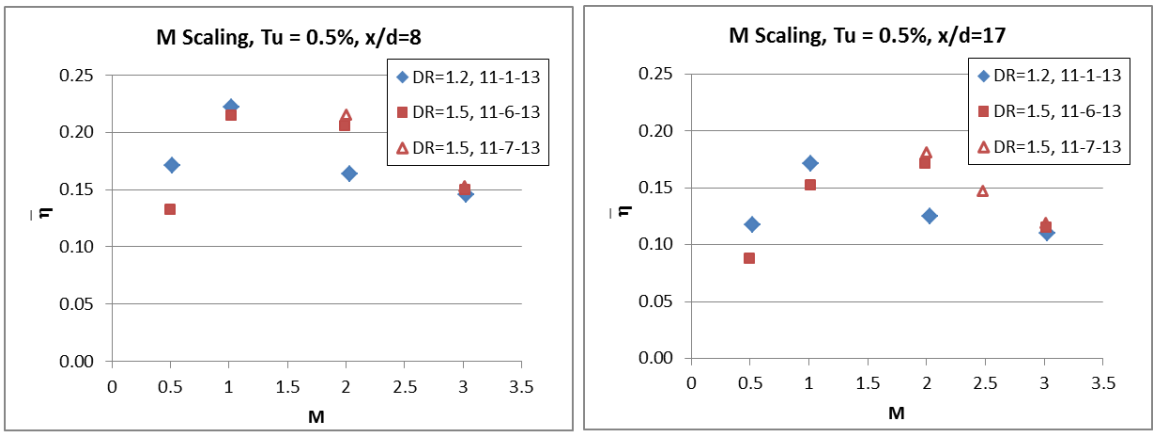

a) b)

Figure 0-50 Scaling with M at Tu = 0.5% and a) x/d = 8 and b) x/d = 17 using the new coolant piping system and the UT Polyurethane coupon.

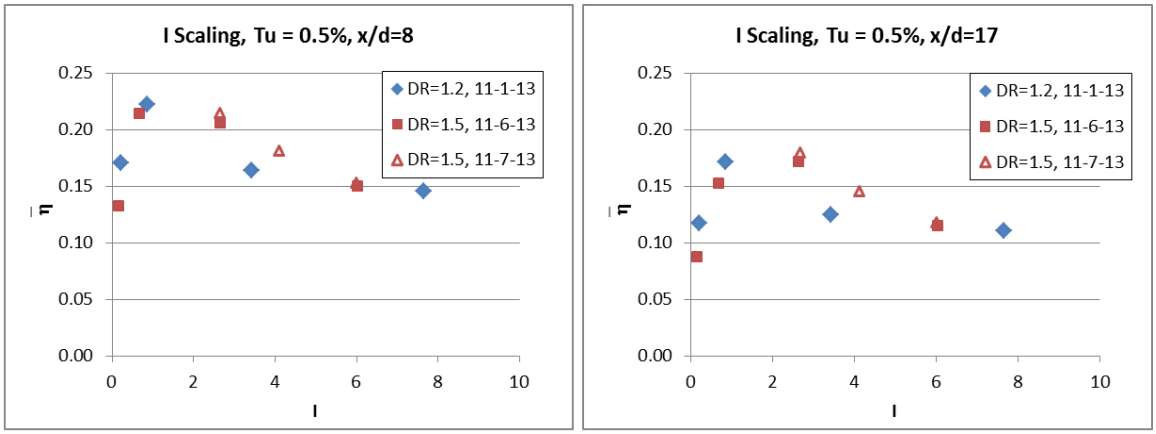

a) b)

Figure 0-51 Scaling with I at Tu = 0.5% and a) x/d = 8 and b) x/d = 17 using the new coolant piping system and the UT Polyurethane coupon.

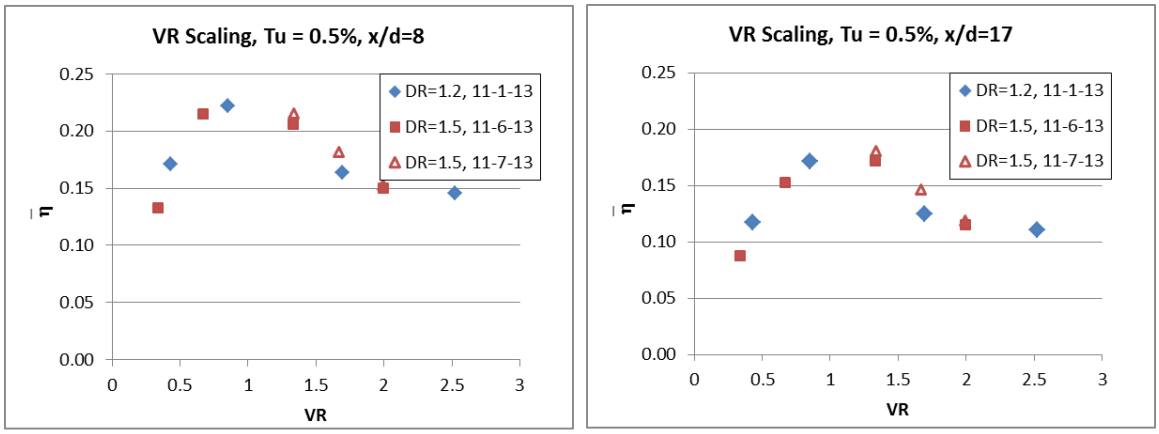

a) b)

Figure 0-52 Scaling with *VR* at *Tu* = 0.5% and a) *x*/*d* = 8 and b) *x*/*d* = 17 using the new coolant piping system and the UT Polyurethane coupon.

1.8.9.2 Scaling at Moderate Turbulence Intensity, *Tu* = 5.0%

Original Coolant Piping System

A similar analysis was completed at moderate turbulence intensity. Figure 0-53, Figure 0-54, Figure 0-55 show scaling of laterally averaged adiabatic effectiveness with *M*, *I*, and *VR*, respectively. The results are presented at *x*/*d* = 8 and 17. Again, velocity ratio is the best scaling parameter, but upon examining Figure 0-55, there appears to be a little more divergence between the data at *DR* = 1.2 and 1.5 at *VR* ≈ 2.

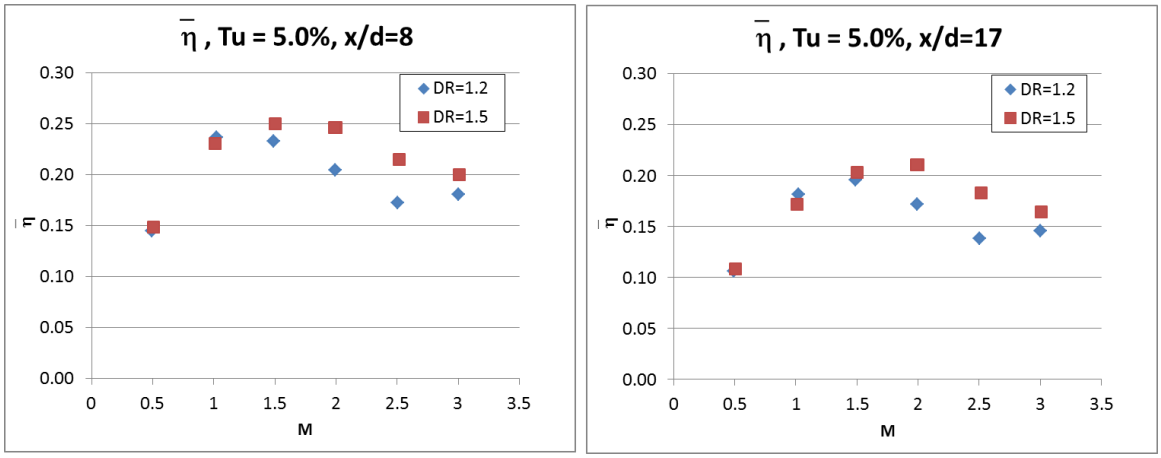

a) b)

Figure 0-53 Scaling with M at Tu = 5.0% and a) x/d = 8 and b) x/d = 17 using the original coolant piping system and the UT Polyurethane coupon.

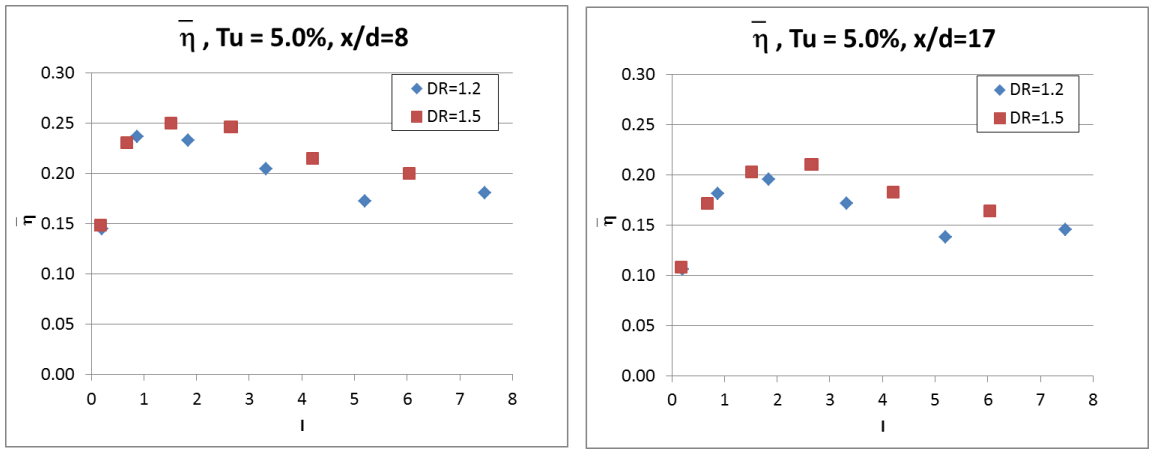

a) b)

Figure 0-54 Scaling with I at Tu = 5.0% and a) x/d = 8 and b) x/d = 17 using the original coolant piping system and the UT Polyurethane coupon.

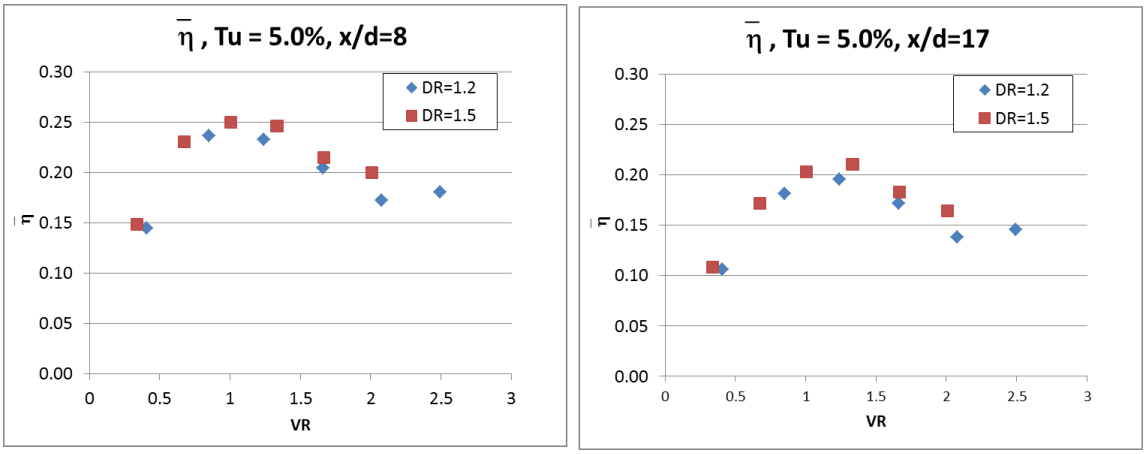

a) b)

Figure 0-55 Scaling with *VR* at *Tu* = 5.0% and a) *x*/*d* = 8 and b) *x*/*d* = 17 using the original coolant piping system and the UT Polyurethane coupon.

New Coolant Piping System

More data was taken at *Tu* = 5.0% with the new coolant piping system, but testing was completed at *DR* = 1.2, 1.4, and 1.6 instead of 1.2 and 1.5. Figure 0-56, Figure 0-57, and Figure 0-58 show scaling of the laterally averaged adiabatic effectiveness with *M*, *I*, and *VR*, respectively. The matched *VR* plots scale the data the best, but the scaling is not as good as at low turbulence intensity. At *VR* > 2.5, the data between *DR* = 1.2 and 1.6 collapses, but the data at *DR* = 1.4 is about $\bar{\eta}$ = 0.03 higher, which is outside the test-to-test uncertainty of the experiments. Some repeat data points were taken at *DR* = 1.4 on another day to verify that the *DR* = 1.4 data did not collapse with the *DR* = 1.2 and 1.6 data at higher *VR*. Those points are shown in black on Figure 0-58. They are slightly lower than the original *DR* = 1.4 data, but still don't collapse with the *DR* = 1.2 and 1.6 data.

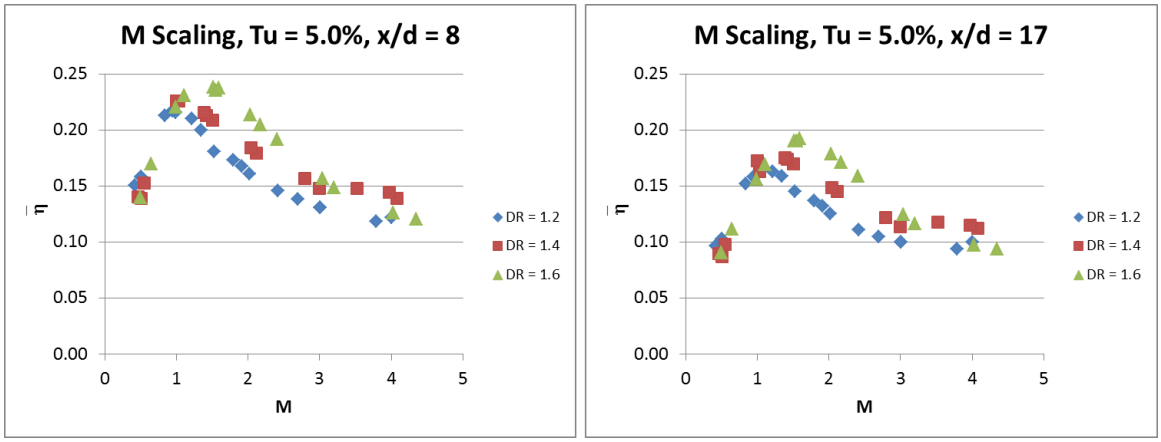

a) b)

Figure 0-56 Scaling with M at Tu = 5.0% and a) x/d = 8 and b) x/d = 17 using the new coolant piping system and the UT Polyurethane coupon.

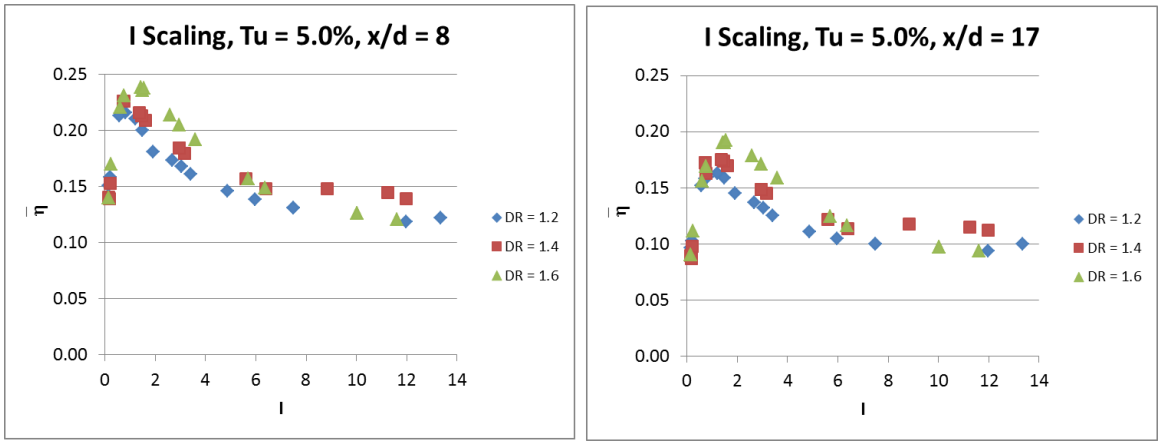

a) b)

Figure 0-57 Scaling with I at Tu = 5.0% and a) x/d = 8 and b) x/d = 17 using the new coolant piping system and the UT Polyurethane coupon.

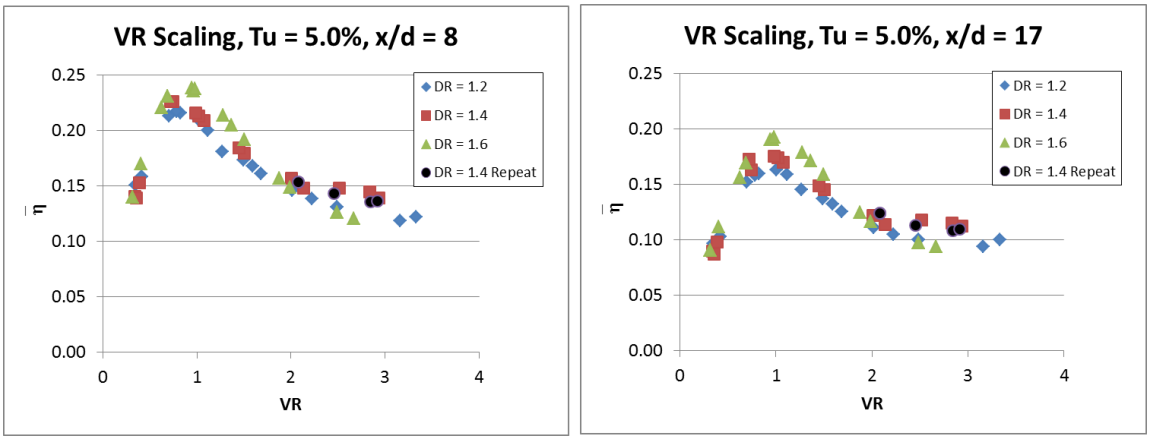

a) b)

Figure 0-58 Scaling with *VR* at *Tu* = 5.0% and a) *x*/*d* = 8 and b) *x*/*d* = 17 using the new coolant piping system and the UT Polyurethane coupon.

Figure 0-59 shows an additional plot of scaling with *VR* at *x*/*d* =3 to demonstrate that the scaling also works at positions upstream of *x*/*d* = 8 and 17. Actually, at *x*/*d* = 3, the scaling seems to work slightly better.

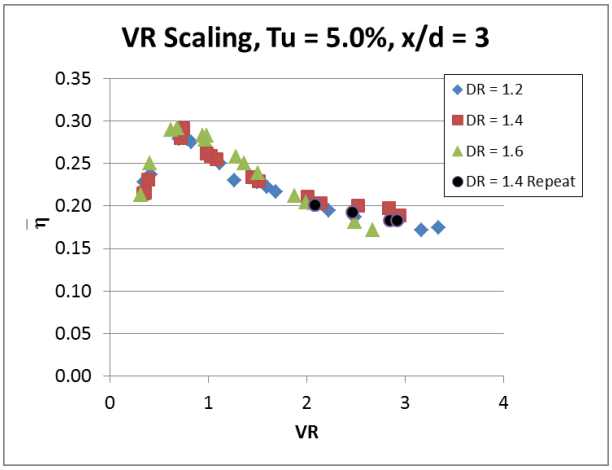

Figure 0-59 Scaling with *VR* at *Tu* = 5.0% and *x*/*d* = 3 using the new coolant piping system and the UT Polyurethane coupon.

This section has shown that at Tu = 0.5%, the velocity ratio serves as an excellent scaling parameter, whether the coolant piping was in the original or new configuration. At Tu = 5.0%, the velocity ratio was the best scaling parameter, but showed more scatter in the scaling than what was present at low turbulence. Still, the scaling with VR at Tu = 5.0% is fairly decent and could be used as a reliable scaling parameter, at least for this hole geometry. If tighter scaling is required, the velocity ratio could be used to create a scaling correlation.

1.8.10 Effect of Reynolds Number on Adiabatic Effectiveness

The effect of the mainstream Reynolds number on adiabatic effectiveness was tested using the UT Polyurethane, d = 4 mm coupon. The mainstream Reynolds number is defined using the mainstream velocity, mainstream kinematic viscosity, and the metering hole diameter, which is shown in Equation 0-3.

$$Re_{\infty} = \frac{U_{\infty} d}{\nu_{\infty}}$$

Equation 0-3

When the UT Polyurethane, d = 4 mm coupon was first tested, the mainstream velocity was maintained at 9.9 m/s, like the other tests that used d = 9 mm holes, which reduced the mainstream Reynolds number from 5600 to 2500 . An additional test was run with the mainstream velocity increased to 22.25 m/s to match the Reynolds number of 5600 used for the d = 9 mm tests. The ratio of boundary layer thickness to hole diameter was not exactly matched between the two experiments, which were both tested without a boundary layer trip. At Re_{∞} = 2500, $\delta = 1.9d$ and at Re_{∞} = 5600, δ was estimated to be

1.5*d*. This estimation was discussed in Section 1.8.3. The boundary layer was about 30% thicker at Re_∞ = 2500 than at 5600.

Figure 0-60 presented laterally averaged adiabatic effectiveness results at *DR* = 1.2. The matched Re_∞ results are shown in solid lines and the low Re_∞ are shown in dashed lines. The largest difference from varying the mainstream Reynolds number is seen at *M* = 0.5. At low Re_∞ the effectiveness is much lower coming out of the holes and $\bar{\eta}$ = 0.20 lower at *x*/*d* = 0 than all of the other blowing ratios. The results at *M* =1.0 and 2.0 are fairly similar until the effectiveness drops at *M* = 3.0 for both Reynolds numbers. At *M* = 0.5, increasing Re_∞ increased $\bar{\eta}$, but at *M* = 3.0, the opposite occurred and increasing Re_∞ decreased $\bar{\eta}$.

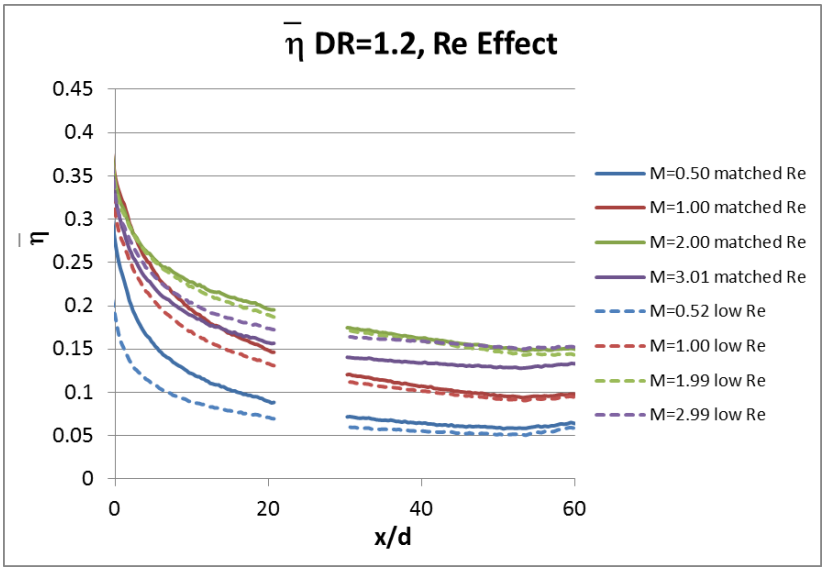

Figure 0-60 Effect of Reynolds number on laterally averaged adiabatic effectiveness at *DR* = 1.2 using the UT Polyurethane, *d* = 4mm.

Figure 0-61 and Figure 0-62 show surface contours of adiabatic effectiveness at *M* = 0.5 and *DR* = 1.2 for low Re_∞ and matched Re_∞, respectively. At low Re_∞, the

effectiveness downstream of the holes is very low. It appears as though the coolant does not fill out the shaped hole expansion and there is mainstream ingestion in the hole. The matched Re_∞ data, shown in Figure 0-62, shows higher effectiveness downstream of the jets. It is possible that at this blowing ratio and density ratio, increasing the mainstream velocity pushes down on the coolant jet, which fills out the shaped hole expansion and increases the effectiveness.

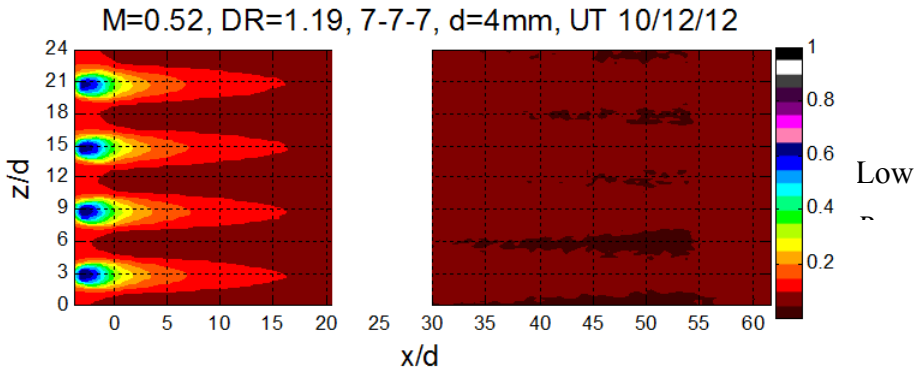

Figure 0-61 Surface contour of adiabatic effectiveness at M = 0.52 and DR = 1.19 at low Re_∞ using the UT Polyurethane, d = 4mm coupon.

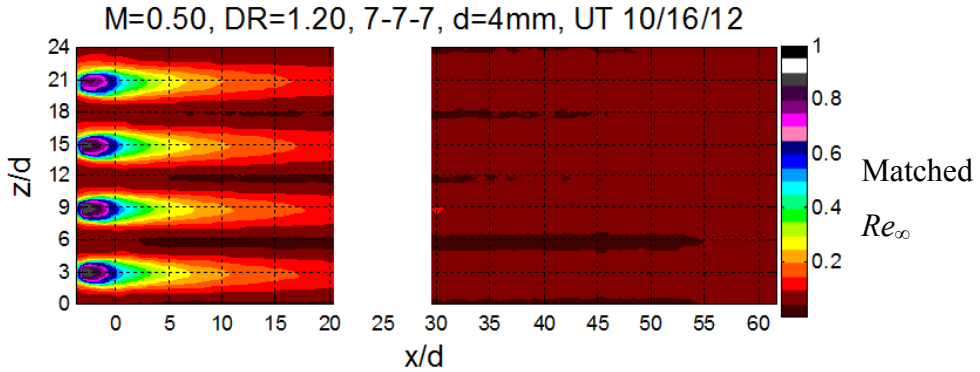

Figure 0-62 Surface contour of adiabatic effectiveness at M = 0.50 and DR = 1.49 at low Re_∞ using the UT Polyurethane, d = 4mm coupon.

Figure 0-63 and Figure 0-64 show similar contours at M = 3.0 and DR = 1.2 for low Re_∞ and matched Re_∞, respectively. As mentioned, this blowing ratio shows the opposite trend as what was seen at M = 0.5. Here, increasing Re_∞ decreases η. At low Re_∞, the jets spread slightly wider, which increases the laterally averaged adiabatic effectiveness, but interestingly, the effectiveness values on the jet centerlines are similar between the two mainstream Reynolds number levels. At this blowing ratio and density ratio, increasing Re_∞ seems to reduce the effectiveness at the lateral edges of the jets, perhaps due to increased turbulence intensity or separation at the edges of the jets.

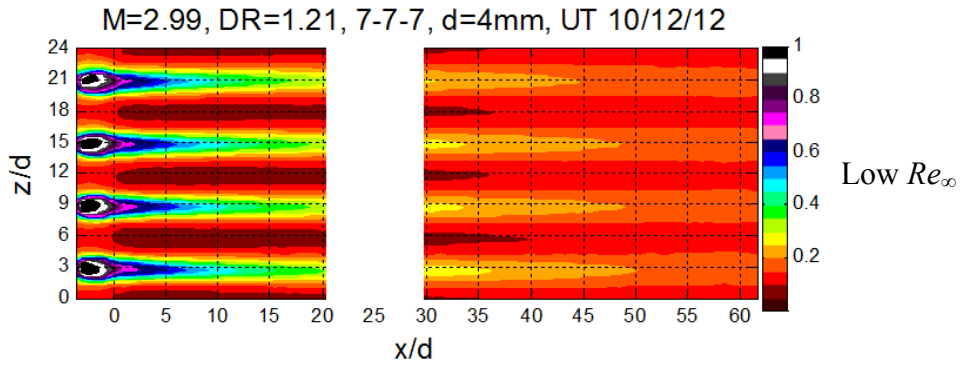

Figure 0-63 Surface contour of adiabatic effectiveness at M = 2.99 and DR = 1.21 at low Re_∞ using the UT Polyurethane, d = 4mm coupon.

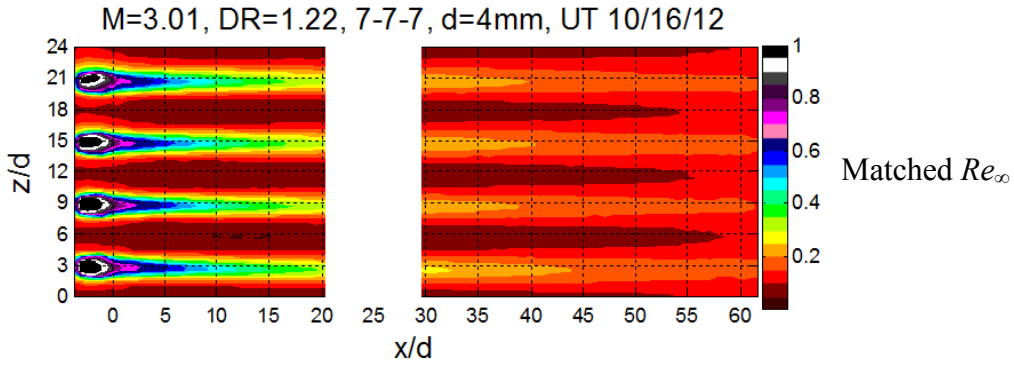

Figure 0-64 Surface contour of adiabatic effectiveness at M = 3.01 and DR = 1.22 at low Re_∞ using the UT Polyurethane, d = 4 mm coupon.

Figure 0-65 shows a comparison of laterally averaged adiabatic effectiveness values for low Re_∞ and matched Re_∞ at DR = 1.5. The results are similar at M = 0.5 and 1.0, but diverge at $M \geq 1.5$, at which increasing Re_∞ increases $\bar{\eta}$, which is the opposite trend seen at M = 3.0 and DR = 1.2.

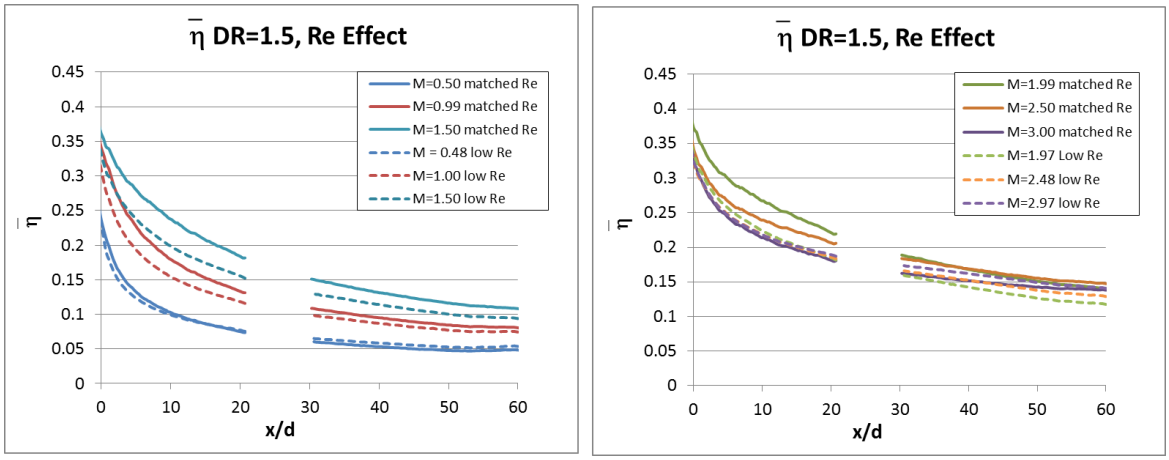

Figure 0-65 Effect of Reynolds number on laterally averaged adiabatic effectiveness at DR = 1.5 using the UT Polyurethane, d = 4 mm.

Figure 0-66 and Figure 0-67 show surface contour plots of adiabatic effectiveness at M = 2.0 and DR = 1.5 for low Re_∞ and matched Re_∞, respectively. M = 2.0 was chosen because it shows the largest difference in effectiveness values between the two Re_∞ cases, but the trend it shows is representative of the comparison between the two Re_∞ values at the M = 1.5 and above. The jets between the two contours spread about the same amount laterally, but the centerline effectiveness values in the core of the jets are higher at the matched Re_∞ value. More than doubling the Reynolds number would cause the hydrodynamic boundary layer to be thinner, which should improve film cooling performance, which is what is seen here.

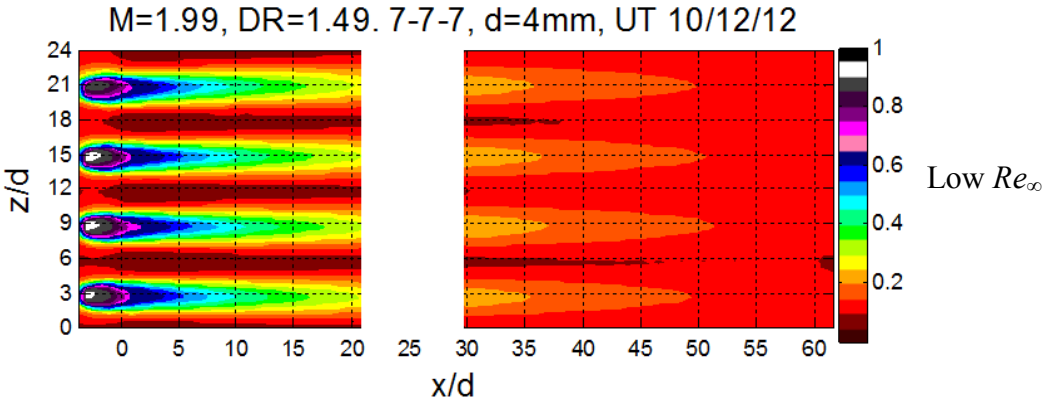

Figure 0-66 Surface contour of adiabatic effectiveness at M = 1.99 and DR = 1.49 at low Re_∞ using the UT Polyurethane, d = 4 mm coupon.

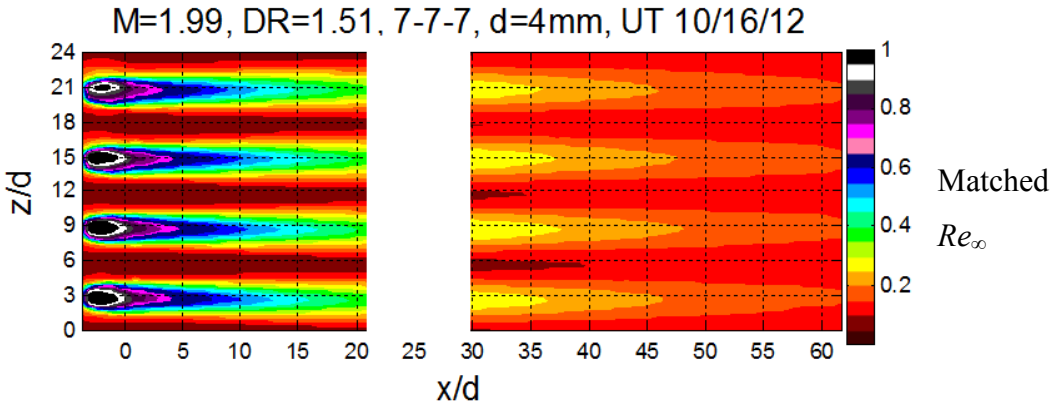

Figure 0-67 Surface contour of adiabatic effectiveness at M = 1.99 and DR = 1.51 at low Re_∞ using the UT Polyurethane, d = 4 mm coupon.

1.8.11 Comparison of 7°-7°-7° Shaped Hole Performance to Shaped Hole Performance in Literature

There are many shaped hole studies in literature, but considering only studies on a flat plate with zero pressure gradient at high density ratio reduces the number of comparable studies. Also, to be able to compare laterally averaged adiabatic effectiveness

results between studies, the pitch between holes needs to be the same, p/d = 6, which narrows the applicable studies further. Laterally averaged adiabatic effectiveness results using shaped holes cannot be easily adjusted because jets from shaped holes tend to spread and interact, which is a three dimensional process, so $\bar{\eta}$ values cannot be simply adjusted for different pitches. The studies that compared the best to this study were all completed at the same laboratory at Karlruhe Institute of Technology (KIT). The testing conditions and hole geometries for relevant studies at low turbulence intensity are summarized in Table 0-5.

Table 0-5 Comparison of hole geometries and testing parameters for studies at low *Tu*

	UT	Gritsch et al. [42]		Saumweber & Schulz [9]
Shaped Hole Type	Laidback Fan-shaped	Fan-shaped	Laidback Fan-shaped	Fan-shaped
Lateral Exp.	7°	14°	14°	14°
Forward Exp.	7°	0°	15°	0°
Surface Angle	30°	30°	30°	30°
AR	2.5	3.0	3.1	3.0
L/d	6	6	6	6
p/d	6	6	6	6
DR	1.5	1.85	1.85	1.75
Tu	0.5%	< 2%	< 2%	< 2%
Ma_∞	0.03	0.3	0.3	0.3
Ma_c	0	0	0	0

Gritsch et al. [42] tested two shaped holes, a fan-shaped hole with a 14° lateral expansion and a laidback fan-shaped hole with a 14° lateral expansion and 15° degree forward expansion. These geometries were used in several studies published by Karslruhe Institute of Technology. Diagrams of the shaped holes are shown in Figure 0-68. Note that the laidback fan-shaped hole, labeled as b), has a forward expansion, but it only extends 1*d* into the hole and is small, while the lateral expansion starts 4*d* into the hole.

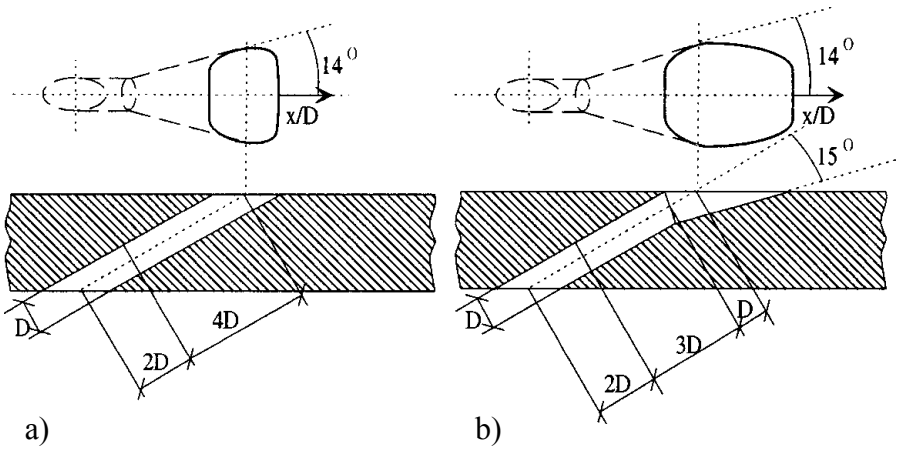

Figure 0-68 Diagram of a) fan-shaped and b) laidback fan-shaped hole geometries commonly tested at KIT [42].

Aside from the difference in shaped hole geometries between UT and KIT, KIT ran their experiments at a higher mainstream Mach number and their low turbulence intensity is less the 2% while it's 0.5% at UT. KIT also uses higher density ratios of 1.75 and 1.85 versus 1.5 at UT. Since the studies used different density ratios, it would be preferable to compare the results via matched velocity ratios, since Figure 0-6 shows that the laterally averaged adiabatic effectiveness scales best with *VR* for the 7°-7°-7° hole. However, there are very few test conditions where *VR* was matched between the two studies. Matching momentum flux ratio would also be better than matching blowing ratio,

but again, there are very few test conditions between the studies that result in matching momentum flux ratio values. As a result, matching blowing ratios will be used to compare the data. Figure 0-69 shows a comparison of laterally averaged adiabatic effectiveness at low *Tu* and the studies listed in Table 0-5 at $M = 0.5$, 1.0, 1.5, and 2.5. In the legend, the terms "LB FS" stand for laidback fan-shaped film cooling holes and "FS" stands for fan-shaped film cooling holes. It should also be noted that $x/d = 0$ is defined at the center of the metering hole for Saumweber and Schulz [9], but is defined at the downstream edge of the hole breakout for the rest of the studies in this figure. Without having the exact breakout dimensions of the hole geometries, an x/d shift could not be made for Saumweber & Schulz's data.

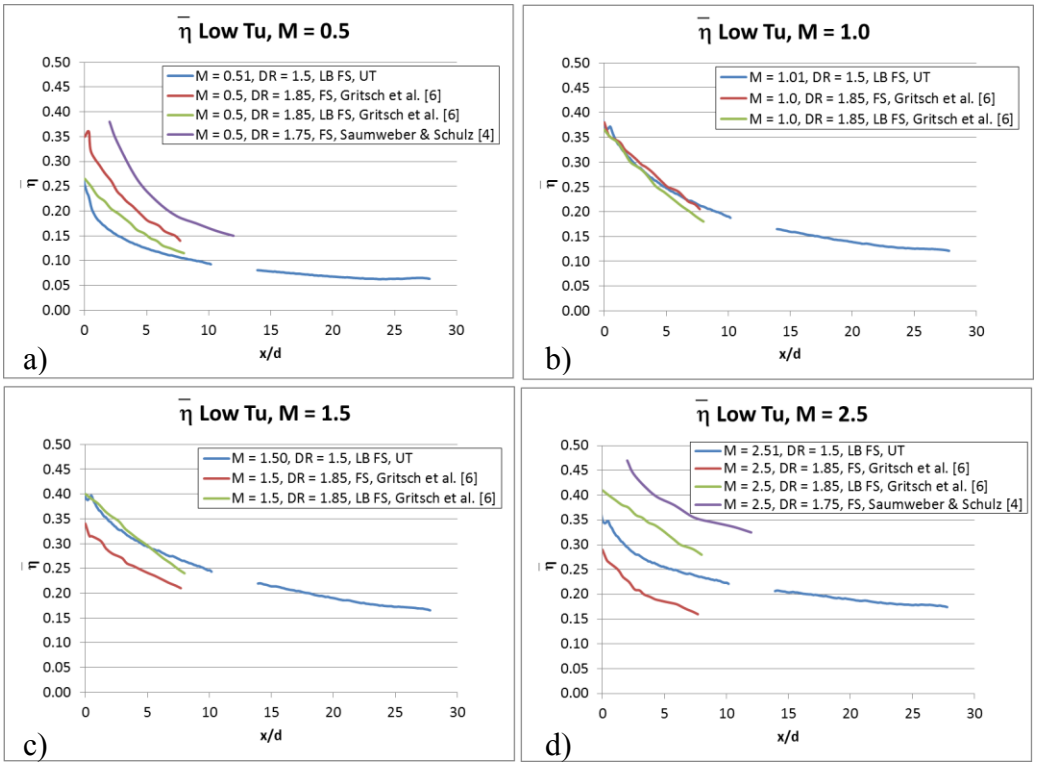

Figure 0-69 UT's laterally averaged adiabatic effectiveness data compared to Gritsch et al. [42] and Saumweber & Schulz [9] at p/d=6, low *Tu* and a) $M = 0.5$ b) $M = 1.0$ c) $M = 1.5$ and d) $M = 2.5$. For additional testing parameters see Table 0-5.

The data from KIT only extended to x/d = 8 in Gritsch et al. [42] and x/d = 12 in Saumweber and Schulz [9]. The laterally averaged adiabatic effectiveness is fairly similar between UT and Gritsch et al. [42], despite the different hole geometries at M = 1.0 and 1.5. However, at M = 0.5 and 2.5, there is a large span in the results between those measured at UT and the two KIT studies. These blowing ratios are interesting because at M = 0.5, the film cooling effectiveness is sensitive because the coolant may or may not be filling out the shaped hole expansions well. At M = 2.5, there could be some degree of separation beginning to take place, and indeed, these blowing ratios are where the results between the studies vary the most. At M = 0.5, UT's data is the lowest. There is even a $\bar{\eta}$ = 0.05 difference between the identical fan-shaped holes tested at KIT (red and purple lines). The only difference in testing conditions between these two data sets is the density ratio, which is labeled on the legend in Figure 0-69 a). The effect of density ratio is usually small, so the fact that there is this large of a difference at M = 0.5 suggests that this blowing ratio is very sensitive to testing conditions. At DR = 1.75 (purple), the jets perform better than at DR = 1.85 (red). This could be because the velocity of the coolant is higher at DR = 1.75, and the coolant fills out the holes better than at DR = 1.85. The same trend was seen at DR = 1.2 and 1.5 at M = 0.5 for UT's data, which is shown in Figure 0-1.

At M = 2.5, there is an even larger difference between all of the studies. As mentioned, it is likely that separation may be taking effect with some of the data sets since the effectiveness drops instead of increases. The fan-shaped holes from Saumweber and Schulz [9] and the laidback fan-shaped hole from Gritsch et al. [42] continue to perform well, while the laterally averaged adiabatic effectiveness from the same shaped hole in Gritsch [42] drops, as does the 7°-7°-7° hole at UT.

A similar analysis is presented below for moderate turbulence intensity. Table 0-6 compares the hole geometries and testing parameters between the relevant studies. Again, the most applicable studies were completed at the Karlsruhe Institute of Technology. The

study by Gritsch [29] tested several shaped hole geometries, two of which will be used for comparison, and they are labeled C and E.

Table 0-6 Comparison of hole geometries and testing parameters for studies at moderate *Tu*

	UT	Gritsch et al. [29]		Saumweber & Schulz [9]	Saumweber & Schulz [22]	Saumweber & Schulz [18]
Shaped Hole Type	LB FS	LB FS, C	LB FS, E	Fan-shaped	Fan-shaped	Fan-shaped
Lateral Exp.	7°	7°	4°	14°	14°	6°
Forward Exp.	7°	11°	8°	0°	0°	0°
Surf. Angle	30°	30°	30°	30°	30°	30°
AR	2.5	3.5	4.2	3.0	3.0	Not provided
L/d	6	7.5	6	6	6	6
p/d	6	6	6	6	6	6
DR	1.5	1.7	1.7	1.75	1.75	1.75
Tu	5.0%	4%	4%	7.5%	5.2%	5.2%
Ma_∞	0.03	0.3	0.3	0.3	0.3	0.3
Ma_c	0	0	0	0	0	0

Figure 0-70 compares UT's 7°-7°-7° laterally averaged adiabatic effectiveness with results from Gritsch et al. [29] and Saumweber and Schulz [9, 22, 18]. In this figure, $x/d = 0$ is defined at the center of the metering hole exit for all of the data presented. At $M = 0.5$, all of the studies have similar $\bar{\eta}$ performance. At $M = 1.5$, the results at KIT are grouped together well, with UT's data being significantly lower immediately downstream of the holes. This is because the shaped hole geometries used by Gritsch et al. [29] and presumably Saumweber and Schulz [22] had larger breakout widths per pitch than the 7°-7°-7°. If it is assumed that the coolant fills out the entire shaped hole expansion, the

wider the hole, the higher the laterally averaged adiabatic effectiveness. If it is assumed that the coolant exits the holes at $\eta = 1$, the breakout width per pitch should be equal to the laterally averaged adiabatic effectiveness. Gritsch et al. [29] list the breakout width per pitch as 0.49 for hole C and 0.43 for hole E, while it's only 0.35 for the 7°-7°-7°. This explains why $\bar{\eta} = 0.35$ at $x/d = 2.36$ (the downstream edge of the hole breakout), and KIT's values are also roughly the same values as the breakout width per pitch at the downstream edge of the hole breakout. Farther downstream, the results are similar between the studies. At $M = 2.5$, there is more variation in performance between the studies. The performance from Saumweber & Schulz [18] (purple) and UT's 7°-7°-7° dropped at this blowing ratio, presumably due to jet separation. The hole geometry from Saumweber & Schulz [18] was a 6° laterally expanded fan-shaped hole. Its area ratio was not listed, but most likely quite small compared to the other holes. This hole geometry, as well as the 7°-7°-7°, had smallest area ratios of the shaped hole geometries compared in this figure, which is why their performance degraded due to separation while the other shaped hole geometries did not. Since the two holes have smaller area ratios, the momentum of the jets exiting the holes will be higher than the jets exiting holes with larger area ratios, which causes jets exiting the smaller *AR* holes to separate at lower blowing ratios.

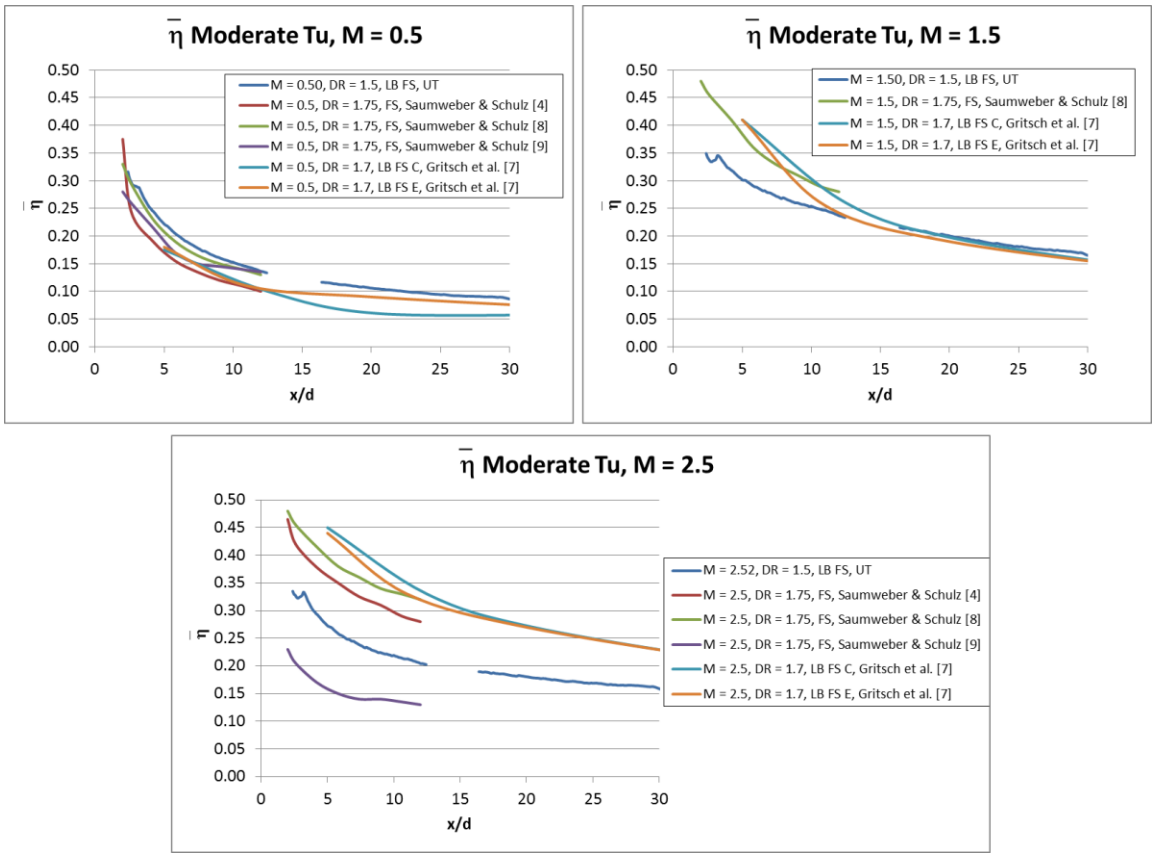

Figure 0-70 UT's laterally averaged adiabatic effectiveness data compared to Saumweber & Schulz [9, 22, 18] and Gritsch et al. [29] at p/d = 6, moderate Tu and a) M = 0.5 b) M = 1.5 and c) M = 2.5. For additional testing parameters see Table 0-6.

Given the result just discussed at M = 2.5 in Figure 0-70, it would be easy to think the wider the expansion angle, the better the performance. This may be true on a flat plate facility with coolant fed via a plenum, but in practice, where there is cross-flow, curvature, and unsteady effects, the widely expanded holes may not perform as well. As the lateral expansion angle is incrased, a separation bubble forms in the center of the diffuser (this is discussed in Section 1.1.5), which splits the coolant into two jets which fill out each side of the coolant hole. This separation can be advantageous on a flat plate

facility, which has been shown in Figure 0-69 and Figure 0-70, but the separation region makes the coolant flow very sensitive to inlet and mainstream conditions, which can cause the jet to bias to one side of the hole expansion and underperform. Figure 0-71 is an example of the change in performance than can be seen from having the coolant fed via a plenum condition (top) or a cross-flow condition at $Ma_c = 0.1$ (bottom).

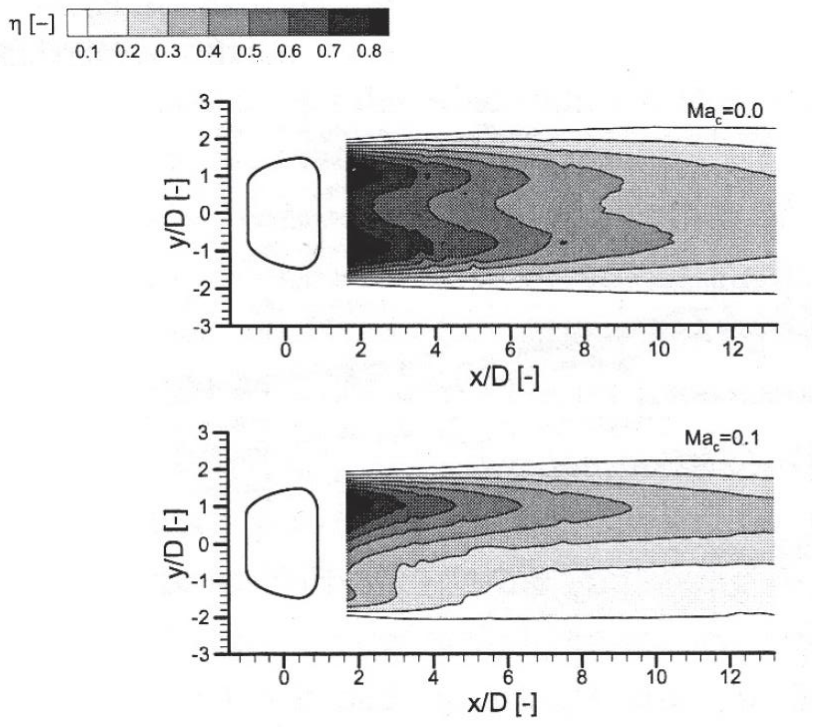

Figure 0-71 Effect of cross-flow on a 14° laterally expanded fan-shaped hole [22].

In conclusion, the performance of PSU's 7°-7°-7° shaped hole is consistent with shaped hole performance in literature. The variation in performance between PSU's hole and what is in literature can mostly be attributed to differences in the shaped hole geometries it is compared to.

1.8.12 COOLANT TEMPERATURE MEASUREMENT LOCATION

The uncertainty analysis in Section 1.7.8 showed that there was a bias error in the coolant temperature measurement due to not accounting for warming between where the temperature was measured in the plenum to where the coolant enters the coolant holes. To see what effect this would have on the data, the laterally averaged adiabatic effectiveness was recalculated using the coolant temperature bias errors found in the uncertainty analysis. Table 0-7 shows the adjustments made to the coolant temperature to account for the warming from the plenum temperature measurement location to the coolant hole entrances. The "Plenum" column is the measured plenum temperature, the "Bias Error" column is the bias error associated with measuring the coolant 1.5 in. into the plenum versus at the hole entrance. "Hole Ent." is the temperature that accounts for the bias error by adding the plenum temperature and the bias error together. "Ub Hole Ent." is the bias uncertainty associated with the temperature measurement and the location of the thermocouple. The table also includes the adjusted density ratios and blowing ratios that account for the coolant temperature bias as well as adjustments to the density that were discussed in Section 1.7.1.

Table 0-7 Adjustments made for coolant temperature bias error in the UT polyurethane experiment.

DR	M	Plenum [K]	Bias [K]	Hole Ent. [K]	Ub Hole Ent. [K]	%
1.19	0.50	252.3	3.99	256.3	3.50	1.37
1.20	0.99	252.6	1.25	253.9	1.00	0.39
1.21	2.00	250.0	1.12	251.1	0.50	0.20
1.22	3.01	248.7	1.12	249.8	0.10	0.04
1.45	0.50	204.2	6.00	210.2	6.00	2.85
1.47	1.01	204.0	3.60	207.6	3.00	1.45
1.47	1.49	203.9	2.39	206.3	2.00	0.97
1.48	1.99	203.5	1.21	204.7	0.90	0.44
1.50	2.50	201.5	1.75	203.2	0.70	0.34
1.50	3.00	198.9	1.95	200.9	0.80	0.40

The largest adjustments in coolant temperature are at $M = 0.5$ at $DR = 1.2$ and 1.5. Figure 0-72 shows the effect that adjusting the coolant temperature has on laterally averaged adiabatic effectiveness at $DR = 1.5$ and Figure 0-73 shows the same data at $DR = 1.2$.

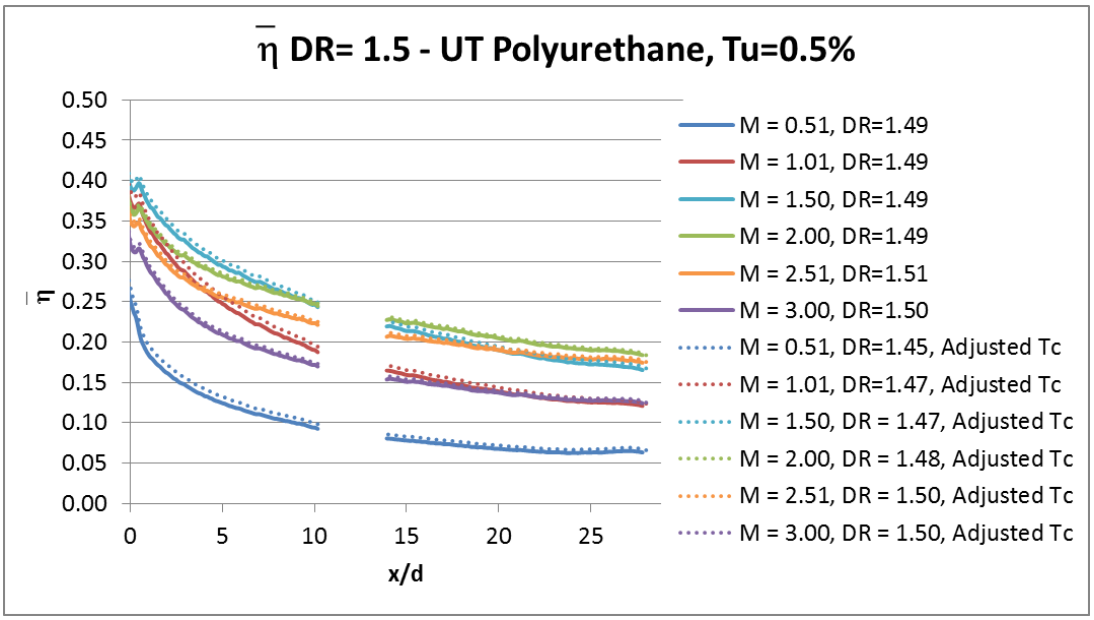

Figure 0-72 Effect of adjusting coolant temperature to correct for the bias error of the coolant temperature measurement location at $DR = 1.5$

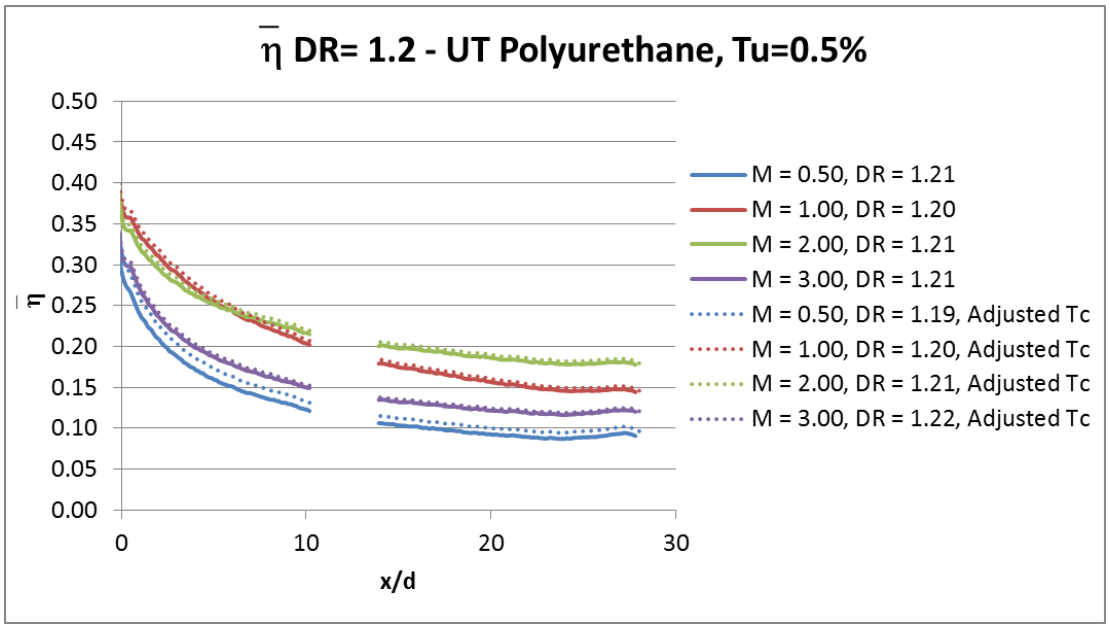

Figure 0-73 Effect of adjusting coolant temperature to correct for the bias error of the coolant temperature measurement location at *DR* = 1.2

Decreasing the coolant temperature has very little effect on the laterally averaged adiabatic effectiveness values. The effect is seen most at *M* = 0.5, *DR* = 1.2. This is because at *DR* = 1.2, the temperature difference between the coolant and mainstream is half the size as at *DR* = 1.5, so a bias to the coolant temperature has a larger effect than it would at *DR* = 1.5. From this result, it can be concluded that the bias error from the coolant temperature location is small, and there is little need to adjust all of the data for comparison to data where the coolant temperature is defined at the coolant hole exit.

1.8.13 Summary of 7°-7°-7° Adiabatic Effectiveness Study

The goal of the 7°-7°-7° adiabatic effectiveness study was to verify its film cooling performance by testing it on flat plate facilities at Penn State University (PSU)

and the University of Texas at Austin (UT). Doing this would prove that the data was correct and could be used as a standard for comparison for future shaped hole studies and CFD simulations. However, when the results did not match between the laboratories, several other factors that can affect shaped hole film cooling performance were investigated. These highlighted the extreme sensitivity of shaped hole performance to many parameters. The summary of what was found is below.

Material/Machining Differences

In the first experiments used for this project, UT and PSU used two different coupon materials which were machined at their respective schools. UT constructed their test coupon out of polyurethane, and PSU used polystyrene. To see if the difference in film cooling performance between UT's and PSU's tests was due to material or machining differences, UT sent PSU a polyurethane coupon that was machined at UT and PSU sent UT a polystyrene coupon that was machined at PSU. Both labs tested these coupons and found that each coupon performed differently. This indicated that there is an effect of material and machining differences. Later, PSU manufactured the PSU Smooth Polystyrene coupon, which had a better machining job than their original PSU Polystyrene Hatch that they tested. They found that the performance between the two coupons was similar, but deviated outside their experimental uncertainty at two of the higher blowing ratios, which also proves that machining has an effect on the adiabatic effectiveness performance.

As another effort, PSU sent UT the original PSU Polystyrene Hatch coupon that they originally tested. When UT tested this coupon, the results at $DR = 1.5$ matched extremely well, and the results at $DR = 1.2$ were similar. This showed that if both labs tested the exact same hole geometry, which takes out any effects due to machining or material differences, that they could get agreeable results.

Mainstream Acceleration

One theory as to why the adiabatic effectiveness results between UT and PSU did not match was that UT's test section height was shorter than PSU's (15.2d versus 34.5d), which would mean that the jets were occupying more of the wind tunnel volume at UT. This could cause the mainstream velocity to accelerate, which could keep UT's coolant jets attached to the surface at higher blowing ratios. First, a Pitot-static probe was used to measure the mainstream velocity while the jets were operating, and it was measured that the mainstream was 1.7% higher when the jets were operating than when there were not. Then, a reduced scale coupon was made so that the test section height to diameter ratio matched PSU's. This test coupon was labeled the UT Polyurethane, d = 4 mm coupon. When the coupon was tested, and the mainstream velocity was increased to match the Re_∞ = 5600 that was used for the tests with the d = 9 mm coolant holes. It was found that the laterally averaged adiabatic effectiveness was the same between the experiments with d = 4 mm and d = 9 mm holes, except at $M \geq 2.0$, where the jets from the d = 4 mm remained more effective than the jets from the d = 9 mm holes. The difference in performance at higher blowing ratios, where effects of jet detachment start to take place, was attributed to machining differences and/or surface roughness to hole diameter ratio differences from reducing the coolant holes to less than half of their original size. The mainstream velocity acceleration was ruled out as a cause of the difference in film cooling performance between tests at PSU and UT because, if anything, reducing the hole diameter should decrease the adiabatic effectiveness, since the mainstream velocity acceleration should be reduced and the jets could separate from the surface easier.

Coolant Entrance Effects

Coolant entrance effects were tested in two ways. First off, UT changed their internal plenum geometry to one that was similar to what was used at PSU. The UT Polystyrene coupon was used for this test. Originally, this coupon was also tested with the original UT internal plenum design, but it was later discovered that the test had a leak

and was invalid. Without a comparison of the UT Polystyrene coupon operating with both types of internal plenum geometries, not much could be concluded on the effect of the internal plenum geometry. However, one thing that was learned from the UT Polyurethane/PSU internal plenum design test was that altering the plenum geometry caused the coolant jets to be non-uniform hole-to-hole. Because of this, that internal plenum design was not used for any other experiments.

Next, the wind tunnel was altered for another project, and in the process, the coolant piping leading up to the coolant plenum was changed. The UT Polyurethane coupon was re-tested, and the results were different than the original results, and more similar to PSU's results. The new coolant piping configuration was similar to what was used at PSU. The change in performance from changing the coolant piping configuration suggests that coolant piping was affecting the coolant flow field at the hole entrance, despite the coolant traveling through a plenum that was designed to evenly distribute the coolant. This proved that film cooling performance from shaped holes is very sensitive to coolant entrance effects.

Data Summary

The following figures summarize most of the laterally averaged adiabatic effectiveness results that were used to compare the data taken at UT and PSU. By plotting all of the data together, it shows the variation in results and provides a more realistic value of the uncertainty that is associated with measuring adiabatic effectiveness using shaped holes. This shows the uncertainty that accounts for the variation in hole machining, coupon material, and coolant piping setup, which are variables that are not normally included in an uncertainty analysis.

Figure 0-74 shows the variation in results at DR = 1.2 at M = 0.5, 1.0, 2.0, and 3.0. In the plot legends, "CP" stands for coolant piping, since the UT Polyurethane coupon was tested with an original coolant piping configuration and a new cooling piping configuration. For more information on the coupon titles and testing conditions, refer to

Table 0-3 and Table 0-4. At $M = 0.5$ and 1.0, while the coolant jets were fully attached to the surface and filling out the shaped hole diffusers, the variation in performance between the tests is fairly consistent, with $\bar{\eta} \pm 0.02$ at $M = 0.5$. At $M = 1.0$, all of the data is grouped together very tightly at $\bar{\eta} \pm 0.01$ except for the data from the UT Polystyrene experiment. Of all of the experiments that were run, the UT Polystyrene experiment, which also used an internal plenum geometry that was similar to what was in PSU's plenum, is the most inconsistent in all of the figures, even at $DR = 1.5$. At $M = 2.0$, the results diverge more, as the performance of the UT Polyurethane test with the original coolant piping configuration (blue) stayed high, while the performance for the rest of the tests, except the one completed with the UT Polystyrene, dropped. At $M = 3.0$, the laterally averaged adiabatic effectiveness for the majority of the experiments dropped farther, with the results grouped at $\bar{\eta} \pm 0.03$, with exception of the data from the UT Polystyrene test being an outlier. From this figure it can be concluded that when the coolant jets were fully attached to the surface and filling out the shaped holes, there was fairly consistent performance, within $\bar{\eta} \pm 0.03$. However, at higher blowing ratios, $M \geq 2.0$, there was much more variation in performance as the experiments using different coupons and testing configurations showed various degrees of decreased adiabatic effectiveness performance, most likely due to varying levels of jet detachment. It is quite possible that the sensitivity of film cooling performance with machining, coupon material, and coolant entrance effects is exacerbated at higher blowing ratios when the coolant jets begin to detach.

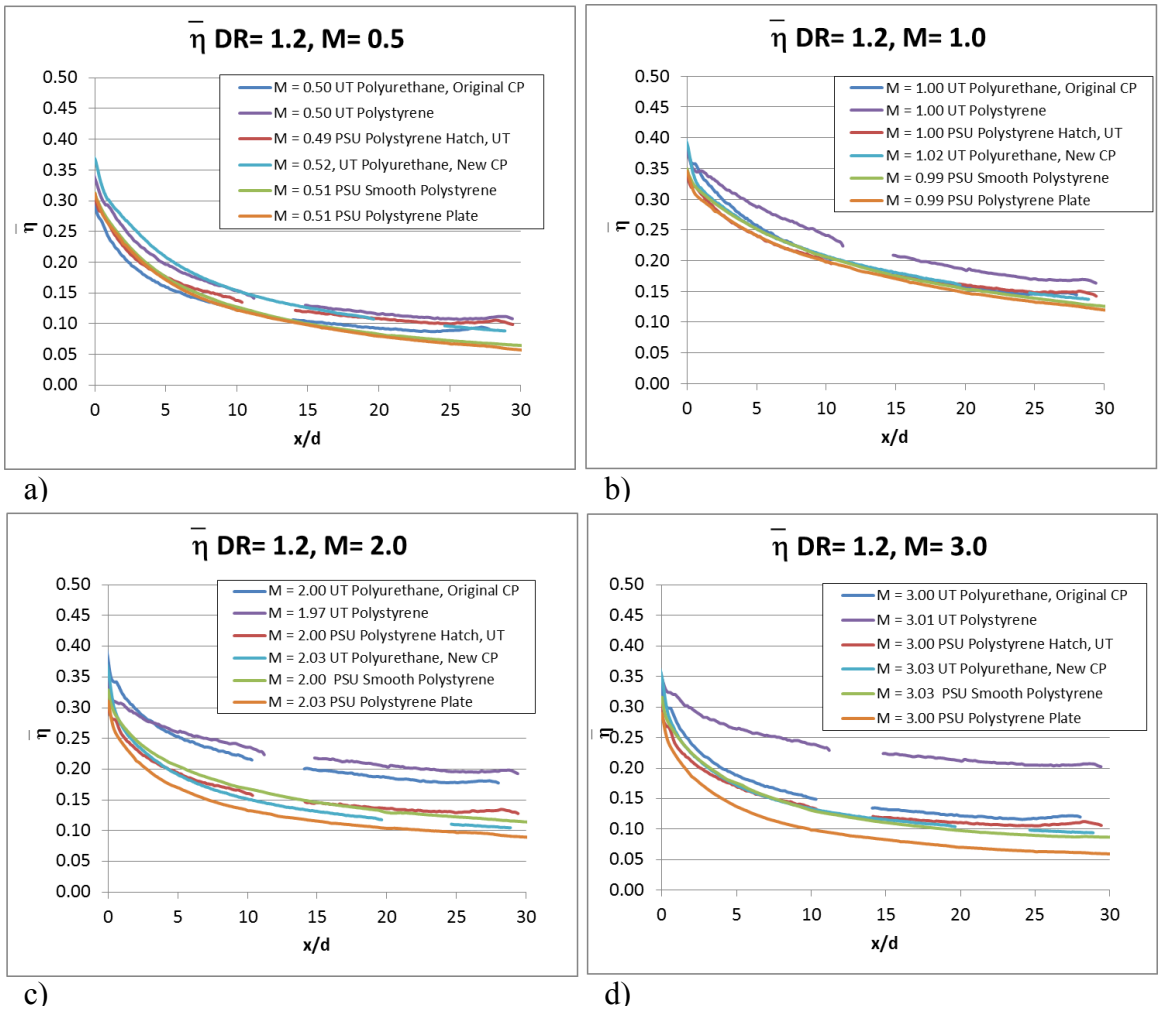

Figure 0-74 Summary of laterally averaged adiabatic effectiveness results at $DR = 1.2$ and a) $M = 0.5$, b) $M = 1.0$, c) $M = 2.0$, and d) $M = 3.0$

Figure 0-75 shows similar plots at $DR = 1.5$, which shows a similar trend as what was seen at $DR = 1.2$. At $M = 0.5$ most of the test data is grouped together rather tightly except for the UT Polyurethane test with the original coolant piping (blue). Section 1.8.2 discussed that the cause of this was that the coolant did not fill out the diffuser and there was possibly some mainstream ingestion in the hole. Interestingly, this behavior was not

observed with the UT Polystyrene coupon and PSU Polystyrene Hatch that were also tested at UT with the original coolant piping system. At M = 1.0 and 1.5, the data is grouped together for all tests, with $\bar{\eta}$ ± 0.02. At M = 2.0, the effects of jet separation started to take effect during some of the tests more than others, so the scatter in the results increased. At M = 2.5, the variation between the results from the experiments increased even more. By M = 3.0, the span of the data decreased, except for the UT Polystyrene test, which was an outlier as it was at M = 3.0 and DR = 1.2.

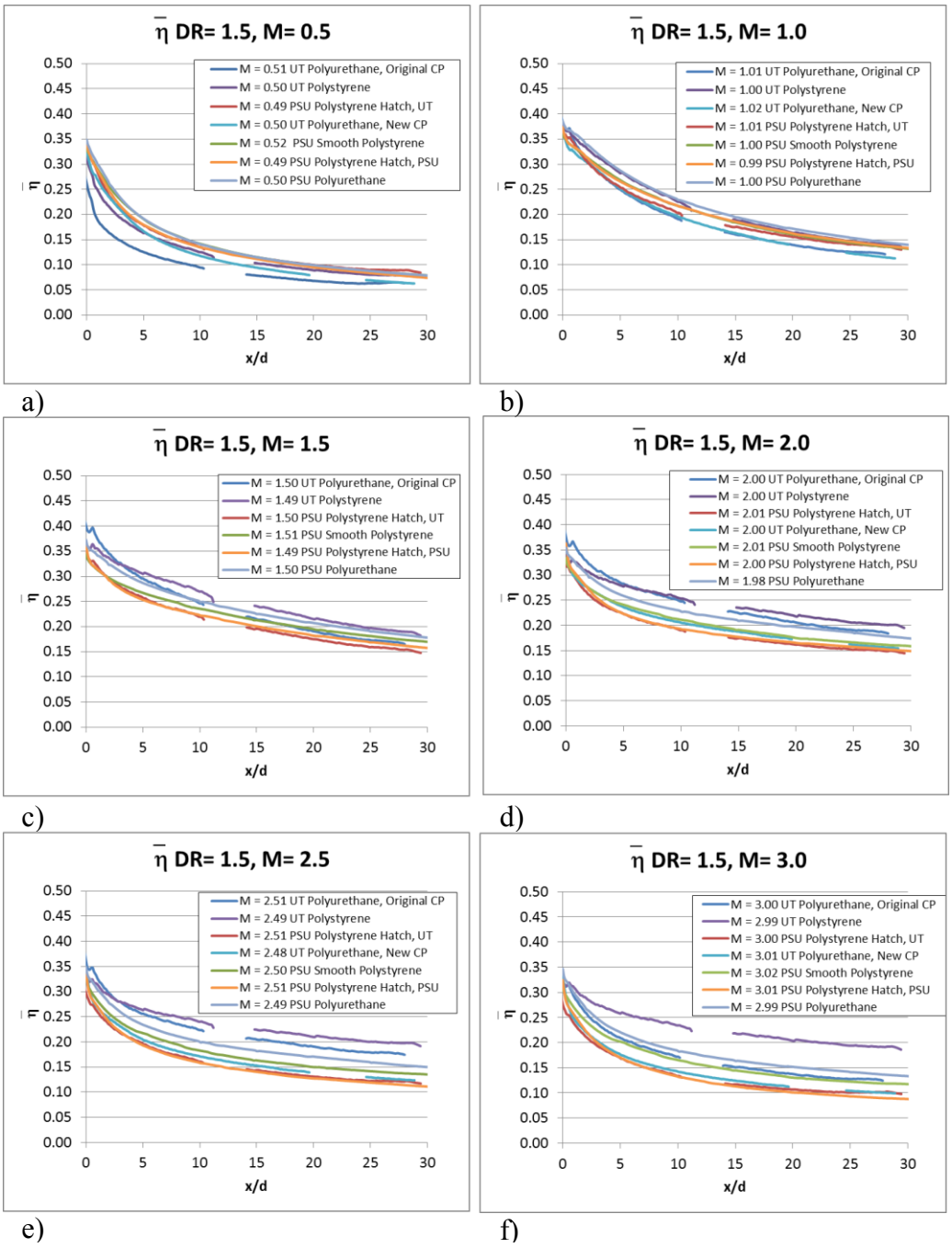

Figure 0-75 Summary of laterally averaged adiabatic effectiveness results at $DR = 1.5$ and a) $M = 0.5$, b) $M = 1.0$, c) $M = 1.5$, d) $M = 2.0$, e) $M = 2.5$, and f) $M = 3.0$

Figure 0-74 and Figure 0-75 show that when different coolant piping, coupon materials, and machining are taken into account, the uncertainty of a film cooling experiment is much higher than what is typically reported in an uncertainty analysis. At low blowing ratios when the jets are fully attached and filling out the shaped hole expansion, the performance between the experiments was more uniform, usually in the $\bar{\eta}$ ± 0.02-0.03 range. However, at higher blowing ratios, when the coolant jets begin to detach, the variation in performance is much wider as different tests showed different degrees of jet separation. This is most likely the regime where the details of machining, material, and coolant entrance effects become important and cause the jets to separate differently.

In addition to comparing the performance of the 7°-7°-7° with PSU at various testing conditions and with multiple test coupons, a few other testing conditions were analyzed, which are summarized below.

Effect of Mainstream Turbulence Intensity

The effect of mainstream turbulence intensity at Tu = 0.5% and 5.0% were compared using data taken with the UT Polyurethane coupon. The effect of increasing the turbulence intensity was small, just within experimental uncertainty, except at M = 0.5 and DR = 1.5. At this condition, increasing the turbulence intensity increased the adiabatic effectiveness performance significantly. At low turbulence intensity, the laterally averaged adiabatic effectiveness was quite low due to the coolant not filling on the shaped hole expansion. It is possible that the increased turbulence intensity spread the jet and caused it to fill out the expansion, which improved the performance.

Scaling Adiabatic Effectiveness at Multiple Density Ratios

The blowing ratio, momentum flux ratio, and velocity ratio were analyzed as scaling parameters at Tu = 0.5% and 5.0%. The data used to analyze the scaling was

taken using the UT Polyurethane coupon and both the original and new coolant piping configurations were used. The results using the two coolant piping configurations were consistent and showed excellent scaling with velocity ratio at low turbulence intensity. At moderate turbulence intensity, velocity ratio was still the best scaling parameter, but there was more scatter in the scaling than what was present at low turbulence intensity. The velocity ratio can be used as a reliable scaling parameter at both low and moderate turbulence, and if tighter scaling is desired at moderate turbulence intensity, a scaling function could be created that would depend on the velocity ratio and density ratio.

Effect of Mainstream Reynolds Number

The UT Polyurethane, d = 4 mm coupon was used to study the effect of mainstream Reynolds number. In one experiment, the mainstream Reynolds number was held at 5600 (the value used for the rest of the tests in this study) and in another experiment, the mainstream Reynolds number was reduced by about 60% to 2500. Comparing the results showed that increasing the mainstream Reynolds number increased the film cooling performance. This could be due to the difference in boundary layer thickness as the mainstream Reynolds number was increased, which would be consistent with what is in literature. At Re_∞ = 2500, δ/d = 1.9, and at Re_∞ = 5600, δ/d = 1.5.

Effect of Coolant Temperature Measurement Location

While completing the uncertainty analysis, it was found that obtaining an accurate measurement of the coolant temperature at low flow rates is not easy. Placing a thermocouple in the plenum does not account for the warming of the coolant that takes place between the measurement location in the plenum and the coolant hole entrances. However, if thermocouples are installed at the coolant hole entrances, the temperature readings between the thermocouples show large variations between them. These issues are typically confined to low blowing ratios, where the coolant flow rates are low and the

coolant is in the plenum longer and the internal heat transfer coefficient is reduced. The uncertainty analysis in Chapter 2 quantified a bias error and bias uncertainties associated with measuring the coolant temperature 1.5 in. beneath the hole entrance inside the plenum. When these bias errors were used to correct the coolant temperature values, they had very little, and in most cases negligible, effect on the adiabatic effectiveness values.

When the 7°-7°-7° performance was compared to relevant studies in literature, it was found that the performance was comparable. The shaped hole studies that were compared to the 7°-7°-7° results used shaped hole geometries that were quite different, and the density ratios were between 1.7 and 1.8, while $DR = 1.5$ was used in this study. However, when the shaped holes were fully attached and filling out the shaped hole expansions, the performance was quite similar. At higher blowing ratios ($M \geq 2$), the jets performed differently as the different shaped hole geometries affected the degree of coolant jet separation.

1.9 Heat Transfer Coefficient Measurements

Heat transfer coefficients were measured downstream of the same 7°-7°-7° shaped hole discussed in Section 1.8. The UT Polyurethane coupon was used for the measurements which were taken at density ratios of 1.0, 1.2, and 1.5 and at blowing ratios of 0.5, 1.0, 1.5, 2.0, 2.5, and 3.0. This section discusses the effect of density ratio on heat transfer coefficients, including scaling parameters. Thermal field measurements are also presented, which show the jet profiles above a heated and unheated wall.

1.9.1 LATERALLY AVERAGED HEAT TRANSFER COEFFICIENT AUGMENTATION

Figure 3-76 (a)-(c) show laterally averaged heat transfer coefficient augmentation at DR = 1.0, 1.2, and 1.5, respectively. The holes are spaced 6d, so looking at the laterally averaged values dampens the local increases in h_f/h_0 that occur downstream of the jets. At DR = 1.0, the laterally averaged heat transfer coefficient augmentation was close to unity for M = 0.50 to M = 1.49, and as the blowing ratio was increased, the laterally averaged heat transfer coefficient augmentation increased up to about 1.26 just downstream of the jets at M = 3.0. A similar trend was seen at DR = 1.2 for which the laterally averaged heat transfer coefficient augmentation was about unity up until M = 1.5. At $M \geq 2.0$, $\overline{h_f/h_0}$ increased with the peak at M = 2.5 being 1.17 just downstream of the coolant holes. For DR = 1.5, $\overline{h_f/h_0}$ remained fairly flat between 1.0 and 1.07, increasing slightly with increasing blowing ratio. Figure 3-76 shows that for a given blowing ratio, there is an effect of density ratio on heat transfer coefficient augmentation, with the results at DR = 1.0 showing the largest enhancement in heat transfer coefficient. As the density ratio is increased, the heat transfer coefficient augmentation decreases. The variation of heat transfer coefficient augmentation with density ratio is outside the uncertainty of the measurements. Figure 3-78 shows contours of h_f/h_0 for these measurements, and the difference in h_f/h_0 in the core of the jets between density ratios is outside the uncertainty of $h_f/h_0 \pm 0.12$ at DR = 1.2 and 1.5 and $h_f/h_0 \pm 0.08$ at DR = 1.0.

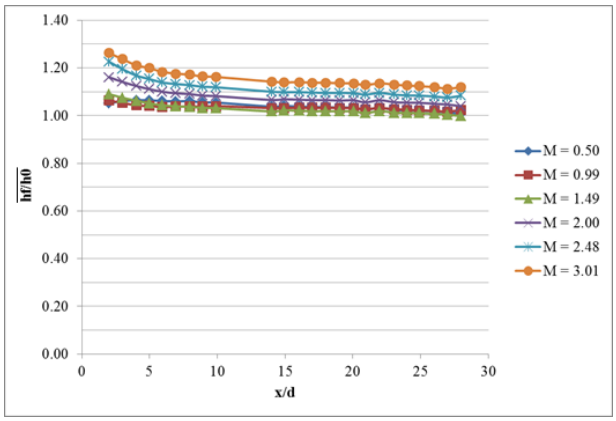

a) Laterally averaged h_f/h_0 at DR=1.0.

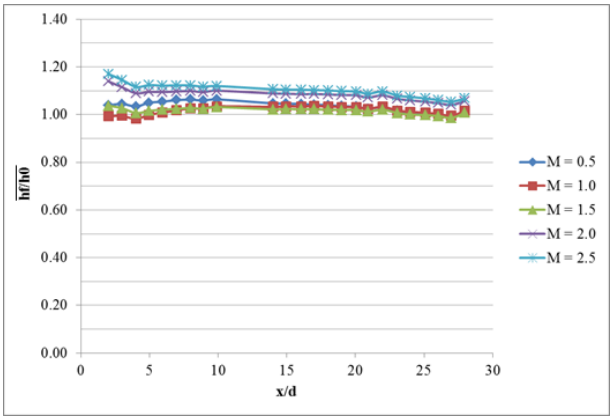

b) Laterally averaged h_f/h_0 at DR=1.2.

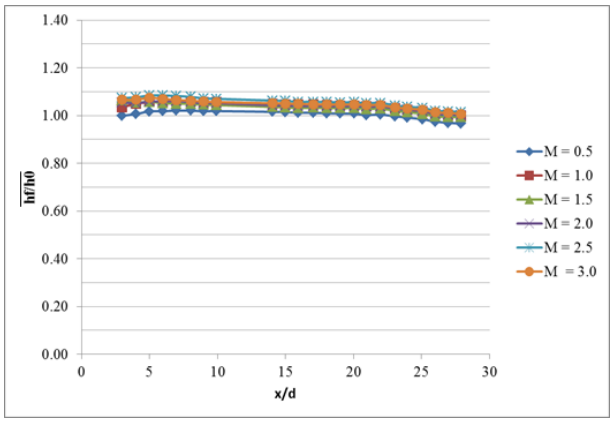

c) Laterally averaged h_f/h_0 at DR=1.5.

Figure 0-76 Laterally averaged h_f/h_0 at a) DR=1.0 b) DR=1.2 c) DR=1.5.

1.9.2 COMPARISON OF $\overline{H_f/H_0}$ TO LITERATURE

The vast majority of the heat transfer coefficient measurements using shaped holes at $DR > 1.0$ in literature were completed at Karlsruhe Institute of Technology. The study that compares best to this research was completed by Saumweber and Schulz [9]. Table 0-8 compares the geometry and testing parameters between the two studies. Both used plenum conditions, moderate turbulence levels, and the same hole spacing, surface angle, and hole length. However, Saumweber and Schulz used a much higher mainstream velocity and the holes shapes were quite different. Their lateral hole expansion was twice the lateral hole expansion used in this study and their hole had no forward expansion. The heat transfer coefficients were also measured differently. Saumweber and Schulz used superposition, which is explained in Section 1.1.2, and this study used direct measurement of T_w and T_{aw} to find the heat transfer coefficient augmentation.

Table 0-8: Comparison of testing parameters between current study and Saumweber and Schulz [9]

	Current Study	Saumweber & Schulz [9]
DR	1.5	1.75
Ma_m	0.03	0.3
Ma_c	0	0
Tu	5.0%	7.5%
p/d	6	6
α	30°	30°
β	7°	14°
ε	7°	0°
γ	0°	0°
$L/d_{metering}$	2.5	2
L/d_{total}	6	6

Figure 0-77 compares the results from this study to those from Saumweber and Schulz [9] at $M = 0.5$ and $M = 2.5$. The results are at different density ratios, but even if momentum ratios or velocity ratios were matched, the conclusions of the comparison would not change much. At $M = 0.5$, the comparison between the two studies is fairly good, but at $M = 2.5$, there is a large deviation, with Saumweber and Schulz's $\overline{h_f/h_0}$ values at $x/d = 4$ being twice those of the present study. It should be pointed out that Saumweber and Schulz defined $x/d = 0$ at the center of the metering hole exit, so the data in the current study has been shifted to match their coordinate definition.

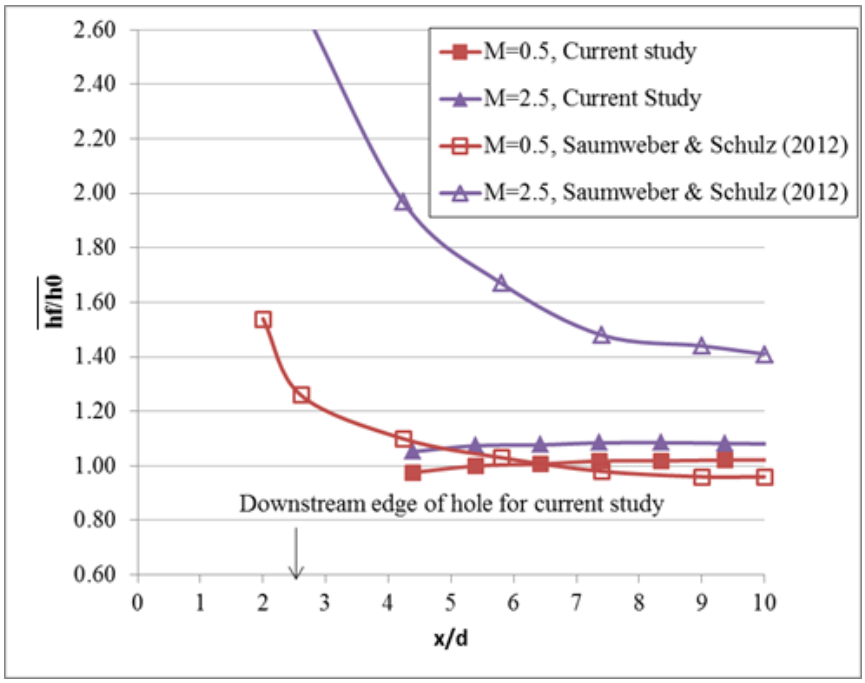

Figure 0-77 Laterally averaged h_f/h_0 comparison between the current study and Saumweber and Schulz [9].

1.9.3 SPATIAL DISTRIBUTIONS OF H_F/H_0

Spatial distributions of the heat transfer coefficient augmentation were examined for all blowing ratios and density ratios. There was a consistent trend of low, nearly uniform distributions of h_f/h_0 = 1.0 to 1.1 while the jets were attached to the surface from M = 0.5 to 1.5. Contour plots of h_f/h_0 at M = 1.5 for all density ratios are presented in Figure 3-78 a)-c). Note that the surface contour color bars are in increments of h_f/h_0 = 0.08. The centerlines of the coolant holes were located at z/d = 3 and 9, and it is evident that increases in h_f/h_0 occurred downstream of the coolant holes, with the region between coolant holes remaining at nominally h_f/h_0 = 1. Although distinct increases to levels of h_f/h_0 > 1.2 occurred immediately downstream of the coolant holes for DR = 1.0 and 1.5, no increase was observed at DR = 1.2. This may be because, even though the velocity ratio based upon the metering hole diameter was 1.25, the velocity ratio exiting the holes was much closer to 1.0 due to the coolant decelerating as it expanded into a larger area in the diffuser. Under this scenario, the velocity ratio at DR = 1.0 would still be larger than 1.0 and at DR = 1.5 would be less than 1. As the velocity ratio approaches 1 at DR = 1.2, the shear layer will be weaker, promoting less turbulence and a lowering the heat transfer coefficient.

For blowing ratios of M > 2.0, when the coolant jets start to detach from the surface, there is a distinct increase in h_f/h_0. Contour plots of h_f/h_0 at M = 2.5 for all density ratios are presented in Figure 3-78 d)-f). What is immediately obvious is the significant differences in h_f/h_0 for the varying density ratios. The maximum increase occurred at DR = 1.0 with peak levels of h_f/h_0 > 1.6 within 2d of the coolant hole exit. The heat transfer coefficient augmentation decreased with increasing density ratio, with a maximum peak of h_f/h_0 > 1.2 at DR = 1.5. The variation of h_f/h_0 with density ratio is not well established in literature, as different researchers have shown that it increases with increasing density ratio [57], has no effect [25], and is inconclusive [58, 24].

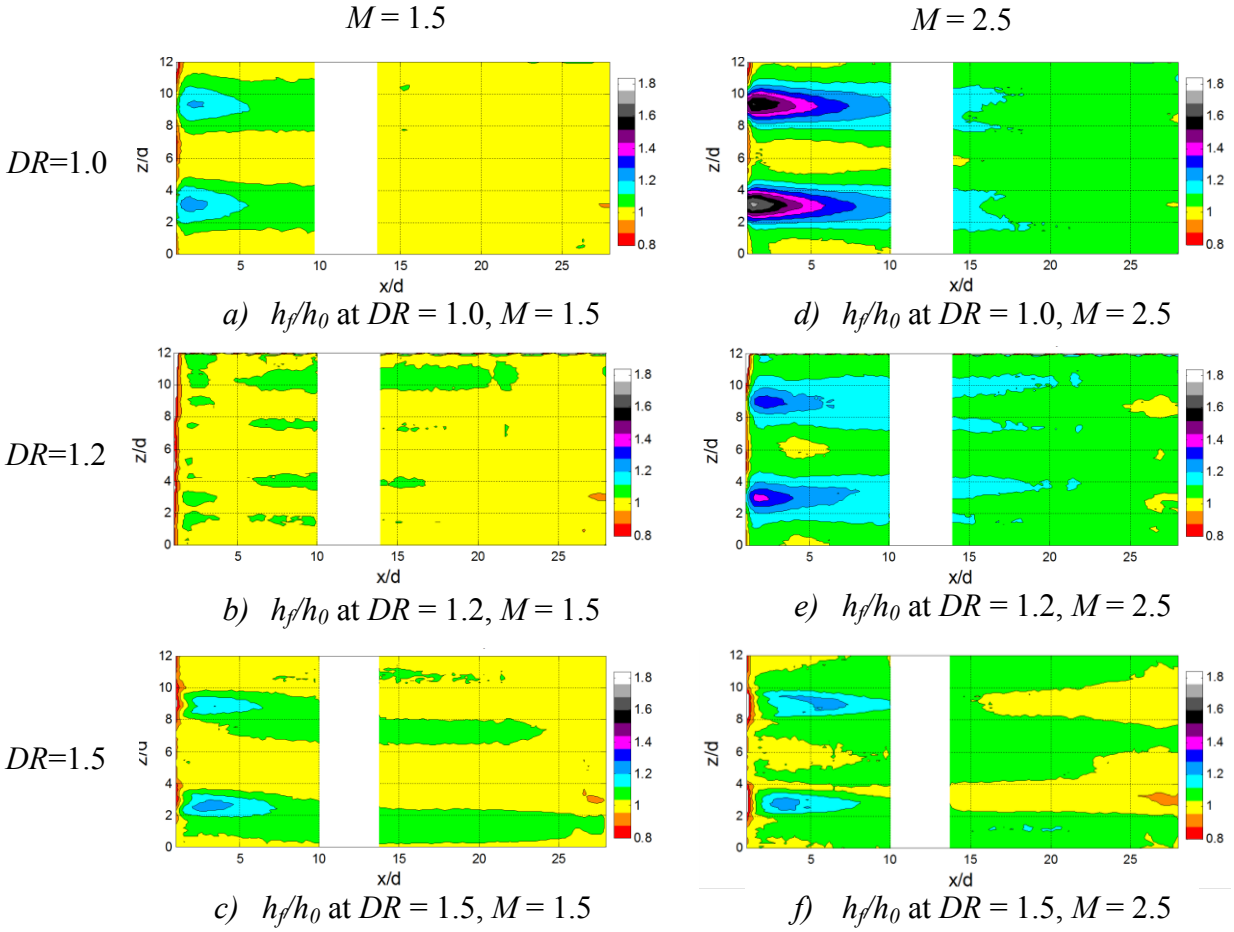

Figure 0-78 h_f/h_0 comparison at DR = 1.0, 1.2, and 1.5 and M = 1.5, 2.5

In order to highlight the importance of accurate measurements of the adiabatic and heated surface temperatures to obtain the appropriate driving temperature for heat transfer, lateral profiles at x/d = 5 are presented in Figure 3-79 a) and b) for M = 1.5 and 2.5, respectively. The associated lateral h_f/h_0 distributions are presented in Figure 3-79 c) and d). From Figure 3-79 a) and b), it is clear that there is a close tracking between the heated surface temperature and the adiabatic surface temperature so that the ΔT between the two was almost constant. These plots emphasize the importance of very accurate surface temperature measurements because a slight error would be greatly magnified

when using the difference between the two temperatures to determine the heat transfer coefficient. The lateral distributions of h_f/h_0 at M = 1.5, shown in Figure 3-79 c), have similarly small peak enhancements for DR = 1.0 and 1.5 and no enhancement at DR = 1.2. At the higher blowing ratio of M = 2.5, shown in Figure 3-79 d), the DR = 1.0 case had a peak level of h_f/h_0 twice as large as for the higher density ratios.

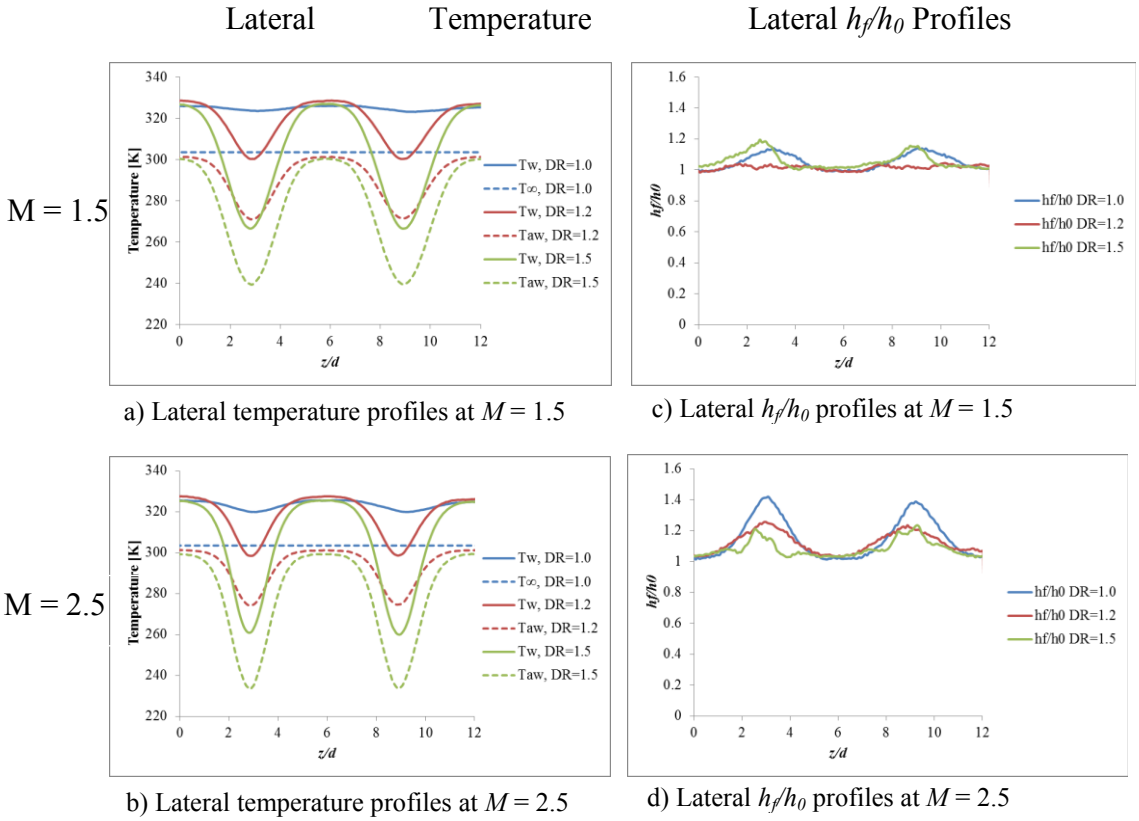

a) Lateral temperature profiles at M = 1.5

c) Lateral h_f/h_0 profiles at M = 1.5

b) Lateral temperature profiles at M = 2.5

d) Lateral h_f/h_0 profiles at M = 2.5

Figure 0-79 Lateral temperature and h_f/h_0 profiles at x/d = 5, DR = 1.0, 1.2, and 1.5, and M = 1.5, and 2.5

1.9.4 SCALING

Since much of the heat transfer coefficient augmentation data in literature is measured at unit density ratio while real gas turbines operate at DR = 1.8-2.0, the effect of density ratio on the heat transfer coefficient augmentation discussed previously is an important observation. However, the variations with density ratio that were shown in Figure 3-78 were based on making comparisons with matched blowing ratios. To examine the possibility that h_f/h_0 distributions at varying density ratios might scale with a different parameter, contour plots of h_f/h_0 with matched blowing ratio, momentum flux ratio, and velocity ratio are compared in Figure 3-80. All of these comparisons are at M = 2.0 or higher, i.e. in the higher range of blowing ratios where there was a significant effect of density ratio. Although none of these parameters resulted in perfect scaling of the h_f/h_0 distributions for different density ratios, the matched velocity ratio was clearly superior to the matched blowing ratio or the matched momentum flux ratio comparisons. For a matched VR = 2.0, the DR = 1.0 case had a peak h_f/h_0 in the core of the jet of about 1.4, while for DR = 1.5 it was about 1.3. This was a much closer correspondence than for the other potential matching parameters examined.

Matched *M*

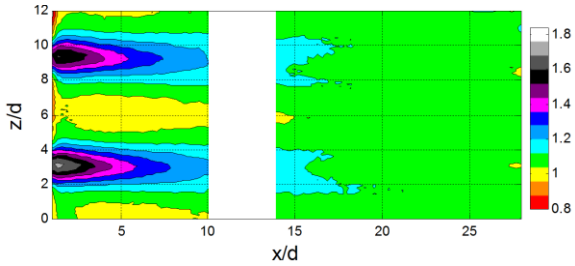

a) h_f/h_0 at $DR = 1.0$, $M = 2.5$

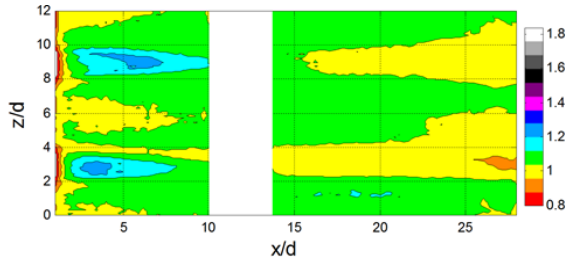

b) h_f/h_0 at $DR = 1.5$, $M = 2.5$

Matched *I*

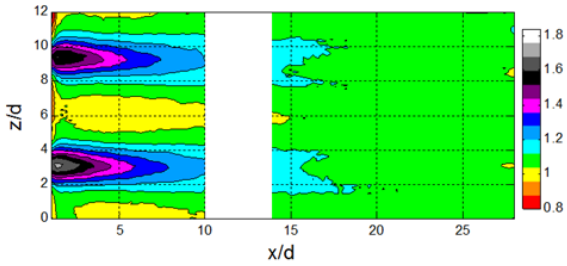

c) h_f/h_0 at $DR = 1.0$, $M = 2.5$, $I = 6.1$

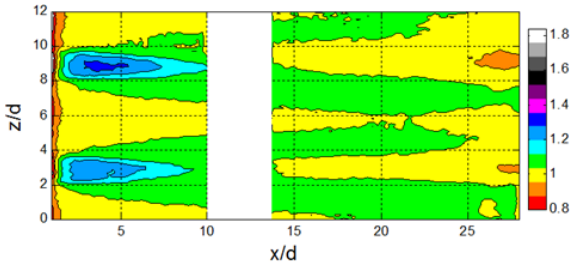

d) h_f/h_0 at $DR = 1.5$, $M = 3.0$, $I = 6.0$

Matched *VR*

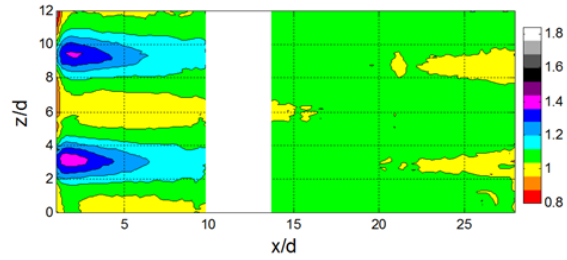

e) h_f/h_0 at $DR = 1.0$, $M = 2.0$, $VR = 2$

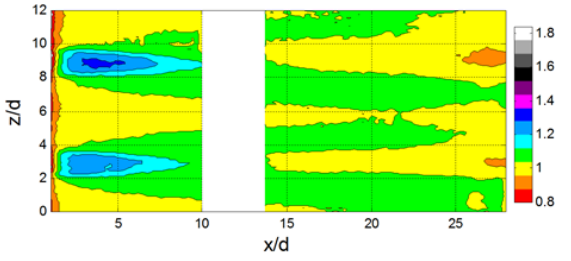

f) h_f/h_0 at $DR = 1.5$, $M = 3.0$, $VR = 2$

Figure 0-80 Scaling of h_f/h_0 with M, I, and VR.

1.9.5 EFFECT OF JET COUNTER-ROTATING VORTICES

Farther downstream, several of the h_f/h_0 contours presented in Figure 3-80 show a decrease in heat transfer coefficient augmentation along the centerline of the jets and enhanced heat transfer on the edges of the jets. This can be attributed to the jets' counter-rotating vortices. As the vortices begin to move toward one another in the z direction, they sweep warm air next to the heat flux plate towards the center of the jet. As the vortices join from opposite directions, they carry the warmer coolant vertically, which thickens the boundary layer and decreases the heat transfer coefficient. As the vortices turn and move away from each other, they circle back down and impinge on the surface, increasing the heat transfer on the edges of the jets. This vortices effect has been seen in several heat transfer coefficient studies [25, 28, 58, 26].

1.9.6 THERMAL FIELD MEASUREMENTS

2-D thermal field contours

The thermal field above the wall was measured with the heat flux plate on and off to observe the relationship between the measured adiabatic wall temperature and the temperature profile above the heated wall. A 1 mil (25 μm) diameter thermocouple was used to measure the thermal field in the centerline of the jet at x/d = 3, 5, 10, and 14.66. In addition, a lateral profile of the jet was measured at x/d = 4.66. The coolant was maintained at DR = 1.2, unless otherwise noted. Figure 3-81 shows lateral contours of nondimensional temperature, θ, at x/d = 4.66, M = 2.0, and DR = 1.2. The contour on the left was measured with the heat flux plate off and the contour on the right was measured with the heat flux plate on. The contour colors are in increments of θ = 0.05, which corresponds to 2.5 K at DR = 1.2.

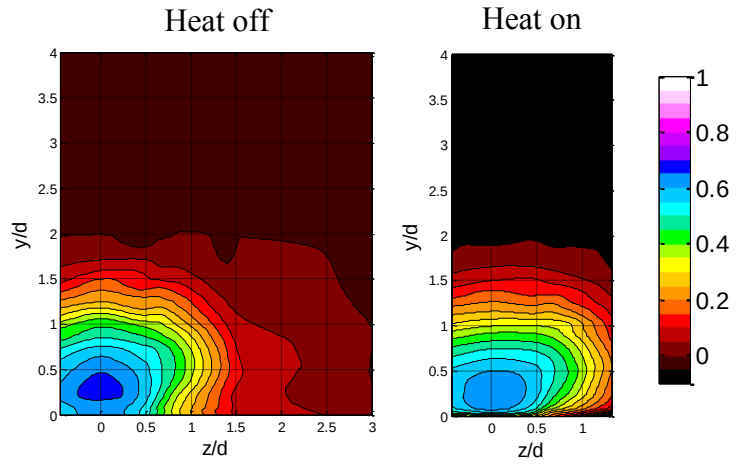

Figure 0-81 Contours of dimensionless temperature, θ, at x/d = 4.66, M = 2.0, DR = 1.2 with the heat off (left) and the heat on (right).

Focusing on the contour with the heat flux plate off, the core of the jet is lifted slightly above the wall, indicating that the jet is slightly detached, which corroborates with the adiabatic effectiveness data in Figure 0-1 a). When the heat flux plate is turned on, the core of the jet becomes warmer, while the surrounding contour levels show little change. This is confirmed in Figure 3-82, which shows thermal profiles of the jet at a) the jet centerline at z/d = 0 and b) just off the jet centerline at z/d = 0.44 with the heat flux plate on and off. The peak of the θ profile at the centerline of the jet has clearly decreased over the heated surface, but the θ peak for the profiles off the centerline show no change between the heated and non-heated surfaces. The heating of only the core of the coolant jet is most likely due the counter-rotating vortex pair that is associated with film cooling. The vortices sweep the warmer air over the heated surface towards the center of the jet, thickening the thermal boundary layer. Surface temperature measurements taken with the IR camera during the heat transfer coefficient experiments are shown in the thermal field plots as open symbols. Notice that the blue thermal field measurements taken above the adiabatic wall align well with the adiabatic wall temperature measurements taken with the IR camera. For the heated wall, there was a

very sharp temperature gradient near the wall, and the thermal field measurement closest to the wall was consistently colder than the IR surface temperature measurement. This was probably because, despite the small diameter of the probe, there was not enough resolution in the measurements to discern the very thin thermal boundary layer.

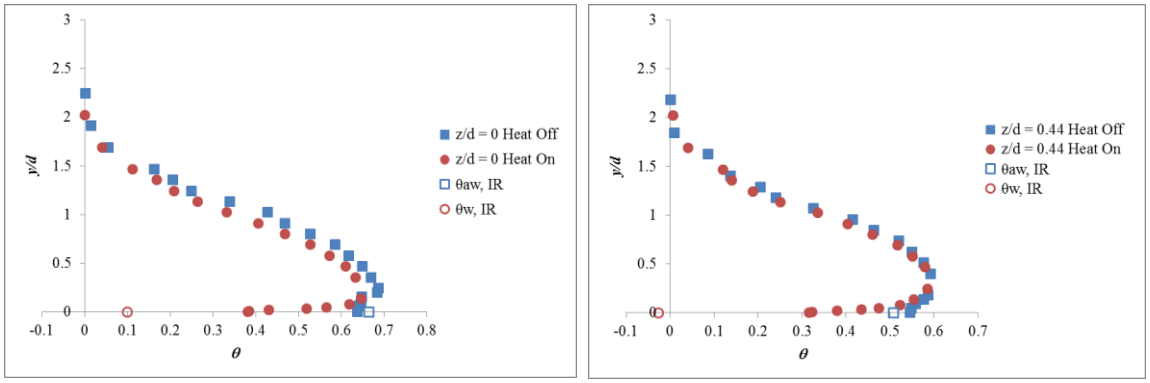

a) $z/d = 0$ b) $z/d = 0.44$

Figure 0-82 Thermal profiles of a jet at $x/d = 4.66$, $M = 2.0$, $DR = 1.2$ with the heat flux plate on and off at a) $z/d = 0$ and b) $z/d = 0.44$

Centerline temperature profiles farther downstream showed increased heating of the coolant jet core with increasing distance downstream. Figure 3-83 shows thermal field measurements at $z/d = 0$, $M = 2.0$, $DR = 1.2$, and a) $x/d = 3$ b) $x/d = 5$, c) $x/d = 10$ and d) $x/d = 14.66$. As the jet moves farther downstream, the coolant at the centerline of the jets gets warmer, again suggesting that the counter-rotating vortices sweep the warm coolant next to the heat flux plate to the centerline of the jet, thickening the thermal boundary layer. The warming with increasing downstream distance cannot be attributed solely to a typical growing thermal boundary layer. At $x/d = 14.66$, which is about 12 cm downstream from the start of the heat flux plate and the start of a new thermal boundary layer, the boundary layer thickness would have to be 8-9 mm thick to cause the thermal field profiles between the heated and non-heated profiles to differ at that distance above the wall, which would be much faster boundary layer growth than expected.

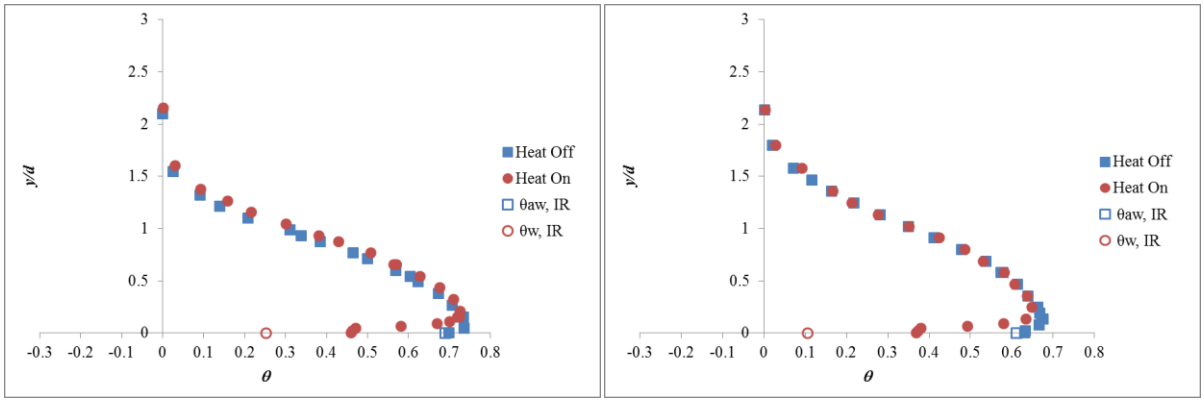

a) $x/d = 3$ b) $x/d = 5$

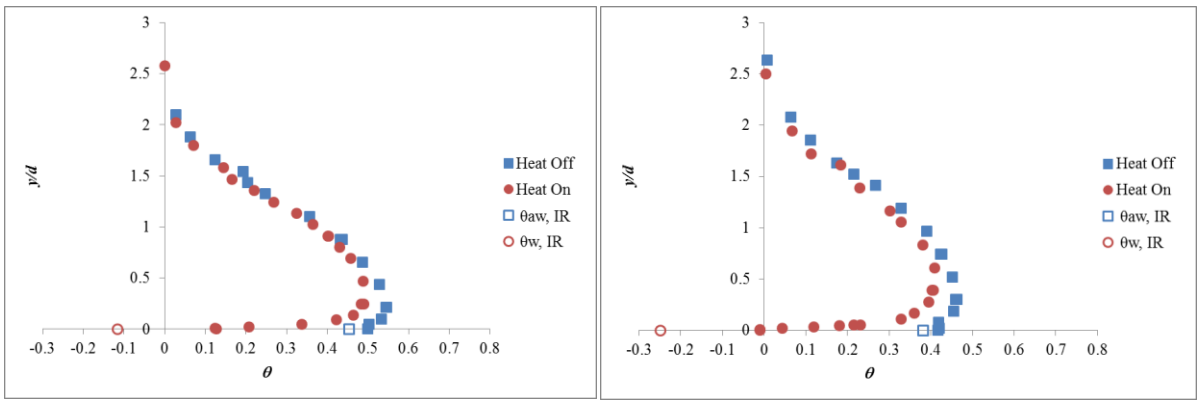

c) $x/d = 10$ d) $x/d = 14.66$

Figure 0-83 Thermal field measurements in the centerline of the jet at $M = 2.0$, $DR = 1.2$

Effect of Blowing Ratio

Figure 3-84 compares thermal field measurements above an unheated wall for $M = 2.0$ and 3.0 at $DR = 1.2$, $z/d = 0$, and a) $x/d = 0$ b) $x/d = 5$ c) $x/d = 10$ and d) $x/d = 14.66$. At $x/d = 0$, the jet is attached coming out of the hole at both blowing ratios. By $x/d = 5$, the core of the jets at $M = 2.0$ and 3.0 have slightly detached. Figure 3-84 b)-d) shows that the detachment of the jet is localized very near the wall, and the peak core temperatures of the thermal profiles match up quite well. The increased coolant for $M =$

3.0 extends farther in the y direction, as would be expected, but the temperature of the coolant core remains the same. The surface temperatures between $M = 2.0$ and 3.0 are not very different at the jet centerline, but $\bar{\eta}$ at $M = 3$ is about 30% lower than at $M = 2$, which is shown in Figure 0-1 a). Contours of adiabatic effectiveness show that the reduced $\bar{\eta}$ results from the jets narrowing, which is a common symptom of jet separation, not because the effectiveness along the centerline decreases.

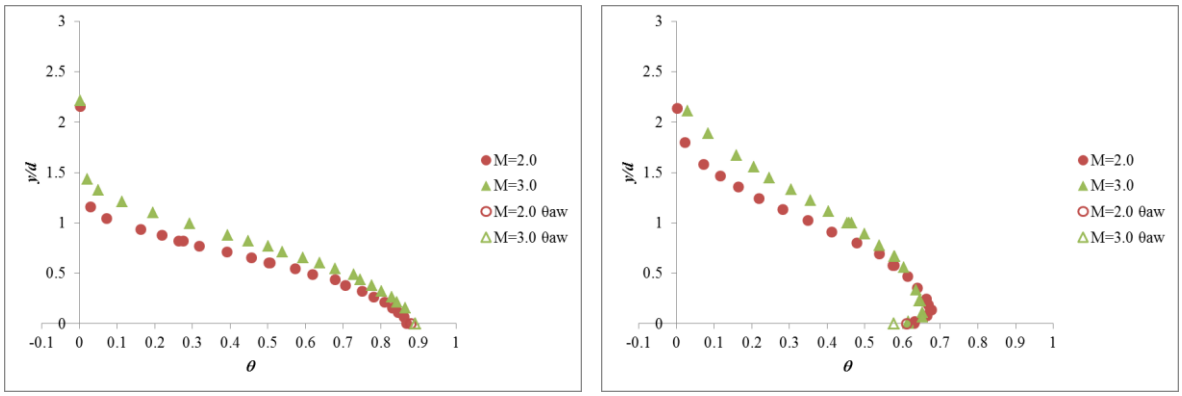

a) $x/d = 0$ b) $x/d = 5$

c) $x/d = 10$ d) $x/d = 14.66$

Figure 0-84 Comparison of thermal field profiles with the heat flux plate off at $M = 2.0$ and 3.0 at $DR = 1.2$ and a) $x/d = 3$ b) $x/d = 5$, c) $x/d = 10$ and d) $x/d = 14.66$

What is interesting to note is that when shaped holes do start to separate, as is the case at M = 3.0, the jets remain relatively close to the wall. Jets from cylindrical holes tend to lift off much farther into the mainstream when the separate, making them less effective. An example of the thermal field that would be expected from cylindrical holes is shown in Figure 0-85. These centerline profiles were measured by Stewart and Bogard [59] downstream of cylindrical holes on a nearly zero pressure gradient location on the suction side of a vane. At DR = 1.2 and M = 2.41, the core of the jet has lifted y/d = 1.5 off the wall by x/d = 5 and x/d = 10. With the shaped hole thermal field profiles in Figure 3-84 b) and c), the jet remains closer to the wall at y/d = 0.2. This shows the benefit of shaped holes, even when they have started to separate.

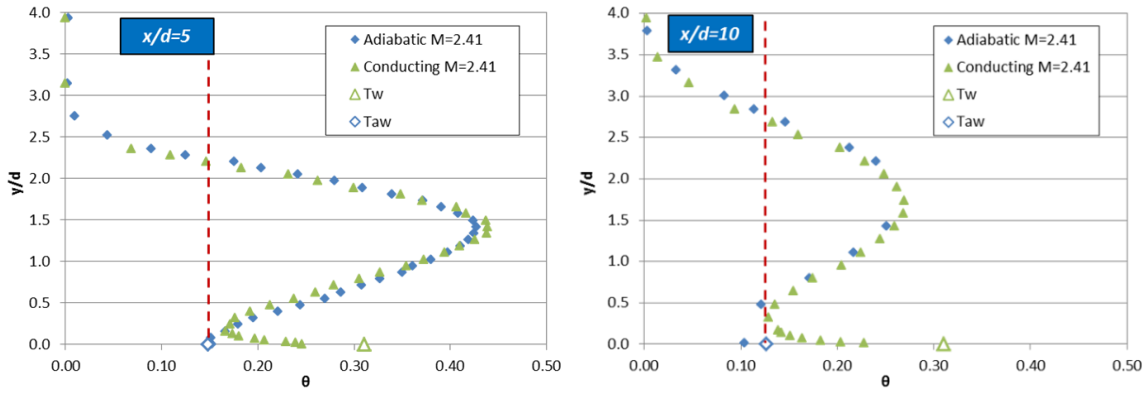

a) b)

Figure 0-85 Centerline thermal field profiles downstream of cylindrical holes on the suction side of a vane at DR = 1.2, M = 2.41, and a) x/d = 5 b) x/d = 10 [59].

Effect of Density Ratio

Figure 3-86 shows centerline thermal field profiles for DR = 1.2 and 1.5 at M = 2.0 for a) the heat flux plate off and b) and heat flux plate on at x/d = 5. What is interesting about these figures is that even though the thermal fields were measured at

two different density ratios, the profiles above the wall are almost the identical when the temperature is nondimensionalized as θ. Referring to the adiabatic effectiveness performance in Figure 0-1, at DR = 1.2 and M = 2.0, the jet has started to separate, while the jets at DR = 1.5 and M = 2.0 are better attached. The thermal field profiles show that the jet separation is localized immediately above the wall, while the rest of the jet profile remains undisturbed.

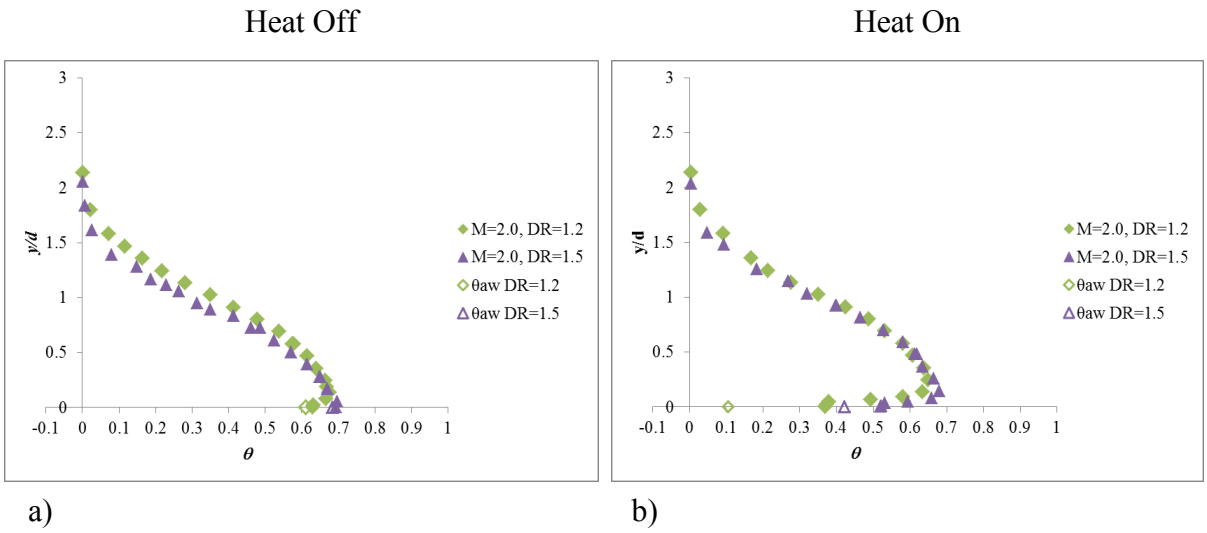

Figure 0-86 Comparison of thermal field profiles at M = 2.0, z/d = 0, and x/d = 5 and DR = 1.2 and 1.5 with the heat flux plate a) off and b) on

CONCLUSIONS

Conclusions from 7°-7°-7° Shaped Hole Adiabatic Effectiveness Study

The original goal of this portion of the dissertation was to validate the performance of the 7°-7°-7° shaped hole geometry on a flat plate facility at two different research labs: one lab at the University of Texas at Austin (UT) and the other at Penn State University (PSU). The scope of this project changed when the adiabatic effectiveness results between the two labs did not match. Several testing parameters and causes were investigated to try to determine what caused the discrepancy in results. In the end, it was concluded that shaped holes are extremely sensitive to machining, substrate material, and coolant entrance effects, especially at high blowing ratios where the jets start to detach from the surface.

1. Sensitivity to Machining and Substrate Material

UT and PSU tested several coupons that were machined out of polyurethane and polystyrene to observe the effect of the coupon substrate material and who machined the coupon. The summary of these test coupons is in Table 0-1. It was found that when UT and PSU tested polyurethane coupons machined at UT (UT Polyurethane and PSU Polyurethane), that the results at DR =1.5 agreed well except at M = 0.5. The discrepancy at M = 0.5 was possibly due to differences in coolant entrance effects from using different plenum and coolant piping designs between the two laboratories. Analysis of the contours of adiabatic effectiveness showed that the coolant did not fill out the shaped hole at M = 0.5 at UT, while it did at PSU. This data was shown in Figure 0-13 and Figure 0-14.

Table 0-1 Polyurethane and polystyrene coupons machining and testing location.

Coupon	Machining Location	Testing Location
UT Polyurethane	UT	UT
UT Polystyrene	PSU	UT
PSU Polystyrene Hatch	PSU	PSU, UT
PSU Polyurethane	UT	PSU

The results from the polystyrene coupons that were machined at PSU (UT Polystyrene and PSU Polystyrene Hatch) did not compare well at any blowing ratio at *DR* = 1.2. At *DR* = 1.5, the results between the two labs agreed well at *M* = 0.5 and 1.0, but as the blowing ratio was increased, the laterally averaged adiabatic effectiveness remained high at UT, while it dropped PSU. These results were shown in Figure 0-23 and Figure 0-24. There are a few reasons that the results did not match. First of all, the UT Polystyrene coupon was tested with a plenum that had been reconfigured internally to match PSU's plenum design. The contours of adiabatic effectiveness showed that the coolant exited non-uniformly from the jets, which was not seen when the same coupon was testing on a plenum with the original UT internal plenum geometry. Secondly, UT and PSU had different coolant piping designs, which could have caused the coolant flow to behave differently inside the plenums in terms of the velocity profile and turbulence intensity. Thirdly, there could have been machining differences between the UT Polystyrene and UT Polystyrene Hatch coupons, even though they were machined by the same machinist. Polystyrene is soft, and it could be that reproducing the same shaped hole geometry is more difficult with this material. This is supported by viewing the quality of machining of the coupons, which is shown in Appendix A. In addition, PSU machined an additional polystyrene coupon, called the PSU Smooth Polystyrene. When the results from this coupon were compared to results from the PSU Polystyrene Hatch,

both tested at PSU, it was found that the difference in performance was slightly outside PSU's uncertainty at two higher blowing ratios.

Finally, UT and PSU tested the same coupon, the PSU Polystyrene Hatch. By testing the same coupon, any variations due to coupon material and machining variability were eliminated. At DR = 1.5, the laterally averaged adiabatic effectiveness matched very well at all blowing ratios. At DR = 1.2, the results were similar, but it was observed that UT had higher effectiveness between the jets than what was seen at PSU. When an adjustment of UT's data was made for this presumed bias, the results at DR = 1.2 agreed much better. In the end, testing the same coupon showed that the results between the two labs were very similar.

2. Sensitivity to Coolant Entrance Effects

The machining and substrate material of the test coupon was not the only factor that was found to be important in film cooling performance between the two laboratories. When UT changed the coolant piping leading up to the plenum for another project, the UT Polystyrene coupon was retested. It was found that when the cooling piping was changed to resemble the coolant piping configuration at PSU more closely, that the laterally averaged adiabatic effectiveness results changed to match PSU's results better.

This study was unique in that it analyzed several film cooling testing parameters that have not been analyzed in the past, such as the coupon substrate material, coupon machining, internal plenum geometry, and coolant piping design, using two different testing facilities. Figure 0-74 and Figure 0-75 show a summary of the laterally averaged adiabatic effectiveness results from all of the studies just described. Plotting all of these results together includes the uncertainty associated with all of the testing parameters just described, which are not typically included in an uncertainty analysis. While the jets were attached and filling out the coolant holes ($M \leq 1.5$ at DR = 1.2 and 1.5), the variation of the data was about $\bar{\eta} \pm 0.02$. However, as the blowing ratio increased, the test results diverged significantly. At high blowing ratios, when the jets start to detach from the

surface, the shaped hole performance becomes more sensitive to differences in the coupon material, coupon machining, and coolant entrance effects. This is an important result, since the impact of these variables on the performance of shaped holes was significant, and are not typically accounted for. While inherently obvious, this study reinforced that gas turbine designers should use robust shaped hole geometries that do not show signs of separation from the surface at the operating conditions they are used at. This is because the degree of separation and performance in this regime in an actual turbine part is hard to predict in a laboratory setting without matching the machining tolerances and imperfections of the shaped holes used in actual turbine components. In addition, turbine designers should use data where the internal flow between the experiment and actual turbine components is matched as closely as possible because the shaped holes tested in this project showed a sensitivity to the internal plenum design as well as the coolant piping configuration leading up to the plenum. The plenum condition used in this study is not representative of most coolant conditions in actual turbine components, which often have cross-flow and variable inlet coolant flow conditions, so new tests would be required to simulate actual coolant inlet flow conditions.

In the course of completing this project, the effects of mainstream turbulence intensity, scaling adiabatic effectiveness at multiple density ratios, and mainstream Reynolds number were also analyzed and are summarized below.

3. Effect of Mainstream Turbulence Intensity

UT tested the UT Polystyrene coupon at Tu = 0.5% and 5.0% at DR = 1.2 and 1.5. At both density ratios, the effect of turbulence intensity was within uncertainty, so no definite conclusions could be drawn. However, at M = 0.5 and DR = 1.5, increasing the mainstream turbulence intensity increased the laterally averaged adiabatic effectiveness significantly, outside the range of uncertainty, which was shown in Figure 0-46. At low turbulence intensity, the coolant did not fill out the shaped hole at this testing condition.

When the turbulence intensity was increased, it caused the jets to spread in the hole, which increased the performance.

4. Scaling Adiabatic Effectiveness at Multiple Density Ratios

Understanding how adiabatic effectiveness scales with density ratio is important because it would allow researchers and turbine designers to use adiabatic effectiveness results at one density ratio to predict the performance at a different density ratio. This is especially useful since many film cooling studies do not match the density ratio of 2.0 that is actually used in gas turbine engines. In addition, understanding how the performance of jets scales would provide insight into the flow physics of the jets. Scaling of adiabatic effectiveness with density ratio was analyzed at Tu = 0.5% and 5.0% using two different coolant piping configurations. The blowing ratio, momentum flux ratio, and velocity ratio were analyzed as scaling parameters. At Tu = 0.5%, the laterally averaged adiabatic effectiveness scaled the best with velocity ratio, which grouped the data at DR = 1.2, 1.5, and 1.73 together quite tightly (Figure 0-49 and Figure 0-52). At Tu = 5.0%, the velocity ratio was again the best scaling parameter, but it did not group the data together as tightly as at low turbulence intensity (Figure 0-55 and Figure 0-58). The velocity ratio served as a reliable scaling parameter at both mainstream turbulence intensities. Even though the coolant piping configuration affected adiabatic effectiveness values, it had no effect on the scaling. The blowing ratio was shown to be a poorest scaling parameter of those analyzed, which is an important result because most studies use the blowing ratio to characterize the coolant flow rate.

5. Effect of Mainstream Reynolds Number

To test the effect of the mainstream Reynolds number, which is defined with the characteristic length being the metering hole diameter, the UT Polyurethane, d = 4 mm was tested at two mainstream Reynolds numbers. In one experiment, the mainstream Reynolds number was held at 5600 (the value used for the rest of the tests in this study)

and in another experiment, the mainstream Reynolds number was reduced by about 60% to 2500. Comparing the results showed that increasing the mainstream Reynolds number increased the film cooling performance anywhere from $\bar{\eta} = 0$ to 0.05, depending on the blowing ratio and density ratio. This could be due to the difference in boundary layer thickness as the mainstream Reynolds number was increased, which would be consistent with what is in literature. At $Re_\infty = 2500$, $\delta/d = 1.9$, and at $Re_\infty = 5600$, $\delta/d = 1.5$. These results were shown in Figure 0-60 and Figure 0-65.

Conclusions from Heat Transfer Coefficient Measurements at Multiple Density Ratios

Heat transfer coefficients at $DR = 1.0$, 1.2, and 1.5 were determined using direct measurements of T_w, T_{aw}, and q'', which has not been published before. This technique has the benefit that it does not rely on extrapolations or assumptions of 1-D heat transfer, and it realistically simulates the thermal field and boundary layer above the wall. At $M =$ 0.5-1.5, when the jets were attached to the surface, the heat transfer coefficient augmentation downstream of the coolant holes was quite low, less than 1.2, at all density ratios. However, for $M = 2.0$-3.0, the jets started to detach from the surface and the heat transfer coefficient augmentation increased. The maximum h_f/h_0 was 1.8 at $DR = 1.0$ and $M = 3.0$. These results show that when the jets are attached, any increased heat transfer into the turbine component produced by the film cooling from the shaped holes is small compared to the enhanced cooling they provide. Once the jets detach from the surface, the benefit of adding shaped holes may come into question, since the adiabatic effectiveness decreases and the heat transfer coefficient augmentation increases.

The heat transfer coefficient augmentation results at $DR = 1.0$, 1.2, and 1.5 were compared by matching M, I, and VR. While none of these parameters scaled the results exactly, scaling with VR was clearly superior to scaling with M or I. Therefore, it would be best to match VR when comparing heat transfer coefficients at different density ratios.

In addition, thermal field measurements showed that the adiabatic wall temperature provided an appropriate driving temperature for heat transfer.

Many of the contours of h_f/h_0 farther downstream of the holes showed a splitting pattern where the heat transfer coefficient augmentation was lower along the jet centerline and increased on the edges of the jet. This can be attributed to the counter-rotating vortices that pull hotter air that is warmed by the heat flux plate into the core of the jet, which increases the thermal boundary layer thickness and decreases heat transfer coefficient. Thermal field profiles supported this theory since the measurements showed that the centerline of the jet was warming faster than the edges of the jet.

Even though the adiabatic effectiveness performance at $M = 3.0$ at $DR = 1.2$ drops off due to jet detachment, thermal field measurements show that the detachment of the jet is localized to very near the wall, and most of the jet, including the coldest peak, remained unchanged compared to the profile at $M = 2.0$ where the jet was better attached to the surface.

The study of heat transfer coefficient augmentation at multiple density ratios should motivate turbine component designers to think about how the heat transfer coefficient augmentation results they use were measured. The heat transfer coefficients measured for this dissertation were different depending on the density ratio, with results at $DR = 1.0$ being distinctly higher than those measured at $DR = 1.2$ and 1.5, especially when the jets were detached at high blowing ratios. This is a key finding since many researchers and turbine designers presume that the heat transfer coefficient augmentation is relatively insensitive to density ratio. However, more research is needed to establish the exact scaling relationship between heat transfer coefficient augmentation and density ratio.

Recommendations for Future Work

Scaling for Multiple Hole Geometries

The work in this dissertation found that the 7°-7°-7° shaped hole designed at PSU scaled best with velocity ratio, but it would be interesting to see if this scaling would hold for other shaped hole geometries and cylindrical holes.

Heat Transfer Coefficient Augmentation Measurements on a Matched Bi Facility

The Turbulence and Turbine Cooling Research Laboratory at the UT has used conducting vane models that match the *Bi* of vanes in a real engine to simulate conjugate effects of internal and external convection as well as conduction through the vane wall. A new facility could be set up that would use a flat plate or other model geometry that would match the *Bi* as well as the internal flow conditions. An infrared camera would view the top of the model (the wall temperature) and an additional infrared camera would view underneath, or inside, the coolant model (the internal surface temperature). Using these temperatures as boundary conditions, a finite element analysis could be used to calculate the heat flux, and then the heat transfer coefficient could be found. The advantage of this method is that the internal coolant flow conditions could be simulated. By using a conducting model, the thermal boundary layer could be simulated more closely (most heat transfer coefficient augmentation studies choose either a constant heat flux or constant temperature boundary condition) and the effect of upstream thermal boundary layer development would be included. In addition, instead of the wall being heated, like with the constant heat flux foil used in this dissertation, the wall would be cooled, which is more realistic.

Effect of Coolant Entrance Conditions on Film Cooling with Cylindrical and Shaped Holes

The research in this dissertation found that shaped hole geometries were very sensitive to inlet flow conditions. A follow-up study could include a more detailed study

on the effects of varying inlet flow conditions on shaped hole and cylindrical hole adiabatic effectiveness performance. The study could systematically vary the coolant cross-flow, turbulence intensity, turbulent length scale, and mean coolant velocity profile.

APPENDIX A: PHOTOGRAPHS OF TEST COUPONS

UT Polyurethane (Machined at UT)

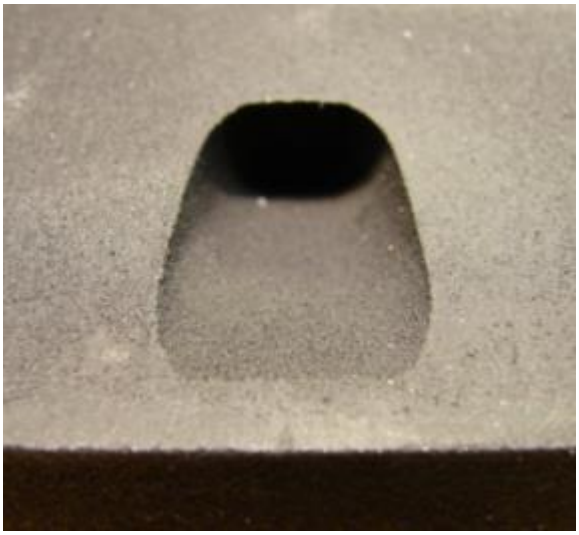

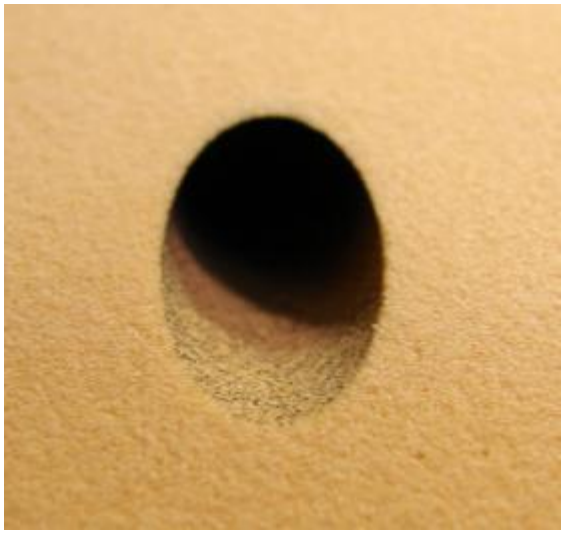

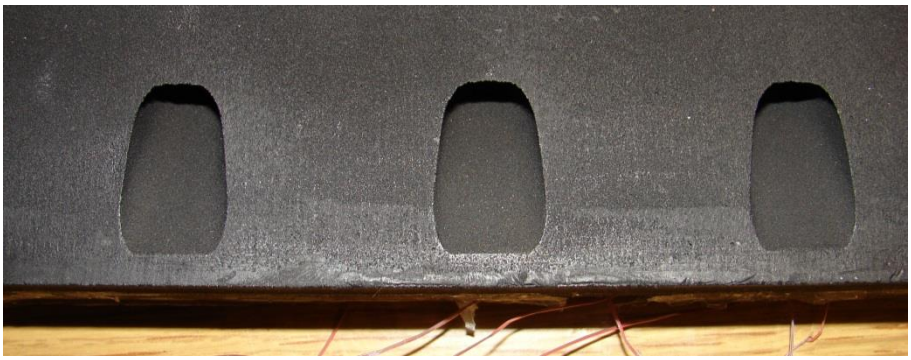

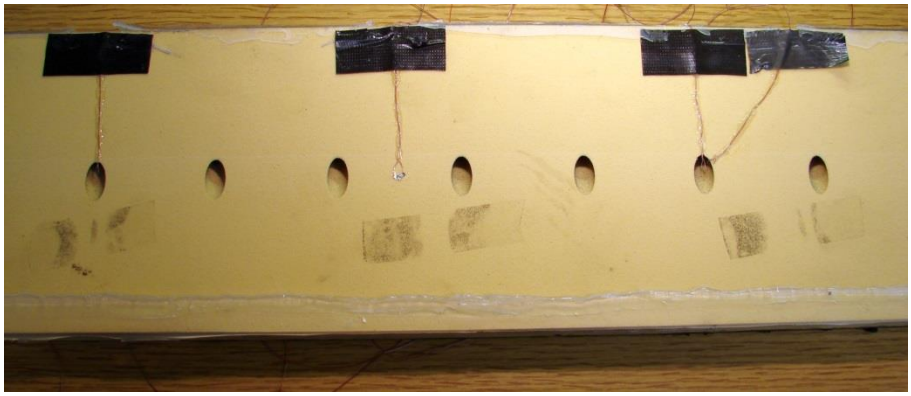

UT Polystyrene (Machined at PSU)

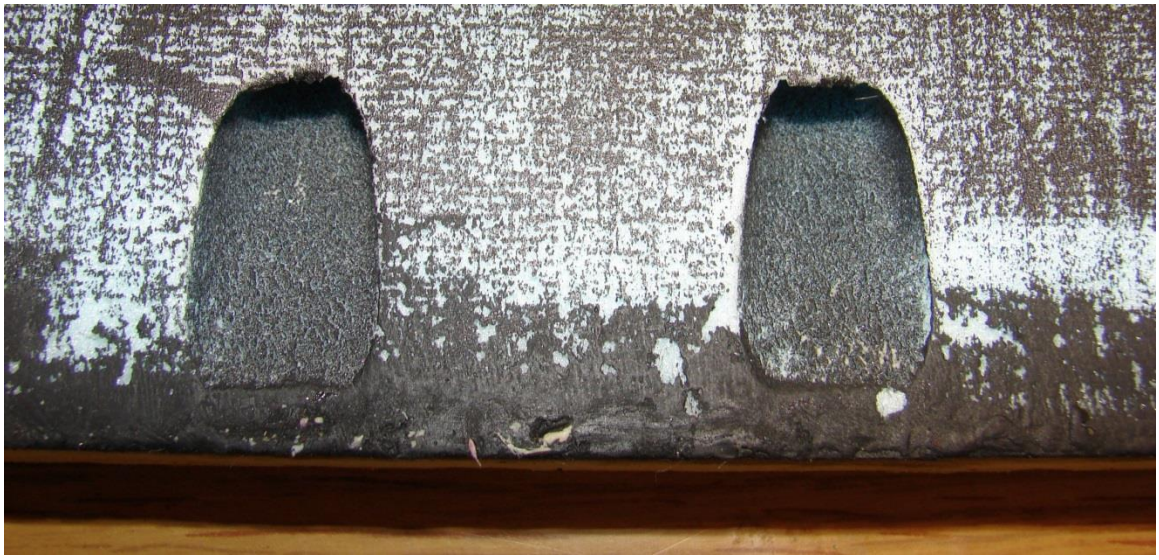

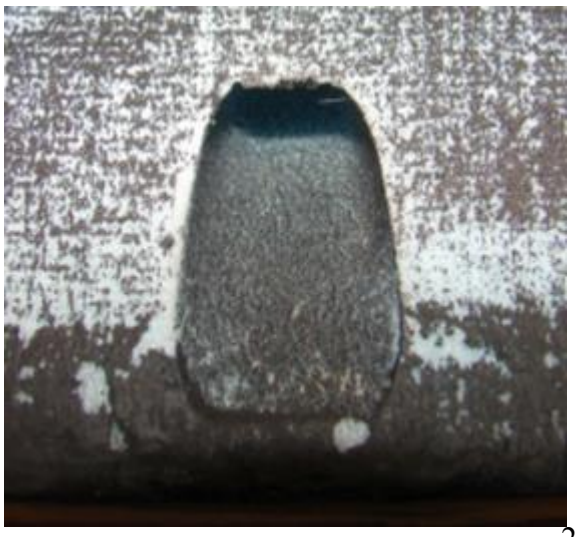

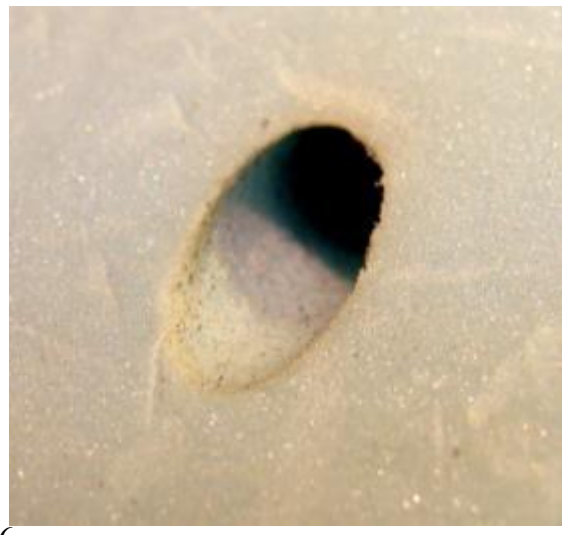

PSU Polystyrene Hatch (Machined at PSU)

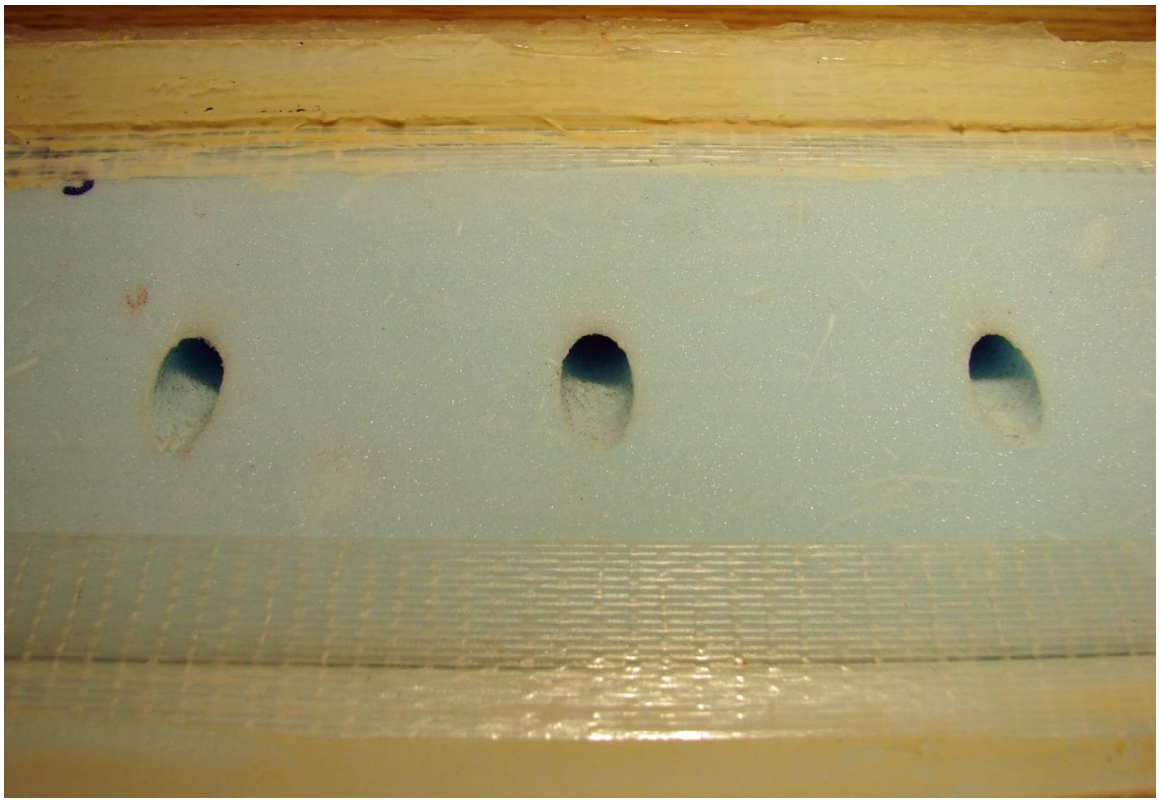

Close-ups of same holes shown above.

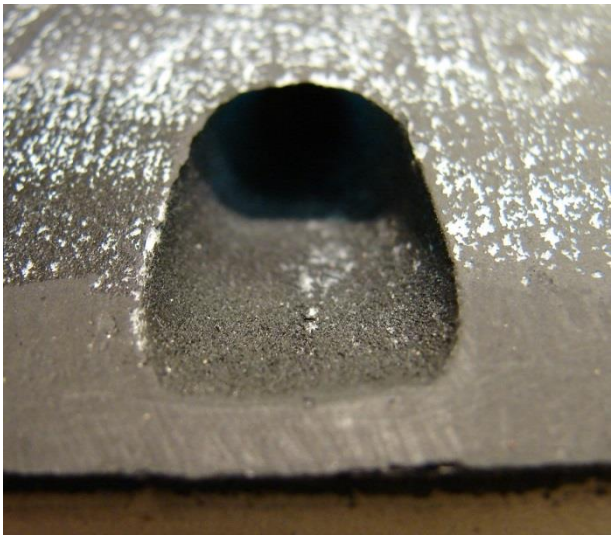

WORKS CITED

[1] "Brayton Cycle," 29 Jan. 2012. [Online]. Available: http://en.wikipedia.org/wiki/Brayton_cycle. [Accessed Mar. 2012].

[2] "Film Cooling of Turbine Blades in Gas Turbines," Ecole Polytechnique Federale de Lausanne Group of Thermal Turbomachinery, [Online]. Available: http://lttwww.epfl.ch/research/htprojects/filmcool.htm. [Accessed 12 March 2012].

[3] D. G. Bogard and K. A. Thole, "Gas Turbine Film Cooling," *Journal of Propulsion and Power,* vol. 22, no. 2, pp. 249-270, 2006.

[4] K. L. Harrison and D. G. Bogard, "Temperature of the Adiabatic Wall Temperature in Film Cooling to Predict Wall Heat Flux and Temperature," *GT2008-51424,* 2008.

[5] E. R. G. Eckert, "Gas-To-Gas Film Cooling," *Inzhenergno-Fizicheskii Zhurnal,* vol. 19, no. 3, pp. 426-440, September 1970.

[6] E. R. G. Eckert, "Analysis of Film Cooling and Full-Coverage Film Cooling of Gas Turbine Blades," *Journal of Engineering for Gas Turbines and Power,* vol. 106, pp. 206-213, 1984.

[7] P. J. Loftus and T. V. Jones, "The Effect of Temperature Ratios on the Film Cooling Process," *Journal of Engineering for Gas Turbines and Power,* vol. 105, no. 3, pp. 615-620, 1983.

[8] M. Gritch, S. Baldauf, M. Martiny, A. Schulz and S. Wittig, "The Superposition Approach to Local Heat Transfer Coefficients in High Density Ratio Film Cooling Flows," *ASME Paper 99-GT-168,* 1999.

[9] C. Saumweber and A. Schulz, "Free-Stream Effects on the Cooling Performance of Cylindrical and Fan-Shaped Cooling Holes," *Journal of Turbomachinery,* vol. 134, no. 6, 2012.

[10] H. Ammari, N. Hay and D. Lampard, "The Effect of Density Ratio on the Heat Transfer Coefficient From a Film-Cooled Flat Plate," *Journal of Turbomachinery,* vol. 112, pp. 444-450, 1990.

[11] R. J. Goldstein and H. H. Cho, "A Review of Mass Transfer Measurements Using Naphthalene Sublimination," *Journal of Experimental Thermal and Fluid Science,* vol. 10, pp. 416-434, 1995.

[12] S. V. Ekkad and J.-C. Han, "A Transient Liquid Crystal Thermography Technique for Gas Turbine Heat Transfer Measurements," *Journal of Measurement Science Technology,* vol. 11, pp. 957-968, 2000.

[13] A. K. Sinha, D. G. Bogard and M. E. Crawford, "Film-Cooling Effectiveness Downstream of a Single Row of Holes With Variable Density Ratio," *Journal of Turbomachinery,* vol. 113, no. 3, pp. 442-449, 1991.

[14] R. S. Bunker, "A Review of Shaped Hole Turbine Film-Cooling Technology," *Journal of Heat Transfer,* vol. 127, pp. 441-453, April 2005.

[15] C. Saumweber, A. Schulz and S. Wittig, "Free-Stream Turbulence Effects on Film Cooling with Shaped Holes," *Journal of Turbomachinery,* vol. 125, pp. 65-73, 2003.

[16] B. A. Haven, D. K. Yamagata and M. Kurosaka, "Anti-Kidney Pair of Vortices in Shaped Holes and Their Influence on Film Cooling Effectiveness," in *Proceedings of the ASME International Gas Turbine & Aeroengine Congress & Exposition*, Orlando, 1997.

[17] C. M. Bell, H. Hamakawa and P. M. Ligrani, "Film Cooling From Shaped Holes," *Journal of Heat Transfer,* vol. 122, no. 2, pp. 224-232, 2000.

[18] C. Saumweber and A. Schulz, "Effect of Geometry Variations on the Cooling Performance of Fan-Shaped Cooling Holes," *Journal of Turbomachinery,* vol. 134, no. 6, pp. 061008-1-16, 2012.

[19] M. Gritsch, A. Schulz and S. Wittig, "Adiabatic Wall Effectiveness Measurements of Film-Cooling Holes with Expanded Exits," *Journal of Turbomachinery,* vol. 120, no. 3, pp. 549-556, 1998.

[20] C. H. Lim, G. Pullan and P. Ireland, "Influence of Film Cooling Hole Angles and Geometries on Aerodynamic Loss and Net Heat Flux Reduction," *Journal of Turbomachinery,* vol. 135, no. 5, pp. 051019-1-13, 2013.

[21] J. E. Sargison, S. M. Guo, M. L. G. Oldfield and A. J. Rawlinson, "The Variation of Heat Transfer Coefficient, Adiabatic Effectiveness and Aerodynamic Loss with Film Cooling Hole Shape," *Annals of the New York Academy of Sciences,* vol. 934, pp. 361-368, 2001.

[22] C. Saumweber and A. Schulz, "Comparison of the Cooling Performance of Cylindrical and Fan-Shaped Cooling Holes with Special Emphasis on the Effect of Internal Coolant Cross-Flow," in *Proceedings of ASME Turbo Expo 2008: Power for Land, Sea and Air*, Berlin, 2008.

[23] S. Baldauf, M. Scheurlen, A. Schulz and S. Wittig, "Heat Flux Redution from Film Cooling and Correlation of Heat Transfer Coefficients From Thermographic Measurements at Enginelike Conditions," *Journal of Turbomachinery,* vol. 124, pp. 699-709, 2002.

[24] S. V. Ekkad, D. Zapata and J. C. Han, "Heat Transfer Coefficients Over a Flat Surface with Air and $C0_2$ Injection Through Compound Angle Holes Using a Transient Liquid Crystal Image Method," *Journal of Turbomachinery,* vol. 119, pp. 580-586, July 1997.

[25] H. D. Ammari, N. Hay and D. Lampard, "The Effect of Density Ratio on the Heat Transfer Coefficient From a Film-Cooled Flat Plate," *Journal of Tubomachinery,* vol. 112, pp. 444-450, July 1990.

[26] R. J. Goldstein, P. Jin and R. L. Olson, "Film Cooling Effectiveness and Mass/Heat

Transfer Coefficient Downstream of One Row of Discrete Holes," *Journal of Turbomachinery,* vol. 121, pp. 225-232, April 1999.

[27] C. Saumweber, A. Schulz, S. Wittig and M. Gritsch, "Effects of Entrance Crossflow Direction to Film Cooling Holes," *Annals of the New York Academy of Sciences: Heat Transfer in Gas Turbine Systems,* vol. 934, no. 1, pp. 401-408, 2001.

[28] M. Gritsch, A. Schulz and S. Wittig, "Film-cooling Holes with Expanded Exits: Near-Hole Heat Transfer Coefficients," *International Journal of Heat and Fluid Flow,* vol. 21, pp. 146-155, 2000.

[29] M. Gritsch, W. Colban, H. Schar and K. Dobbeling, "Effect of Hole Geometry on the Thermal Performance of Fan-Shaped Film Cooling Holes," *Journal of Turbomachinery,* vol. 127, no. 4, pp. 718-724, 2005.

[30] W. F. Colban, K. A. Thole and D. Bogard, "A Film-Cooling Correlation for Shaped Holes on a Flat-Plate Surface," *Journal of Turbomachinery,* vol. 133, no. 1, pp. 011002-1-11, 2011.

[31] B. Laveau and R. S. Abhari, "Influence of Flow Structure on Shaped Hole Film Cooling Performance," in *Proceedings of ASME Turbo Expo 2010: Power for Land, Sea, and Air*, Glasgow, 2010.

[32] K. Thole, M. Gritsch, A. Schulz and S. Wittig, "Flowfield Measurements for Film-Cooling Holes With Expanded Exits," *Journal of Turbomachinery,* vol. 120, no. 2, pp. 327-336, 1998.

[33] K.-D. Lee and K.-Y. Kim, "Shape Optimization of a Laidback Fan-Shaped Film-Cooling Hole to Enhance Cooling Performance," in *Proceedings of ASME Turbo Expo 2010: Power for Land, Sea, and Air*, Glasgow, 2010.

[34] C. Heneka, A. Schulz, H. Bauer, A. Heselhaus and M. Crawford, "Film Cooling Performance of Sharp Edged Diffuser Holes With Lateral Inclination," *Journal of Turbomachinery,* vol. 134, no. 4, pp. 041015-1-8, 2012.

[35] E. Lutum and B. V. Johnson, "Influence of the Hole Length-to-Diameter Ratio on Film Cooling with Cylindrical Holes," *Journal of Turbomachinery,* vol. 121, no. 2, pp. 209-217, 1999.

[36] R. J. Goldstein, E. R. G. Eckert and F. Burggraf, "Effects of Hole Geometry and Density on Three-dimensional Film Cooling," *Int. J. Heat Mass Transfer,* vol. 17, pp. 595-607, 1974.

[37] N. W. Foster and D. Lampard, "Effects of Density and Velocity Ratio on Discrete Hole Film Cooling," *AIAA Journal,* vol. 13, no. 8, pp. 1112-1114, 1975.

[38] D. R. Pedersen, "Film Cooling with Large Density Differences Between the Mainstream and the Secondary Fluid Measured by the Heat-Mass Transfer Analogy," *Journal of Heat Transfer,* vol. 99, no. 4, pp. 620-627, 1977.

[39] C. J. P. Forth, P. J. Loftus and T. V. Jones, "Scaling Parameters in Film-Cooling," in *8th International Heat Transfer Conference*, 1986.

[40] C. Liess, "Experimental Investigation of Film Cooling With Ejection From a Row of Holes for the Application to Gas Turbine Blades," *Journal of Engineering for Power,* vol. 97, no. 1, pp. 21-27, 1975.

[41] J. P. Bons, C. D. MacArthur and R. B. Rivir, "The Effect of High Free-Stream Turbulence on Film Cooling Effectiveness," *Journal of Turbomachinery,* vol. 118, no. 4, pp. 814-825, 1996.

[42] M. Gritsch, A. Schulz and S. Wittig, "Effect of Internal Coolant Crossflow on the Effectiveness of Shaped Film-Cooling Holes," *Journal of Turbomachinery,* vol. 125, no. 3, pp. 547-554, 2003.

[43] S. P. Porter, A. D. Henderson and G. J. Walker, "Influence of Inlet Velocity Ratio on the Outlet Flow Uniformity of a Fan-shaped Film Cooling Hole," in *Proceedings of ASME Turbo Expo 2009: Power for Land, Sea, and Water*, Orlando, 2009.

[44] D. G. Hyams and J. H. Leylek, "A Detailed Analysis of Film Cooling Physics: Part

III--Streamwise Injection with Shaped Holes," *Journal of Turbomachinery,* vol. 122, no. 1, pp. 122-132, 2000.

[45] B. Sen, D. L. Schmidt and D. G. Bogard, "Film Cooling with Compound Angle Holes: Heat Transfer," *Journal of Turbomachinery,* vol. 118, pp. 800-806, 1996.

[46] V. L. Eriksen and R. J. Goldstein, "Heat Transfer and Film Cooling Following Injection Through Inclined Circular Tubes," *Journal of Heat Transfer,* vol. 96, no. 2, pp. 239-245, October 1974.

[47] Y. Yu, S. Gogineni, C.-H. Yen, T. I.-P. Shih and M. K. Chyu, "Film Cooling Effectiveness and Heat Transfer Coefficient Distributions Around Diffusion Shaped Holes," *Journal of Heat Transfer,* vol. 124, pp. 820-827, October 2002.

[48] A. Kohli and D. G. Bogard, "Adiabatic Effectiveness, Thermal Fields, and Velocity Fields for Film Cooling with Large Angle Injection," *Journal of Turbomachinery,* vol. 119, pp. 352-358, 1997.

[49] A. Kohli and D. G. Bogard, "Fluctuating Thermal Field in the Near-Hole Region for Film Cooling Flows," *Journal of Turbomachinery,* vol. 120, pp. 86-91, 1998.

[50] C. Y. Ho and T. K. Chu, "Electrical Resistivity and Thermal Conductivity of Nine Selected AISI Stainless Steels," CINDAS, West Lafayette, 1977.

[51] S. J. M. F. A. Kline, "Describing Uncertainties in Single Sample Experiments," *Mechanical Engineering,* vol. 75, no. 1, pp. 3-8, January 1953.

[52] R. J. Moffat, "Using Uncertainty Analysis in the Planning of an Experiment," *Journal of Fluids Engineering,* vol. 107, no. 2, pp. 173-178, 1985.

[53] G. E. Mattingly, "Volume Flow Measurements," in *Fluid Mechanics Measurements*, 2nd ed., Washington, D.C., Taylor & Francis, 1996, pp. 301-365.

[54] Dow, "Styrofoam Sheathing," The Dow Chemical Company, 2013. [Online]. Available: http://building.dow.com/na/en/products/insulation/ressheathing.htm. [Accessed 28 August 2013].

[55] General Plastics Manufacturing Company, "LAST-A-FOAM® R-3315 Rigid Polyurethane Foam," General Plastics Manufacturing Company, Tacoma, 2010.

[56] K. Kadotani and R. Goldstein, "Effect of Mainstream Variables on Jets Issuing from a Row of Inclined Round Holes," *Transactions of the American Society of Mechanical Engineers,* vol. 101, pp. 298-304, 1979.

[57] A. J. H. Teekaram, C. J. P. Forth and T. V. Jones, "The Use of Foreign Gas to Simulate the Effects of Density Ratios in Film Cooling," *Journal of Turbomachinery,* vol. 111, pp. 57-62, 1989.

[58] S. Baldauf, A. Schulz and S. Wittig, "High Resolution Measurements of Local Heat Transfer Coefficients by Discrete Hole Film Cooling," *Journal of Turbomachinery,* vol. 123, no. 4, pp. 749-759, 1999.

[59] W. R. Stewart and D. G. Bogard, "Experimental Thermal Field Measurements of Film Cooling Above the Suction Surface of a Turbine Vane," in *Proceedings of the ASME Turbo Expo 2014*, Dusseldorf, 2014.